Kinematics, motion analysis and path planning for four kinds of wheeled mobile robots

Yongji Wang

Ph. D. Thesis

University of Edinburgh

1995

Dedicated to

my wife, Lu Jiang, and my son, Daniel Wang

Abstract

This dissertation presents a comprehensive and systematic investigation into some fundamental issues relating to creating an autonomous wheeled mobile robot (WMR).

The forms of WMRs with various structures developed in the past are first classified into four groups according to the method of steering and powering. The four groups are: a. ordinary car-like robots (including passenger cars, single unit trucks, single unit buses and articulated trucks); b. dual drive robots (dual drive motors with various casters); c. synchro drive and steering robots; and d. omnidirectional robots.

The concepts of inverse and direct kinematics widely used in non-mobile manipulators are, for the first time, introduced to WMRs, and a unified treatment of the kinematics for the four kinds of WMRs is presented. A motion feasibility and smoothness analysis for each of them is carried out, revealing the motion characteristics resulting from each of the different mechanical structures. This provides a better understanding of their motion characteristics and forms the basis for discussing the path planning problem. The concept of deviation angle interval is defined and used to explain the strange phenomenon of a pirouette. The conditions and formula for pure translation, pure rotation, straight line motion and circular motion are developed. In order to verify the correctness and to illustrate the advantages of the developed kinematic model, the simulation results from the present model are compared with the existing standards from other kinematic models.

Path planning is essential for creating an autonomous robot. Various methods for dealing with the find-path problem have been developed in the past. Based on the motion analysis of the four kinds of WMRs, a critical review of the presently available algorithms for moving a WMR among known static obstacles from a given start location to a given goal location is presented, and the suitability of the existing algorithms to each of the four kinds of WMRs is examined. The study shows that most of these algorithms suffer from the fundamental drawback that kinematics of the robot has not been taken into account, and thus there is no guarantee that the paths generated by these algorithms are always

collision-free and executable. Finally, a formal formulation of the findpath problem for the most widely used car-like and the dual drive robots is given and then a robust, efficient and reliable algorithm, taking into account nonholonomic constraint and steering angle limit, is developed. Some important criteria for the avoidance of collisions and steering angle saturations are derived.

Declaration

This thesis is submitted in part fulfillment of the requirements for the degree of Doctor of Philosophy at the University of Edinburgh. Unless otherwise stated, the work described is original and has not been previously submitted in whole, or in part, for any degree at this, or at any other, University.

Yongji Wang

University of Edinburgh

January 1995

Acknowledgments

I would like to thank the many people who have contributed their time to helping with this thesis. First, I wish to acknowledge the help of my former supervisor, Dr. D. J. Todd, who originally suggested wheeled mobile robots as a topic for my research. I also owe a great debt to my supervisors, Dr. J. W. Roberts and Dr. J. A. Linnett, who were pleased to act as my supervisors at the difficult time when Dr. D. J. Todd died two years ago.

Also thanks to Dr. A. S. T. Lue, Dr. G. Alder, Dr. M. P. Cartwell, Dr. Weidong Peng, Dr. Kaiyuan Cai, Mr. K. H. Wong and many others for their valuable encouragement and help.

I am grateful for the financial support of K. C. Wong Education Foundation, Hong Kong, for providing living expenses, the Committee of Vice-Chancellors and Principals of the Universities of the United Kingdom (CVCP) and the Mechanical Engineering Department of Edinburgh University for offering tuition fees during my PhD research, which enabled me to carry out this work.

Finally, I would like to express my deep appreciation to Lu Jiang, my wife, and to Daniel Wang, my son, not only for their support of my work, interest in the subject, and constant inspiration, but also for their endless patience at all stages of the manuscript preparation.

Yongji Wang

Contents

Chapter 1

Introduction

1.1 Introduction

A robot is a versatile mechanical device equipped with actuators and sensors under the control of a computer system. It operates in a workspace within the real world. This workspace is populated by physical objects and subject to the laws of nature. The robot performs tasks by executing motions in the workspace.

Robots take a bewildering variety of forms: arms of all shapes, vehicles with all possible arrangements of wheels and legs, and devices which although clearly robotic are neither vehicles nor arms.

Arms are one kind of mechanical device widely adopted in Robotics. They are made of several moving objects (called links) connected by joints, e.g. revolute joints (hinges) and prismatic joints (sliding joints). Each joint constraints the relative movements of the two objects it connects. A typical example of such a device is a robot arm (manipulator).

The first robotic systems to find widespread success in industrial applications were those commonly referred to as manipulators. When compared with the dedicated machines and conveyors that they replaced, these robots appear quite versatile. They can be easily reprogrammed to perform a variety of functions, and they have a far wider field of possible actions than the dedicated hardware systems. Which is to say that they are usually associated with a higher degree of control intelligence, and that this intelligence has more manipulative operations as a result of the flexible hardware structure.

1.2 Need for wheeled mobile robots

Despite the strong advantages of manipulators, they have some serious limitations. Most of these limitations come as a direct result of their immobility. A robot arm can only

manipulate objects that it can reach. As most industrial manipulators are fixed in place, their workspace is limited by the maximum extension of their linkages. Components have to be brought to the robot and taken away again by conveyors and other mechanical feed devices. To overcome the problems caused by the limited reach of robot arms, two approaches are under investigation.

One is the flexible manufacturing cell, where the manipulator is fixed in place and the machines that it services are placed around it. As the manipulator can reach several machines, it can service one while the others are performing their tasks, and it can transfer components, from one machine to the next. This approach works best when the machines are small enough to fit close to the robot. This approach, however, has a shortcoming. If a fixed manipulator fails, it usually becomes a liability. Since manipulators are not mobile, and they tend to be mounted in locations central to the flow of the product, when a failure occurs, the disabled robot may block, or partially block the flow of productions. Additionally, the personnel and equipment required to repair or replace the robot may cause further congestion.

A second approach is to mobilize the manipulator by, for example, mounting it on a wheeled robot, so that it can move from one machine to another. Before a general purpose mobile robot can move freely in a factory, home, farm or military environment, we have to achieve an "intelligent" connection between perception (sensing and understanding the environment), planning (trajectory generation and path planning) and action (control of robot motion within the environment). This is the emphasis of most of the research into Autonomous Land Vehicles (ALVs).

In the past, a manufacturer set up his plant on the basis of an expected long product run. Such a factory changed little from day to day and in order to achieve continuous throughput, the manufacturer kept large stocks of raw materials and parts. With the advent of computer-aided design for manufacturing and computer-controlled inventory systems, all this has changed. Now, customers expect a variety of operations and fast delivery. The rising cost of keeping large inventories has stimulated the development of just-in-time

manufacturing. One of the most serious problems in this environment is the transport of parts and subassemblies between manufacturing cells. Often industrial parts must be quickly transferred from one cell to another to keep production going. Automated Guided Vehicles (AGVs) are the most commonly used transport systems at present in industry. In the car manufacturing industry, for example, manipulator arms are fixed in place in a work cell (for welding, painting, gluing, sealing, and so on), and the car chassis is moved from cell to cell using an AGV.

The shortcoming of AGV systems is that they lack flexibility. The motion of these vehicles is restricted to certain predefined paths. Once the guidance mechanism is installed, it is expensive to alter. In some environment, traditional AGVs are too cumbersome and inflexible. Smaller and more flexible mobile robots are needed.

The need for mobile robots in factories can also be observed from the fact that changing a plant with a large number of manipulators from one product or process to a significantly different one may require a considerable expenditure of time and money. Much of this expenditure is the result of the fixed manipulators and the conveyor systems that are typically associated with the robots.

As a result, it is inevitable that mobile robots will find increased popularity in manufacturing applications. The combination of manipulators and mobile robots will be very powerful.

In addition to the needs in manufacturing industry, mobile robots will find applications in several other fields. Todd [205] gives a detailed discussion of the potential applications of the mobile robots. They include mining in the high health risks environment, deep-sea operation, space exploration, nuclear and explosive materials handling, security industry, agriculture, military, publicity entertainment, and domestic service.

Among the popularly developed mobile robots are wheeled mobile robots, tracked mobile robots, and legged mobile robots. Most mobile robots so far, like land vehicles in general, have used wheels since this is the simplest method of locomotion. Wheels are abandoned

only when there is a pressing reason. Tracks are intended as a sort of portable railway, a temporary smooth road for a wheeled robot, which spreads the load on soft ground and bridge gaps. Legged robots may be chosen as another alternative to wheeled robots only in the cases where transport occurs on harder environment, such as a rough ground, or in buildings (in particular, on stairs). In this thesis, attention is focused on wheeled robots.

Some special types of mobile robots have been reported recently, but they are still in the process of development and research. Koshiyama et.al [95] described a new type of mobile robot that has a spherical wheel, an arched body, and motion controlling mechanisms installed inside the wheel. Shan et.al [176] at the University of Michigan reported the design and motion planning for a mechanical snake robot which is designed mainly for the places that are too dangerous and too small for people to enter. The structure of this robot enables it to move without the traditional wheels.

1.3 Evolution of wheeled mobile robots

Autonomous wheeled mobile robots (AWMRs) are in the process of extensive development. The nature and the structure of AWMRs should be judged upon their evolution.

One of the first serious wheeled mobile robots (Shakey, Fig. 1.1) was developed at Stanford Research Institute (SRI). This project was ambitious for its time (1966-1972), especially as there were no small computers and so Shakey had to be controlled by a fixed computer (a PDP-10 in the final version) over a radio link. However, it was able to solve very simple problems of perception, motion planning and control.

The project's goals were to develop techniques and concepts in Artificial Intelligence (AI) to enable a robot to function autonomously in a realistic environment. The main thrust of the research was in the area of planning actions, solving problems, recovering from mistakes and learning in the sense of storing and re-using plans. The main sensors were a TV camera (with motorized pan, tilt, focus and aperture control), mechanically tough sensors, driving wheel shaft encodes and a rangefinder. Although the project was not

directly concerned with computer vision, some computer vision software had to be provided and integrated with the rest of the system. This was some of the earliest work in operational machine vision. At this time, it was appreciated that machine vision was a fundamental problem for further research.

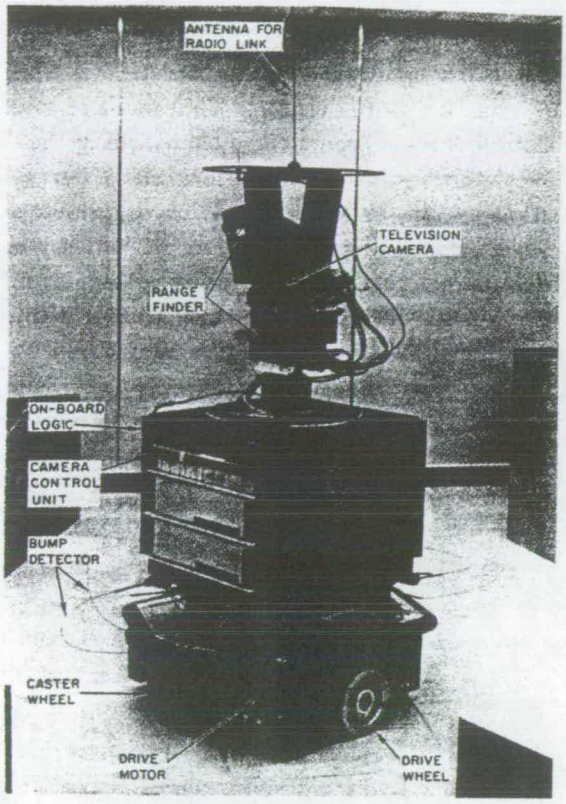

Fig. 1.1 Stanford Research Institute's Shakey

Shakey was driven by two large stepper motors. As well as the two driving wheels there were two load-bearing castors. The robot moved in an environment consisting of several rooms connected by doors and containing a few large irregular objects such as cubes and wedges. Because it moved in a highly irregular and jerky manner, it was given the name Shakey.

The robot's position in the world was determined by so-called "dead reckoning", i.e., by keeping track of the actual motion. However, actual motion was judged upon the information of wheel rotation, and error due to slippage caused the system to miscalculate

Shakey's position. Thus the vision system was unable to incorporate objects correctly into the grid model. Because of this, it was noted that effective reorientation techniques would be an important area for future study.

In the early 70's NASA, in cooperation with Jet Propulsion Laboratory (JPL), initiated a program oriented to reduce ground support requirements, provide real-time control, improve reliability and performance in support of space exploration, space assembly, automation of manufacturing facilities, and achieve the autonomous goal-directed coordination of location, manipulation, perception and cognition in a close-to-reality environment.

The basic hardware configuration used in the JPL robot consisted of a mobile vehicle equipped with a manipulator and some sensors (laser range-finder, stereo TV cameras, tactile sensors and proximity sensors). The navigation system was based on a gyrocompass and optical encoders on the wheels for dead-reckoning. The system of perception-motion coordination was based on the results of the hand-eye SRI project.

The robot was able to analyze a scene for evaluating traversability in a simplified environment, for example, a laboratory with a limited number of obstacles and proper illumination, and had to plan a path to the goal and follow that path. The model of the world used in this project was still a grid model.

From 1973 to 1981, work was done at the AI Laboratory, Stanford University by Hans Moravec on developing a remote controlled TV equipped mobile robot. This robot used stereo imaging to locate objects and to deduce its own motion.

This system underwent further development and modernization later at the Robotic Institute of Carnegie-Mellon University. The new Moravec's robot was cylindrical, about a meter tall and 30 cm in diameter. It had three individually steerable wheel assemblies which gave it a full three degrees of freedom of mobility.

At this time (1979), CNRS Research Center in France developed its own concept of a simplified wheeled mobile robot system named Hilare. The structure of this vehicle is

similar to that used in Shakey. The difference between them is that Hilare was equipped with a 3D vision system together with a video camera. Ultrasonic devices were utilized as proximity detectors for close-in obstacle detection and for following the wall. Infrared beacons were mounted in the corners of the room to give the absolute positioning information.

A relatively autonomous mobile robot system with an ultrasonic system and obstacle avoidance capabilities was developed by the Mechanical Engineering Laboratory of Ministry of International Trade and Industry (MITI) in Japan. This robot was designed to serve as a guide dog for blind people. The robot obeys spoken commands. Communication between man and the robot is over a flexible wire link. Control commands such as LEFT, RIGHT, STRAIGHT and STOP, are transmitted by control switches on the harness. Alarms from the robot to man signalling danger are transmitted over the link in the form of mild shocks to the blind person's hand. Ultrasonic transducers are used in a feedback system between man and the robot, so they can walk fast or slow, but a distance of one meter between the two is always maintained.

Robart-I was probably one of the first robots to be totally autonomous and exhibiting a high level of sophistication. It was built at the Naval Postgraduate School, USA, to serve as a feasibility demonstration for an autonomous robot. Robart was supposed to patrol a site in a random manner sensing fire, smoke, flooding, toxic gas, intrusion. etc., and take appropriate warning action if any of these conditions was found. This is a mobile warning system, whose motion is random wandering rather than goal oriented.

A motion routine is randomly chosen from a preprogrammed set of sixteen routines that filled in the gaps. Some of these routines would move the robot to a new vantage point, where it might elect to stop and re-enter the surveillance mode. Motion under these situations usually involved moving straight ahead, unless it saw an object, in which case it would swerve to one side or the other as appropriate.

Comparatively speaking, the early stage of the mobile robots focused more on the high-level intelligent control, computer vision, and navigation and little attention to low-level

problems such as the kinematics and motion feasibility was paid. The main contribution of this stage lies in the fact that they developed some techniques and concepts in AI and discovered some fundamental issues that must be solved before a commercial autonomous robot can be constructed. Among them, machine vision, path planning and representation of the world, and reasoning are some examples which became major fields of further research.

1.4 Types of wheeled mobile robots

A wheeled mobile robot is a wheeled vehicle which executes the commands from computers rather than from a driver. Therefore, from the viewpoint of structures, we don't distinguish clearly mobile robots from vehicles. For convenience, we use wheeled mobile robots to represent a wide class of devices which move on wheels. The research on wheeled mobile robots can contribute insights to the problems related to man-driven vehicles and the problems associated with intelligent and autonomous robots.

The development of mechanical structure for wheeled vehicles has a very long history. The forms of the vehicles can be classified according to the steering and powering of the vehicle.

1.4.1 Ordinary car-like robots

The most widely used type of wheeled mobile robots today is called the ordinary car-like robots, as shown in Fig. 1.2. From the viewpoint of steering and power, this type of robots includes 1) front wheel steering (four-wheel or three-wheel) and rear wheel differential powering, as shown in Fig. 1.2 (a) and (b); 2) front wheel steering and powering (especially for the three wheel car-like vehicle), as shown in Fig. 1.2 (c).

1.4.2 Dual drive robots

The basic dual-motor four-wheel robot design has been widely adopted for use on experimental mobile robots (Fig. 1.3 (a)). This design has also been popular with hobby and publicity robot designers. This popularity is due to its simplicity of construction and

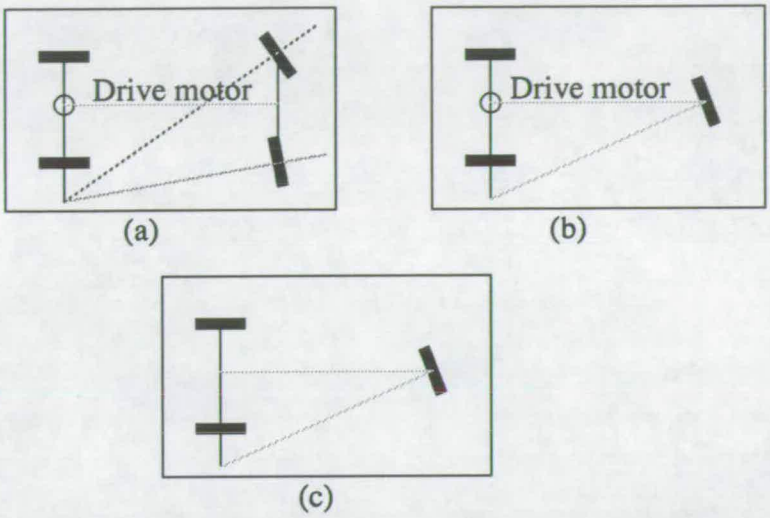

Fig. 1.2 (a) 4-wheel car-like vehicle with front wheel steering and rear wheel powering
(b) 3-wheel car-like vehicle with front wheel steering and rear wheel powering
(c) 3-wheel car-like vehicle with front wheel steering and powering

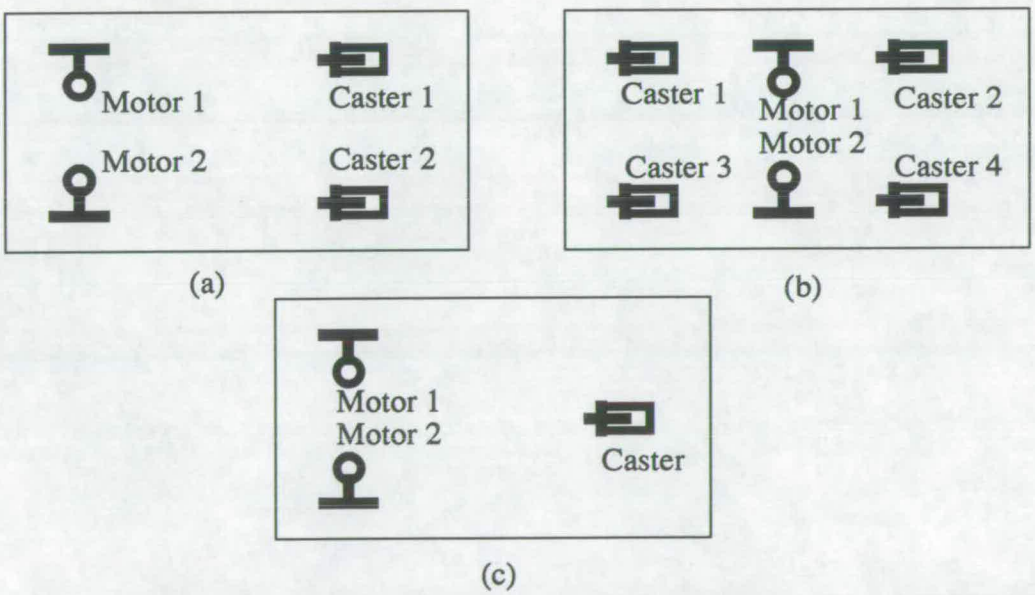

Fig. 1.3 Dual drive systems (a) two front casters (b) four casters (c) one caster

low cost. There are many variations on the fundamental configuration. Fig. 1.3 (b) and (c) show two variations. One is the dual-motor six-wheel design and the other is the dual-motor three-wheel design. Although these systems have different caster numbers, they use two independent drive motors to power and steer the robots. The driven wheels are fixed parallel to each other, while the other wheel or wheels are free to pivot. Steering is accomplished by causing one of the driven wheels to rotate faster than the other.

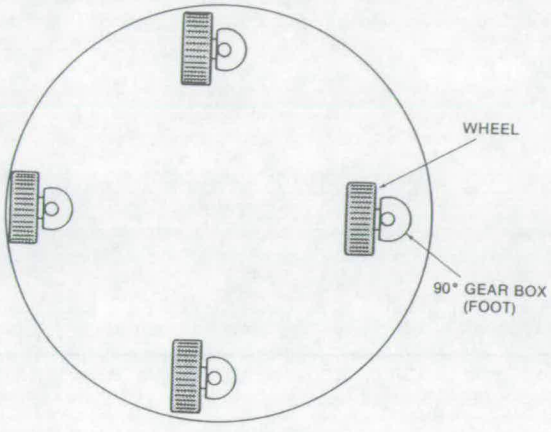

(A) Bottom view.

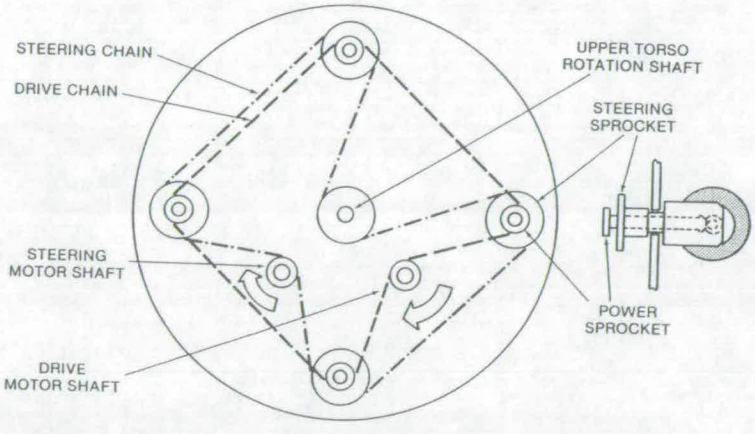

(B) Top view.

Fig. 1.4 Synchro drive and steering using chain coupling

Relatively, tight turns may be accomplished by powering one wheel in a forward direction and the other in a reverse direction. In this thesis, those with two independent drive motors are referred to as dual drive systems.

1.4.3 Synchro drive and steering robots

The synchro drive and steering system shown in Fig. 1.4 features three or more wheels (in

this case four) that are mechanically synchronized to each other for both steering and power [69]. Synchronization can be accomplished by the use of chains (as shown) or by gears. Each wheeled "foot" assembly contains a 90° mitre gear arrangement as shown in Fig. 1.5. The housing of the "foot" is driven by the steering chain, while the inner shaft is connected to the drive chain.

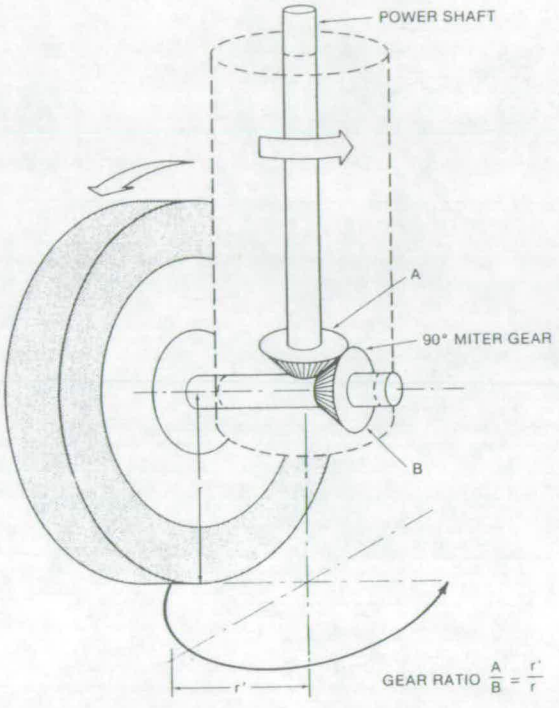

Fig. 1.5 Steering action of the synchro drive and steering foot assembly

In this thesis, we will prove that the system can offer some interesting characteristics, which can make the path planning problem for this kind of robots quite simple. When it is

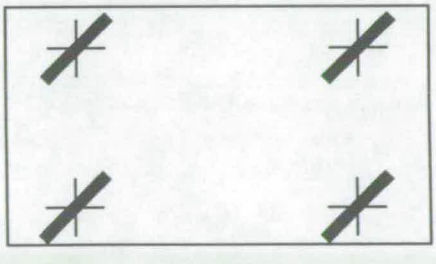

Fig. 1.6 Schematic for the synchro drive and steering (4-wheel)

driven along any path, since the wheels steer together, the base does not change its

rotational orientation. For this reason, it may play a very important role in the designing of an autonomous robot system. Fig. 1.6 shows the schematic for the synchro drive and steering system.

1.4.4 Omnidirectional robots

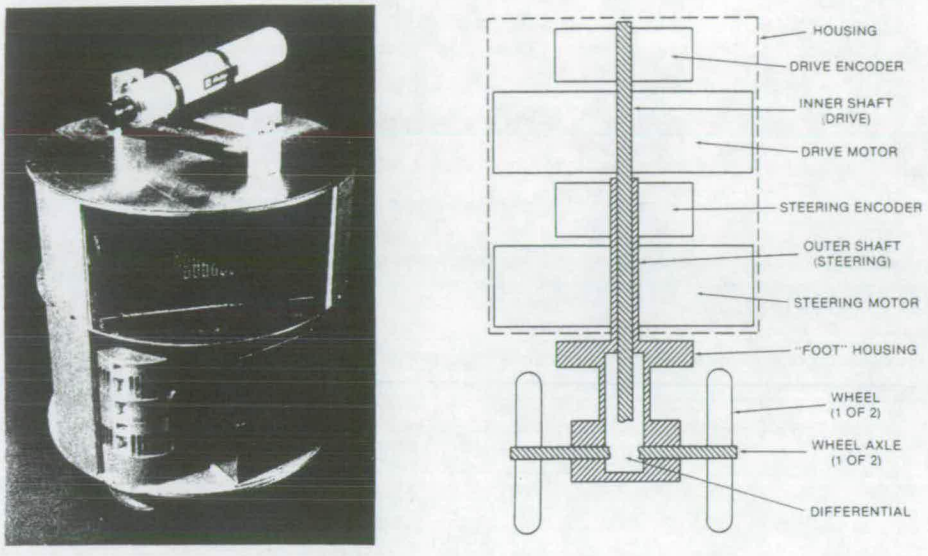

(a) (b)

Fig. 1.7 (a) CNU Rover (b) The CMU Rover wheel drive assembly (cross section)

Fig. 1.7 shows the structure of the CMU Rover constructed at Carnegie Mellon University by Dr. Hans Moravec [69]. The purpose of this design is to improve the flexibility of the robot. The feature of this robot is that each "foot" is totally independent for both steering and power. The "feet" also have a wheel on each side, powered through a differential. Each "foot" assembly contains an encoder for both steering and power, allowing the drive computer to precisely control it. For its degrees of freedom, its control is of course more complex than the other systems. An alternative structure which is also called omnidirectional robot HERMIES-III (Hostile Environment Robotic Machine Intelligence Experiment Series) has been developed by the researchers at Oak Ridge National Laboratory, USA [159]. The chassis has two steerable powered drive wheels A, B, and four corner caster wheels, as shown in Fig. 1.8. Four motors are used to separately steer and power the two wheels. The common feature of these two robots is that they can carry

out omnidirectional motion through independent steering and powering although their structures (the number of the motors used and the number of the casters) are different.

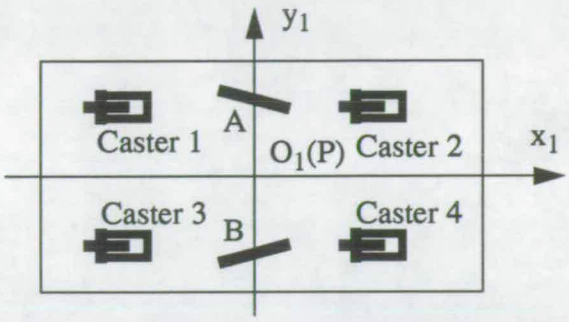

Fig. 1. 8 Structure of the omnidirectional HERMIES-III robot

1.5 Aims of the research

The aim of this thesis is to investigate the issues relating to creating an autonomous robot. A unified treatment of the four kinds of robots will be given. The problems investigated include:

1.5.1 Inverse and direct kinematics

Kinematics is the science of motion which treats motion without regard to the forces which cause it. Within the science of kinematics one studies the position, velocity, acceleration, and all higher order derivatives of the position variables (with respect to time or other variables). Kinematics forms the basis for a feasibility analysis of the mechanism, motion feasibility, dynamics and control, trajectory planning, and more complicated problems for an autonomous intelligent robot, such as path planning. As discussed above, there are several different types of mobile robot structure which result in different kinematic constraints. The aim of chapter 2 is to develop the inverse and the direct kinematics for each of the four kinds of wheeled robots.

1.5.2 Motion smoothness and feasibility

The location of a mobile robot moving on a plane can be uniquely described by three

parameters, i.e. the position (x_p, y_p) of a reference point P and the orientation angle θ of the robot. If we know the configuration (x_p, y_p, θ) of a robot and their time derivatives, then we can find the location of any other point (x, y) on the robot as well as their derivatives. There exists a nonholonomic kinematic constraint for a car-like robot and the dual drive robot, which restricts some motion of the robot. In addition to this, for a car-like robot, there is a steering angle limit, which also makes some motion infeasible. All of these make the analysis of motion feasibility challenging.

Generally speaking, robot motion should be as smooth as possible to reduce vibration, noise and wear effects. The degree of smoothness will depend on the degree of continuity of the reference path, therefore, smoothness is directly associated with the continuity of the curves. In order to reach a smooth and feasible motion, we will in chapter 3 investigate the factors which have effects on a smooth and feasible motion for the four kinds of robots. The conclusions drawn in this chapter will be used in the following chapters.

1.5.3 Applications of kinematics in geometric design for highway and street

A driver can manipulate a car or a long articulated lorry around a corner easily. This is because the geometric standards for highway and street have been adopted to design curbs at corners using design vehicles [232].

Sustained increases in truck weights and dimensions have occurred over the past decade in North America and other parts of the world [232]. The principal stimulus behind these changes is the reduction in unit transportation costs with increasing payload. The substantial increase in gross vehicle mass (GVM) and the length required to achieve these increases in productivity have important implications for the criteria used for the design of various components of highway infrastructure. Hutchinson [75] has discussed in detail the impacts caused by this trend, and pointed out that current standards used for the geometric design and capacity analysis of urban roads are based mainly on the properties of automobiles, with some allowance for truck characteristics. The models used were adequate when the weights, dimensions and performance characteristics of trucks were

not dramatically different from those of passenger car. A conclusion made by him is that the many design procedures used for infrastructure, including the design of intersection of urban streets, should be revised to incorporate this new change.

The low-speed cornering of large trucks on urban streets and intersections is a major problem in terms of public safety and traffic congestion. These problems can be alleviated in two manners: (1) modify the roadway dimensions to allow large vehicles to pass more easily; or (2) modify the size or maneuverability of the large trucks. Both of them depend on a correct low-speed kinematic model which can describe the transient motion of the truck when its reference point follows a prespecified path.

In chapter 4, the simulation results from the kinematics developed in chapters 2 and 3 will be compared with the stands available for the following purposes:

1. To verify the correctness of the model.

2. To illustrate that the model can offer a perfect solution to any dimension of vehicle and vehicle combination.

3. To understand that a kinematic model is essential for determining the swept volume of a vehicle ant therefore can not be ignored in the path planning problem for mobile robots.

1.5.5 Path planning

One of the ultimate goals in Robotics is to create autonomous robots. Such robots will accept high-level descriptions of the tasks and execute them without further human intervention. The input descriptions will specify what the user wants the robots to do rather than how to do it. Based on the input descriptions, the robots must be able to automatically plan the actions needed to reach the goals and then traverse the paths through its environment.

To achieve this, one central theme is path planning. The simplest path planning problem can be described as: Given a start position S and orientation of the wheeled robot, a goal

position G and orientation, and the positions of the obstacles, find a safe path from S to G which is collision-free and satisfies the goal orientation (the start orientation is naturally satisfactory).

It is important to recognize the difference between path planning problem and path generation problem. The former attempts to find a collision-free path among a set of obstacles while the latter is designed to find a path without taking the obstacles into consideration.

During the past two decades, various methods for dealing with the basic findpath problem and its various extensions have been developed. However, a fundamental problem of these researches is the ignorance of the kinematic characteristics of the different kinds of wheeled mobile robots.

In chapter 5, we first give a critical review of the path planning algorithms presently available for wheeled robots and then discuss their suitability for different kinds of wheeled robots.

In chapter 6, we first give a formal formulation for the findpath problem for the most widely used car-like robots and the dual drive robots based on the conclusions made from previous chapters, and then develop a robust, efficient, and reliable algorithm for a car-like robot, taking nonholonomic constraint and steering angle limit into account. This algorithm may also apply to a dual drive robot.

Finally, chapter 7 summarizes the main contributions made in this thesis and suggests avenues for future research.

Chapter 2

Inverse and direct kinematics for four kinds of wheeled mobile robots

2.1 Introduction

Before the development of kinematics for the four kinds of robots, it seems helpful to briefly introduce the concepts used in the analysis of a manipulator, reveal why these concepts are used, and then discuss the meaning of inverse and direct kinematics for wheeled robots. After a brief review of the related research on robot kinematics, we will establish the kinematics for each of the four kinds of robots and discuss the advantages of the model established in this chapter.

2.1.1 Inverse and direct kinematics for manipulators

A kinematic analysis of manipulators always distinguishes the direct kinematics from the inverse kinematics. The direct kinematics consists of computing the position and orientation of the end-effector of the manipulator given a set of joint angles, whereas the inverse kinematics involves finding all possible sets of the joint angles for a given position and orientation of the end-effector. Of these two, the direct kinematic analysis is simpler, with a straightforward solution for the unique position and orientation of the end-effector corresponding to the given set of joint angles. On the other hand, the feasibility of an inverse kinematic solution is quite dependent on the manipulator structure. For certain manipulator designs, the inverse kinematics can not be solved at all in analytic form. The questions of existence of a solution and of multiple solutions to the inverse kinematics, arise. The difficulty of the inverse kinematic solution has had practical effects on the trajectory planning and control of a manipulator.

The existence or nonexistence of an inverse kinematic solution defines the workspace of a given manipulator. The lack of a solution means that the manipulator cannot attain the

desired position and orientation because it lies outside of the manipulator's workspace.

2.1.2 Jacobian: Velocities, singularities and static forces

The direct and inverse problems of kinematics of a manipulator mainly deal with static positioning problem. One may wish to analyze manipulators in motion. In performing velocity analysis of a manipulator, a matrix quantity called the Jacobian of the manipulator is used. The Jacobian specifies a mapping from velocities in joint space to velocities in Cartesian space. The nature of this mapping changes as the configuration of the manipulator varies. At certain points, called Singularities, this mapping is not invertible. This results in joint rates approaching infinity as the singularity is approached. An understanding of the phenomenon is important to designers and users of manipulators.

The Jacobian matrix can also find application in dealing with the contact force between a manipulator and its contact surface. Manipulators do not always move through space; sometimes they are also required to contact a workpiece or work surface. In this case the problem arises: given a desired contact force and moment, what set of joint torques are required to generate them? Once again, the Jacobian matrix of the manipulator arises quite naturally in the solution of this problem.

2.1.3 Dynamics

There are two problems related to the dynamics of a manipulator that we wish to solve. The first problem is to find the required vector of joint torques given the joint's position, velocity, and acceleration. This formulation of dynamics is useful for the problem of controlling the manipulator. The second problem is to calculate how the mechanism will move under application of a set of joint torques. That is, given a torque vector, calculate the joint's position, velocity, and acceleration. This is useful for simulating the motion of a manipulator.

2.1.4 Inverse and direct kinematics for wheeled mobile robots

The description of position and orientation of a manipulator is always given in Cartesian

Space whereas the execution of the motion of a manipulator is realized by actuating the joints in Joint Space. Thus, the calculation of the transformation between Cartesian Space and Joint Space, including position, velocity and acceleration, is necessary. The establishment of the concepts of inverse and direct kinematics and jacobian is to make the calculation of the translation easier. Similarly, a relationship between location description and execution of a wheeled mobile robot must be established. For a wheeled mobile robot, it is useful to introduce the concept of the joint variables and the Cartesian variables. For the structure difference of the four kinds of robots, we generally define the joint variables as the powering and steering variables and the Cartesian variables as the position of the reference point, the orientation angle and their derivatives. Essentially, the inverse and direct kinematics describes the mapping between the description variables of the robot and the execution variables.

Note that the concept of inverse and direct kinematics we used here for a wheeled mobile robot involves not only relationships among the static position, orientation, and the steering angle of the robot and so on, but also their time derivatives. This is different from the case of a manipulator. In this thesis, the concept of Jacobian is not used, although other researchers have used it [108, 109, 131], because the working principles of a manipulator and a wheeled robot are totally different.

2.1.5 Related research on kinematics for wheeled mobile robots

It is well-known that the kinematics of a manipulator form the basis of its dynamics, control, trajectory planning, and path planning. At the beginning of research on manipulators, kinematics was developed and now it is widely accepted. Similarly, the kinematics of a wheeled mobile robot is of central importance for its dynamics, control, trajectory planning, and path planning. However, although research on wheeled robots has been conducted for twenty years, there does not exist an established kinematics for them. This can be observed from two facts. First, when a large drawbar truck turns left and the front right wheel's path is given as a circle, how to precisely determine the locus of other dangerous points on the truck is still an open issue in research for highway design [16, 57,

75]. Second, for lack of a complete description of the motion for a vehicle, the effects of kinematics on the trajectory generation, path planning and control problems have not been sufficiently investigated [210--215]. For example, for the purpose of control of a wheeled mobile robot such as a car-like robot, whether autonomous or not, the problem of determining the needed steering angle for tracking a specified path must be answered. However, a general solution to this problem has not been given. Following is a brief review of the study of kinematics carried out by researchers from different fields.

A driving hazard problem was proposed by Baylis [12] and revisited by Bender [14]. The problem can be described as follows: when making a right turn at a crossroad on British roadways, one moves to the right as far as possible on one's side of the roadway and then turns. Unfortunately, the rear of the vehicle swings leftward as the right turn is begun - toward the unsuspecting driver passing on the left (Fig. 2.1). This can be quite noticeable if the turning vehicle is a long bus. Hence, the problem - just how far to the left will the back corner of the bus (P in Fig. 2.1) swing towards the left as the bus driver negotiates the right turn - was proposed.

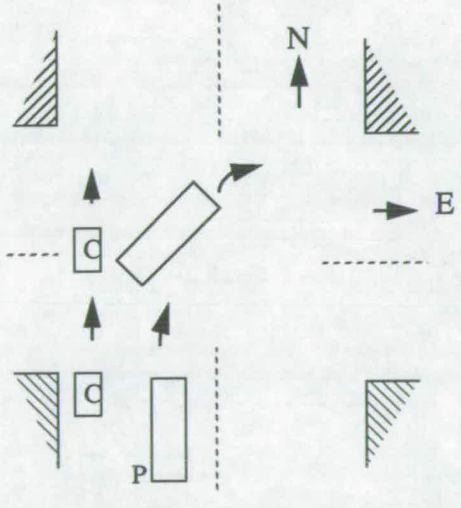

Fig. 2.1. A driving hazard problem

Another similar problem, studied by Freedman and Riemenschneider [58], is how to determine the path of the rear wheels of a bus while the front wheel of the bus tracks a given path. The solution to this problem is useful for highway design and for the

placement of curbs at intersections.

A third problem, which is related to the previous ones but a little more complicated, arises from the motion of a trailer-truck and was dealt with by Fossum and Lewis [55] and Alexander [3]. A comprehensive discussion of the maneuvering of vehicles such as buses or articulated trucks was carried out by Alexander and Maddocks [4, 5]. In their work, attention was focused on intrinsic properties of rigid-body trajectories, such as curvature and centers of rotation. They derived a relation between the radius of rotation of the body and the radii of curvatures of the trajectories of the wheels. Based on that relation, the problems of circular steering, offtracking, and optimal steering were considered.

In addition to the aforementioned researchers from the mathematical field, many others [60, 65-67, 84-86, 194] have focused their attentions on kinematics of mobile robots, and different methods have been developed. Muir and Newman [131, 132] formulated the kinematics for omnidirectional wheeled mobile robots. Their development parallels the development of kinematics for manipulator arms and draws heavily upon the concepts of manipulator kinematics. However, the kinematic modelling of wheeled robots differs from the modelling of manipulators because the wheels are always in contact with the ground. Their formulation does not grasp the essential requirement of a wheeled vehicle and makes the kinematic description more complicated. The kinematics developed by Alexander and Maddocks [5] has been adopted by Kyriakopoulos and Saridis [98]. However, the problem of this formulation is that the constraint equation is not given and orientation angle is assumed to be independent of the path.

The motion problems of wheeled vehicles have also attracted the interest of many researchers devoted to road design for vehicles, especially large vehicles [16, 64, 173, 189]. As stated in reference [64], the formula used in references [64, 235] may break down for long units on short-radius curve.

Obviously, establishment of kinematics for each of the four kinds of wheeled robots is of importance not only for robotics but also for highway design. In this chapter, a different method, called the constraint satisfaction, will be developed. Compared with the other

available models, it has the following advantages:

- The mathematical model is general in the sense that the reference point can be chosen at any point on the vehicle, not only on the mid-point of the rear axle (used by most of the researchers in robotics), on the front left wheel (defined in highway and street design standards), or on the vertex of the robot body (chosen by most path planning algorithms).

- The model can apply to any dimension of rigid vehicle or vehicle combination, not only to small vehicles, because it gives a transient description of the motion for a vehicle.

- The steering angle needed for a reference point to trace a specified path can be given, which is essential for automatically controlling a mobile robot by computers and useful for highway design to determine the minimum turning radius when the steering angle limit is taken into consideration.

- The model is applicable to any kinds of path, for example, a straight line, a circle, or a more general curve y=f(x).

- The analytic solutions to straight line motion and circular motion can be developed, which make the computation of the swept space by the vehicle more efficient and accurate.

- The model distinguishes the inverse kinematics from the direct kinematics.

2.2 Motion description of rigid robot body and ideal rolling condition for each wheel

In this section, we first develop the motion description of robot rigid body and then discuss the ideal rolling condition which each wheel mounted on the rigid body must satisfy.

2.2.1 Global and local reference coordinate frames

Fig. 2.2 is a plan view of a general robot model investigated. From the point of view of the

operating function, wheels used in the robot can be categorized into two types: rotatable wheels and fixed wheels. If a wheel can rotate about a vertical axle, it is defined as a rotatable wheel; otherwise, it is defined as a fixed wheel. Based on this definition, the front steered wheels of a car-like robot are rotatable wheels and its two rear wheels on the fixed axle are fixed wheels. However, when they are described by a mathematical model, a fixed wheel may be regarded as a special rotatable wheel. Therefore, in Fig. 2.2, all the wheels are given in the form of rotatable wheels. A global reference coordinate frame (Oxy) is introduced to describe the motion of the robot in terms of the position of the reference point (x_p,y_p) and the orientation angle θ of the robot. We define a local reference

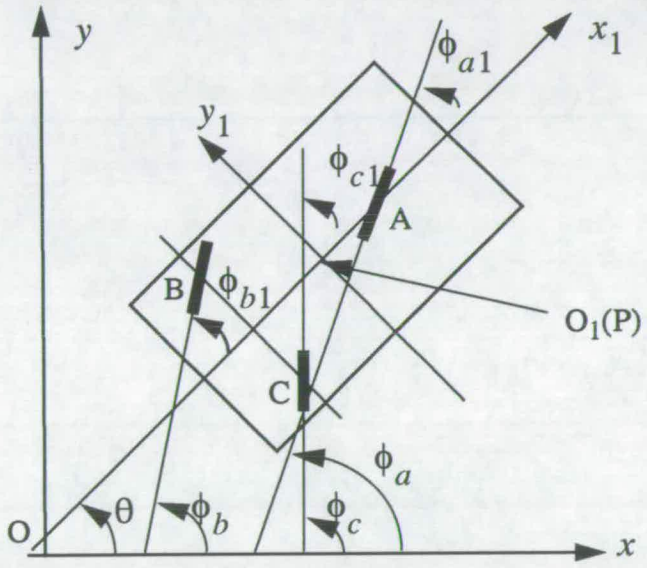

Fig. 2.2 Global (Oxy) and local ($O_1x_1y_1$) reference coordinate frames reference point P coincides with O_1

coordinate frame ($O_1x_1y_1$), whose origin is placed at the reference point P of the robot with y_1-axis parallel to the rear axle BC of the robot. We use M to represent any point in the rigid robot body when discussing the motion of the rigid robot body, and also use it to represent a wheel connected to the corresponding point when discussing steering angle. The coordinates of point M are denoted by M (x_m,y_m) in terms of the global reference frame and M (x_{m1},y_{m1}) in terms of the local reference frame. Therefore, the coordinates of

the central point of a wheel are constants with respect to the local reference frame.

2.2.2 Motion description of robot body

The coordinates of point M in the global frame are related to the coordinates of point M measured in the local frame by the transformation:

$$\begin{bmatrix} x_m \\ y_m \end{bmatrix} = \begin{bmatrix} x_{m1}\cos\theta - y_{m1}\sin\theta + x_p \\ x_{m1}\sin\theta + y_{m1}\cos\theta + y_p \end{bmatrix} \tag{2. 1}$$

In this thesis, when x and y are functions of time t, we use $\dot{x}$ and $\ddot{x}$ to denote $\frac{dx}{dt}$ and $\frac{d^2x}{dt^2}$ respectively. Differentiating (2.1) with respect to time, we have

$$\begin{bmatrix} \dot{x}_m \\ \dot{y}_m \end{bmatrix} = \begin{bmatrix} (-x_{m1}\sin\theta - y_{m1}\cos\theta)\,\dot{\theta} + \dot{x}_p \\ (x_{m1}\cos\theta - y_{m1}\sin\theta)\,\dot{\theta} + \dot{y}_p \end{bmatrix} \tag{2. 2}$$

where $\dot{x}_m$, $\dot{y}_m$ $\dot{x}_p$, and $\dot{y}_p$ are the absolute velocity components of point M and reference point P along the x and y-axes in terms of the global reference frame; and $\dot{\theta}$ is the absolute angular velocity of the robot body. Differentiating (2.2) again, we have the absolute acceleration expressions:

$$\begin{bmatrix} \ddot{x}_m \\ \ddot{y}_m \end{bmatrix} = \begin{bmatrix} (-x_{m1}\cos\theta + y_{m1}\sin\theta)\,\dot{\theta}^2 + (-x_{m1}\sin\theta - y_{m1}\cos\theta)\,\ddot{\theta} + \ddot{x}_p \\ (-x_{m1}\sin\theta - y_{m1}\cos\theta)\,\dot{\theta}^2 + (x_{m1}\cos\theta - y_{m1}\sin\theta)\,\ddot{\theta} + \ddot{y}_p \end{bmatrix} \tag{2. 3}$$

Eqs. (2.1)--(2.3) give the mathematical description of any point on the robot body in terms of the reference point position, velocity, acceleration, and the orientation angle, as well as their derivatives.

2.2.3 Ideal rolling condition and motion description of each wheel

The angle ϕ_m (m = a, b, and c) is defined as that between the vertical plane of the wheel M

and the positive x axis; and ϕ_{m1} is measured from the vertical plane of the wheel M to the positive x_1 axis (Fig. 2.2). It is noted that ϕ_m, θ, and ϕ_{m1} are all in the range from -180° to $+180^\circ$ and their relation can be written as

$$\phi_m = \phi_{m1} + \theta \tag{2.4}$$

For any type of wheeled robots, the general requirement for the mechanical design is that all the wheels connected to the rigid body should roll without any side-slip. When the whole robot is considered, the following ideal rolling conditions must be satisfied:

- The direction of every wheel rolling forward or backward, whether steered or not, must coincide with the tangent to the robot body trajectory through the corresponding wheel center.
- The velocity of every wheel center point must equal to the product of wheel rotating angular velocity about its own horizontal axle and its radius.

Mathematically, the foregoing conditions can be expressed as

$$tan(\phi_m) = \frac{d}{d(x_m)}(y_m) = \frac{\dot{y}_m}{\dot{x}_m} \tag{2.5}$$

and

$$v_m = r\omega_m \tag{2.6}$$

where ω_m (m = a, b, and c) represents the angular velocity of wheels A, B, and C respectively; v_m the velocity of the center point of wheels A, B, and C; and r the radius of every wheel. Here, v_m is equal to the vector sum of $\dot{x}_m$ and $\dot{y}_m$

$$(v_m)^2 = (\dot{x}_m)^2 + (\dot{y}_m)^2 \tag{2.7}$$

From (2.4) and (2.5) we can obtain ϕ_{m1}, the relative angle to the robot orientation line,

which is the steering angle for the steering wheel

$$\phi_{m1} = arc\tan\left(\frac{\dot{y}_m}{\dot{x}_m}\right) - \theta \tag{2.8}$$

2.3 Mathematical model for car-like robots

For a car-like robot, in order to make it move along a path, steering is necessary. Steering is normally affected by changing the heading of the front steering mechanism. In order to change its speed, the velocity from the motor must be adjusted. So two problems, one being the inverse of the other, are investigated. The first of these is to determine the location of the robot and its higher derivatives when the steering angle, its derivatives and the driven velocity from the motor are given. This is referred to as the direct or forward problem. The second problem, which is referred to as the inverse problem, is given a desired path of the reference point and its derivatives, to calculate the required steering angle, its derivatives, and the driven velocities. The inverse problem is clearly relevant to the control of the robot.

2.3.1 General constraint equation

As defined, when the wheels are fixed wheels, their relative angles to the robot orientation line are constants. For a car-like robot, the rear wheels B and C are fixed wheels. If we choose y_1 axis parallel to the rear axle BC, then $\phi_{b1} = \phi_{c1} = 0$. From (2.8), the following constraints are imposed:

$$\tan\theta = \frac{\dot{y}_b}{\dot{x}_b} \tag{2.9}$$

and

$$\tan\theta = \frac{\dot{y}_c}{\dot{x}_c} \tag{2.10}$$

Substituting (2.2) into (2.9) and (2.10) respectively and simplifying, we obtain

$$x_{b1}\dot{\theta} = \dot{x}_p \sin\theta - \dot{y}_p \cos\theta \tag{2.11}$$

$$x_{c1}\dot{\theta} = \dot{x}_p \sin\theta - \dot{y}_p \cos\theta \tag{2.12}$$

As defined above, y_1 axis is parallel to the robot's rear axle, so that $x_{b1} = x_{c1} = \underline{x}$. Eqs. (2.11) and (2.12) become the same one:

$$\underline{x}\dot{\theta} = \dot{x}_p \sin\theta - \dot{y}_p \cos\theta \tag{2.13}$$

Eq. (2.13) is what we need to solve for the robot's orientation angle θ when the reference point velocity components $\dot{x}_p$ and $\dot{y}_p$ are specified. Due to the fact that this equation describes the general relationship among the reference point's position relative to the rear axle, its velocity, and the robot's orientation angle as well as its first derivative when the reference point is chosen at any point on the robot, it is called the general constraint equation.

It can be noted that y_{b1} and y_{c1} are not included in (2.13), which illustrates the fact that only $\underline{x}$ has effects on a robot's orientation angle.

Eq. (2.13) indicates that

- If a robot has more than one fixed horizontal axle, two constraint equations are imposed. It is obvious that the two equations conflict with one another, then the robot cannot move properly. Therefore, ideally, in a rigid robot the number of the fixed horizontal axles cannot exceed one.

- When different fixed wheels in a robot have the same x-coordinates in terms of the local reference frame, that means they are mounted on the same fixed horizontal axle, and only one constraint is imposed.

Differentiating (2.13), we can obtain the expression of rotational angular acceleration of

the robot

$$\underline{x}\ddot{\theta} = \ddot{x}_p \sin\theta - \ddot{y}_p \cos\theta + (\dot{x}_p \cos\theta + \dot{y}_p \sin\theta)\,\dot{\theta} \tag{2. 14}$$

2.3.2 Mechanical design for front wheels

Steering angle limit, an inherent characteristic of a car-like robot, results from the mechanical design of the steering mechanism. We will here introduce the concept of the Jeantaud condition which is used to guide the mechanical design of the front steering wheels so that the front steering wheels satisfy the ideal rolling condition, and meanwhile, add only one constraint to the motion of a vehicle. Fig. 2.3 shows a vehicle cornering without any side-slip of the wheels. At low speeds, there is a simple relation between the position of the steering linkage and the steering wheel angle, and the turning behavior

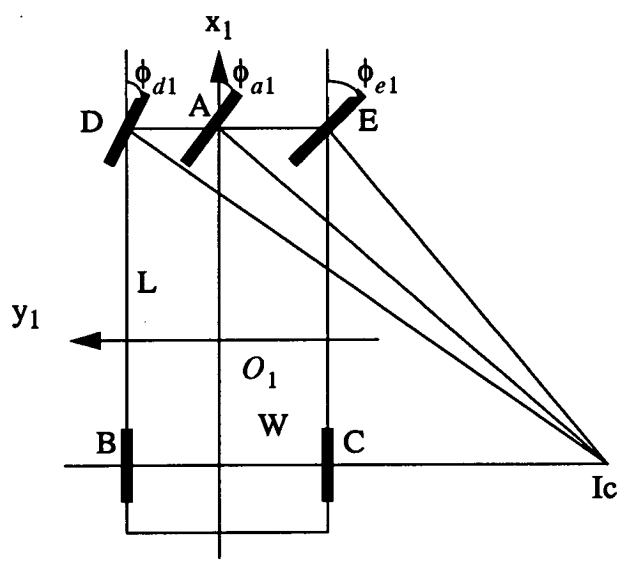

Fig. 2.3 Vehicle cornering with unique center of rotation

mainly depends on the geometry of the steering linkage. The prime consideration in the design of the steering system geometry is to satisfy this relation for minimum tire scrub during cornering. This requires that during the turn all tires should be in pure rolling without lateral sliding. Let us assume for simplicity that the planes of all four wheels, two front wheels (D, E) and two rear wheels (B, C), are vertical. Then the condition to be satisfied is this: the perpendicular to the planes of the front wheels, drawn through their

centers, must meet at a projected point on the back axle. This establishes the proper relationship between the steering angle of the inside front wheel ϕ_{e1} and that of the outside front wheel ϕ_{d1}. When the local right hand coordinate frame $O_1x_1y_1$ is introduced, as shown in Fig. 2.3, it is evident that ϕ_{d1} and ϕ_{e1} are negative angles. Therefore, in Fig. 2.3, it can be seen readily that ϕ_{e1} and ϕ_{d1} should satisfy the following relationship:

$$\cot\phi_{d1} - \cot\phi_{e1} = -\frac{W}{L} \tag{2. 15}$$

where W is the track and L is the wheelbase of the vehicle, respectively. Eq. (2.15) is usually referred to as the Jeantaud condition, which must be fulfilled in the mechanical design if tire wear is to be kept to a minimum [219].

A mechanism that might be used in the steering of a four-wheeled vehicle with theoretically perfect satisfaction of the Jeantaud condition has been designed using suitably shaped oval wheels (or cams), which engage without slipping [200]. In practice, the Ackermann layout [68] has sufficient approximation to the Jeantaud condition and is widely used, although it does not completely achieve the Jeantaud condition and is only accurate in three positions; straight-ahead, and one position in each lock. Since pneumatic tires are used, any slight inaccuracy can be overcome by the deflection of the tires.

It is obvious that the steering angle of the inside front wheel, ϕ_{e1}, is greater than that of the outside front wheel, ϕ_{d1}, when a vehicle turns. In our study of the motion of the car-like four-wheel vehicle, to gain simplicity without losing generality, we introduce a virtual steering angle ϕ_{a1} when we discuss the steering angle needed to follow a prespecified path, where ϕ_{a1} is the angle between the path of the midpoint of the two front wheels and the center line of the vehicle (Fig. 2.3).

2.3.3 Satisfaction of the Jeantaud condition

In the following, we prove that the kinematical model established in the foregoing satisfies

Jeantaud condition (2.15). Suppose that the coordinates of the outside front wheel D, the inside front wheel E, and the two rear wheels B and C are denoted by $D(x_{d1}, y_{d1})$, $E(x_{e1}, y_{e1})$, $B(x_{b1}, y_{b1})$, and $C(x_{c1}, y_{c1})$, respectively in terms of the local reference frame. Then we have the following equations (see Fig. 2.3):

$$\begin{bmatrix} x_{b1} \\ y_{b1} \end{bmatrix} = \begin{bmatrix} x_{c1} \\ y_{d1} \end{bmatrix} \tag{2.16}$$

$$\begin{bmatrix} x_{e1} \\ y_{e1} \end{bmatrix} = \begin{bmatrix} x_{d1} \\ y_{c1} \end{bmatrix} \tag{2.17}$$

$$\begin{bmatrix} x_{d1} - x_{b1} \\ y_{b1} - y_{c1} \end{bmatrix} = \begin{bmatrix} x_{e1} - x_{c1} \\ y_{d1} - y_{e1} \end{bmatrix} = \begin{bmatrix} L \\ W \end{bmatrix} \tag{2.18}$$

From (2.8), we obtain the following relationship:

$$\cot(\phi_{m1}) = \frac{\dot{x}_m + \dot{y}_m \tan\theta}{\dot{y}_m - \dot{x}_m \tan\theta} \tag{2.19}$$

Substituting (2.2) into (2.19) gives

$$\cot(\phi_{m1}) = \frac{-y_{m1}\dot{\theta} + \dot{x}_p \cos\theta + \dot{y}_p \sin\theta}{x_{m1}\dot{\theta} + \dot{y}_p \cos\theta - \dot{x}_p \sin\theta} \tag{2.20}$$

When choosing M to be D and E, respectively, and taking (2.13), (2.16)--(2.18) into account, we have

$$\cot(\phi_{d1}) - \cot(\phi_{e1}) = \frac{\dot{\theta}(y_{e1} - y_{d1})}{\dot{\theta}(x_{d1} - x_{b1})} = -\frac{W}{L} \tag{2.21}$$

Eq. (2.21) illustrates that our mathematical model satisfies the Jeantaud condition, and

therefore its correctness is verified.

2.3.4 Procedure for solving inverse kinematics

The inverse kinematics means that given the position of a reference point on the robot and its first and second derivatives, find the needed steering angle, the driving velocity, and the acceleration of the middle point of the rear axle (this is due to the fact that a rear differential driving system is used for car-like robot). It can be seen that to solve the inverse kinematic problem, the key problem is to solve the general constraint equation (2.13). Once θ and $\dot{\theta}$ are known, the position and absolute velocity of any point can be determined by (2.1) and (2.2) and the steering angle can be solved from (2.8). The simulation result and analysis in more detail will be given in chapter 3.

2.3.5 Curvature, radius of instantaneous rotation, and their relationship

The expressions for the curvature and the radius of instantaneous rotation of any point in the robot will be given in this subsection by using the basic kinematic description developed previously with respect to the position of the reference point, the robot orientation angle, and their derivatives. Some conclusions will also be made.

As $\frac{dy}{dx} = \frac{dy}{dt} / \frac{dx}{dt} = \frac{\dot{y}}{\dot{x}}$, while $\frac{d^2y}{dx^2} = \frac{d}{dx}(\frac{\dot{y}}{\dot{x}}) = \frac{d}{dt}(\frac{\dot{y}}{\dot{x}}) \cdot \frac{dt}{dx} = \frac{\dot{x}\ddot{y} - \ddot{x}\dot{y}}{\dot{x}^3}$. Therefore, for any point M in the robot, the curvature κ_m can be expressed by the following formula:

$$\kappa_m = \frac{\frac{d^2y_m}{d(x_m)^2}}{\left(1 + \left(\frac{dy_m}{dx_m}\right)^2\right)^{3/2}} = \frac{\dot{x}_m\ddot{y}_m - \dot{y}_m\ddot{x}_m}{((\dot{x}_m)^2 + (\dot{y}_m)^2)^{3/2}} \qquad (2.22)$$

Let R_m be the radius of instantaneous rotation of point M in the robot. Then R_m is defined

as the ratio of v_m to $\dot{\theta}$

$$R_m = \frac{v_m}{\dot{\theta}} = \frac{((\dot{x}_m)^2 + (\dot{y}_m)^2)^{1/2}}{\dot{\theta}} \tag{2.23}$$

Taking (2.8) into consideration, we obtain the relationship between κ_m and R_m

$$R_m \cdot \kappa_m = \frac{((\dot{x}_m)^2 + (\dot{y}_m)^2)^{1/2}}{\dot{\theta}} \cdot \frac{\dot{x}_m \ddot{y}_m - \dot{y}_m \ddot{x}_m}{((\dot{x}_m)^2 + (\dot{y}_m)^2)^{3/2}} = 1 + \frac{\dot{\phi}_{m1}}{\dot{\theta}} \tag{2.24}$$

Eq. (2.24) reaches the same result as proposition 2 obtained by Alexander and Maddocks [4], which results in the following conclusion:

- If a point lies in the fixed axle, then $\dot{\phi}_{m1} = 0$, and the center of instantaneous rotation of a point in the robot and its center of curvature do coincide, otherwise, these two points do not necessarily coincide.

This proposition is useful for avoiding the common misunderstanding that the center of instantaneous rotation of any point in the robot and its center of curvature always coincide.

2.3.6 Direct kinematics for car-like robots

Given a steering angle ϕ_{a1} and a velocity $\upsilon(t)$ of the middle point Z of the rear axle as well as their derivatives, the direct kinematics consists of computing the position of the reference point P and the orientation angle of the robot, as well as their first and second derivatives. Although we can derive the direct kinematics from the inverse kinematics, it is more straightforward to use a geometrical method. As shown in Fig. 2.4, the velocity υ can be decomposed into the velocity components along the x and y axes. We have

$$\dot{x}_z = \upsilon \cos\theta \tag{2.25}$$

$$\dot{y}_z = \upsilon \sin\theta \tag{2.26}$$

The rotational speed of the robot can be expressed as follows:

$$\dot{\theta} = \frac{\upsilon(t)\tan(\phi_{a1}(t))}{L} \tag{2.27}$$

We can integrate and differentiate these equations, respectively, to obtain

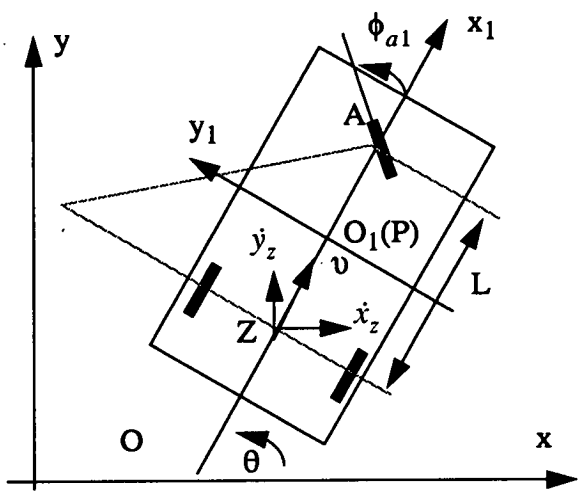

Fig. 2. 4 Geometry for direct kinematics

$$\theta(t) = \theta(0) + \int_0^t \{\frac{\upsilon(t)\tan(\phi_{a1}(t))}{L}\}\, dt \tag{2.28}$$

$$x_z(t) = x_z(0) + \int_0^t \{\upsilon(t)\cos(\theta(t))\}\, dt \tag{2.29}$$

$$y_z(t) = y_z(0) + \int_0^t \{\upsilon(t)\sin(\theta(t))\}\, dt \tag{2.30}$$

$$\ddot{\theta}(t) = \frac{\upsilon(t)}{L}(\sec(\phi_{a1}))^2 \cdot \dot{\phi}_{a1} + \frac{\dot{\upsilon}(t)}{L}\tan(\phi_{a1}(t)) \tag{2.31}$$

$$\ddot{x}_z(t) = \dot{\upsilon}(t)\cos(\theta) - \upsilon(t)\sin(\theta)\,\dot{\theta} \tag{2.32}$$

$$\ddot{y}_z(t) = \dot{\upsilon}(t)\sin(\theta) + \upsilon(t)\cos(\theta)\,\dot{\theta} \tag{2.33}$$

After solving (2.28) to (2.33), we can obtain the position of the reference point P and its

first and second derivatives using (2.1)--(2.3).

2.3.7 Mathematical model for combined vehicles

In the previous sections, a mathematical model for dealing with the motion of a rigid vehicle has been developed. Before studying the motion of a combined vehicle, it is useful to distinguish a vehicle unit from a combined vehicle. A vehicle unit is composed of: (1) a rigid body; (2) a fixed axle on which some wheels are mounted; and (3) some steering wheels or a hitch point. In this sense, a rigid vehicle is a single-unit vehicle with two front steering wheels like that shown in Fig. 2.3, while a combined vehicle, such as an articulated vehicle or a drawbar vehicle, can be regarded as a combination of two or more vehicle units linked in series at their hitch points (Fig. 2.5).

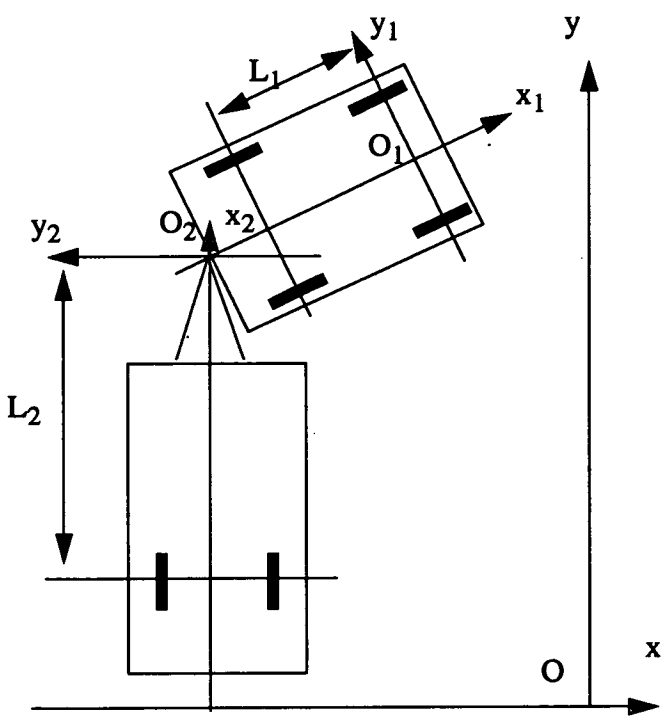

Fig. 2.5 A schematic for an articulated vehicle

It is worthy of note that from a motion analysis standpoint, multiple axles of an axle group operating together within a single suspension system which is simplified as a rigid body, are treated as though they were a single axle located at the geometric center of the group

[64].

Fig. 2.5 shows a combined vehicle model. The first vehicle unit is one with two steering wheels, while the second has a hitch point instead of two steering wheels. Two local reference coordinate frames ($O_1x_1y_1$) and ($O_2x_2y_2$) are put on the two vehicle units, respectively. For convenience, the origin of the second frame coincides with the hitch point. We know that for the first vehicle unit, if the position and velocity of the reference point $O_1(P_1)$ are given, then the orientation angle of vehicle unit 1 can be obtained by solving the general constraint differential equation (2.13), and then the position and velocity of the hitch point $O_2(P_2)$ which is a point in the vehicle unit 1 can be calculated using (2.1) and (2.2). This means that the position and velocity of the second vehicle unit's reference point O_2 have been obtained. Consequently, by means of the identical procedure used in the calculations for vehicle unit one, the position and velocity and other interesting parameters of all the points in the second vehicle unit can be calculated. If more than two vehicle units are serially linked, the procedure for dealing with the motion problem of the complicated vehicle is analogous to the above one. In every step, a numerical method must be used to solve a simple first-order differential equation (2.13).

2.4 Mathematical model for dual drive robots

2.4.1 Inverse kinematics for dual drive robots

The steering and powering of the dual drive robot is accomplished by changing the velocity of two rear wheels B and C. Therefore, the purpose of the inverse kinematics is to solve the needed velocities υ_b and υ_c when $\dot{x}_p$ and $\dot{y}_p$ are given. Since the dual drive robot

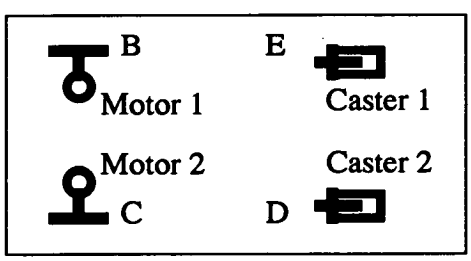

Fig. 2.6 Dual drive system with two front casters

still has two fixed wheels B and C which are parallel, as shown in Fig. 2.6, there is no need to repeat the derivation for the general constraint equation and other equations describing the motion of the rigid body. In deriving the inverse kinematics of the car-like robot, we have in fact established the inverse kinematics for the dual drive robot. That is, (2.13), (2.14) and (2.2) can also be used to solve for the orientation angle, angular rate of rotation, and the driving velocities υ_b and υ_c. The only difference in analyzing the inverse kinematics from a car-like robot is that we do not need to consider the steering angle limit.

2.4.2 Direct kinematics for dual drive robots

Suppose the velocities υ_b and υ_c are given, then we have (see Fig. 2.7)

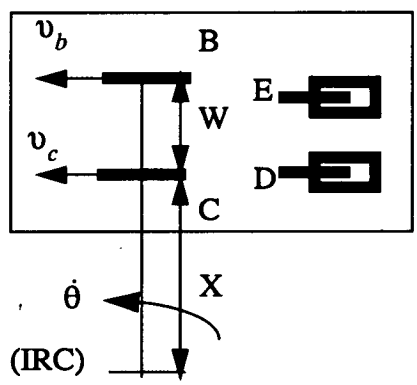

Fig. 2.7 Illustration of instantaneous rotation center (IRC)

$$\upsilon_b = (W+X)\,\dot{\theta} \tag{2.34}$$

$$\upsilon_c = X\dot{\theta} \tag{2.35}$$

where X is the distance from wheel C to the centre of instantaneous rotation; W is the wheelbase. From (2.34) and (2.35), we get

$$\dot{\theta} = (\upsilon_b - \upsilon_c)/W \tag{2.36}$$

Thus, the orientation angle can be obtained by integrating the above equation.

$$\theta = \theta_0 + \int_0^t ((\upsilon_b - \upsilon_c)/W)\,dt \tag{2.37}$$

The position of wheel B is

$$x_b = x_b(0) + \int_0^t (v_b \cdot \cos\theta)\, dt \tag{2.38}$$

$$y_b = y_b(0) + \int_0^t (v_b \cdot \sin\theta)\, dt \tag{2.39}$$

Eqs. (2.1) to (2.3) also apply to solve the position of the reference point and its derivatives.

2.4.3 Motion of casters

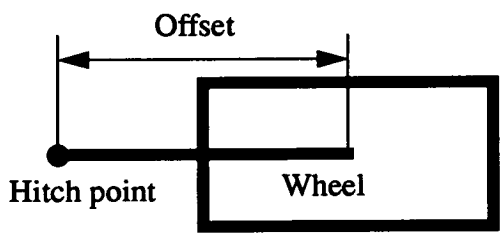

Fig. 2.8 Top view of a caster

The function of casters is to support a robot. They add no constraints to the whole robot, and their motion always follows the robot body. Each caster can be regarded as a small robot unit which has a fixed wheel, as shown in Fig. 2.8. Once the motion of the robot body is solved (it may be solved by either inverse kinematics or direct kinematics in different circumstance), then the motion of the hitch point (through which point, the caster is connected to the rigid body) can be obtained. If we treat a caster as a robot unit like that discussed in the previous section, the motion of the caster can be solved using the inverse kinematics.

2.5 Mathematical model for synchro drive and steering robots

2.5.1 Inverse kinematics

As stated in chapter 1, the wheels of the synchro drive and steering system are mechanically synchronized to each other for both steering and power. Figure 2.9 illustrates the functional diagram of its steering and power. As the synchronization is

accomplished by the use of chains or by gears, the mechanism requires that each wheel of A, B, C and D must have the identical steering angle and the identical velocity at any moment. Therefore, mathematically, the constraint imposed by the synchro steering is

$$\phi_{a1} = \phi_{b1} = \phi_{c1} = \phi_{d1} = \phi(t) \tag{2.40}$$

and the constraint imposed by the synchro power is

$$\dot{x}_a = \dot{x}_b = \dot{x}_c = \dot{x}_d \tag{2.41}$$

$$\dot{y}_a = \dot{y}_b = \dot{y}_c = \dot{y}_d \tag{2.42}$$

For all wheeled robots, the wheels on the rigid body should satisfy the ideal rolling

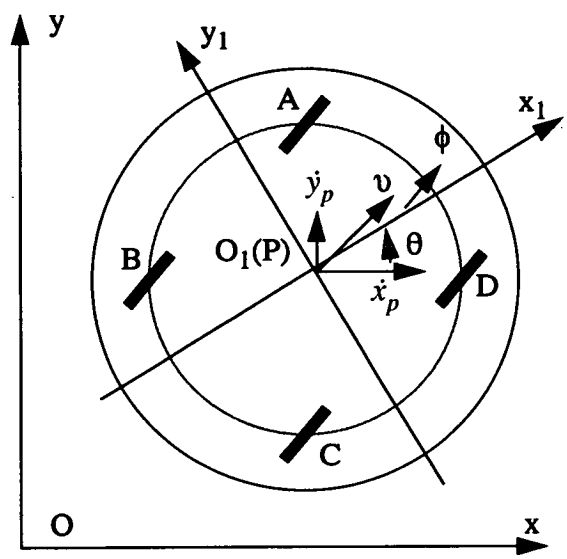

Fig. 2.9 Functional schematic for the synchro drive carriage system

conditions described by (2.5) and (2.6). In addition, (2.1) to (2.3) that describe the motion of the rigid body and (2.8) describing the steering angle, also apply to the synchro drive and steering system. Thus, from (2.2), (2.8), and (2.40), we have

$$\tan(\theta+\phi) = \frac{(x_{m1}\cos\theta - y_{m1}\sin\theta)\,\dot{\theta} + \dot{y}_p}{(-x_{m1}\sin\theta - y_{m1}\cos\theta)\,\dot{\theta} + \dot{x}_p}, m = a, b, c, d \tag{2.43}$$

The only solution to the foregoing set of equations is

$$\dot{\theta} = 0 \Rightarrow \theta = \theta_0 \tag{2.44}$$

This is the general constraint equation for a synchro drive and steering robot. It is clear that the motion of the rigid body for this kind of robot is always a translation.

The general constraint equation (2.44) generated from the synchro steering requirement must also satisfy (2.41) and (2.42) resulting from the synchro drive requirement. It is straightforward to verify that this is true. This indicates that the design of the synchro drive and steering system is valid. Eqs. (2.41) and (2.42) become

$$\begin{bmatrix} \dot{x}_m \\ \dot{y}_m \end{bmatrix} = \begin{bmatrix} \dot{x}_p \\ \dot{y}_p \end{bmatrix}, m = a, b, c, d \tag{2.45}$$

The expressions for the steering angle and the rotating angular rate of all the wheels are

$$\phi = arc\tan(\dot{y}_p/\dot{x}_p) - \theta_0 = arc\tan(f'(x_p)) - \theta_0 \tag{2.46}$$

$$\omega = (\sqrt{\dot{x}_p^2 + \dot{y}_p^2})/r \tag{2.47}$$

2.5.2 Direct kinematics

In the following we give the direct kinematics using the geometrical method (see Fig. 2.9). Suppose $\phi(t)$ and $\upsilon(t)$ are given, then

$$\dot{x}_p = \upsilon(t)\cos(\phi + \theta) \tag{2.48}$$

$$\dot{y}_p = \upsilon(t)\sin(\phi + \theta) \tag{2.49}$$

$$\theta = \theta_0 \tag{2.50}$$

$$x_p = x_p(0) + \int_0^t \{\upsilon(t)\cos(\phi + \theta)\}\, dt \tag{2.51}$$

$$y_p = y_p(0) + \int_0^t \{ \upsilon(t) \sin(\phi + \theta) \} dt \tag{2.52}$$

$$\ddot{x}_p = \dot{\upsilon}(t) \cos(\phi + \theta) - \upsilon(t) \sin(\phi + \theta) \dot{\phi} \tag{2.53}$$

$$\ddot{y}_p = \dot{\upsilon}(t) \sin(\phi + \theta) + \upsilon(t) \cos(\phi + \theta) \dot{\phi} \tag{2.54}$$

where $\upsilon(t)$ represents the translation velocity of the rigid body; ϕ the steering angle; P is the reference point which may be chosen at any point.

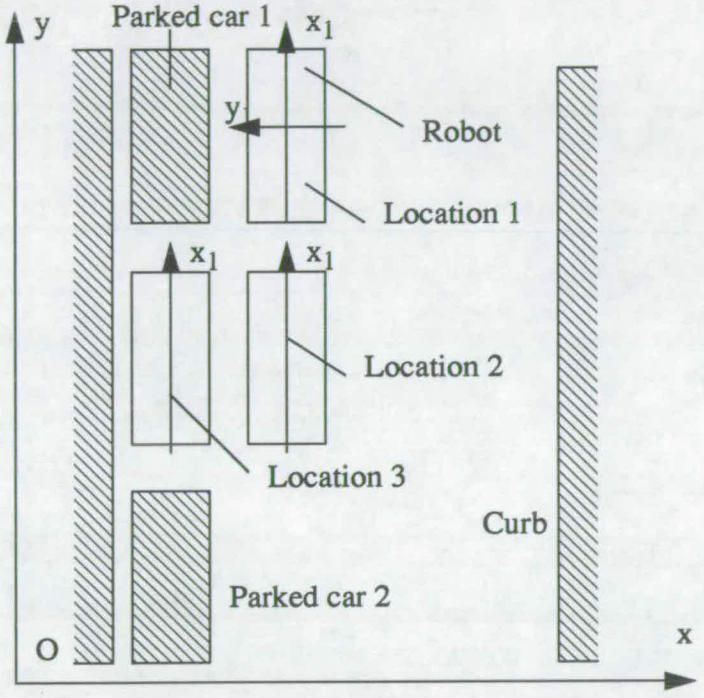

Fig. 2.10 Illustration of a parallel parking for four kinds of robots

2.6 Mathematical model for omnidirectional robots

2.6.1 Implication of omnidirectional robots

Before developing the kinematics of an omnidirectional robot for HERMIES-III, we will discuss the meaning of omnidirectional. In the past, although a few researchers used this term, in fact nobody clarified its meaning using the expressions of the reference path and the orientation angle. For example, the synchro drive and steering robot was thought to be

an omnidirectional robot [137], although it is not correct to think of the synchro-drive and steering robot as an omnidirectional one. We begin by considering the motivation for designing such a mobile robot with steerable wheels.

Generally speaking, the motivation to design an omnidirectional robot is to provide it with more flexible maneuverability than the conventional robots like the car-like or dual drive types. Maneuverability is still a portmanteau, meaning different things in different circumstances. In the present context, the two most important aspects of maneuverability are:

- The ability to turn sharply, and
- The ability to keep within a narrow path when turning.

The most familiar example of the maneuvering required by a robot is a parallel parking, as shown in Fig. 2.10. The goal is to move the robot into a space (location 3) between two parked cars 1 and 2 (they may be two other obstacles). It is straightforward to prove using the general constraint equation (2.13) that for the robots subject to the constraint equation (2.13), it is impossible to move the robot directly from location 2 into location 3 without changing the orientation. For a car-like robot, the strategy adopted for such a parallel parking is to move the robot to location 2, stop, and then the following manipulations are performed: turning the steering wheels to the left limit, backing, straightening the wheels, backing, turning the wheels to the other limit, backing, and straightening the wheels (several iterations may be required by an unskilled driver). The optimum path is arc-line-arc. Of course, this path can also be traced by the dual driving robot although the needed operations are different. However, if the location 1 is occupied by obstacles, it is difficult for them to maneuver into location 3 in this way.

If the robot is synchro drive and steering, such a requirement of maneuvering from location 2 to 3 can be met. This example illustrates the advantage of a synchro drive and steering robot over a car-like or a dual drive robot. In another example of turning a corner shown in Fig.11, however, the car-like robot and the dual drive robot may succeed in

moving from location 1 to 2 while the synchro drive one can not. These two examples of required maneuvering, which may occur very often in practice, indicate that all of these three kinds of robots posses their own limitations. The common feature of the three kinds of robots is that among the three parameters of x_p, y_p and θ describing the location of a robot one is dependent on the other two by the form of constraint equation (2.13), or the orientation angle is restricted by (2.44). As a result, some kinds of maneuvering for them are restricted.

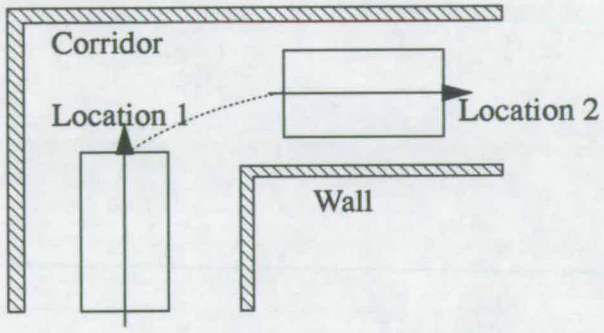

Fig. 2.11 A robot turning around a corner

The purpose of designing an omnidirectional robot is to overcome these limitations. Therefore, an omnidirectional robot should be able to execute any desired path $y_p = f(x_p)$ and have any desired orientation angle θ along the path. In other words, the three parameters x_p, y_p and θ should be independent of each other. This kind of robot is called an omnidirectional robot or a free moving robot.

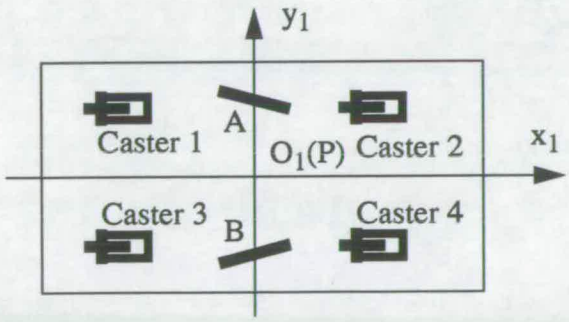

Fig. 2.12 Structure of the omnidirectional HERMIES-III robot

A platform with steerable drive wheels can use the steering degrees of freedom to reduce

the maneuvering difficulty. HERMIES-III, which was reported to have two drive steerable wheels A and B (see Fig. 2.12), functions as such a platform [159]. The original wheel control system for the HERMIES-III did not allow the drive wheels to be steered. An improved system that allows the wheels to be steered has been designed, constructed, and tested. The experimental results show that rotation about an instantaneous Center of rotation (ICR) can result in a substantial error, and the error can not be eliminated. In the following we will explain the difficulty of eliminating the error from the viewpoint of structure.

Generally, the first consideration associated with the control system design is how many wheels should be driven and steered. For any mechanism, the number of degrees of freedom it possesses is the number of independent variables which would have to be specified in order to locate all parts of the mechanism. An omnidirectional wheeled robot has only three degrees of freedom due to the independence of its three parameters when moving in a plane, therefore, the total number of drive and steering for wheels should be equal to three, the number of degrees of freedom of the robot. The number of the control variables for the HERMIES-III, however, is four (two for drive and two for steering). In this sense, HERMIES-III is an overactuated system which has more actuators for drive and steering than the degrees of freedom of the robot. The shortcoming of such an overactuated system is that it is difficult to accurately coordinate the four variables for a desired motion. Each of the four is described by x_p, y_p and θ, and thus, one of the four variables must depend on the other three. In practice, it is more reasonable to have the system with wheels A and B steered and one of them, instead of two, driven.

2.6.2 Inverse kinematics

The meaning of the inverse kinematics for an omnidirectional wheeled robot is different from that of the other three kinds of robots. The difference is that the orientation angle of the robot as well as the reference point's position and their derivatives must be given to calculate the needed steering angle ϕ_{m1} and drive angular rate ω_m. In this case, there is no

general constraint equation. Eqs. (2.1) to (2.8) can also be used for this purpose.

2.6.3 Direct kinematics

In deriving the direct kinematics for an omnidirectional robot like HERMIES-III, we assume that both of wheels A and B are steered and only wheel A is driven. As shown in Fig. 2.13, if the steering angles ϕ_{a1} and ϕ_{b1} are given, then the position of the ICR is uniquely determined. The velocity of wheel B is a function of ϕ_{a1}, ϕ_{b1}, and $\upsilon_a(t)$.

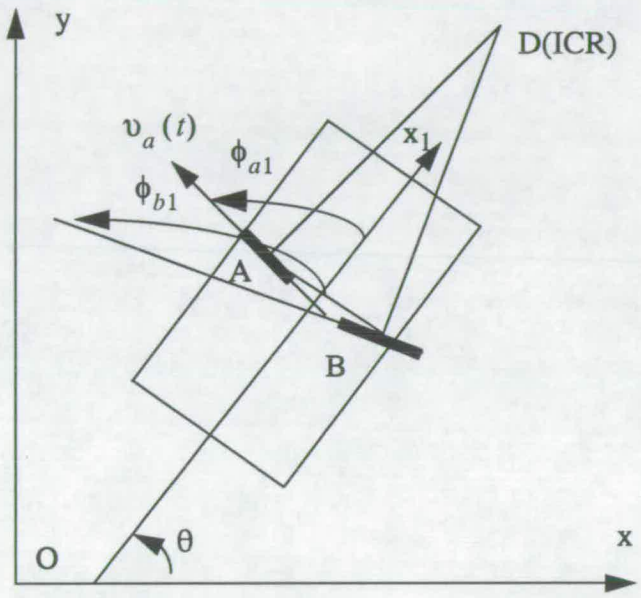

Fig. 2.13 A schematic for the omnidirectional robot

Fig. 2.13 shows that υ_a can be decomposed in x and y axes

$$\dot{x}_a = \upsilon_a \cos(\phi_{a1} + \theta) \tag{2.55}$$

$$\dot{y}_a = \upsilon_a \sin(\phi_{a1} + \theta) \tag{2.56}$$

where θ is still an unknown function that must be derived. We use the geometric method in the following (it can also be derived from the inverse kinematics using the algebraic method).

Since the directions of line AD and BD are perpendicular to wheels A and B, respectively,

from Fig. 2.13, we have

$$\angle ADB = \phi_{b1} - \phi_{a1} \tag{2.57}$$

Suppose the orientation line x_1 axis is perpendicular to the line joining the two wheels A and B, then

$$\angle ABD = 180° - \phi_{b1} \tag{2.58}$$

The length of AD can be obtained from the sine theorem

$$AD = \frac{AB\sin(\angle ABD)}{\sin(\angle ADB)} = \frac{W\sin(\phi_{b1})}{\sin(\phi_{b1} - \phi_{a1})} \tag{2.59}$$

where W represents the distance between the two wheels. Thus

$$\dot{\theta} = \frac{\upsilon_a}{AD} = \upsilon_a \cdot \frac{\sin(\phi_{b1} - \phi_{a1})}{W \cdot \sin(\phi_{b1})} \tag{2.60}$$

Integrating (2.60), (2.55), and (2.56) respectively gives

$$\theta = \theta(0) + \int_0^t \left(\upsilon_a \cdot \frac{\sin(\phi_{b1} - \phi_{a1})}{W \cdot \sin(\phi_{b1})} \right) dt \tag{2.61}$$

$$x_a = x_a(0) + \int_0^t (\upsilon_a \cos(\phi_{a1} + \theta))\, dt \tag{2.62}$$

$$y_a = y_a(0) + \int_0^t (\upsilon_a \sin(\phi_{a1} + \theta))\, dt \tag{2.63}$$

2.7 Summary

So far, the concepts of inverse and direct kinematics widely used in manipulators are, for the first time, introduced to wheeled mobile robots, and a unified treatment of the kinematics for each of the four kinds of robots has be presented. Its applications will be seen in the following chapters. Compared with the other kinematic models available, the

model established in this chapter has the following advantages:

- The mathematical model is general in the sense that the reference point can be chosen at any point on the vehicle, not only on the mid-point of the rear axle (used by most of the researchers in robotics), on the front left wheel (defined in highway and street design standards), or on the vertex of the robot body (chosen by most path planning algorithms).

- The model can apply to any dimension of rigid vehicle or vehicle combination, not only to small vehicles, because it gives a transient description of the motion for a vehicle.

- The steering angle needed for a reference point to trace a specified path can be given, which is essential for automatically controlling a mobile robot by computers and useful for highway design to determine the minimum turning radius when the steering angle limit is taken into consideration.

- The model is applicable to any kinds of path, for example, a straight line, a circle, or a more general curve y=f(x).

- The analytic solutions to straight line motion and circular motion can be developed, which make the computation of the swept space by the vehicle more efficient and accurate.

- The model distinguishes the inverse kinematics from the direct kinematics.

Chapter 3

Motion smoothness and feasibility of wheeled mobile robots

3.1 Introduction

The aim of this chapter is to investigate the motion smoothness and feasibility for wheeled robots using the kinematic models established in chapter 2.

When a robot (it may be an autonomous robot, an automated guided vehicle, a car or a truck) is required to run from a start point to a goal point in the workspace, a path has to be planned and a point on the robot is designated to follow this path. The path is usually called the reference path and the point is called the reference point P (it is also called the guidepoint [137] and the reference vertex [114]).

The reference path for an automatically guided vehicle around factories or offices generally comprises a concatenation of line-circular segments [84, 218]. The path generated by the available algorithms for an autonomous robot depends on the assumption of the shapes of the obstacles in the workspace and the autonomous robot, and the algorithms. It generally consists of a collection of line-line, line-circular segments. For example, under the assumption of polygonal obstacles and polygonal robot body, the path generated by the visibility graph method [114, 115] and the cell decomposition method [101] comprises line-line segments, as shown in Figure 3.1 (a). The path generated by the generalized visibility graph [103] is a combination of line-line and line-circular segments, as shown in Figure 3.1 (b). The common feature of these reference paths is that at the transition point between segments, the path is not smooth enough. For example, at the line-line transition point, the first derivative of the path with respect to x_p is not continuous, and at the line-circular transition point, the second derivative of the path with respect to x_p is not continuous. In general, the smoothness of the reference path can be

described by the continuity of the nth derivative of the path. The natural problem is how the smoothness of the reference path and other factors determine the motion smoothness and feasibility for the four kinds of robots classified in chapter 1.

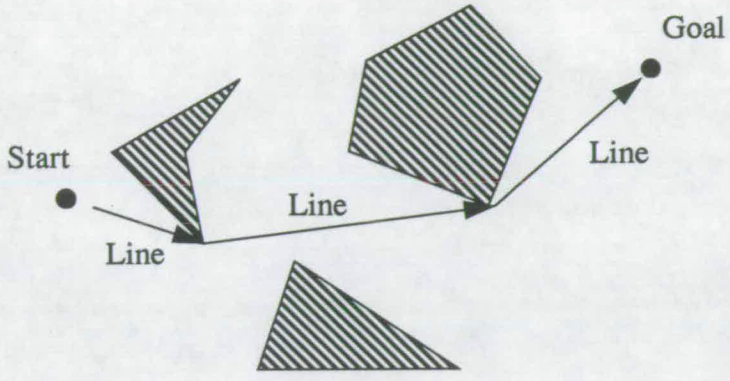

Fig. 3.1 (a) A typical line-line planned path for robots

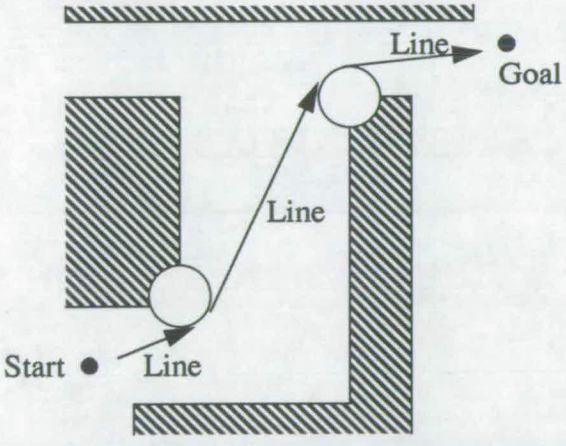

Fig. 3.1 (b) A typical line-circular planned path for robots

Among the four kinds of robots, the most commonly used robots today are car-like and the dual drive types. Most of this chapter will be devoted to discussion of these two kinds of robots. The dual drive robot can be thought of as a car-like robot which has no steering angle limit. Therefore, all the conclusions derived directly from the general constraint equation (2.13) for a car-like robot also apply to a dual drive robot if no steering angle

limit is taken into consideration. For example, when discussing the orientation angle for them, we will use the phrase "the robots subject to the general constraint equation" to represent both of these two kinds of robots, and the conclusions are suitable for both of them.

For all kinds of robots, robot orientation angle is the first important parameter which should be investigated. Since a robot is modelled as a rigid body with wheels mounted on it, the orientation angle totally determines the space swept by the robot when it moves along the reference path. Therefore, the analysis of the orientation angle change will find wide applications in the places where collision with obstacles must be avoided. In addition to this, discontinuity of the orientation angle at transition points will occur if the reference point is not chosen correctly. This implies that the requirement of tracing the planned path by the reference point is not feasible and the motion is infeasible.

For a car-like robot, steering angle is an important parameter featuring its motion smoothness and feasibility. To make a robot move along a path, steering is necessary. Steering is normally affected by changing the heading of the steering wheels (for four wheel robots) or the single steering wheel (for three wheel robots) through the steering system. As we know, the design of the steering geometry must satisfy the Jeantaud condition. In practice, the turning capability of most of the steering mechanisms in use is limited, and it can be described by inequality constraints. Due to the steering angle limit, not all the paths are executable. At any time, only when the robot steering angle needed to follow a given path satisfies these constraints is the robot able to follow the reference path. In this sense, a study of the factors which will affect the steering angle is of importance.

Another reason for studying steering angle lies in the fact that even when the steering angle limit is not exceeded in following a path, a discontinuity of the steering angle may occur at a transition point. The only way for a robot to cope with this discontinuity is to stop at the corresponding point, wait for the required adjustment of the steering angle, and then start again. Clearly, too many unnecessary stops are unacceptable.

In addition to the shape of the reference path, the steering angle and orientation angle of a

robot depend on many other factors. The most important two are the reference point position and the initial orientation angle. The choice of the reference point is the first thing to be considered. In the past, for different purposes, there are mainly three positions which are chosen as the reference points, e.g. one of the vertices of the rigid polygonal body for simplifying the path planning algorithms [114], the middle point of the rear axle for the control of car-like robot or the dual drive robot [228], and the geometric center of the robot for finding a good representation of free space [60, 66]. In fact, the choice of the reference point may be somewhat arbitrary, yet its choice does affect the kinematics and dynamics of the robot. The desired steering and drive functions of the robot, the space swept out by the robot, the actuators needed to drive the robot and the control method to be devised for the robot all are functions of the position of the reference point. Hence, the analysis of the effect of the reference point position on the motion feasibility of the robot is necessary.

The necessity of investigating the initial orientation angle can be seen from tracing the line-line combination shown in Figure 3.1 (a). When the robot arrives the end of the first line segment, the orientation angle at that point will become the initial orientation angle for the second line segment; the orientation angle at the end of the second line will, in turn, become the initial angle for the third line, and so on. When the robot changes lanes consisting of circular-circular segments, there also exists an initial value problem.

Most of the robots in use or in development today are steered by a single wheel or wheel pair [36, 194]. It has been proved in chapter 2 that from the steering viewpoint, a robot steered by a single wheel is an equivalent to that steered by a wheel pair. So in this study, we only consider the former kind of robot to analyze the motion feasibility of the robot.

Although many researchers have focused their attentions on the study of the motion of trucks [31] and the motion of automated guided vehicles or autonomous robots [63, 70], to date, the author has not been aware of the detailed analysis of the dependence of the motion feasibility of wheeled robots on the shape of the reference path, the reference point position and the initial orientation angle of a robot. This chapter, based on the inverse

kinematic model established in previous chapter, investigates this problem when a robot is required to follow a general path $y_p = f(x_p)$. Some typical motions, i.e., pure translation, pure rotation, general straight line motion and circular motion are also analyzed.

3.2 Conditions of a pure translation and a pure rotation for car-like robots and dual-drive robots

3.2.1 Necessary and sufficient conditions of a pure translation

Definition 3.1: If the orientation angle of a robot is always a constant θ_0 during its motion, then the motion is called a pure translation.

In the following we will give the necessary and sufficient conditions of a pure translation for a car-like robot or a dual drive robot.

Theorem 3.1: *The necessary and sufficient conditions of a pure translation for a wheeled robot which is subject to the general constraint (2.13) are that the reference path* $y_p = f(x_p)$ *is a straight line which passes through the initial point* (x_{pi}, y_{pi}) *and has the slope of* $tan(\theta_0)$.

Proof. Necessary condition

If the motion of the robot is a pure translation, then $\theta = \theta_0$. In this case, from (2.13), it can be obtained that $f'(x_p) = \dfrac{dy_p}{dx_p} = \tan(\theta_0)$. The solution to this equation is $y_p = \tan\theta_0 \cdot x_p + b$, where b is a constant determined by the initial values (x_{pi}, y_{pi}). So the reference path is a straight line which passes through the initial point (x_{pi}, y_{pi}) and has the slope of $\tan(\theta_0)$.

Sufficient condition

Suppose the reference path is given as the form $y_p = \tan\theta_0 \cdot x_p + b$. Differentiating it

gives $f'(x_p) = \frac{dy_p}{dx_p} = \tan\theta_0$. In this case, (2.13) becomes $\underline{x} \cdot \cos\theta_0 \cdot \frac{d\theta}{dx_p} = \sin(\theta - \theta_0)$, and the solution to this equation is $\theta = \theta_0$, so the motion is a pure translation.

Note that this theorem holds wherever the reference point is chosen. However, condition of a pure rotation for robots subject to the constraint equation (2.13) discussed in the following depends on the position of the reference point.

3.2.2 Necessary condition of a pure rotation

Definition 3.2: If the motion of a robot satisfies: $\dot{x}_p = 0$, $\dot{y}_p = 0$, and $\dot{\theta} \neq 0$, then the motion is called a pure rotation.

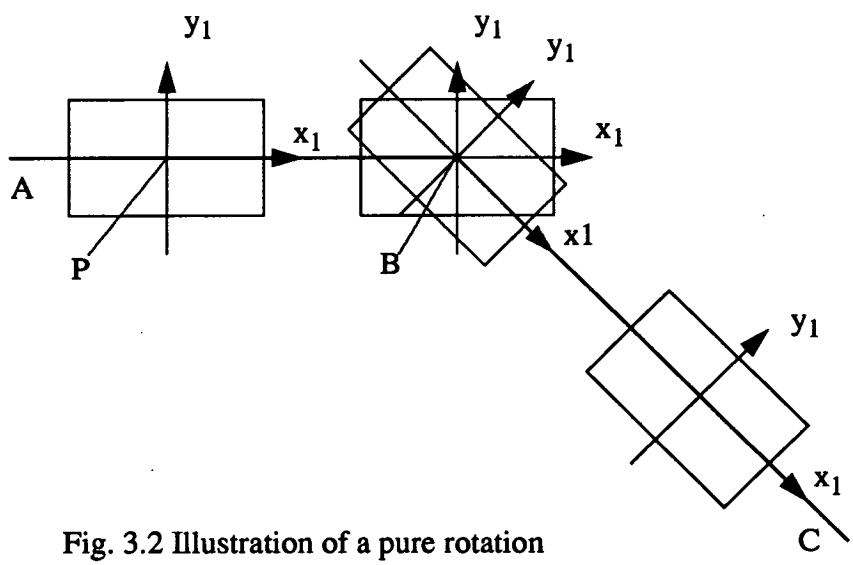

Fig. 3.2 Illustration of a pure rotation

Let us consider the motion of a robot subject to the constraint equation (2.13), as shown in Fig. 3.2. The robot is required to move from the initial point A to the intersection point B of the two straight line segments AB and BC, stop at B, and then turn without moving the reference point P (we call such a motion as a pure rotation) until the orientation angle of the robot coincides with the straight line segment BC. This problem arises from the execution of the generated path using the method presented by Brooks [23]. In this

method, the robot and the obstacles are assumed to be polygons and the generated path consists of line-line segments. The reference point is chosen so that the $max_{1 \le i \le n}(d_i)$ is minimized as the candidate of the reference point, where d_i represents the distance of the ith vertex of the robot from the reference point (for more details, see [23]). For a rectangular robot, the reference point chosen based on this definition is located at the geometrical center. In most cases, this point is not at the rear fixed axle for a car-like or a dual drive robot. The question we are interested in here is if the reference point is not at the rear axle, whether or not such a pure rotation can occur.

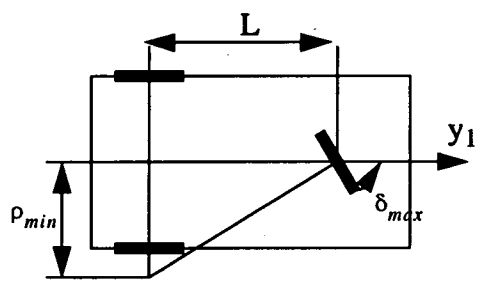

Fig. 3.3 Illustration of the minimum distance from the middle point of the rear axle to the instantaneous rotation center for a robot with steering angle limit

In the following we will prove a theorem describing the necessary condition of a pure rotation for a robot subject to the kinematic constraint equation (2.13).

Theorem 3.2: *For a robot subject to the kinematic constraint equation (2.13), only when the reference point is at the rear fixed axle, does a pure rotation occur.*

Proof. If the motion is a pure rotation, then $\dot{x}_p = 0$, $\dot{y}_p = 0$, and $\dot{\theta} \neq 0$. (if $\dot{x}_p = 0$, $\dot{y}_p = 0$, and $\dot{\theta} = 0$, then the robot does not move at all). In this case, the unique solution of the general constraint equation (2.13), which satisfies this requirement, is $\underline{x} = 0$. That means the reference point must be at the rear fixed axle.

Note that steering angle limit is an intrinsic characteristic of the car-like robot. In theorem 3.2, it is not taken into account. Suppose the steering angle limit is δ_{max}, then the minimum distance of the instantaneous rotation center to the middle point of the rear axle

ρ_{min} can be expressed in the following form (see Fig. 3.3)

$$\rho_{min} = L/(\tan\delta_{max}) \tag{3.1}$$

From (3.1), it can be observed that for a car-like robot which has steering angle limit (that means $\delta_{max} \neq \pm 90°$), even if the reference is at the middle point of the rear axle, the motion of a pure rotation can not occur. For the dual drive robot, since steering is accomplished by changing the ratio of the velocities of the two driving wheels, only when the reference point is located at the rear axle, does a pure rotation occur.

3.3 Continuities of orientation angle and steering angle

The motion smoothness of robots can be judged upon the continuities of the nth derivatives of the orientation angle and steering angle. An interesting problem investigated here is to determine the dependence of the continuities of the orientation angle and steering angle on that of the nth derivative of the reference path with respect to x_p.

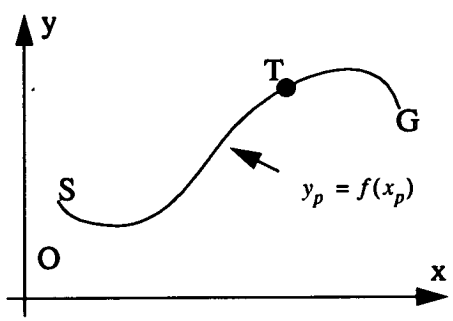

Fig. 3. 4 Illustration of an independent variable to velocity

A geometric curve, which is generated by a path planning algorithm and is required to be followed by the reference point P of the robot, is called a path. Mathematically, a curve can be represented as a general form in x-y plane

$$y_p = f(x_p) \tag{3.2}$$

Some characteristics associated with its shape, such as its derivatives and curvature, are referred to as its geometric characteristics. A trajectory is defined as the time course along a path. One can choose velocity from various schedules for a geometrically defined path, which results in various velocity profiles. Fig. 3.4 shows such an example. When a robot is required to trace the reference path from start point S to goal point G through the point T at different velocities, if every time, the robot's orientation angle has fixed value at point T, then we call the orientation angle an independent variable of its velocity. More generally, if a variable is only affected by the geometrical characteristics rather than by robot's velocities at any point along the path, it is called an independent variable of velocities. The purpose of defining such an independent variable is to show that once a reference path is infeasible for a robot, then adjusting its velocity and steering angle do not change its motion feasibility. We can see in the following that θ, ϕ_{a1} are such defined independent variables.

Eqs. (2.8) and (2.13) can not be directly used for showing the independence as they include time variable. From (2.13), another form of the general constraint equation can be derived as

$$\pm d\theta = (\sin\theta - f'(x_p)\cos\theta)\, dx_p \tag{3.3}$$

where $f'(x_p)$ denotes the slope of the reference path $y_p = f(x_p)$ at x_p. It follows from differential equation (3.3) that the orientation angle of the robot is only a function of x-axis coordinate of the reference point.

From (3.2), (3.3), and (2.8), we can obtain the expression of steering angle as follows (the detailed derivation is omitted):

$$\phi_{m1} = arc\tan\left(\frac{f'(x_p)\cos\theta - \sin\theta + x_{m1}\dfrac{d\theta}{dx_p}}{f'(x_p)\sin\theta + \cos\theta - y_{m1}\dfrac{d\theta}{dx_p}}\right) \tag{3.4}$$

Eqs. (3.3) and (3.4) indicate that θ and ϕ_{a1} are independent variables.

Since the reference point at different positions will produce different effects on the orientation angle and steering angle, in the following two cases, $\underline{x} = 0$ and $\underline{x} \neq 0$, will be considered when the continuities of orientation angle and steering angle are discussed.

Case 1: $\underline{x} = 0$

As defined above, $\underline{x} = 0$ corresponds to the position where the reference point is chosen at the rear axle. In this case, (3.3) gives

$$\theta = arc\tan\left(f'(x_p)\right) \tag{3.5}$$

Substituting (3.5) into (3.4) and simplifying lead to

$$\phi_{a1} = arc\tan\left(\frac{L\kappa_p}{1 - y_{a1}\kappa_p}\right) \tag{3.6}$$

where $\kappa_p = \dfrac{f''(x_p)}{\left(1 + \left(f'(x_p)\right)^2\right)^{\frac{3}{2}}}$ represents the curvature of the reference path at x_p, $f''(x_p)$ represents the second derivative of the reference path with respect to x_p, and $L = x_{a1} - \underline{x}$ represents the wheelbase of the robot. If the reference point is at the midpoint of the rear axle, then $y_{a1} = 0$ and we obtain the widely used formula:

$$\phi_{a1} = arc\tan\left(L\kappa_p\right) \tag{3.7}$$

It is noted that (3.5) and (3.7) are independent of the initial orientation angle at any point on the path, that is the direction of the orientation of the robot must coincide with the tangent of the reference path.

Eq. (3.5) indicates that robot's orientation angle possesses the same continuity as the first derivative of the reference path. At the line-line transition point shown in Fig. 3.1 (a),

$f'(x_p)$ is not continuous. Consequently, the orientation of the robot is also not continuous. However, at the line-circular transition point shown in Fig. 3.1 (b), robot's orientation angle is continuous as $f'(x_p)$ at this point is continuous.

Eq. (3.7) shows the dependence of the continuity of the steering angle on that of the followed path. The sufficient and necessary conditions for the continuity of the steering angle along the path is the continuity of the second derivative of the path at every point. So at the line-line and line-circular transition points, steering angle is not continuous. This prevents the robot from efficient and smooth motion.

Using an inductive method, we can prove the following theorems:

Theorem 3.3: *If the (n+1)th derivative of the reference path at any point with respect to x_p is continuous, then the nth derivative of the orientation angle of the robot at the corresponding point with respect to x_p is continuous.*

Theorem 3.4: *If the (n+2)th derivative of the reference path at any point with respect to x_p is continuous, then the nth derivative of the steering angle of the robot at the corresponding point with respect to x_p is continuous.*

Case 2: $\underline{x} \neq 0$

When the reference point is chosen away from the rear axle of the robot, $\underline{x} \neq 0$. In this case, orientation angle is the solution of the first order differential equation (3.3) and is a function of $f'(x_p)$ and the initial orientation angle θ_0 of the robot. When the robot traverses the line-line transition point, although $f'(x_p)$ at that point is not continuous, orientation angle will be continuous because the orientation angle at the end of the first line segment will become the initial angle of the succeeding line segment. The first derivative of the orientation angle with respect to x_p possesses the same continuity as

$f'(x_p)$ does. From (3.3) and (3.4), steering angle can be derived as:

$$\phi_{a1} = arc\tan\left(\frac{L(\sin\theta - f'(x_p)\cos\theta)}{(\underline{x}\cos\theta - y_{a1}\sin\theta) + f'(x_p)(\underline{x}\sin\theta + y_{a1}\cos\theta)}\right) \tag{3.8}$$

It can be seen from (3.8) that for most cases, the steering angle is not continuous at the line-line transition point because the orientation angle is continuous and $f'(x_p)$ is not; the steering angle is continuous at the line-circle transition point because both orientation angle and $f'(x_p)$ are continuous.

Since the solution of the orientation angle θ depends on the initial orientation angle θ_0 when $\underline{x} \neq 0$, the continuity of the orientation angle θ may hold occasionally even if $f'(x_p)$ is not continuous at some transition point. However, the possibility is rare. Generally, we have the following theorems:

Theorem 3.5: *If the nth derivative of the reference path at any point with respect to x_p is continuous, then the nth derivative of the orientation angle of the robot at the corresponding point with respect to x_p is continuous.*

Theorem 3.6: *If the (n+1)th derivative of the reference path at any point with respect to x_p is continuous, then the nth derivative of the steering angle of the robot at the corresponding point with respect to x_p is continuous.*

From theorems 3.3 to 3.6, it is easily seen that the position of the reference point does have a significant effect on the motion feasibility of the robot. Following the same path, moving the reference point away from the rear axle of the robot will improve the smoothness of the motion and steering performance.

3.4 Steering angle limit and feasible deviation angle intervals

The pure translation and rotation discussed in 3.2 are two basic motions adopted in the study of wheeled robots. However, they are not enough to describe a more general motion.

To analyze the motion feasibility of a car-like robot, the existence of steering angle limit can not be neglected. The consideration of it helps understand the critical conditions for distinguishing a feasible motion from an infeasible one.

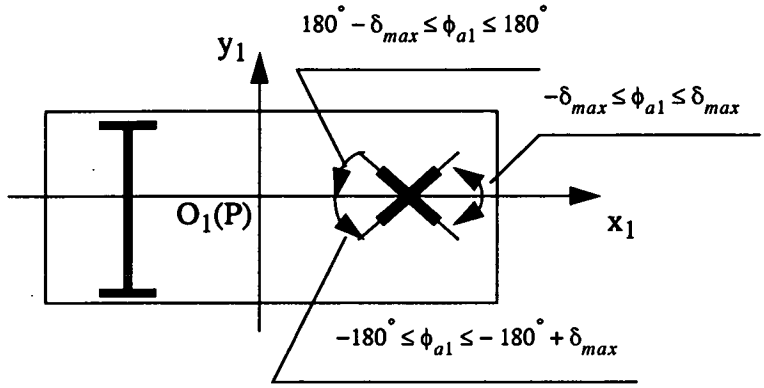

Fig. 3.5. Illustration of the steering angle inequality constraints

In this section, a new concept of deviation angle will be introduced to further discuss the motion feasibility of a car-like robot when the reference path is given as a general form $y_p = f(x_p)$ and the steering angle limit is taken into account.

In the range of $-180^\circ \le \phi_{a1} \le 180^\circ$, the limited steering angle can be expressed by the following inequality constraints:

$$-\delta_{max} \le \phi_{a1} \le \delta_{max},\ 180^\circ - \delta_{max} \le \phi_{a1} \le 180^\circ,\ -180^\circ \le \phi_{a1} \le -180^\circ + \delta_{max} \qquad (3.9)$$

where δ_{max} is a positive constant and represents the maximum deviation of the steering wheel from x_1-axis, see Fig. 3.5. When the steering angle is in the range of $-\delta_{max} \le \phi_{a1} \le \delta_{max}$, it means that the direction of the velocity at the midpoint of the rear axle is the same as that of the positive direction of the x_1-axis; when the steering angle falls into the range of $180^\circ - \delta_{max} \le \phi_{a1} \le 180^\circ$ or $-180^\circ \le \phi_{a1} \le -180^\circ + \delta_{max}$, the direction of the velocity at the midpoint of the rear axle is along the negative direction of the x_1-axis. We usually refer to the former as a forward motion and the latter as a

backward motion.

Let α represent the motion direction of the reference point P, θ represent the orientation angle of the robot at point x_p on the path $f(x_p)$, as shown in Fig. 3.6. Then α can be expressed as:

$$\tan(\alpha) = \frac{\dot{y}_p}{\dot{x}_p} = f'(x_p) \tag{3.10}$$

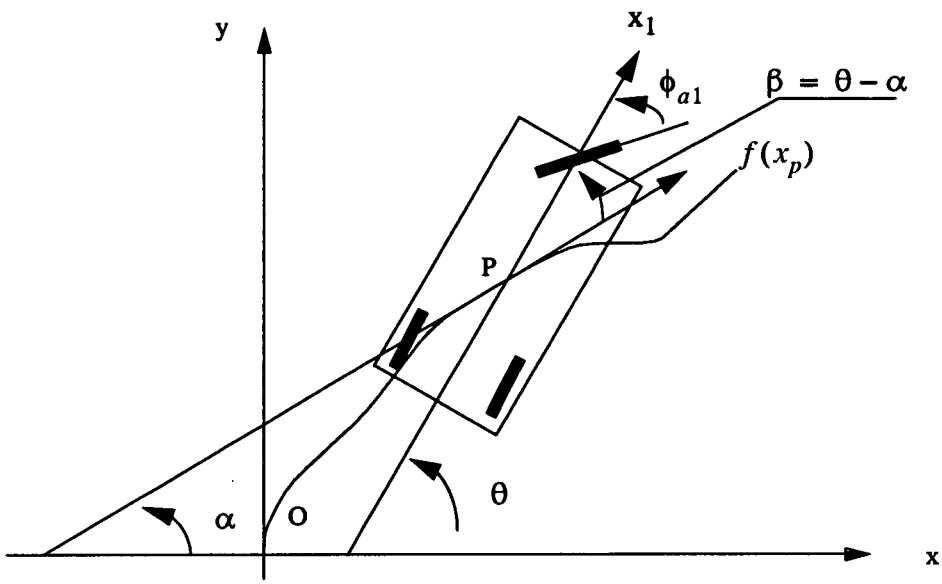

Fig. 3.6. Illustration of the deviation angle β

We define $\beta = \theta - \alpha$ as the deviation angle of the vehicle at point x_p. Substituting (3.10) into (3.8), we have

$$\phi_{a1} = arc\tan\left(\frac{L\sin\beta}{\underline{x}\cos\beta - y_{a1}\sin\beta}\right) \tag{3.11}$$

Differentiating (3.11) with respect to β gives

$$\frac{d\phi_{a1}}{d\beta} = \frac{\underline{x}\cdot L}{(L\sin\beta)^2 + (\underline{x}\cos\beta - y_{a1}\sin\beta)^2} \tag{3.12}$$

It is clear that when $\underline{x} < 0$, $\frac{d\phi_{a1}}{d\beta} < 0$, steering angle ϕ_{a1} is monotonic decreasing with respect to β; when $\underline{x} > 0$, $\frac{d\phi_{a1}}{d\beta} > 0$, steering angle ϕ_{a1} is monotonic increasing. A typical relationship between steering angle and the deviation angle is shown in Fig. 3.7.

Since the steering angle varies monotonically with respect to the deviation angle, there exist four critical deviation angles β_1, β_2, β_3 and β_4, corresponding to the four critical steering angles δ_{max}, $-\delta_{max}$, $180^\circ - \delta_{max}$ and $-180^\circ + \delta_{max}$. The corresponding feasible intervals of the deviation angles for $\underline{x} < 0$ and $\underline{x} > 0$ are shown in Tables 3.1 and 3.2, respectively.

From Tables 3.1 and 3.2, we can draw the conclusion that if the steering angle limit is taken into consideration, only when the deviation angle falls into the four feasible intervals, i.e., the neighborhood of 0° and that of ±180°, can the steering angle limit be satisfied. We call these four intervals as the feasible deviation intervals, and the corresponding orientation angle intervals as feasible orientation intervals.

For a given steering angle limit, in the following, we discuss the effect of $\underline{x}$ on the maximum deviation angle. From (3.11), it is easy to obtain

$$\beta = arc\tan\left(\frac{\underline{x}\tan(\phi_{a1})}{L + y_{a1}\tan(\phi_{a1})}\right) \tag{3.13}$$

It can be observed from (3.13) that the farther (the larger the value of the $|\underline{x}|$) the reference point is chosen from the rear axle, the larger the magnitude of the permitted deviation angle. When the reference point is chosen at the rear axle, $\beta = 0$. It should be noted that above analysis applies to the initial position.

3.5 Analysis of straight line motion

In this and next sections, we use the general constraint equation (2.13) or (3.3) to analyze

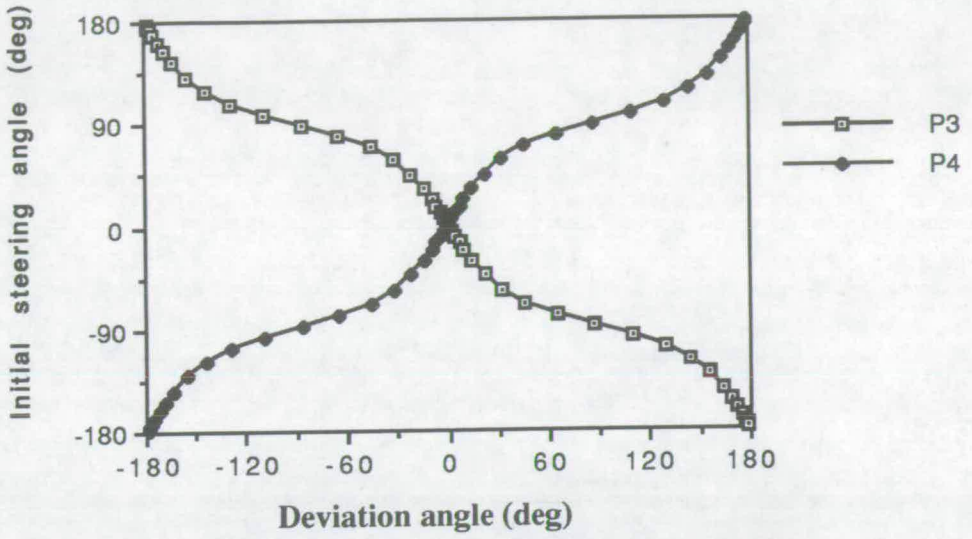

Fig. 3.7 The relationship between the steering angle and the deviation angle when the reference points are in front of the rear axle (P3) and behind the rear axle (P4), respectively.

Table 3.1 The corresponding relationship between critical steering angles and critical deviation angles when reference point is in front of the rear axle

$x < 0$				
Interval ϕ_{a1}	$(0^\circ, \delta_{max})$	$(-\delta_{max}, 0^\circ)$	$(180^\circ - \delta_{max}, 180^\circ)$	$(-180^\circ, -180^\circ + \delta_{max})$
Interval β	$(\beta_1, 0^\circ)$	$(0^\circ, \beta_2)$	$(-180^\circ, \beta_3)$	$(\beta_4, 180^\circ)$
Signs	β_1 (-)	β_2 (+)	β_3 (-)	β_4 (+)

Table 3.2 The corresponding relationship between critical steering angles and critical deviation angles when reference point is behind the rear axle

$x > 0$				
Interval ϕ_{a1}	$(0^\circ, \delta_{max})$	$(-\delta_{max}, 0^\circ)$	$(180^\circ - \delta_{max}, 180^\circ)$	$(-180^\circ, -180^\circ + \delta_{max})$
Interval β	$(0^\circ, \beta_1)$	$(\beta_2, 0^\circ)$	$(\beta_3, 180^\circ)$	$(-180^\circ, \beta_4)$
Signs	β_1 (+)	β_2 (-)	β_3 (+)	β_4 (-)

two other typical robot motions: 1) straight line motion, 2) circular motion. The straight line motion and circular motion are chosen as examples because of the following reasons: 1) most analyses especially for practical applications assume that the reference path is a circle or a straight line; for example, the offtracking problem for highway design is defined only for a circular turn and then a straight line motion [231]. In a path planning problem, most of the generated paths also consist of circles and straight lines [101]; 2) the closed-form solutions can be derived and the effects of some parameters, such as the circular radius, the driving velocity, and the position of the reference point, on the driving characteristics can be illustrated clearly using them.

Definition 3.3: If the reference path is a straight line, then the motion of a robot is called a straight line motion.

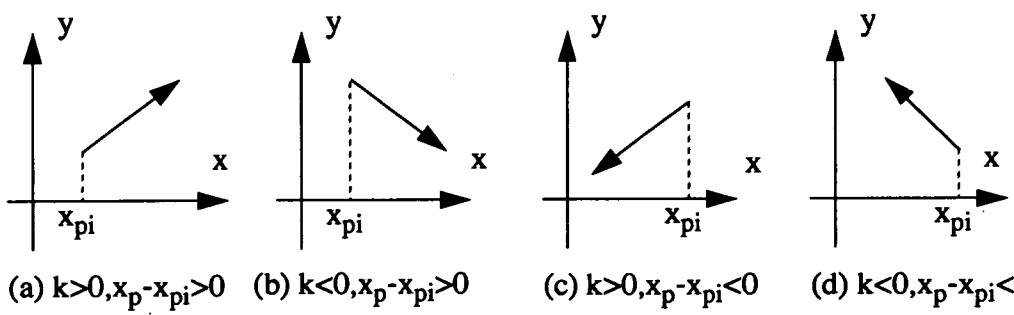

Fig. 3.8. Illustration of the signs of k and (x_p-x_{pi}) for a straight line motion

From this definition and theorem 3.1, it can be seen that a pure translation is only a special case of a general straight line motion where the initial orientation angle coincides with the direction of the straight line. In this section, we first derive a closed-form expression for the orientation angle and then analyze the effects of the position of the reference point and the initial orientation angle on the orientation angle and steering angle of the robot when the limit of steering mechanism is taken into consideration.

Let us consider the case where a robot moves along a straight line as shown in Fig. 3.8 at any velocity. Without losing generality, suppose the reference path is described by the

following equation

$$y_p = kx_p + b \tag{3.14}$$

where k is the slope of the straight line and b is the intercept on y axis, hence:

$$f'(x_p) = k \tag{3.15}$$

Substituting (3.15) into (3.3), we have

$$\underline{x} \cdot d\theta = (\sin\theta - k\cos\theta)\, dx_p = \sqrt{1+k^2}\sin(\theta - \alpha)\, dx_p \tag{3.16}$$

where $\alpha = arc\tan(k)$, a constant, is defined as that in (3.10). The solution of (3.16) is

$$\theta = 2arc\tan\left(\tan\frac{\beta_0}{2} \cdot e^c\right) + \alpha,\ c = \frac{\sqrt{1+k^2}}{\underline{x}}(x_p - x_{pi}) \tag{3.17}$$

where x_{pi} is the initial x-coordinate, $\beta_0 = \theta_0 - \alpha_0$ is the initial deviation angle. In this formula, the signs of k and x_p-x_{pi} indicate the moving direction, as shown in Fig. 3.8. θ_0, the initial orientation angle, is in the range of ±180°.

When a robot moves along a straight line parallel to y axis, (3.17) is not applicable. In this case, the solution to orientation angle is

$$\theta = 2arc\tan\left(\tan\frac{\theta_0 - 90°}{2} \cdot e^c\right) + 90°,\ c = \frac{y_p - y_{pi}}{\underline{x}} \tag{3.18}$$

In the following analysis of the straight line motion, for simplicity, suppose the straight line is the x-axis, the start point is located at the origin and the motion direction is along the positive direction of the x-axis. As defined above, in this case, $x_{pi} = y_{pi} = 0$, and $\alpha = 0$, the deviation angle β of the robot is equal to its orientation angle θ. The

orientation angle (3.17) becomes

$$\theta = 2arc\tan\left(\tan\left(\frac{\theta_0}{2}\right)e^c\right) \tag{3.19}$$

where $c = \frac{x_p}{\underline{x}}$. Differentiating (3.19) with respect to x_p, we have

$$\frac{d\theta}{dx_p} = \frac{2\tan\left(\frac{\theta_0}{2}\right)e^c}{\underline{x}\left(1+\left(\tan\left(\frac{\theta_0}{2}\right)e^c\right)^2\right)} \tag{3.20}$$

The monotonicity of θ with respect to the passed length x_p is shown in Table 3.3.

Table 3.3 The monotonicity of the orientation angle with respect to x_p when the reference point is chosen away from the rear axle (MI = Monotonic Increasing, M D = Monotonic Decreasing)

	$\underline{x} < 0$		$\underline{x} > 0$	
	$0° < \theta_0 < 180°$	$-180° < \theta_0 < 0°$	$0° < \theta_0 < 180°$	$-180° < \theta_0 < 0°$
θ versus x_p	M D	M I	M I	M D

Case 1: $\underline{x} < 0$

In this case, since θ is monotonic decreasing (MD) with respect to x_p when $0^\circ < \theta_0 < 180^\circ$ whereas θ is monotonic increasing (M I) when $-180^\circ < \theta_0 < 0^\circ$. If no steering angle limit is taken into consideration, then whatever the initial orientation angle is in the range from $-180°$ to $180°$, when $x_p \to \infty$, then $\theta \to 0$. When the steering angle limit is not neglected, it can be seen from Tables 3.1 and 3.3 that if the initial orientation angle falls into the feasible interval of $(\theta_1, 0^\circ)$ or $(0^\circ, \theta_2)$ which corresponds to $(\beta_1, 0^\circ)$ or

$(0^\circ, \beta_2)$, respectively, when $x_p \to \infty$, then $\theta \to 0$. The orientation angle is always kept in the feasible interval, and consequently, the steering angle limit is always satisfied; on the other hand, if the initial orientation angle falls into the other feasible interval of $(-180^\circ, \theta_3)$ or $(180^\circ, \theta_4)$ which corresponds to $(-180^\circ, \beta_3)$ or $(\beta_4, 180^\circ)$, respectively, as x_p increases, the orientation angle will approach θ_3 or θ_4 within a limited passed length. This means that steering angle limit will be reached within a limited passed length. After that, the reference path can not be traced any more.

Case 2: $\underline{x} > 0$

In this case, since θ is monotonic increasing (MI) with respect to x_p when $0^\circ < \theta_0 < 180^\circ$ whereas θ is monotonic decreasing (MD) when $-180^\circ < \theta_0 < 0^\circ$. If no steering angle limit is taken into consideration, whatever the initial orientation angle falls into the range of $0^\circ < \theta_0 < 180^\circ$, $-180^\circ < \theta_0 < 0^\circ$, when $x_p \to \infty$, then $\theta \to \pm 180^\circ$. Using the similar analysis, we can conclude that only when the initial orientation angle is in the feasible range of $(-180^\circ, \theta_3)$ or $(180^\circ, \theta_4)$, can the robot trace the straight line for any length.

Case 3: $\underline{x} = 0$

This means that the initial orientation angle must only be 0° or $\pm 180^\circ$. The locus of any point is also a straight line and the motion of the robot must be a pure translation. Otherwise, the robot can not move.

3.6 Analysis of circular motion

Definition 3.4: If the reference path is a circular arc, then the motion of a robot is called a circular motion.

A circular motion in clockwise direction is called a right turn circular motion and a circular motion in counter-clockwise direction is called a left turn circular motion. Fig. 3.9

shows a right turn circular motion.

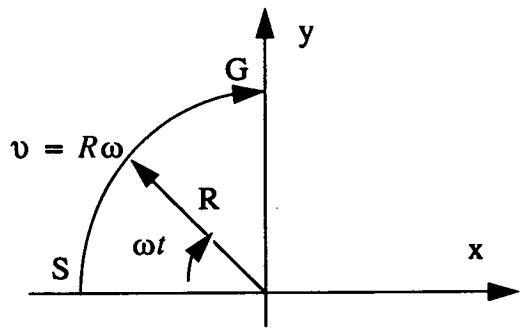

Fig. 3.9 A schematic for a right turn circular motion

The previously discussed pure rotation is a special case of a general circular motion where the center of instantaneous rotation always coincides with the reference point and the radius of the circular motion is zero. In this section, we only consider the right turn motion of a robot travelling along a circle of radius R from S to G, see Fig. 3.9. As discussed previously, some parameters, such as the robot's orientation angle and steering angle, are independent variables to its velocity. Therefore, for convenience and without losing generality, we may use parameterized expressions and assume that the motion of the reference point P can be described by the following equations:

$$\begin{bmatrix} x_p \\ y_p \end{bmatrix} = \begin{bmatrix} -R\cos(\omega t) \\ R\sin(\omega t) \end{bmatrix} \tag{3.21}$$

$$\begin{bmatrix} \dot{x}_p \\ \dot{y}_p \end{bmatrix} = \begin{bmatrix} R\omega\sin(\omega t) \\ R\omega\cos(\omega t) \end{bmatrix} \tag{3.22}$$

where ω represents the angular velocity of the reference point P, ωt represents the radians of the passed arc. Substituting (3.22) into (3.10), we have the expression for the motion direction of the reference point:

$$\alpha = 90° - \omega t \tag{3.23}$$

At the start point, $\omega t = 0$ and $\alpha = 90°$. The feasible initial orientation angle must be in

the neighborhood of ±90°.

The steering angle expression becomes

$$\phi_{a1} = arc\tan\left(\frac{-L}{\underline{x}\tan(\theta+\omega t)+y_{a1}}\right) \tag{3.24}$$

Like the straight line motion, there are three cases for $\underline{x}$, depending on the choice of the reference point P.

Case 1: $\underline{x} < 0$

In this case, by substituting (3.22) into (2.13), we have

$$(-\underline{x})\,\dot{\theta} = \dot{y}_p\cos\theta - \dot{x}_p\sin\theta = R\omega\cos(\omega t+\theta) \tag{3.25}$$

For convenience, put $k = -R/\underline{x}$. Because (3.25) is not an equation in t and θ with separable variables, the method of changing the variables must be used to solve it. The substitution $z=\omega t+\theta$ gives $\dot{z} = \omega+\dot{\theta}$. Substituting them into (3.25) gives

$$\frac{dz}{dt} = \omega\cdot(1+k\cos z) \tag{3.26}$$

Integrating (3.26) gives

$$\int_0^t dt = \int_{z_0}^{z}\frac{dz}{\omega\cdot(1+k\cos z)} \tag{3.27}$$

where $z_0 = \theta(0) = \theta_0$ is the initial orientation angle of the robot at start point S. Eq. (3.27) is a integral of rational function of $\cos\theta$. Put $z' = \tan(z/2)$, $dz' = \frac{1}{2}\cdot(\sec z/2)^2\cdot dz$

so that $dz = \frac{2}{1+(z')^2} \cdot dz'$, hence:

$$\omega t = \int_{z'_0}^{z'} \frac{2dz'}{(1+k)+(1-k)(z')^2} \tag{3.28}$$

The solution from (3.28) is

$$\omega t = \begin{cases} \frac{1}{b} arc\tan\left(\frac{z'}{a}\right) - \frac{1}{b} arc\tan\left(\frac{z'_0}{a}\right), a = \sqrt{\frac{1+k}{1-k}}, b = \frac{\sqrt{1-k^2}}{2}, k < 1 \\ (z' - z'_0), k = 1 \\ \frac{1}{d} \cdot \left(ln\frac{c+z'}{c-z'} - ln\frac{c+z'_0}{c-z'_0} \right), c = \sqrt{\frac{k+1}{k-1}}, d = \sqrt{k^2-1}, k > 1 \end{cases} \tag{3.29}$$

Considering the substitutions we used above, we finally obtain the expression for θ in terms of k, ω, z'_0 and t:

$$\theta = \begin{cases} 2arc\tan\left(a \cdot \frac{z'_0 + a \cdot \tan(\omega t \cdot b)}{a - (z'_0 \cdot \tan(\omega t \cdot b))} \right) - \omega t, k < 1 \\ 2\,\mathrm{atan}(\omega t + z'_0) - \omega t, k = 1 \\ 2arc\tan\left(c \cdot \frac{(c+z'_0) \cdot e^{\omega t d} - (c-z'_0)}{(c+z'_0) \cdot e^{\omega t d} + (c-z'_0)} \right) - \omega t, k > 1 \end{cases} \tag{3.30}$$

Eq. (3.30) indicates that the orientation angle is a function of initial orientation angle, the k and ωt, independent of ω and $R\omega$. That means velocity has no effect on the orientation angle.

Substituting (3.21) into (2.1) and simplifying, we obtain

$$\begin{bmatrix} x_m \\ y_m \end{bmatrix} = \begin{bmatrix} L_m \cos(\theta+\gamma) - R\cos\omega t \\ L_m \sin(\theta+\gamma) + R\sin\omega t \end{bmatrix} \tag{3.31}$$

where $\sin\gamma = \frac{y_{m1}}{L_m}, \cos\gamma = \frac{x_{m1}}{L_m}, L_m = \sqrt{x_{m1}^2 + y_{m1}^2}$. In order to understand better the locus of any

point in the robot, squaring the two sides of (3.31), we write

$$x_m^2 + y_m^2 = L_m^2 + R^2 - 2RL_m \cos(\theta + \gamma + \omega t) \tag{3.32}$$

Eq. (3.32) verifies that when the reference point moves along a circle, the locus of the other point is not necessarily a circle. This conclusion will be used for discussing the shortcomings of the path planning algorithms presently available for wheeled robots in the later chapter.

Because the monotonicity of the orientation angle with respect to ωt is not as explicit as that of the straight line motion, so in the following, the simulation result is given. Fig. 3.10 illustrates a schematic of a practical rigid vehicle and its key dimensions [233]. This vehicle will be used as the simulation model here.

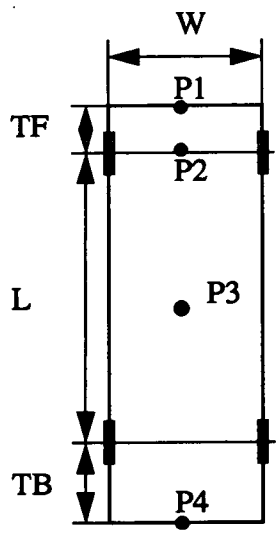

Dimensions (values in meters)	
Body width (W)	2.5
Effective wheelbase (L)	6.2
Front overhang (TF)	1.3
Rear overhang (TB)	2.5

Fig. 3. 10 A schematic of the geometry of a FAT design rigid vehicle

Fig. 3.11 shows the changes of the orientation angle with respect to ωt at different k values and initial orientation angles when ωt changes from 0° to 90°. When the initial orientation angle is in the range from 90° to 120°, the orientation angle is monotonic decreasing and the smaller the k, the slower the change of the orientation angle. When the initial orientation angle is less than 90°, at the beginning, the orientation angle increases

and then decreases. It can also be seen that with the same k and different initial orientation angles, the vehicle's orientation angle tends to be the same value as ωt increases.

Figures 3.12 (a) and (b) show the change of the steering angle with respect to ωt when the initial orientation angle is in the neighborhood of 90° and the reference point are at P3 and P1 (see Fig. 3.10), respectively. Three factors, namely, the reference point position, the initial orientation angle and k, affect the steering angle. The initial steering angle is dependent on the position of the reference point and the initial orientation angle, not on k. As stated above, moving the reference point forward increases the permitted deviation angle, and consequently, makes it easier to satisfy the steering limit. However, as ωt increases, the steering angle tends to a steady value which is independent of the initial orientation angle but dependent on k. Moving the reference point forward makes the magnitude of the steady steering angle increase. In practice, k>1, from (3.24) and (3.30) by putting $\omega t \to \infty$, the following can be obtained

$$\phi_{a1_\infty} = \lim_{\omega t \to \infty} \phi_{a1} = arc\tan\left(\frac{-L}{-x\sqrt{k^2-1}+y_{a1}}\right), (k>1) \tag{3.33}$$

When the reference point is chosen at the center line, namely, $y_{a1} = 0$, the condition of equal initial and steady steering angles is

$$\tan(\theta_0) = \pm\sqrt{k^2-1} \tag{3.34}$$

When the radius of the circular motion is 25m and the initial orientation angles are −60°, −90° and −120°, respectively, the steering angle change with respect to ωt is shown in Fig. 3.13. Since the feasible steering interval corresponding to this case is in the neighborhood of ±180°, the steering angle reaches its saturation limit very quickly. After that, the robot can not move.

In summary, from the above analysis we can draw the following conclusions: only when the initial orientation angle falls into the neighborhood of 90° and the corresponding

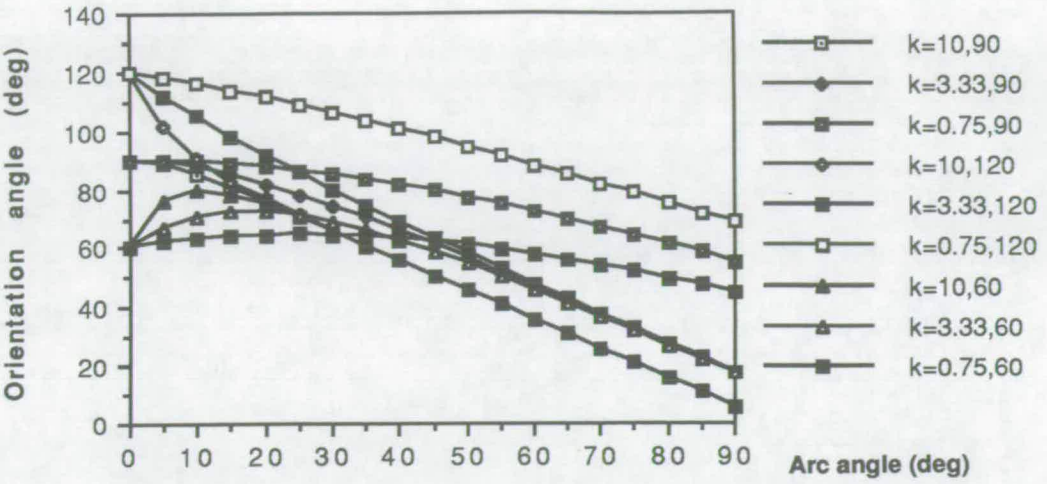

Fig. 3.11 The change of the orientation angle with respect to the passed arc length when the reference point is in front of the rear axle and the initial orientation angle is in the neighborhood of 90°

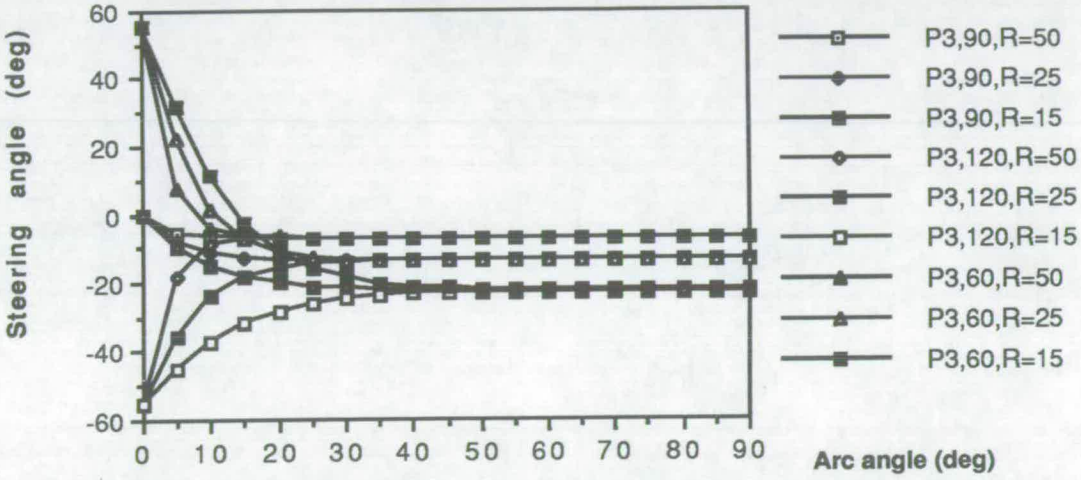

Fig. 3.12 (a) The change of the steering angle with respect to the passed arc length when the reference point is chosen at P3 and the initial orientation angle is in the neighborhood of 90°

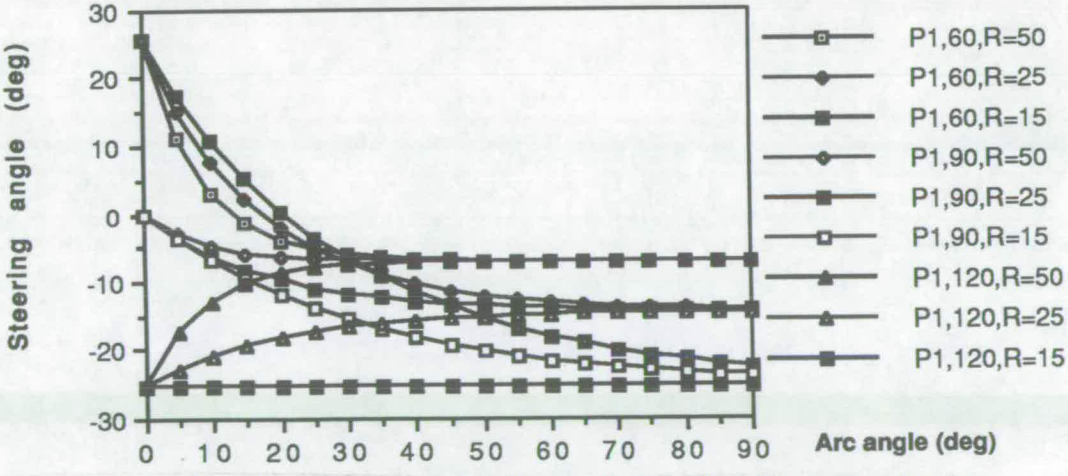

Fig. 3.12 (b) The change of the steering angle with respect to the passed arc length when the reference point is chosen at P1 and the initial orientation angle is in the neighborhood of 90°

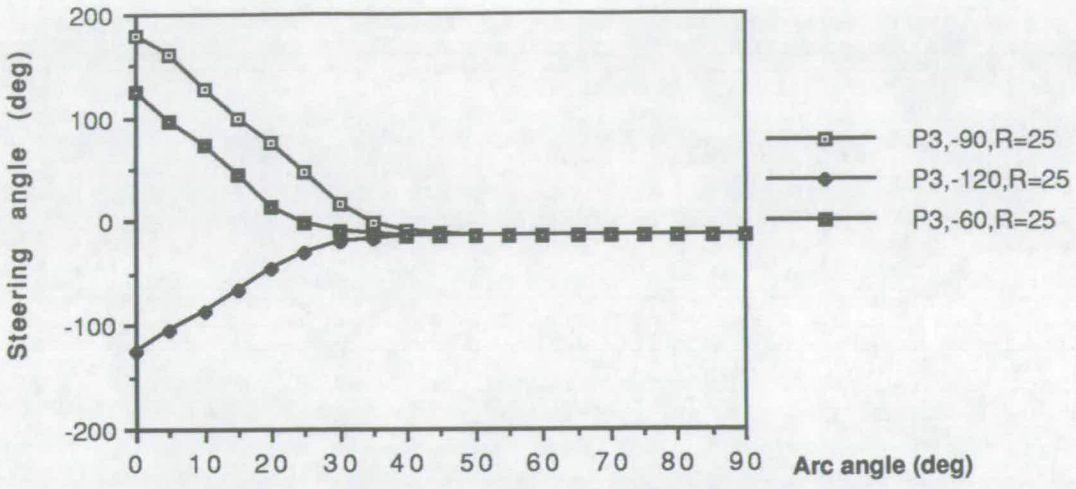

Fig. 3.13 The change of the steering angle with respect to the passed arc length when the reference point is chosen at P3 and the initial orientation angle is in the neighborhood of -90°

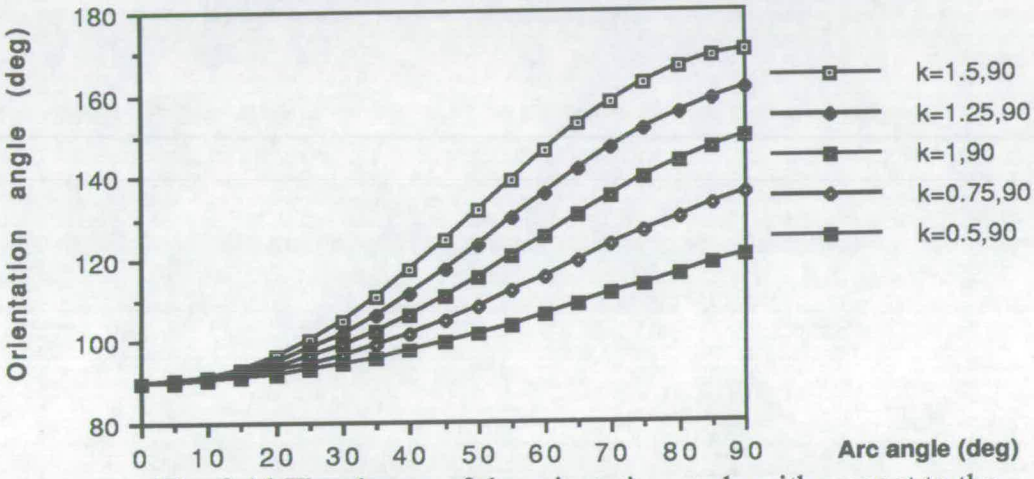

Fig. 3.14 The change of the orientation angle with respect to the passed arc length when the reference point is behind the rear axle and the initial orientation angle is 90°

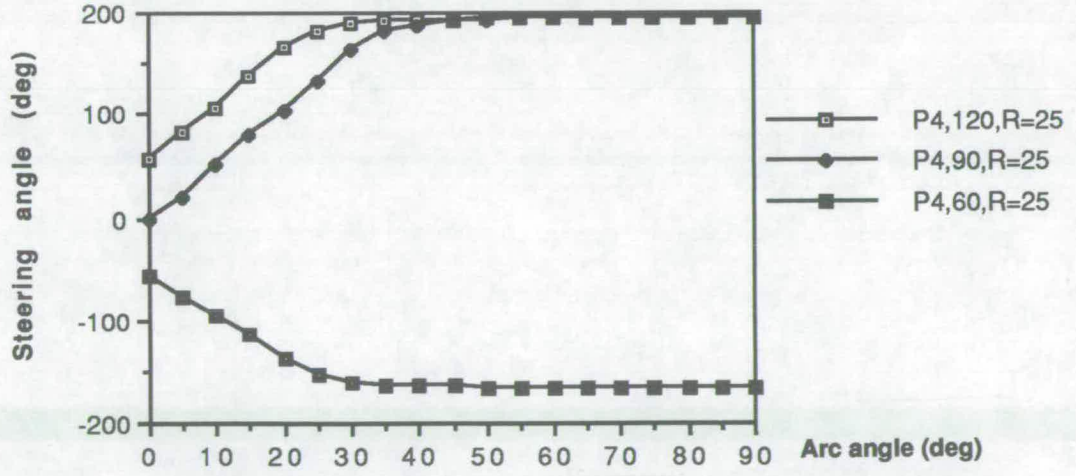

Fig. 3.15 The change of the steering angle with respect to the passed arc length when the reference point is behind the rear axle (P4) and the initial orientation angle is in the neighborhood of 90°

steering angle satisfies the steering angle limit, then the robot can move properly; the required steering angle tends to a steady value. The farther the reference point is chosen from the rear axle, the smaller the required magnitude of the initial steering angle, but the bigger the required magnitude of the steady steering angle.

Case 2: $\underline{x} > 0$

In this case, the reference point P is chosen after the rear axle. For the sake of simplification, the derivation for the expression of the orientation angle is omitted. Using the similar procedure as above, we can obtain the expression of θ as follows:

$$\theta = \begin{cases} 2arc\tan\left(\frac{1}{a}\cdot\frac{az'_0+\tan(\omega t\cdot b)}{1-(az'_0\cdot\tan(\omega t\cdot b))}\right)-\omega t, & k<1 \\ 2arc\tan\left(\frac{z'_0}{1-(\omega t\cdot z'_0)}\right)-\omega t, & k=1 \\ 2arc\tan\left(\frac{1}{c}\cdot\frac{(1+cz'_0)+(cz'_0-1)\cdot e^{\omega td}}{(1+cz'_0)-((cz'_0-1)\cdot e^{\omega td})}\right)-\omega t, & k>1 \end{cases} \quad (3.35)$$

where $k = \frac{R}{\underline{x}}$, a, b, c, d, and z'_0 are defined as they were in the case $\underline{x} < 0$. The steering angle necessary to follow the circle is still determined by (3.24).

Fig. 3.14 shows the change of the orientation angle with respect to ωt when the initial orientation angles are 90°. The heading of the robot turns left while the reference point is making a right turn. This phenomenon is called a pirouette and was reported by researchers on highway design [16]. It is of practical importance for path planning problem. When a pirouette occurs, even if the initial steering angle satisfies the steering limit, the steering angle limit will be reached very quickly. Fig. 3.15 illustrates this point.

Fig. 3.16 is an illustration of orientation angle changes when initial orientation angle are −90°, −120°, and −60°, respectively. Fig. 3.17 shows the corresponding steering angle changes. Clearly, the steering angle limit will be satisfied all the time if initial and steady

steering angles fall into the feasible intervals.

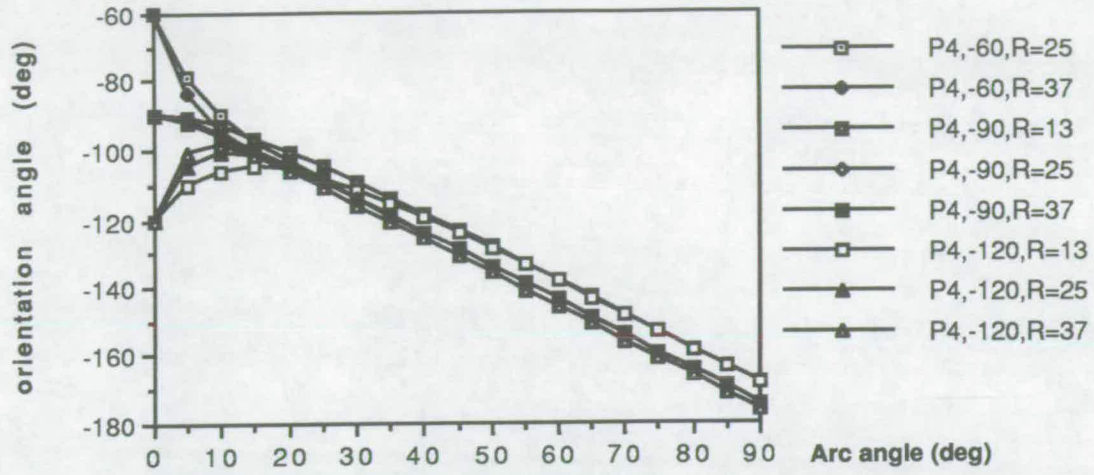

Fig. 3.16 The change of the orientation angle with respect to the passed arc length when the reference point is chosen at P4 and the initial orientation angle is in the neighborhood of -90°

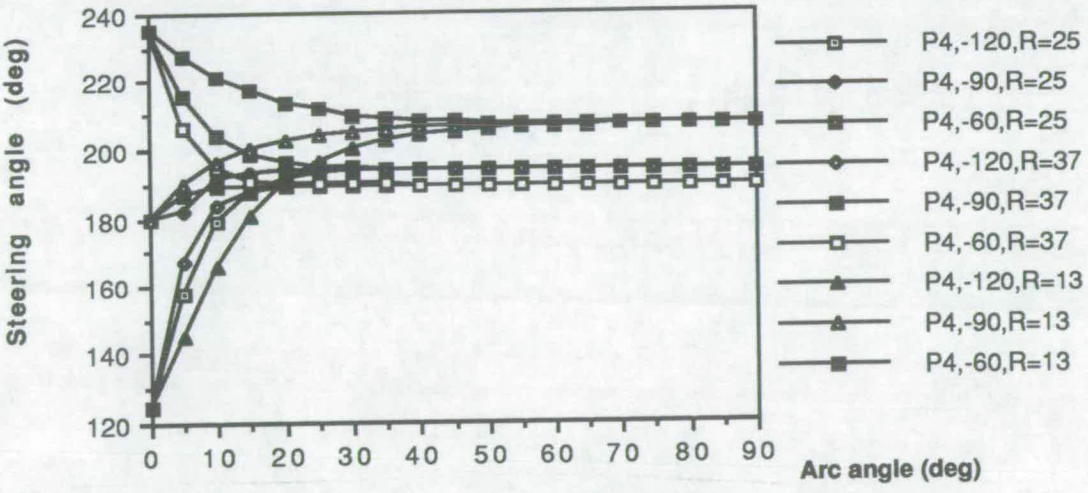

Fig. 3.17 The change of the steering angle with respect to the passed arc length when the reference point is chosen at P4 and the initial orientation angle is in the neighborhood of -90°

Case 3: $\underline{x} = 0$

As mentioned previously, the choice of reference point has very important effect on the orientation angle, and consequently, on all the other parameters. $\underline{x} = 0$ is a special case that means the reference point is chosen at the rear axle connecting the two rear wheels.

Eq. (3.25) yields

$$\theta = 90° - \omega t \tag{3.36}$$

In this case, (3.31) becomes

$$x_m^2 + y_m^2 = x_{m1}^2 + (y_{m1} + R)^2 \tag{3.37}$$

Eq. (3.37) indicates that the path of any point on the robot is a circle. At any instant, the tangent of the reference path coincides with the orientation of the robot, including the initial time.

3.7 Motion smoothness of synchro drive and steering robots

The previous sections in this chapter are devoted to the analyses of motion smoothness and feasibility for a car-like robot or a dual drive robot. The focus of this section will be on the synchro drive and steering robot. From chapter 2, we know the motion of a synchro drive robot can be described as follows:

$$\dot{\theta} = 0 \Rightarrow \theta = \theta_0 \tag{3.38}$$

$$\phi = arc\tan(\dot{y}_p / \dot{x}_p) - \theta_0 = arc\tan(f'(x_p)) - \theta_0 \tag{3.39}$$

$$\omega = (\sqrt{\dot{x}_p^2 + \dot{y}_p^2}) / r \tag{3.40}$$

Although the motion of this type of robot is also a pure translation, the allowed reference path for it is not only a straight line which is the only pure translation allowed for the robots subject to the constraint equation (2.13) (see theorem 3.1), but also any continuous path $y_p = f(x_p)$.

Eq. (3.9) shows that when the robot traverses the line-line transition point, the steering angle is discontinuous at the transition point, and the robot must stop to adjust its steering angle. At the line-circular transition point, the steering angle is continuous and

consequently, the robot can move without stopping.

Generally, we have the following theorem:

Theorem 3.7: *If the (n+1)th derivative of the reference path at any point with respect to x_p is continuous, then the nth derivative of the steering angle of the synchro drive and steering robot at the corresponding point with respect to x_p is continuous.*

3.8 Singularity of omnidirectional robots

In chapter 2, we have established the kinematics of the Omnidirectional robot, and discussed the difficulty of the coordinated control of the four variables υ_a, υ_b, ϕ_{a1}, and ϕ_{b1} to keep all wheels satisfying the ideal rolling condition. The difficulty is caused by the adoption of driving and steering of both wheels A and B simultaneously. In the derivation of the direct kinematics, we assume that one wheel is driven and two wheels are steered.

Theoretically, such a robot can perform any kinds of motions required. In practice, the control is more difficult than imagined. So far, there is no a satisfactory result achieved using this robot.

In the velocity analysis of a manipulator, a matrix quantity called the Jacobian of the manipulator, is introduced to specify a mapping from velocities in Joint space to velocities in Cartesian space. The nature of this mapping changes as the configuration of the manipulators varies. At certain points, called Singularities, this mapping is not veritable. An understanding of the phenomenon is important to designers and users of manipulators.

When a manipulator is in a singular configuration, it loses one or more degrees of freedom as viewed from Cartesian space. The physical explanation of the singularity is that at a singular point, the inverse Jacobian blows up. This results in joint rates approaching infinity as the singularity is approached.

For an omnidirectional robot, a similar phenomenon to the singularities of a manipulator

occurs when the steering angles ϕ_{a1}, ϕ_{b1} approach certain values. In these cases, the needed υ_a for a given $\dot{\theta}$ will tend to infinity.

We rewrite (2.60), (2.62), and (2.63) here:

$$\upsilon_a = \frac{W \cdot \sin(\phi_{b1})}{\sin(\phi_{b1} - \phi_{a1})} \cdot \dot{\theta} \tag{3.41}$$

$$x_a = x_a(0) + \int_0^t (\upsilon_a \cdot \cos(\phi_{a1} + \theta))\, dt \tag{3.42}$$

$$y_a = y_a(0) + \int_0^t (\upsilon_a \cdot \sin(\phi_{a1} + \theta))\, dt \tag{3.43}$$

Case 1: $\phi_{a1} = \phi_{b1}$ and $\phi_{b1} \neq 0$

This means that both wheels are parallel but not pointing forward (see Fig. 2.13). Clearly, from (3.41), it follows that if $\dot{\theta} \neq 0$, then υ_a tends to infinity. The singularity occurs.

The only motion which can avoid an infinity υ_a is

$$\dot{\theta} = 0 \rightarrow \theta = \theta_0 \tag{3.44}$$

The motion is a pure translation. Furthermore, if the steering angles ϕ_{a1} and ϕ_{b1} keep constant, then from (3.42) and (3.43), we can deduce that the reference path is a straight line, whether the υ_a is a constant or not. The expression for the reference path is

$$y_a = y_a(0) + \tan(\phi_{a1} + \theta_0) \cdot (x_a - x_a(0)) \tag{3.45}$$

It should be noted that the direction of the robot is not pointing forward. If the steering

angle varies during the motion, then the reference path is a curve.

Case 2: $\phi_{a1} = \phi_{b1} = 0$

In this case, the structure is like that of the dual drive robot. However, the υ_b is unknown. From (3.41), we can not determine the orientation angle. The robot lost a degree of freedom and the motion of the robot is undetermined.

Case 3: $\phi_{a1} \neq \phi_{b1}$ **and** $\phi_{b1} = 0$

In this case, even if $\dot{\theta} \neq 0$, $\upsilon_a = 0$ still holds. The motion is a pure rotation.

Above analysis shows that an omnidirectional robot is easy to suffer from the singularity problem and more attention should be paid.

3.9 Summary

In this chapter, we have investigated in detail the dependence of the orientation angle and steering angle on the shape of the reference path, the initial orientation angle and the position of the reference point, taking steering angle limit into consideration. The problem solved is how to judge the motion smoothness and feasibility of a robot when it is required to follow a path and, if feasible, how to determine the required steering angle and the velocity.

The continuity of the orientation angle is the first requirement for a smooth and feasible motion. However, if we choose the reference point on the rear axle of the robot and the first derivative of the reference path possesses a discontinuity point, a discontinuity will occur. This means that the reference path is infeasible. Moving the reference point away from the rear axle improves not only the continuity of the orientation angle, but also that of the steering angle, when the same path is followed. A continuous steering angle means that continuous motion without stopping at the transition points of the path is possible.

Steering angle limit is the main factor affecting the maneuvering capacity of the car-like

robot. Theoretically, if no steering limit exists, any continuous reference path can be traced if the reference point is chosen away from the rear axle. In practice, steering angle limit can not be neglected. The concept of the deviation angle interval has been established to describe the motion feasibility of the robot. The advantage of developing the concept is that at any time, the feasible deviation angle intervals are always in the neighborhood of $0°$ and $\pm 180°$. Through the analyses of straight line motion and circular motion, it is further revealed that when the reference point is in front of the rear axle, if the initial deviation angle falls into the feasible interval in the neighborhood of $0°$, then the robot can trace the straight line or circular arc for any length. However, if the initial deviation angle falls into the other feasible interval, i.e., the neighborhood of $\pm 180°$, a pirouette will occur and the steering limit will be reached very quickly; after that, the robot can not trace the reference path any more. When the reference point is chosen behind the rear axle of the robot, the initial orientation angle falls into the neighborhood of $90°$ and the corresponding deviation angle interval falls into the neighborhood of $0°$, a pirouette will occur and the steering limit will be reached very quickly; after that, the robot can not trace the reference path any more.

The above result tells us that if the robot moves forward, the reference point should be chosen in front of the rear axle whereas the reference point should be chosen behind the rear axle when the robot moves backward.

For following a circular path, the position of the reference point affects both the initial steering angle and the steady state steering angle. The farther the reference point is chosen from the rear axle, the smaller the magnitude of the initial steering angle, but the bigger the magnitude of the steady state steering angle. Therefore, a trade-off must be made

The aim of this chapter is to offer a better understanding of the motion of the robot. The results have been tested on a kinematic model of a typical vehicle. Even if the reference point is not at the mass center of the robot, we still can calculate the motion of the mass center of the robot using this model. This is important for the analysis of the dynamics of

the robot. More applications associated with kinematics of a wheeled robot are expected.

The factors investigated in this chapter are, of course, not the only constraints that should be considered in order to guarantee feasible motions for a robot. However, they are among the most important ones and can never be ignored. The other dynamic constraints resulting from the limit of the actuators may usually be satisfied by applying the appropriate time-scaling techniques, or called speed adjustment, to critical segments of the reference path [60].

Chapter 4

Applications of kinematics in highway design

4.1 Introduction

The first stage in highway design occurs when it is decided for social, economic or traffic reasons to link together two areas A and B. It is then the engineer's task to select the optimum terminal positions in A and B, and to specify the route between them so as to achieve the best possible balance between construction costs and user costs.

The engineer, with these objectives and constraints in mind, develops a number of feasible alternative 'lines' (horizontal alignment) giving regard to the associated vertical alignment. Evolution of each line can then be accomplished (primary design) in some detail as a guide for the final choice.

Once a route is selected, detailed calculations and drawings must follow as a basis for contract negotiations and work in the field. The horizontal and vertical position of the center line must be known with great accuracy. In this stage, a mathematical model accurate enough to describe the turning behavior of a vehicle is required, and the minimum turning paths of design vehicles have to be calculated.

4.1.1 Design vehicles

The physical characteristics of vehicles and the proportions of various size vehicles using the highways are positive controls in geometric design. Therefore, it is necessary to examine all vehicle types, select general class groups, and establish representative size vehicles within each class for design use. Design vehicles are selected motor vehicles with the weight, dimensions, and operating characteristics used to establish highway design controls to accommodate vehicles of designated classes. For purpose of geometric design,

Table 4.1 Design vehicle dimensions (ft) (after AASHTO's manual, 1990)

Design vehicle type	Symbol	Overall			Front	Rear	WB_1	WB_2	S	T	WB_3	WB_4
		Height	Width	Length								
Passenger car	P	4.25	7	19	3	5	11					
Single unit truck	SU	13.5	8.5	30	4	6	20					
Single unit bus	BUS	13.5	8.5	40	7	8	25					
Articulated bus	A-BUS	10.5	8.5	60	8.5	9.5	18		4[a]	20[a]		
Combination trucks												
Intermediate semitrailer	WB-40	13.5	8.5	50	4	6	13	27				
Large semitrailer	WB-50	13.5	8.5	55	3	2	20	30				
"Double bottom" semi-trailer---full-trailer	WB-60	13.5	8.5	65	2	3	9.7	20	4[b]	5.4[b]	20.9	
Interstate semitrailer	WB-62*	13.5	8.5	69	3	3	20	40-42				
Interstate semitrailer	WB-67**	13.5	8.5	74	3	3	20	45-47				
Triple semitrailer	WB-96	13.5	8.5	102	2.5	3.3	13.5	20.7	3.3[c]	6[c]	21.7	21.7
Triple double semitrailer	WB-114	13.5	8.5	118	2	2	22	40	2[d]	6[d]	44	
Recreation vehicle												
Motor home	MH		8	30	4	6	20					
Car and camper trailer	P/T		8	49	3	10	11	18	5			
Car and boat trailer	P/B		8	42	3	8	11	15	5			
Motor home and boat-trailer	MH/B		8	53	4	8	20	21	6			

* = Design vehicle with 48' trailer as adopted in 1987 STAA (Surface Transportation Assistance Act);
** = Design vehicle with 53' trailer as grandfathered in 1982 STAA;
a = Combined dimension 24, split is estimated; b = Combined dimension 9.4, split is estimated;
c = Combined dimension 9.3, split is estimated; d = Combined dimension 8, split is estimated;
WB1, WB2, WB3, and WB4 are effective vehicle wheelbase; S is the distance from the rear effective axle to the hitch point;
T is the distance from the hitch point to the lead effective axle of the following unit.

each design vehicle has larger physical dimensions and larger minimum turning radius than those of almost all vehicles in its class. The largest of all the several design vehicles are usually accommodated in the design of freeways.

4.1.2 Need for large vehicles and problems

A review of the range of vehicles, their dimensions and turning characteristics made in ***A Policy on Geometric Design of Rural Highways, AASHTO 1965*** concluded that four design vehicles (P, SU, WB-40, and WB-50, see Table 4.1) would be sufficient for purpose of geometric design.

Eight years later, the examination, made in ***A Policy on Design of Urban Highways and Arterial Streets, AASHTO 1973*** [231], of trends in vehicular sizes, however, shown that in addition to the four design vehicles, two other design vehicles are required, a design vehicle representative of many buses in use (BUS) and a design vehicle representative of semitrailer-fulltrailer combination (WB-60).

Sustained increases in truck weights and dimensions have occurred over the past decade in North America and other parts of the world. The principal stimulus behind these changes is the reduction in unit transportation costs with increasing payload [75]. The surface Transportation Assistance Act (STAA) of 1982 provided badly needed new funding for U.S. highway facilities. No thinking person can deny that the 48-ft. semitrailer which is mandated nationwide, has brought about a major upheaval in the arena of geometric design standards [16]. Further, the double-trailer phenomenon has given rise to a renewed interest in the re-examination of truck turning requirements.

In the manual of ***A Policy on Geometric Design of Highways and Streets, AASHTO 1990*** [232], three general classes of vehicles were selected, namely, passenger cars, trucks, and buses/recreational vehicles. The passenger car class includes compacts and subcompacts plus all light vehicles and light delivery trucks (vans and pickups). The truck class includes single-unit trucks, truck tractor-semitrailer combinations, and trucks or truck tractors with semitrailer in combination with full trailers. Buses/recreational vehicles

include single unit buses, articulated buses, motor homes, and passenger cars or motor homes pulling trailers or boats. The number of representative design vehicles within these general classes has increased to 15 (including the six design vehicles which appear in the 1973 manual), and their dimensions are given in Table 4.1.

The substantial increases in geometric dimensions have important implications for the costs of providing highway infrastructure and for highway safety [75]. There are many highway infrastructure design criteria that are needed to be reassessed in the light of recent evidence on the behavior and properties of trucks using North America highway system. This chapter examines one of these properties, namely, the low speed offtracking at intersections using the analytic formula for straight line and circular motions developed in chapters 2 and 3.

A number of authors have pointed to the problems caused by long wheelbase trucks at intersections. Substantial intrusions into adjacent traffic lanes and/or onto curbs and sidewalks occur at the front of the tractor, the rear corners of the trailer, and the rear wheels of the trailer. Smith [189] has noted that these turning difficulties usually involve substantial disruption to the traffic flow at urban intersections, and lead to significant reductions in traffic capacity. Essentially, solutions to these problems are mainly based on the correct determination of the locus of the dangerous points and the swept volume of the vehicle. The model established in the previous chapters can give solutions to them.

4.2 Review of the related work

When a vehicle turns, the rear wheels track inside the path traced by the front wheels. This behavior is called offtracking and can lead to problems when large trucks operate in confined areas. Offtracking has a history of documented study going back at least 33 years [64]. During the period of recorded study, several different definitions have been advanced, each typically reflecting the concerns of the research approach. A detailed explanation of the basic research methodologies and perspectives was presented in the reference [64] to help develop a basis for understanding the concepts used to define and

quantify offtracking. These methodologies include full-scale tests; scale-model tests; mathematical and graphic procedure; and more recently, computer-model simulation.

The earliest offtracking research involved measurements using actual vehicles on test track curves of known radius. After that, scale-model work proved much more expeditious than using actual vehicles, and these tools provided most of the source drawing from which existing turning templates were originally developed. The tractrix integrator is the most widely known and used of the template-drawing scale-model devices.

The mathematical and graphic techniques depend quite explicitly on the geometric relationships demonstrated in offtracking. In the 1964 handbook of the Society of Automotive Engineers (SAE), a formula for offtracking of a single two-axle vehicle was presented as follows:

$$OT = \{WB^2 + [(TR^2 - WB^2)^{1/2} - HT]^2\}^{1/2} - (TR^2 - WB^2)^{1/2} + HT \qquad (4.1)$$

where OT = offtracking; WB = wheelbase; HT = half of the front wheel track; and TR = turning radius of outside front wheel.

This formula is based on the well-known pythagorean theorem and becomes more complex as vehicle combination is considered. The annually published handbooks carefully defined and explained this formula up to and through the 1972 issue. However, beginning with 1973 volume, SAE dropped much of the prior detail and revised the text to introduce the West Highway Institute (WHI) offtracking formula, which is widely used for the design of highway.

The statement included in 1973 SAE volume (pp. 1209) is as follows: ***In recent years, there have been developed data which are accurate enough to use for all practical purpose. The method was developed by the Western Highway Institute..... It is this method, easy to calculate and simple to apply, which is recommended as a general practice*** [64].

A detailed discussion of the WHI formula, its derivation, and its accuracy in comparison with results obtained via other methods were presented in WHI's research Committee

report 3 [235]. The WHI formula can be expressed as follows:

$$OT = R - (R - \sum L^2)^{1/2} \tag{4.2}$$

$$\sum L^2 = WB_1{}^2 - ac_1^2 + ca_1{}^2 - ac_2{}^2 + ca_2{}^2 + WB_2{}^2 \tag{4.3}$$

where R = radius of the circular curve followed by the front axle center; WB_1 = tractor wheelbase; ac_1 = fifth wheel offset; ca_1 = kingpin to rear tandem centre line; ac_2 = center line of rear tandem to pintle hook; ca_2 = pintle hook to centre line of dolly axle; and WB_2 = Full-trailer wheelbase, as shown in Fig. 4.1.

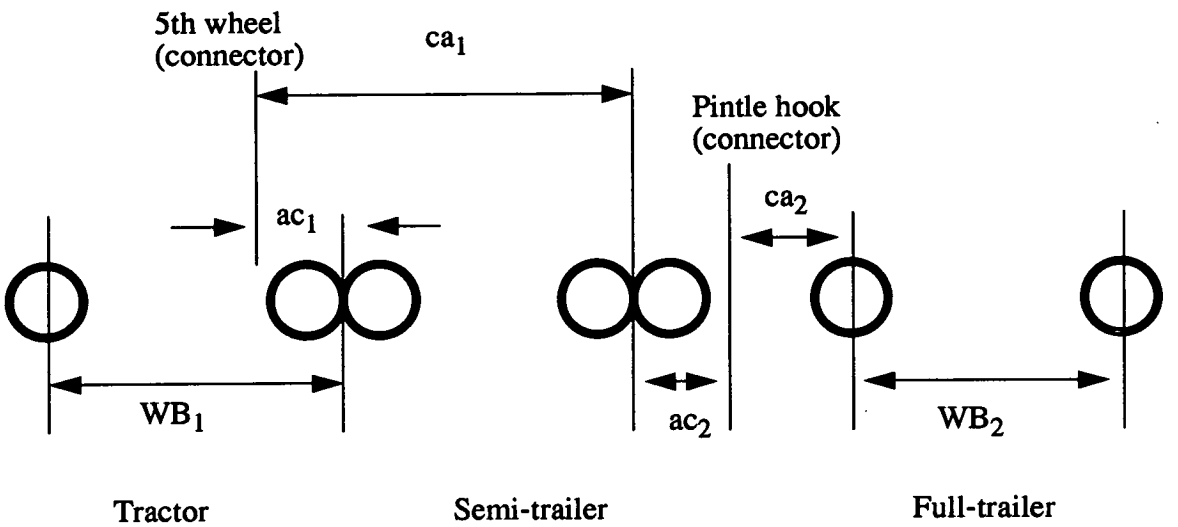

Fig. 4.1 General illustration for a semitrailer full-trailer combination

The problem pointed out by Heald [64] is that the WHI formula may break down for long units on short-radius curves. A practical example of this has been shown in reference [173]. The reason for that can be explained as follows using the analytic formula (3.30) and (3.32) for a circular motion developed in chapter 3.

Before explaining the problem, we need to define a stead state motion as one that is reached when a vehicle or a vehicle combination traces a circle and the number of turns tends to infinity. Essentially, the WHI formula describes the steady-state motion of a vehi-

cle or a vehicle combination, and gives only the maximum offtracking that will eventually be reached for a given vehicle dimension and input radius. However, for many large trucks, the steady state motion is not reached until the vehicle has turned more than 360 degrees. The model presented in this thesis gives a transient description of the vehicles. Using this mathematical model, we can prove that the WHI formula is a special result of this model. This can be observed from (3.30) when ωt tends to infinite. In this case, $\theta + \omega t \rightarrow 2arc\tan(c)$, a constant. The path of each point on the vehicle becomes a circle. The path taken by the hitch point is the input for the trailer, just like the path taken by the front wheel is the input for the tractor. This procedure can be extended to more trailing units.

Eq. (3.30) also indicates that d is an important factor affecting the speed needed to reach the steady state condition. If the radius of the circle is fixed, then the bigger the length of the wheelbase of a truck, the smaller d, and the longer the length of the path passed by the reference point, the larger the error when the WHI formula is used. This explains that the WHI formula can give a reasonable approximation when the truck's wheelbase is small, but is not applicable to very large trucks.

The assumption used in the model and the WHI is the same, i.e., all the wheels roll without slipping. The only difference is that our model gives a transient description of the vehicle while the WHI describes the steady-state motion.

Another method developed in reference [173] gives a transient description of the turning behavior. However, this method is basically a computation simulation of the tractrix integrator and the accuracy is not sufficient enough.

None of the methods discussed thus far is completely satisfactory as an everyday design tool. The model developed in chapter 3 can serve as tool for that purpose.

4.3 Simulation results and discussions

In highway design, the determination of the minimum turning paths of design vehicles is

Table 4.2. Comparison of the results from our model with the existing standards (SD = standard data extracted from AASHTO's manuals, 1973 and 1990, respectively; OURS = results from our model; ER = error)

Design vehicle type	Passenger car			Single unit truck			Single unit bus			Semitrailer intermediate			Combination large		
Symbol	P			SU			BUS			WB-40			WB-50		
Figure	G-1			G-2			G-3			G-4			G-5		
Min. turning radius (ft)	24	24		42	42		42	42		40	40		45	45	
Min. inside radius (ft) 1973	15.3	15.3	0%	28.4	28.5	0.4%	20.3	25.4	25%	19.9	19.4	2.5%	19.8	19.7	0.3%
1990	13.8		11%	27.8		2.5%	24.4		4%	18.9		2.5%	19.2		1.5%
Max. outside radius (ft) 1973	25.8	25.9	0.4%	43.9	44.0	0.2%	47.1	46.5	1.3%	41.2	41.5	0.7%	46.2	46.3	0.2%
1990	25.5		1.6%	44.1		0.2%	46.5		0%	41.5		0%	46.3		0%
Max. steering angle (rad)		-35.6			-35.0			-44.1			-24.0			-28.6	
	SD	OURS	ER	SD	OURS	ER	SD	OURS	ER	SD	OURS	ER	SD	OURS	ER

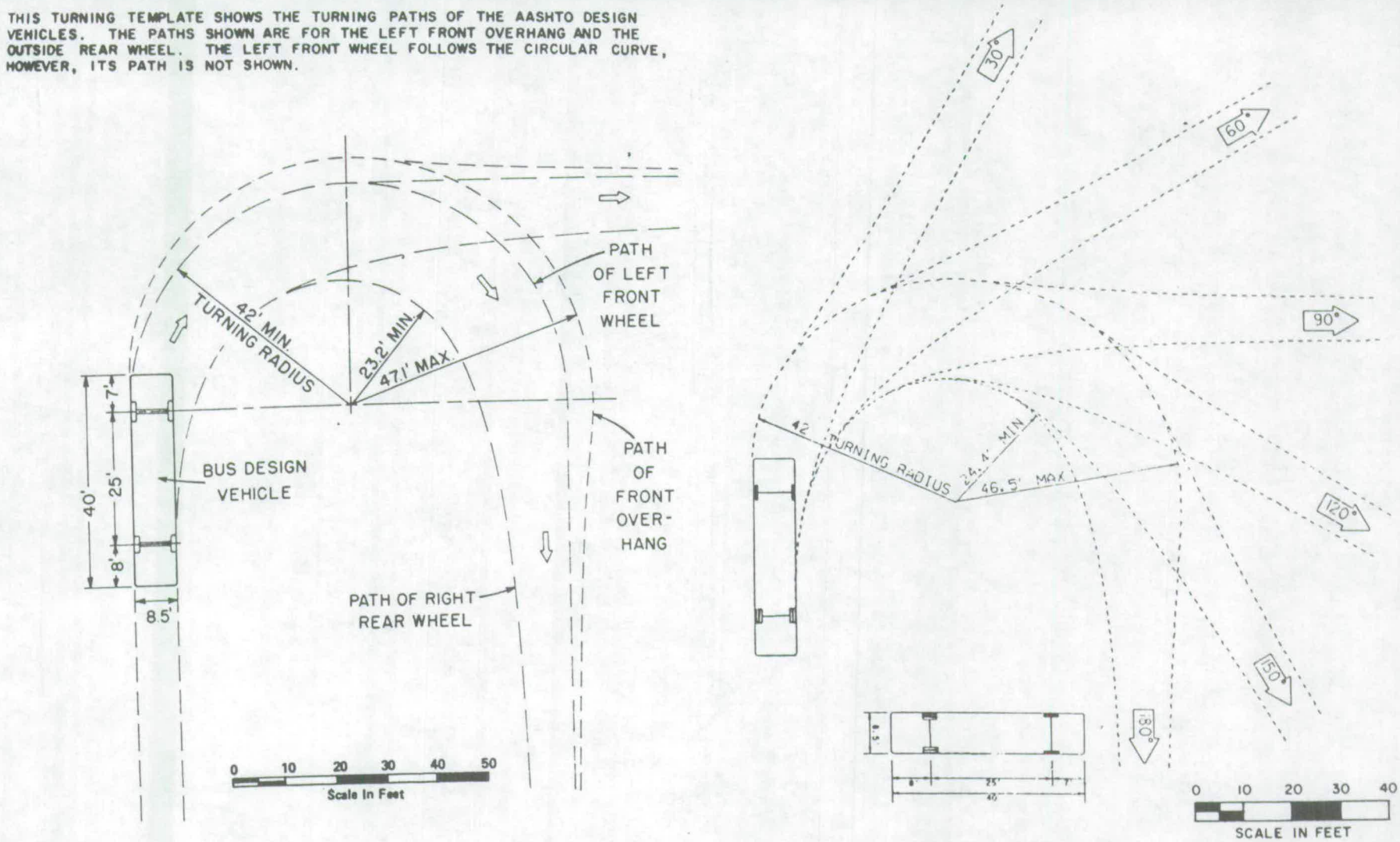

(a) 1973

(b) 1990

Fig. 4.2 Minimum turning paths for design vehicle BUS (after AASHTO's manuals, 1973 and 1990, respectively)

an important problem. In the following the simulation results from the present model are compared with the standards given in ***A policy 1973*** [231] and ***A policy 1990*** [232], respectively. Fig. 4.2 (a) and (b) present only the minimum turning paths for the design vehicle BUS given in ***A policy 1973*** and ***A policy 1990***, respectively. The other figures included in them for P, SU, WB-40, and WB-50 are not cited here for the limitation of the space, but their dimensions are given in Table 4.1.

The boundaries of the turning paths of the several design vehicles when making the sharpest turn are established by the outer trace of the front overhang and the path of the inner rear wheel. This turn assumes that the outer front wheel first follows a circular arc which is the minimum turning radius as determined by the vehicle steering mechanism and then follows a straight line. Thus, the path of the reference point is given as the forms of (3.14) for the straight line motion and (3.21) for the circular turn, respectively. Based on the geometric dimensions given in Table 4.1 (the dimensions of the design vehicles for P, SU, Bus, WB-40, and WB-50 in A policy 1973 and 1990 are identical), the minimum outside and inside wheel paths from this model and from the standards are all shown in Table 4.2.

In the practical programming, the reference point is chosen at the front left wheel, and the initial orientation angle for the circular curve is 90° as required. More attention should be paid to the transition from the circular curve to the straight line (see Fig. 3.9). The calculated orientation angle of the vehicle at the end of the circular curve must be treated as the initial orientation angle for the straight line motion.

In the calculation of the minimum radius and maximum outside radius for the WB-40 and WB-50, the most widely used fourth-order **Runge-Kutta** method [154] was used to solve the general constraint equation (2.13) for the trailer's orientation angle, while the orientation angle of the tractor is calculated directly from the closed-form formula (3.30) for the circular motion and (3.17) for the straight line motion, respectively.

Let us compare our results with the standards. From Table 4.2, it can be observed that the error of the maximum outside radius is smaller than that of the minimum inside radius. This is because the overhang of each vehicle is much smaller than the corresponding

wheelbase. For small vehicles (P and SU) given in ***A policy 1973***, both of the errors are reasonable. However, as the wheelbase increases (BUS), the error of the minimum inside radius increases rapidly, reaching 25%. If a larger vehicle is allowed, then a model that can describe the transient motion of the vehicle is necessary. The model described previously can meet this requirement. For WB-40 and WB-50, the minimum inside radius and maximum outside radius from the simulation are smaller and larger than those from the standards, respectively.

In ***A policy 1990***, the resolution for both minimum and maximum turning radii for large vehicles is significantly improved. However, on the other hand, the resolution for small design vehicle (P and SU) becomes very poor (11%). This phenomenon can not be explained because the 1990 manual did not describe the compensation method used for calculating the minimum and maximum turning radii for various vehicles.

Table 4.2 also shows the maximum steering angle needed for the outer front wheel to follow the circular arc. This is not given in ***A Policy 1973 and A policy 1990.*** In fact, the minimum turning radius should be determined from equation (3.33) provided the dimension of a design vehicle and its maximum steering angle are given.

Chapter 5

On the suitability of path planning algorithms to four kinds of wheeled mobile robots

5.1 Introduction

The path planning problem for wheeled mobile robots has been drawing more and more attention since the late 1960s. Over the last decade, the number of papers published on the related issues has increased rapidly. The motivations behind the research arise mainly from the increasing demands on autonomous wheeled robots. The solution to path planning problem will play an essential role in the development of an autonomous robot.

This problem is well-known as a find-path problem [114], and the complexity involved in solving it has been shown in reference [177]. The problem can be described as: given an object (a wheeled mobile robot) with an initial location and orientation, a goal location and orientation, and a set of obstacles located in workspace, find a continuous path for the object from the initial location and orientation to the goal location and orientation which avoids any collision with obstacles along the path.

In order to solve this problem, a large variety of effort has been made on this seemly simple, but in fact very complicated find-path problem since the early 1970s. Various methods for dealing with the basic find-path problem and its various extensions, such as *Vgraph, Voronoi diagram, exact cell decomposition, approximate cell decomposition and potential field* approaches, have been developed. A systematic discussion on robot motion planning can be found in reference [101].

As pointed out previously, there are four kinds of wheeled mobile robots. The various mechanical structures of these robots result in their different motion characteristics.

Unfortunately, the effects of various mechanical structures on the path planning problem have not been taken seriously and correctly. Most algorithms presently available made the assumption that the robot is a point or a free moving rigid body such as a sofa, a piano or a ladder [72, 116, 174, 175]. However, for the most commonly used car-like and dual drive robots, this assumption is not attainable. One of the questions we are interested in here is what kind of wheeled mobile robots can be treated as a point or a free moving robot and what conditions are needed to achieve it. Our previous work [210--214] showed that all the algorithms available, when applied to a car-like robot with a steering angle limit, can not be guaranteed to generate a safe and executable path. The reason for this is that the point robot or the free moving robot assumption is not applicable to a car-like robot.

The purpose of this chapter is first to give a brief but critical review of the algorithms presently available for wheeled mobile robots and then to investigate their suitability to each of the four kinds of robots. We will only consider the simplest path planning problem, i.e., moving a robot among known, static obstacles from start location to goal location.

Let us introduce some notations and assumptions in advance. Let A be the robot being moved in the workspace W, and B_i (i=1,2,.....,n) be the polygonal obstacles. Findpath can be described as: Find a path for A from configuration S to configuration G such that A is always in W and all configurations of A on the path are safe. This path is called a safe path. In the subsequent sections, the following assumptions are made:

- The locations of B_i are known to high accuracy and the path of A can be controlled to the same precision.
- The robot A is the only robot in W.
- The robot and obstacles are rigid objects, i.e., objects whose points are fixed with respect to one another.

5.2 Review of the path planning approaches

5.2.1 Path planning approaches for a point robot

Consider the problem that a point object A is required to move from position S to position G without colliding with obstacles B_i (i = 1, 2, ..., n). In this case, the area swept out by all possible paths of A that avoids obstacles B_i is simply the complement of B_i. Any path contained in the complement of B_i is legal, and vice-versa. Therefore, we can use the description of the complement of B_i to represent the set of legal paths. This complement is known as the free space for A.

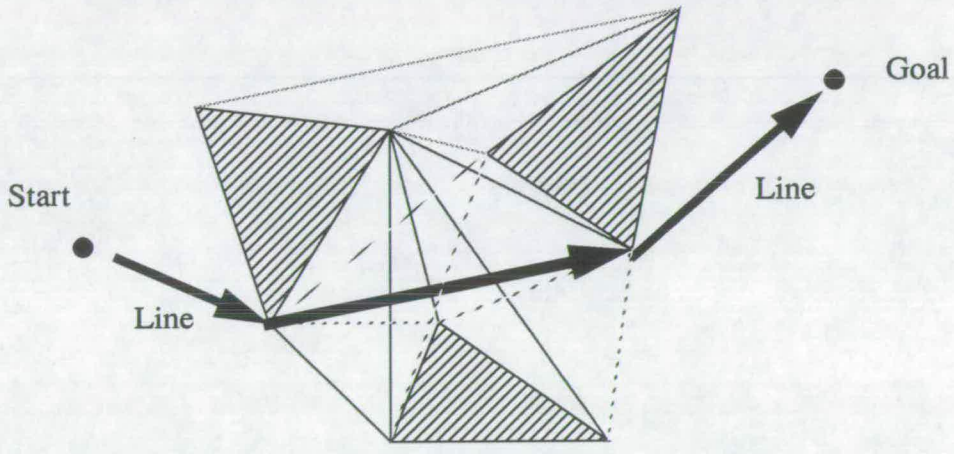

Fig. 5.1 Visibility graph with polygonal obstacles

I. Vgraph approach [115]

The Visibility graph (Vgraph) method is one of the earliest path planning methods. An undirected graph describing the position of the obstacles and the start point S and the goal point G in the workspace is denoted by VG(N,L) where N is the union of S, G and all the obstacles' vertices; L, the link set, is the set of all the links (N_i, N_j) such that a straight line exists connecting the ith element of N to the jth without overlapping any obstacle. The graph VG(N,L) is thus called the 'visibility graph' of N, since the connected vertices in the graph can see (no collision) each other. The Vgraph is shown (dotted lines) in Fig. 5.1

under the assumption of polygonal obstacles. The shortest collision-free path from S to G on the plane is the shortest path in the Vgraph starting from the corresponding node S to the corresponding node G, as also shown in Fig. 5.1. This method for finding the shortest collision-free path for a point in a Vgraph is called the Vgraph algorithm, and the resulting shortest path, if it exists, is composed of straight lines connecting the start point and the goal point and passing through a number of vertices belonging to the different obstacles in the environment.

The advantage of the Vgraph approach is that it is non-heuristic technique which means that it guarantees that the search can find a path if it exists, and the generated path is always the shortest one.

II. Voronoi diagram approach [77]

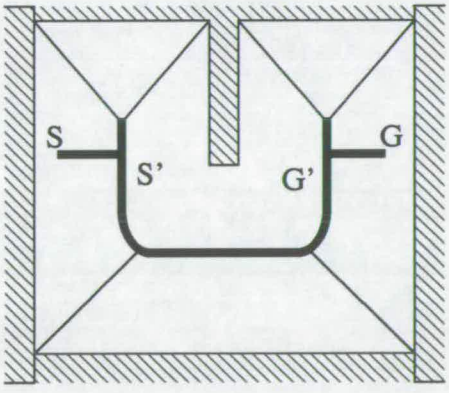

Fig. 5.2 Illustration of Voronoi diagram

The retraction approach consists of defining a continuous mapping of the robot's free space onto a one-dimensional network of curves lying in the free space. In 2-D space, robot's free space is typically retracted onto its Voronoi diagram. This diagram is the set of all the free configurations whose minimal distance to the obstacle region is achieved with at least two points in the boundary of the obstacles. Fig. 5.2 illustrates a Voronoi diagram method. The interesting property of this diagram is that it maximizes the clearance between the robot and the obstacles. Under the assumption of polygonal obstacles, the

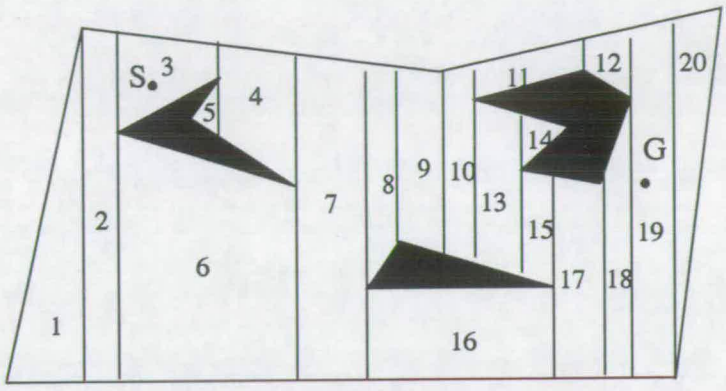

Fig. 5.3 (a) Free space is decomposed into trapezoidal and triangular cells

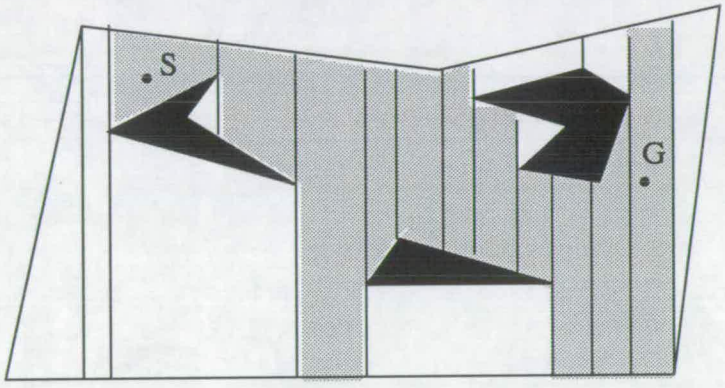

Fig. 5.3 (b) A path in the connectivity graph determines a channel

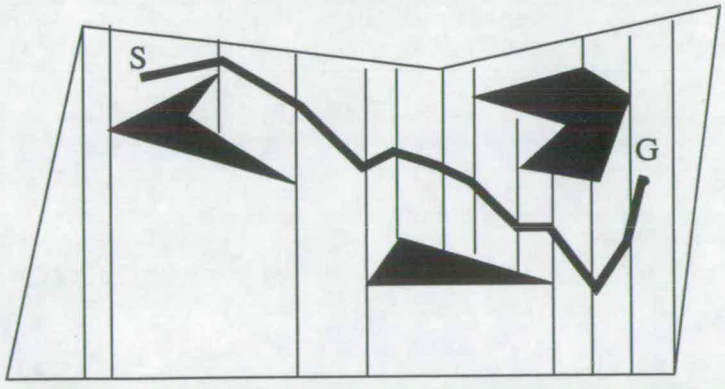

Fig. 5.3 (c) A path is generated by connecting the initial configuration to the goal configuration through the midpoints of the intersections of every successive cell

Voronoi diagram consists of a finite collection of straight line and parabolic curve segments, which we call arcs.

The initial and goal configurations are retracted in the diagram to S' and G' as shown in Fig. 5.2. A path is searched in the diagram between S' and G'. The free path between S and G generated by this approach, consists of three subpaths: the straight line path from S to S', a path in the diagram from S' to G', and the straight line path from G' to G.

III. Exact cell decomposition approach [101]

Exact cell decomposition methods are perhaps the motion planning methods which have been the most extensively studied ones so far. They consist of decomposing the robot's free space into simple regions, called *cells*, such that a path between any two configuration spaces in a cell can be easily generated. A non-directed graph representing the adjacency relation between the cells is then constructed and searched. This graph is called the *connectivity graph.* Its nodes are the cells extracted from the free space and two nodes are connected by a link if and only if the two corresponding cells are adjacent. The outcome of the search is a sequence of cells called a *channel.* A continuous free path can be computed from this sequence.

Fig. 5.3 (a), (b) and (c) illustrate an exact cell decomposition method in a two-dimensional configuration space. The free space is externally bounded by a polygon and internally bounded by three polygons. The free space is exactly decomposed into trapezoidal and triangular cells. These cells are built by drawing vertical rays from the obstacles' vertices. Two cells are adjacent if they share a portion of an edge of non-zero length. Once the connectivity graph has been constructed and a channel found, a free path is computed by connecting the initial configuration to the goal configuration through the midpoints of the intersections of every two successive cells.

IV. Approximate cell decomposition approach [24, 30]

Another cell decomposition approach is known as the approximate cell decomposition approach. It consists again of representing the robot's free space as a collection of cells.

But it differs from the exact approach in that the cells are now required to have a simple prespecified shape, e.g. a rectangloid shape. Such cells do not in general allow us to represent free space exactly. Instead, a conservative approximation of this space is constructed, hence the name of the approach. As with the exact approach, a connectivity graph representing the adjacency relation among the cells is built and searched for a path.

Fig. 5.4 illustrates an approximate cell decomposition method developed by Brooks and Lozano-perez [24]. The free space is externally bounded by a rectangle and internally bounded by three polygons. The rectangles are each given a status which can be:

- Empty: if the rectangle does not intersect an obstacle.
- Full: if the interior of the rectangle everywhere intersects one or more obstacles.
- Mixed: if there are interior points inside and outside the obstacles.

The path is found by searching for a connected set of empty rectangles. If such a path can not be found then mixed rectangles must be divided up into smaller full, mixed and empty rectangles until either a path is found or failure is indicated.

Each decomposition generates four identical new rectangles. Because this type of decomposition can be represented as a tree of degree 4, it is called a "quadtree" decomposition method. At some level of resolution, only the cells whose interiors lie entirely in the free space are used to construct the connectivity graph. If the search of this graph terminates successfully, a path in the free space is easily generated. Otherwise, it may mean that either the resolution of the decomposition is insufficient, or no free path exists between the initial and goal configurations. Often, an approximate cell decomposition method operates in a hierarchical fashion by using a rather coarse resolution at the beginning, and refining it until either a free path is found or a limit resolution is attained.

Provided that they are equipped with both approximate search techniques and exact numerical computation techniques, exact cell decomposition methods are complete, i.e.,

they are guaranteed to find a free path whenever one exists and to return failure otherwise.

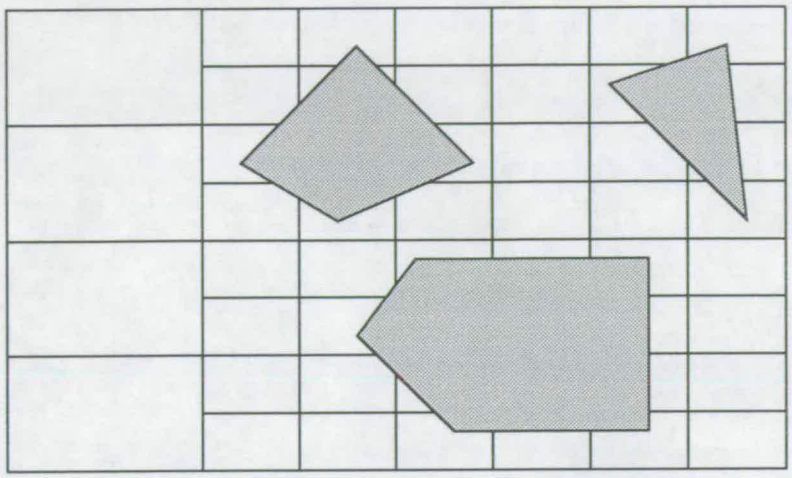

(a)

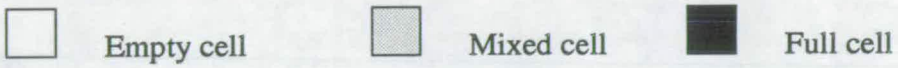

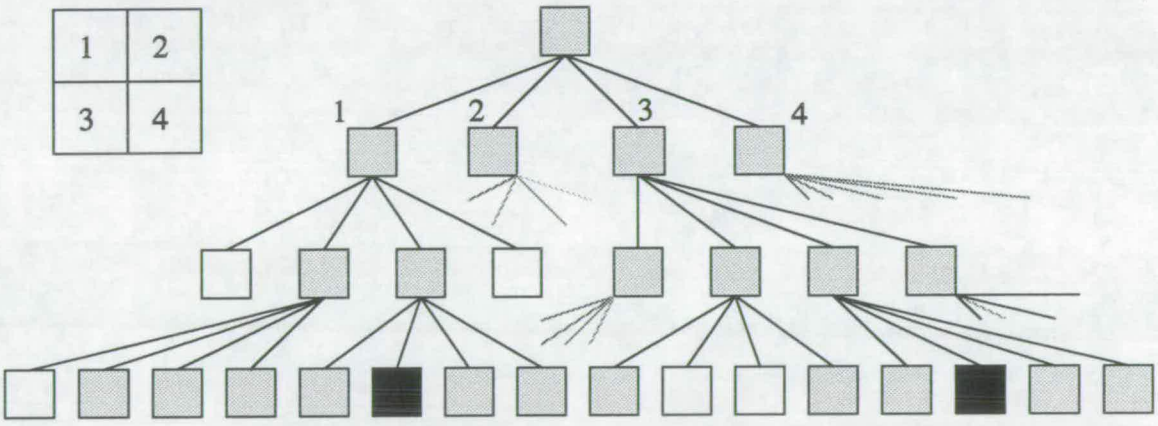

(b)

Fig. 5.4 A quadtree decomposition is obtained by recursively dividing the workspace and the generated Mixed cells into smaller cells. The division of a cell creates four new rectangloid cells of equal dimensions. Figure (a) shows the quadtree decomposition at depth 3. Figure (b) shows a subset of the corresponding tree.

Approximate methods may not be complete; but, for most of them, the precision of the approximation can be tuned and made arbitrarily small at the expense of the running time. Therefore, the methods are said to be "resolution-complete". On the other hand, except in very simple cases, exact methods are mathematically more involved than approximate

ones. Hence, the latter are usually easier to implement.

V. Potential field approach [76, 90]

This approach was pioneered by Khatib [90] and followed by many researchers [76, 208]. It treats the robot represented as a point in configuration space as a particle under the influence of an artificial potential field **U** around obstacles which present potential collision hazards in the workspace. The potential function is typically defined as the sum of an attractive potential pulling the robot toward the goal configuration and a repulsive potential pushing the robot away from the obstacles. Path planning is performed iteratively. At each iteration, the direction of the artificial force induced by the potential function at the current configuration is regarded as the most promising direction of motion, and the path generation proceeds along this direction by some increment.

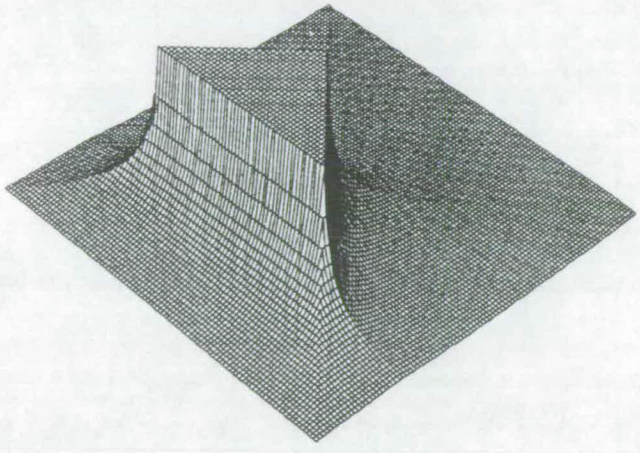

Fig. 5.5 Potential function due to a 2-D triangular obstacle. The potential is arbitrarily large inside the obstacle and decreases roughly as the inverse of the distance outside the obstacle

Fig. 5.5 is an illustration of the potential field due to a 2-D triangular obstacle. The potential is arbitrarily large inside the obstacle and decreases roughly as the inverse of the distance outside the obstacle.

Potential field approach was originally developed as an on-line collision avoidance

approach, applicable when the robot does not have a prior model of the obstacles, but senses them during motion execution [101]. Emphasis was put on real-time efficiency, rather than on guaranteeing the attainment of the goal. Although its efficiency, there are some disadvantages. First, this approach is not a purely geometric one, but dependent on the definition of the potential function. This means that even for the same robot and environment, different definitions of the potential function may lead to contrast results. For example, one may give a successful path and the other may report failure. Second, since an on-line potential field approach essentially acts as a fastest decent optimization procedure, it may get stuck at a local minimum of the potential function other than the goal configuration. Dealing with local minima is the major issue that one has to face in designing a planner based on this approach. It seems to be difficult to define a versatile potential function which has an analytical expression for various obstacle distributions in the workspace and meanwhile has no or few local minimums.

The simplicity of the aforementioned approaches (I--V) stems from the assumption that the robot is a point. Under this assumption, the configuration of a robot is totally determined by the position x and y of the reference point, and the orientation angle of the robot is neglected. This is a good approximation for robots which are much smaller compared with the gaps between the obstacles. In most cases, however, this assumption can cause problems because a movable robot must have its own dimension.

5.2.2 Concept of Cspace Obstacles [114]

It can be seen that the aforementioned approaches require the robot to be a point whilst the obstacles are forbidden regions for that point. If the robot is not a point, then a new set of grown obstacles must be computed which are the forbidden regions for a 'reference point' on the moving object. The new grown obstacles must describe the area where the reference point must not fall to avoid collisions with any of the original obstacles. The operation of computing the new grown obstacles from the original ones and a robot A is called growing obstacle and shrinking the object, and the new grown obstacles are called Cspace Obstacles, denoted as $CO_A(B)$. The formal definition of $CO_A(B)$ can be described

as follows:

$$CO_A(B) = \{x \in Cspace | (A_x \cap B \neq \emptyset)\}$$

Fig. 5.6 shows an example of the $CO_A(B)$ as shaded region when the robot and the obstacles are all polygons and the orientation of A is fixed. The boundary of the generated $CO_A(B)$ consists of line segments.

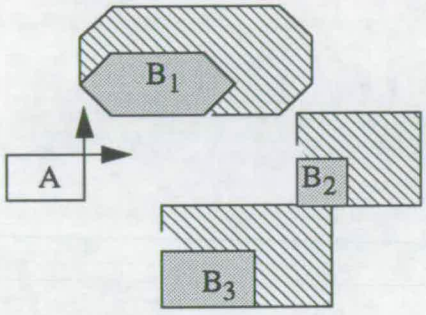

Fig. 5.6 Cspace obstacles due to B for fixed orientation of A

This concept is one of the most important in robotics. The idea was first popularized by Lozano-Perez [114] as a basis of the spatial planning approach for the find-path and find-place problems and then extended by Latombe [101] as a basis of all motion planning approaches suitable for a point robot.

5.2.3 Circular robots: a special case where orientation angle change has no effect on $CO_A(B)$

A simple generation of the first problem (a point object) is to make the robot a circle with a radius R. Under the assumption of polygonal obstacles, choosing the reference point at the center of the robot and then growing the obstacles R units result in a $CO_A(B)$ bounded by line segments and circular arcs. The generated $CO_A(B)$ is called generalized polygons [103], as shown in Fig. 5.7. Obviously, any path contained in the complement of the $CO_A(B)$ is collision-free and vice-versa. This is a special case where the orientation angle

change has no effect on the $CO_A(B)$ and the approaches for a point robot may be directly applied to the generalized $CO_A(B)$.

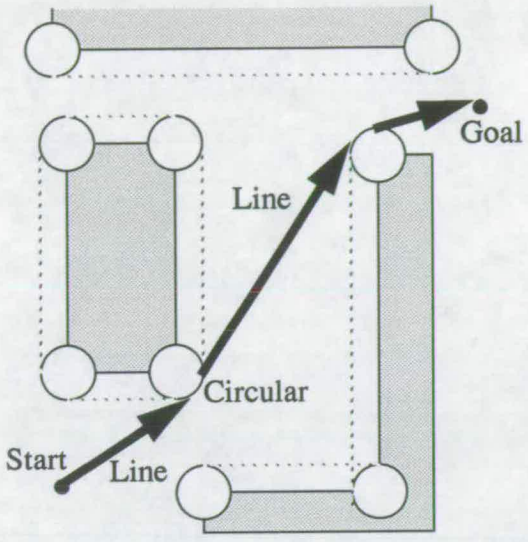

Fig. 5.7 Shortest path generated by the generalized Vgraph method for a circular robot with the reference point on the center

Fig. 5.7 shows an example of the shortest collision-free path generated by the generalized Vgraph method [115]. Note that the shortest path generated using this method consists of a collection of straight lines and circular arcs. In principle, the other four approaches may also be adapted to the generalized polygons. However, to our best knowledge, there are no reports addressing this problem.

5.2.4 Polygonal robots with fixed orientation [114]

It can be seen that the shape of the robot has a very important effect on the path planning problem. A point robot or a circular robot is only a special case. A more general presentation of a robot's shape is a polygon. Under the polygonal assumption, the effect of the orientation change of the robot on the $CO_A(B)$ can not be neglected.

The location of a mobile robot moving on a plane can be uniquely specified by three parameters, i.e., the position (x_p, y_p) of a reference point P and the orientation angle θ of the robot. If we know the configuration (x_p, y_p, θ) of a robot, then we can find the

location of any other point (x, y) on the robot as well as the envelope of the area swept. If the orientation of a polygonal robot A is fixed, only the position of the reference point P is sufficient to specify the robot's configuration. In this case, the find-path problem for A among B_i is equivalent to the find-path problem for a point robot (the reference point) among the $CO_A(B)$. To find a path, two steps are needed:

1. Compute the $CO_A(B)$;

2. Find the path by any one of the approaches for a point robot among $CO_A(B)$.

For the efficiency of computing $CO_A(B)$, the reference point of A is not chosen in the center of the robot, but instead at one of its vertices, and the resulting $CO_A(B)$ is still a set of polygons. In Fig. 5.8, the $CO_A(B)$ has been computed as the shaded region, around which the shortest collision-free path is shown.

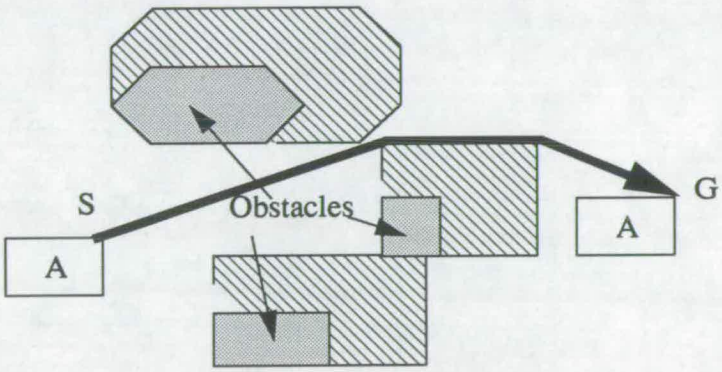

Fig. 5.8 A polygonal robot with fixed orientation

Up to this stage, we have not changed the orientation of the polygonal robot. Problems arise when rotations in a polygonal robot are allowed.

5.2.5 Polygonal robots with variable orientation [115]

When A is a rigid object which is allowed to rotate, an approach of slice projection of the $CO_A(B)$ has been proposed by Lozano-perez [115]. Fig. 5.9 shows an example, given in [115], of this approach by projection of (x, y, θ) on the (x, y) plane. The objects shown

shaded represent the (x, y) projection of three θ-slices of $CO_A(B)$ when A and B are convex polygons. This figure also shows a polygonal approximation to the slice projection and polygonal approximation to swept area from which it derives. These slices represent configurations where A overlaps B for some orientation of A in the specified range of θ. Lozano-perez [115] gave a proof that these slice projections are equivalent to the $CO_A(B)$ of the area swept out by A over the range of orientations of the slice. Obviously, a solution to a findpath problem in any of the slices is a solution to the original problem, but since the slices are an approximation to the $CO_A(B)$, the converse is not necessarily true.

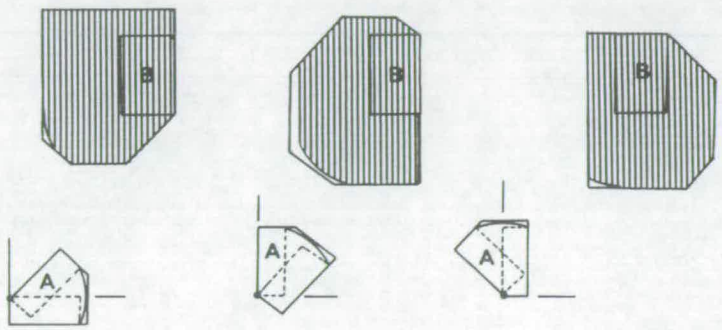

Fig. 5.9 Slice projection of $CO_A(B)$ computed using (x, y)-area swept out by A over a range of θ values

This slice projection method was thought to be complete. That means if there is a path available, this method certainly can find it. In our opinion, there are still some difficulties to use it. In this section, we only analyze the drawbacks of the slice-projection when it is applied to the free moving robot such as an omnidirectional robot, the fundamental drawbacks of all the algorithms available (including the slice projection method) when they are applied to the car-like robots and the dual drive robots will be analyzed in the next section. First, we examine the steps needed for the find-path problem using the slice projection method.

As noticed, when rotations of A are allowed, a number of slice projections of the $CO_A(B)$

are constructed for different ranges of orientations of A. The approach suggested by Lozano-perez [115] for the find-path problem carries out the following steps in turn:

1. Assume a slice orientation angle interval and then constructing the $CO_A(B)$;

2. Use any one of the approaches for a point robot to search for a path among the $CO_A(B)$;

3. Move between slices at configurations that are safe in both slices.

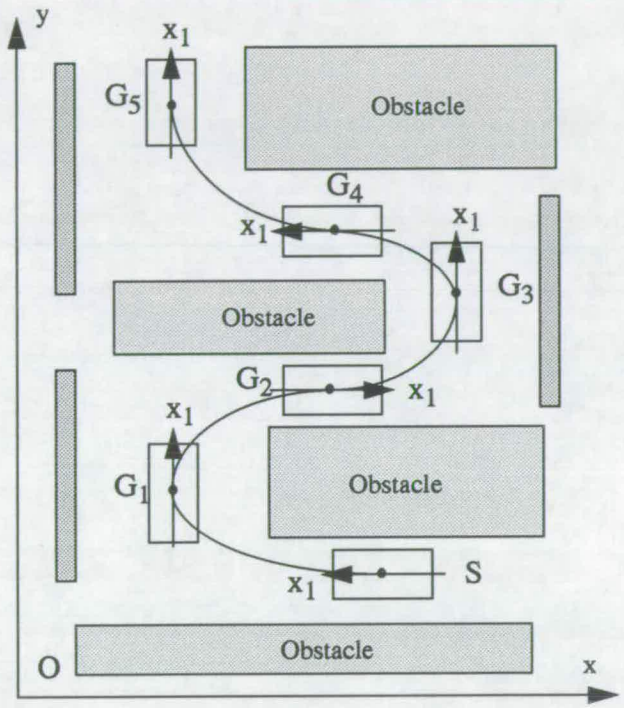

Fig. 5.10 (a) A general case for a polygonal robot with variable orientation

The path generated from the first two steps is only guaranteed to be safe when the orientation angle falls into the range of the slice angle during the whole path. The difficulty of using this method arises from the first step and the third step, i.e., how to choose the range of the slice orientation angle to compute $CO_A(B)$, how far to move forward every time, and how to determine the orientation angle change during each slice. So far, few papers have focused on these problems. A solution suggested by Lozano-Perez for choosing the slice orientation angle is to divide "the complete range of θ (orientation

angle) values" into k smaller ranges, and then, for each of these ranges, find the solution to $CO_A(B)$ in that range of θ. However, he did not explain the meaning of "the complete range of θ values". In addition to that, dividing "the complete range of θ values" into k smaller ranges means that the orientation angle change is monotonic, which is infeasible for some situations.

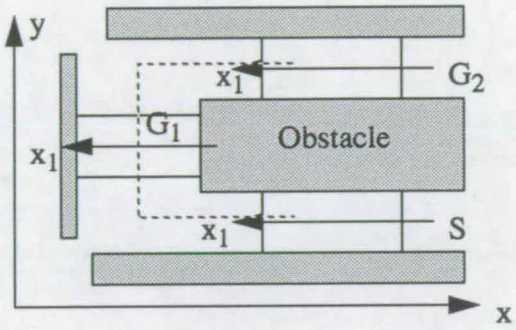

Fig. 5.10 (b) A critical case for a polygonal robot with variable orientation

In order to illustrate the difficulty, let us consider two examples, shown in Fig. 5.10 (a) and (b). In Fig. 5.10 (a), the robot A is required to move safely from S (where the initial orientation angle is 180^o) to G_5 (where the goal orientation angle is 90^o). During the motion from S to G_5, the orientation angle is monotonically decreasing from S to G_2 through G_1, monotonically increasing from G_2 to G_4 through G_3, and then monotonically decreasing from G_4 to G_5. The orientation angle change covers the range of 0^o to 180^o during the whole path. If we could use the range of 0^o to 180^o as the slice angle interval to compute the $CO_A(B)$, then the path found by the above first two steps will be safe and in this case, the third step is not necessary. However, when the reference point is chosen at one of its vertices, this slice projection would be too generous to be useful. For a more complicated environment, orientation angle may varies over the range of 0^o to 360^o. Thus, if the difference between the goal and the initial orientation angles is treated as "the complete range of θ values", the slice projection method can not be applied to this example.

In the second example shown in Fig. 5.10 (b), the robot is required to move from S to G_2.

The only way for this critical situation is to translate the robot along the dashed line. If only the information about the initial and goal orientation location is used, it is also difficult to decide the slice angle projection.

5.3 Suitability of algorithms for four kinds of wheeled robots

The task of path planning for a wheeled mobile robot is to find a continuous sequence of the x_p, y_p and θ, which we call a desired motion. The generated x_p, y_p and θ are then used as inputs to calculate the steering and powering variables needed to accomplish the desired motion. The task of the real time controller is to make the robot execute the desired motion as accurately as possible. At the path planning stage, it is normal to assume that the controller can trace the desired motion accurately.

Definition 5.1: If all the desired motions generated by an algorithm can be executed by a robot, then the algorithm is defined to be suitable to the robot; otherwise, it is defined to be unsuitable to the robot.

In the sequel, we will discuss the suitability of the algorithms available to each of the four kinds of robots.

5.3.1 Synchro drive and steering robots

Analysis of the kinematic characteristics in chapters 2 and 3 tells us that the orientation angle of this kind of robots is always fixed. Therefore all the approaches discussed in 5.2.1 for a point robot can be used to solve the find-path problem once the $CO_A(B)$ is computed using the slice projection method with fixed orientation. We will not discuss this problem any more.

5.3.2 Omnidirectional robots

For this kind of robots, the assumption of the robot as free moving rigid body is correct, because there exists no kinematic constraint equation among the x_p, y_p and θ. This means that any desired motion can be accomplished through steering and powering the wheels.

The factors which must be taken into consideration are only the size and location of the obstacles, and the size of the robot. All the algorithms which consider these factors are suitable to this kind of robots. However, as pointed out previously, how to deal with the change of the orientation angle is still a problem if the slice projection method is used. Because of the complicated structure and the difficulty of control, this kind of robots has not been widely used. Our discussion for path planning is focused on the car-like and dual drive robots.

5.3.3 Existence and uniqueness of orientation angle for car-like and dual drive robots

We know from chapter 2 that the general constraint equations for a car-like robot and a dual drive robot are identical. Provided the reference path for a wheeled robot is a continuous curve y = f (x), e.g., a concatenation of piecewise continuous line-line or line-circle segments, if we can prove the existence and uniqueness of the orientation angle once a reference path is given, then we can understand better the shortcomings of the path planning approaches which treat a car-like robot or a dual drive robot as a free moving rigid body (including the slice projection method).

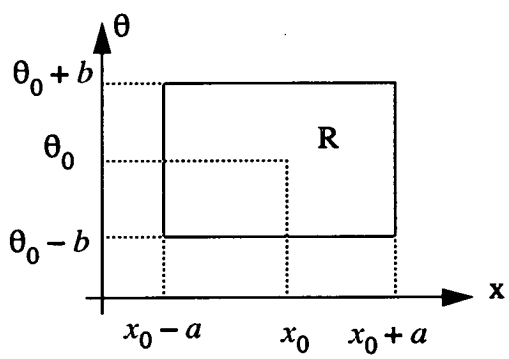

Fig. 5.11 Rectangle R in the existence and uniqueness theorems

Consider an initial value problem of the form

$$\frac{d\theta}{dx} = g(\theta, x), \theta(x_0) = \theta_0 \tag{5.1}$$

Problem of existence: Under what conditions does an initial value problem of the form (5.1) have at least one solution?

Problem of uniqueness: Under what conditions does that problem have only one solution?

The following theorems 5.1 and 5.2 state the conditions [96].

Existence theorem 5.1: *If* $g(\theta, x)$ *is continuous at all points* (θ, x) *in some rectangle R (cf. Fig. 5.11)*

$$R: |x - x_0| < a, |\theta - \theta_0| < b$$

and bounded, say,

$$|g(\theta, x)| \leq K$$

for all (θ, x) *in R, then the initial value problem (5.1) has at least one solution* $\theta(x)$, *which is defined at least for all x in the interval* $|x - x_0| < \alpha$ *where* α *is the smaller of the two numbers a and* b/K.

Uniqueness theorem 5.2: *If* $g(\theta, x)$ *and* $\frac{\partial g}{\partial x}$ *are continuous for all* (θ, x) *in that rectangle R and bounded, say,*

$$(a)\ |g(\theta, x)| \leq K, \text{ and } (b)\ \left|\frac{\partial g}{\partial \theta}\right| \leq M$$

for all (θ, x) *in R, then the initial value problem (5.1) has only one solution* $\theta(x)$, *which is defined at least for all x in that interval* $|x - x_0| < \alpha$.

Using above two theorems, we can prove the following uniqueness theorem 5.3:

Theorem 5.3: *If the reference path* $y_p = f(x_p)$ *and its first derivative* $y'_p = f'(x_p)$ *are*

piecewise continuous for all (x_p, y_p) *in a rectangle* R_1 *(cf. Fig. 5.12)*

$$R_1: |x - x_0| < a_1, |y - y_0| < b_1$$

and bounded, say,

$$(a)\ |f(x_p)| \le K_1, \text{ and } (b)\ \left|\frac{df}{dx_p}\right| \le M_1$$

for all (x_p, y_p) *in* R_1*, then the initial value problem described by constraint equation (2.13) or (3.3) has only one solution.*

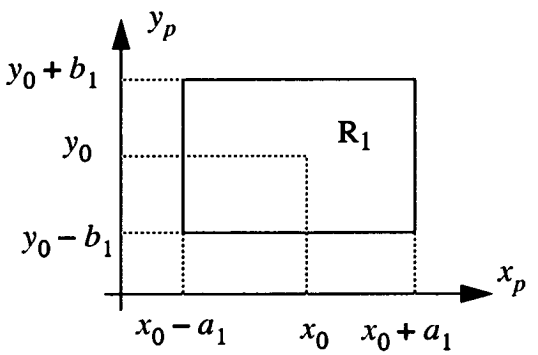

Fig. 5.12 Rectangle R_1 in theorem 5.3

Proof. Let $g(x_p, \theta) = sin\theta - f'(x_p)\cos\theta$, then $\frac{\partial}{\partial\theta}g(x_p, \theta) = \cos\theta + f'(x_p)\sin\theta$. If $y'_p = f'(x_p)$ is piecewise continuous and bounded in R_1, then $g(x_p, \theta)$ and $\frac{\partial}{\partial\theta}g(x_p, \theta)$ are piecewise in R, where $a = a_1$ and b may be any positive constant, and we have

$$|g(x_p, \theta)| \le |\sin\theta| + |f'(x_p)\cos\theta| \le 1 + M_1 = K$$

and

$$\left|\frac{\partial}{\partial\theta}g(x_p, \theta)\right| \le |\cos\theta| + |f(x_p)\sin\theta| \le 1 + M_1 = M$$

It is clear from the uniqueness theorem (5.2) that the initial value problem described by

(2.13) or (3.3) has only one solution.

Note that the existence and uniqueness of the orientation of the car-like or dual drive robot are not equivalent to their motion feasibility. For example, when a reference point of the robot is required to follow a path, even though the orientation angle exists and is unique, the path may be infeasible or inexecutable because the needed steering angle may exceed the steering angle limit.

5.3.4 Car-like and dual drive robots

The shortcomings of the slice projection method and the other approaches, when applied to the car-like and the dual drive robots, can be observed from the uniqueness of the orientation angle we have proven previously. This inherent characteristic indicates that before a reference path $y = f(x)$ is found (if it exists), one can not assume exactly the robot's orientation angle change. On the other hand, to obtain Cspace obstacles, an orientation angle change must be assumed before a reference path is generated. Thus, there is a potential conflict between the assumed orientation angle change and that generated when the reference path is followed by a practical robot. Therefore, even if the Cspace obstacles are computed without considering the kinematic constraint, there is no guarantee that the generated path is really collision-free because of the existence of the kinematic constraint. Checking for collisions is necessary.

From the point of view of constraints taken into account in the existing algorithms, the algorithms available can be categorized into two types. The first type treats a wheeled mobile robot as a free moving rigid body (the robot is assumed as a sofa, a piano or a ladder) which can translate and rotate freely in the work space provided that it does not collide with obstacles, i.e., the motion of a wheeled mobile robot is supposed to be only subject to constraints from the obstacles, rather than from any kinematic constraints. The algorithms falling into the first type, when they are applied to these two kinds of robots, suffer from the fundamental drawback that kinematic constraints resulting from the robot's structure are not taken into account. Therefore, they are not suitable to the car-like and dual drive robots. Fig. 13. shows an example. If the robot is assumed to be a free

moving robot, it is possible for the existing algorithms to generate a path from S to G; however, for a car-like or a dual drive robot, it is straightforward to conclude from theorem 3.1 that the path is inexecutable and G is unreachable.

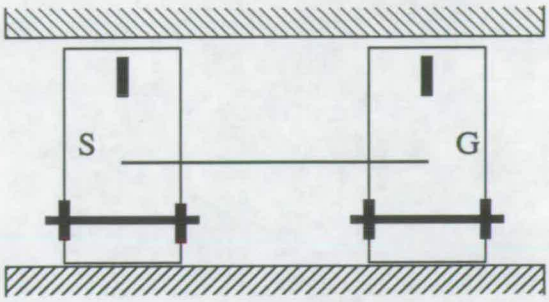

Fig. 5.13 Illustration of the difference between a free moving rigid body and a car-like or a dual drive robot

Another example is shown in Fig. 5.14. In (a) and (b), Robot 1 and Robot 2 have the

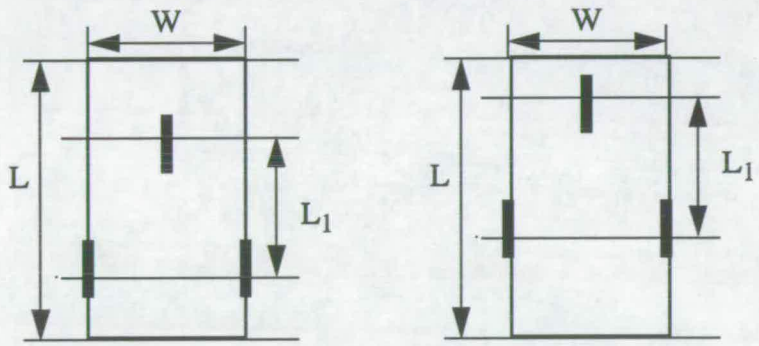

(a) Robot 1 (b) Robot 2

Fig. 5.14 Two robots with same rigid bodies but different wheel positions

identical rigid body shape but different wheel positions. From chapters 2 and 3, we know that their kinematics is different. When the first type of algorithms is utilized to plan the paths for the two robots under the same environment, the path generated must be the same because of their identical body shapes. However, in practice, when the two robots are required to follow the same generated path, the locus of any corresponding points except the two reference points on the two robots will be different. That means the swept spaces by the two robots are different.

The second type of path planning algorithms for wheeled mobile robots does take into

account the steering angle limit imposed by the steering mechanism which defines the minimum radius of curvature of the reference path. Path planning with this kind of constraint is a relatively new area of research. Following the work of Laumond [102], it

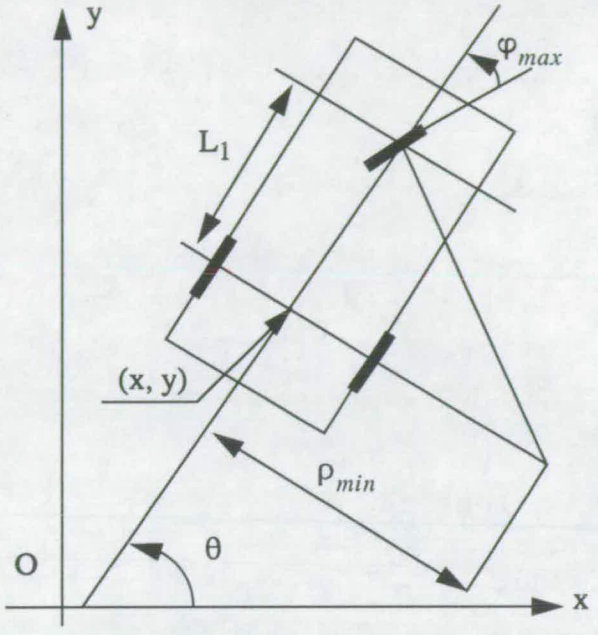

Fig. 5.15 Illustration of nonholonomic constraints
expressed in equations (5.2) - (5.4)

has recently attracted considerable interest [101]. The kinematic constraints considered by the second type of algorithms can be expressed in the following form:

$$\dot{x}^2 + \dot{y}^2 - \rho_{min}\dot{\theta}^2 \geq 0 \tag{5.2}$$

$$-\dot{x}\sin\theta + \dot{y}\cos\theta = 0 \tag{5.3}$$

$$\frac{1}{\rho_{min}} = \frac{1}{L_1}\tan(\varphi_{max}) \tag{5.4}$$

where $\dot{x}$, $\dot{y}$ are the velocity components of the midpoint of the rear axle in x-axis and y-axis in terms of the global reference frame respectively, θ is the orientation angle of the mobile robot, $\dot{\theta}$ is the rotating angular speed of the robot, L_1 is the wheelbase of the robot, ρ_{min} is the minimum radius of curvature of the midpoint of the rear axle, and φ_{max} is the

maximum steering angle determined by the steering mechanism, as shown in Fig. 5.15.

The purpose of developing the second type of algorithms is to remedy the drawback that the radius of curvature of the path generated for the reference point using the first type may be less than ρ_{min}. The second kind of algorithms, however, still suffers from some drawbacks:

1. Eqs. (5.2) to (5.4) hold only when the reference point is chosen at the midpoint of the rear axle. If the reference point is chosen on the other point, say, one of the vertices of the robot body or the mass center, the kinematics will be different.

2. Eqs. (5.2) to (5.4) do not completely describe the relative positions of all the wheels to the rigid body. Therefore, they are not a complete description of the kinematics of a car-like robot. For example, in Fig. 5.14 (a) and (b), the relative positions of the three wheels on both robots are identical, and both of the robots satisfy (5.2) to (5.4). However, the relative positions of the three wheels to each of the two rigid bodies are different, which leads to their different kinematics.

Therefore the second type of algorithms is still not suitable to the car-like and dual drive robots. A complete and formal description of the path planning problem taking account of kinematics for a car-like robot will be given in next chapter.

Note that Brooks's approach [23] mentioned in chapter 3 is a special case. Although the kinematic constraints are not explicitly expressed in this approach, the two basic motions assumed are implicitly compatible with the kinematic constraints only when the reference point is at the fixed axle of the dual drive robot. This is the reason why in some cases the approach is suitable to the dual drive robot. This approach is not suitable to a car-like robot.

5.4 Summary

Path planning is a central theme for creating an autonomous wheeled mobile robot. In this chapter, we have given a brief but critical review of the algorithms presently available for

wheeled mobile robots, and shown their suitability to each of the four kinds of wheeled mobile robots.

The conclusions that can be made are as follows:

1. For synchro drive and steering robots, their motion is always a translation. Therefore all the approaches for a point robot are suitable to this kind of robots once the $CO_A(B)$ is computed using the slice projection method with fixed orientation.

2. For omnidirectional robots, the three parameters x_p, y_p and θ are independent of each other, and there is no general kinematic constraint equation. All the algorithms which consider the size and location of obstacles and the size of the robot are suitable if they can find a desired motion. However, how to deal with the change of the orientation angle when using the slice projection method to find a desired motion remains a problem.

3. For car-like and dual drive robots, their motion is restricted by a general kinematic constraint resulting from the fixed wheels. All the existing algorithms except Brooks's method are not suitable. Under the condition that the reference point is at the fixed axle of the dual drive robot, Brooks's approach is suitable to the dual drive robot, but still unsuitable to the car-like robot.

Chapter 6

Path planning for a wheeled mobile robot with nonholonomic constraint and steering angle limit

6.1 Introduction

In chapters 2 and 3, we have established the kinematic models for the four kinds of robots and analyzed in greater depth their kinematic characteristics. In chapter 5, we have examined the suitability of the available algorithms to each of the four kinds of robots and concluded that the presently available path planning algorithms can not be directly applied to the car-like and dual drive robots. The objective of this chapter is first to give a formal description of the path planning problem and then to develop an algorithm for a car-like robot (CLR) with a steering angle limit. Our attention here is focused on a CLR rather than on a dual-drive robot (DDR) because a DDR can be treated as a special case of a CLR with an equivalent steering angle limit $\delta_{max} = 90°$ (the definition of the δ_{max} is given in chapter 3). In other words, any paths generated for a CLR must be applicable to a DDR with the same size of the robot body and the same relative position of the fixed axle to the robot body.

Since the path planning algorithm presented later will use the same kinematic model as that used in highway design which is usually called geometric design, the algorithm is also called a geometric method.

From previous analysis, it can be seen that the following four points are key ones for the path planning problem for a CLR and must be taken into account.

1. Rotation. Rotation of a CLR when it follows a curved path must occur. Only in one case where the path followed is a straight line and the CLR's initial orientation angle coincides

with the direction of the straight line, does a pure translation occur. However, in practice, this situation rarely appears.

2. Dependence of a CLR's orientation angle on its reference path. The orientation angle is obtained by solving the general constraint equation (2.13) when it follows a specified path. Corresponding to every given initial orientation angle and every generated path, there exists a unique solution to (2.13) for θ. This inherent characteristic of a practical CLR tells us that before a path is found (if it exists), one can not know exactly the CLR's orientation angle when the CLR follows it. Thus, the slice projection method is not applicable to car-like robots.

3. Saturation of the steering mechanism. Whenever a reference path (we call it an approximate global path) for a CLR is generated, the steering angle needed to follow this path must be computed to check the motion feasibility against the steering angle limit.

4. Satisfaction of the goal orientation angle.

6.2 A general formulation of path planning problem for a CLR

In order to satisfy the kinematic constraints, we introduce the following definitions. In path planning problem for a CLR, we call a path from the starting point to the goal point feasible if and only if it satisfies both the requirements of being collision-free and being within the steering angle limit. A feasible path only means it is safe and can be followed, but it offers no guarantee of satisfaction of the goal orientation requirement. We call a feasible path a final path if it satisfies the goal orientation requirement. Obviously, the purpose for planning a path is to find a final path.

We here attempt to give a general formulation of the path planning problem for a CLR while taking into account the kinematic constraints, and then a possible algorithm structure for solving the find-path problem is proposed. First we need to derive the expression of the boundary of a CLR A when its reference point follows a reference path.

Suppose a point with coordinates (x, y) in terms of the global reference frame and (x_1, y_1)

in terms of the local reference frame is located at the boundary of the CLR, then the boundary can be represented as the following implicit form in terms of the local reference frame

$$\Gamma_A(x_1, y_1) = 0 \tag{6.1}$$

where $\Gamma_A(x_1, y_1)$ is compact (i.e. closed and bounded) and continuous functions of the coordinates (x_1, y_1).

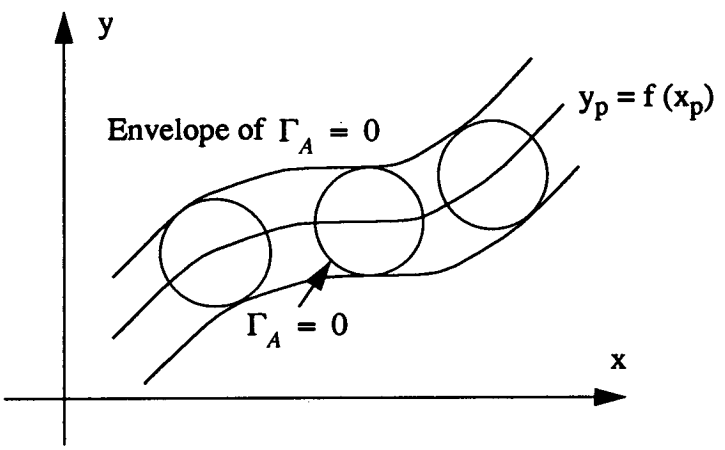

Fig. 6.1 Illustration of the boundary of Robot A

From (2.1), it follows that

$$\begin{bmatrix} x_1 \\ y_1 \end{bmatrix} = \begin{bmatrix} (x - x_p)\cos\theta + (y - y_p)\sin\theta \\ -(x - x_p)\sin\theta + (y - y_p)\cos\theta \end{bmatrix} \tag{6.2}$$

Substituting (6.2) into (6.1) yields

$$\Gamma_A [(x - x_p)\cos\theta + (y - y_p)\sin\theta, -(x - x_p)\sin\theta + (y - y_p)\cos\theta] = 0 \tag{6.3}$$

In (6.3), if the reference path $y_p = f(x_p)$ is given, then the orientation angle can be obtained from the general constraint equation (2.13) or (3.3). Therefore, (6.3) describes a family of the boundary curves for robot A in terms of the global reference frame. Fig. 6.1

shows such an example when robot A is a disc with radius R and the reference point at its center. In this example, $\Gamma_A(x_1, y_1) = x_1^2 + y_1^2 = R^2$. Eq. (6.3) becomes $(x - x_p)^2 + (y - y_p)^2 = R^2$.

The boundary of the ith obstacle can be represented as the following implicit form in terms of the global reference frame

$$\Gamma_{B_i}(x, y) = 0, i = 1, 2, \ldots\ldots, n \qquad (6.4)$$

Suppose the initial position of the CLR is collision-free, and the CLR and obstacles are compact. If there is a path taken by the reference point of the CLR such that the boundary curve of the CLR expressed by (6.3) and the boundary curves of the obstacles expressed by (6.4) do not intersect each other, this path must be a collision-free path. If a collision-free path satisfies the requirement of the steering angle limit, it then becomes a feasible path. The purpose for path planning is to find a final path. Therefore, mathematically, a path planning problem for a CLR can be described formally as:

Given $\Gamma_A(x_1, y_1) = 0$, $\Gamma_{B_i}(x, y) = 0$, the initial position (x_{pi}, y_{pi}) of the reference point and initial orientation angle θ_i of the CLR, and the goal position (x_{pg}, y_{pg}) of the reference point and the goal orientation angle θ_g of the CLR, find a continuous function $y_p = f(x_p)$ as the reference path such that it satisfies the following conditions:

1. $y_{pi} = f(x_{pi})$ and $y_{pg} = f(x_{pg})$.

2. $\underline{x} d\theta = (\sin\theta - f'(x_p)\cos\theta)\, dx_p$.

3. Eqs. (6.3) and (6.4) have no points of intersection.

4. The needed steering angle obtained from (3.8) satisfies the inequality constraint (3.9).

5. The goal orientation obtained from (2.13) at the goal point satisfies θ_g.

As discussed previously, rotation of a robot, namely, the orientation angle change of a robot is the most difficult thing to deal with. A possible way one can do to alleviate this difficulty is first to find an approximate global path as fast as possible without considering the orientation change and then to test it for potential collisions with obstacles and saturations of the steering mechanism taking the kinematic constraints into account. If collisions or saturations are detected, then use the information obtained during the tests to plan a local path for correcting the collisions or saturations. The procedure for testing and correcting continues until a feasible path is found. After that, check the requirement of the goal orientation. If it is not satisfied, another local planning for adjusting the goal orientation angle must be devised. Clearly, this work can only be done after a feasible path has been found. A possible path planning algorithm may consist of the following parts:

1. A coarse subalgorithm for finding an approximate globaEasy to be generated.

2. A testing subalgorithm for testing the potential collisions with obstacles, saturations of the steering mechanism, and the satisfaction of the goal orientation.

3. A local path planning subalgorithm for correcting the collisions and saturations encountered, and for meeting goal orientation.

6.3 Finding an approximate global path for a CLR

There are many ways to generate an approximate global path. Any approach discussed previously may be a candidate. However, a good approximate global path should meet the following requirements:

- Easy to be generated.
- Smooth.
- Adaptive to the environment.
- Easy to be used for checking the potential collisions and saturations.

- Able to offer information for recovery from possible collisions or saturations encountered.

The third point means that the path should be a measure of the sparseness of the workspace. For example, finding a global path should be much easier in an uncluttered environment than that in a cluttered one. According to these requirements, we will here develop an algorithm for finding an approximate global path.

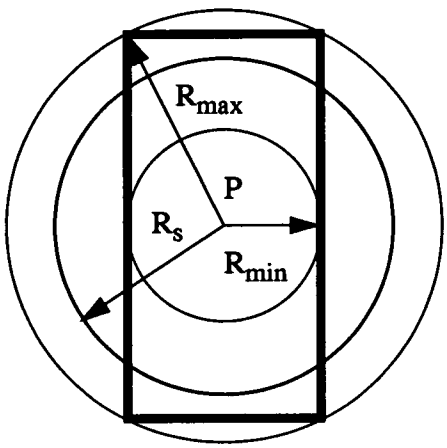

Fig. 6.2 The boundary of the CLR is encompassed by two circles with the same center, different radiuses R_{max} and R_{min}. The shrinking radius R_s between R_{min} and R_{max} is used to generate an global path.

The choice of the reference point is always the first consideration in path planning for a CLR. Its choice is affected by kinematic constraints, the algorithms devised and other factors. For example, when the reference point is chosen at any point on the rear axle (this is the case where most studies do), if the first derivative of the reference path is discontinuous, a discontinuity of the orientation angle will occur at the discontinuous point. Consequently, this will cause discontinuity of the velocity and acceleration of any point in the CLR. This undesired characteristic can be alleviated by moving the reference point away from the rear axle. When the reference point is chosen behind the rear axle, an undesired pirouette may occur. These two situations are examples showing the effect of the kinematic constraints on the choice of the reference point. The algorithmic effect on it

is also clear. For example, in reference [114], when the CLR and obstacles are closed and bounded polygonal bodies, and the slice projection technique is employed, the reference point is chosen at one of the vertices of the CLR to generate a polygonal Cspace obstacles, thus to reduce the computational complexity for the Cspace obstacles and the graph searching procedure followed.

Let the CLR A be a bounded convex polygon, its boundary be Γ_A (marked by the thick lines in Fig. 6.2), and a_i be any point on Γ_A. In this thesis, the reference point is chosen according to the following definition. Choose an arbitrary point on the robot, let d_i be the distance from a_i to this point, then there exists at least one point among all the a_i which maximizes d_i. Denote the distance as $max_{a_i \in \Gamma_A} d_i$. The origin is chosen so that $max_{a_i \in \Gamma_A} d_i$ is minimized over all possible points on the robot. The coordinate axes x_1 and y_1 are chosen so that the direction of the x_1 axis is always perpendicular to the rear axle of the CLR and from the rear axle to the front axle.

For a rectangular rigid robot, the origin generated from this definition is located at the symmetric center; for a circular robot, it is at the center. Obviously, for these two typical robot structures, the definition of the origin leads to the important property that $min_{a_i \in \Gamma_A} d_i$ is maximized. After the reference point is chosen as defined above, let R_{max} denote the $min\,(max_{a_i \in \Gamma_A} d_i)$ and R_{min} denote the $max\,(min_{a_i \in \Gamma_A} d_i)$. Consequently, the difference between R_{max} and R_{min} is also minimized (for a circular robot, it is zero). The boundary of the CLR will be encompassed by two circles, one with the central point at the origin and the radius of R_{max} and the other with the same central point but different radius of R_{min}, as shown in Fig. 6.2.

As pointed out in chapter 5, the shortcoming of the slice projection method [114] is that every time for finding a Cspace obstacle, it must assume an orientation angle range which is difficult to deal with. We here use a different strategy to find a global path. Although the slice projection technique is not adopted, we still employ the concept of Cspace obstacles

to represent the grown obstacles. Our strategy is first to expand the obstacles by a circle with radius R_s rather than a polygon for generating the Cspace obstacles and then to search the Cspace obstacles to find a shortest path. Obviously, this strategy can reduce the computational burden compared with the slice projection method and the smoothness of the generated path is significantly improved.

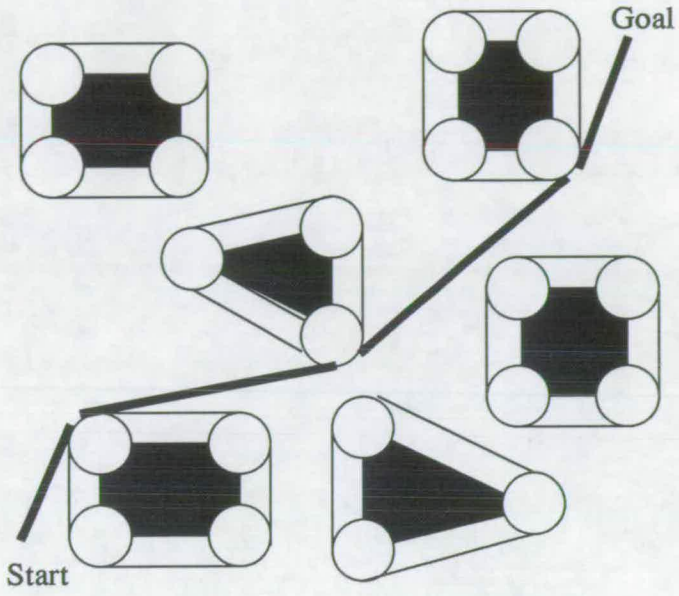

Fig. 6.3 The shortest approximate global path among Cspace obstacles

For every shrinking radius $R_s > R_{min}$, as shown in Fig. 6.2, two steps are required to find an approximate global path for a CLR. The first step is to compute the Cspace obstacles that are called the generalized polygonal obstacles [103]. The second step is to use an algorithm for a point robot to search the Cspace obstacles. Clearly, the encompassed part of the robot by the circle of radius R_s is collision-free if an approximate global path can be found corresponding to the shrinking radius R_s. We will use this property in later sections. A tangent graph method for a point robot among such a generalized polygonal obstacles has been presented in references [103, 112] and can be employed here to generate a shortest approximate global path. Fig. 6.3 shows a typical example.

We return to discuss the benefit from the choice of the reference point. If R_{max} is used to

grow the original polygonal obstacles, any path generated for a point among the Cspace obstacles will certainly be a collision-free path whatever the orientation angle of the CLR is. In this case, test for collision with obstacles is not needed. Since $R_{max} = min\,(max_{a_i \in \Gamma_A} d_i)$, the choice of the reference point makes it most possible to find a collision-free, approximate global path in an uncluttered environment.

On the other hand, if R_{min} is used to grow the obstacles, and no path is found by the algorithm [103, 112] for a point robot among the Cspace obstacles, then it can be concluded that there exists no path for the CLR however it is maneuvered among the obstacles because of the completeness of the algorithm used. In this case, since $R_{min} = max\,(min_{a_i \in \Gamma_A} d_i)$, the choice of the reference point increases the possibility to find that there is no path available in a cluttered environment.

The foregoing two cases are easily handled. If the opposite search results are reached, namely, the first two iterations of using R_{max} and R_{min} fail and succeed, respectively, in finding an approximate global path, then we devise an equal-interval decreasing search scheme for R_s between R_{max} and R_{min}. Divide the interval $[R_{min}, R_{max}]$ into n equal subintervals, and thus, the length of every subinterval equals to $\Delta = \frac{R_{max} - R_{min}}{n}$. Let $R_{s3} = R_{max} - \Delta$ and $R_{si} = R_{s(i-1)} - \Delta$ ($i = 4, 5, \ldots\ldots, n+1$), then use R_{s3} as the next shrinking radius. If the third iteration fails, choose R_{s4}, and so on until an approximate global path for the biggest shrinking radius R_s is found, provided that n is big enough. Note that this is not the only possible search order. In fact, the order of the choice of R_s in $[R_{min}, R_{max}]$ is perfectly arbitrary.

In practice, due to errors from various sources, a robot is never able to exactly follow a prescribed path. A path is error-tolerant if the robot will not come to harm when it makes a small deviation from the path. With this in mind, we call a robust path to be one that maintains a prescribed minimum width (and that is thereby error-tolerant). If uncertainty is taken into account, a safety distance R_{safe} is assumed, then the actual minimum

shrinking radius R_{smin} must be equal to

$$R_{smin} = R_{safe} + R_{min} \tag{6.5}$$

The generated path consists of a concatenation of line-circular segments. The tangent of the path at every transition point is continuous. Since the reference chosen is usually not at the rear axle, from theorems 3.5 and 3.6 we can conclude the continuities of the orientation angle and the steering angle. If an approximate global path can be generated using a large R_s, then the environment is sparse; otherwise, the environment is cluttered. In this sense, R_s is a good measure of the sparseness of the environment. Therefore we can say that the approximate global path generated using this strategy satisfies the first three requirements. The following sections will show its other advantages.

6.4 Detecting satisfaction of the steering angle limit

Once an approximate path is found, the satisfaction of the steering angle must be tested. The formulas needed for the testing have been given in chapter 3. The general procedure consists of two steps:

1. For every point on the path, calculate the deviation angle.

2. Check whether or not the deviation angle falls within the feasible deviation angle intervals.

Theoretically, checking at every point along the path is unrealistic. A natural idea is to check at some special points such that the tests at these points can offer enough information to judge the satisfaction along the whole path. Since the approximate path consists of the special form of curves, i.e. the combination of straight lines and circular arcs (see theorem 6.1), we will give a more efficient checking method.

Theorem 6.1: *The approximate global path for a CLR produced by the tangent graph method for a point robot among the generalized polygonal obstacles consists only of a*

collection of straight lines and circular arcs.

Proof. See reference [103].

6.4.1 Straight line motion

Theorem 6.2: *For a car-like robot moving along a straight line from point Q_1 to point Q_2, if the deviation angles at Q_1 and Q_2 fall into the feasible intervals, then at any point between Q_1 and Q_2, the deviation angle must also fall into the feasible intervals.*

Proof. In order to prove this theorem, we only need to prove that for any straight line motion, the deviation angle β is always monotonic with respect to x_p. For a straight line motion, α is a constant. Thus $\frac{d\beta}{dx_p} = \frac{d\theta}{dx_p} - \frac{d\alpha}{dx_p} = \frac{d\theta}{dx_p}$. From (3.20), we can observe that for any θ_0 and $\underline{x}$, $\frac{d\theta}{dx_p} \geq 0$ or $\frac{d\theta}{dx_p} \leq 0$ holds, and $\frac{d\theta}{dx_p}$ is always monotonic. Therefore, $\frac{d\beta}{dx_p}$ is always monotonic and the proof is complete.

The importance of theorem 6.2 lies in the fact that it significantly reduces the complexity of the test procedure for the satisfaction of the steering angle limit. For every straight line, only two end points are needed to be tested.

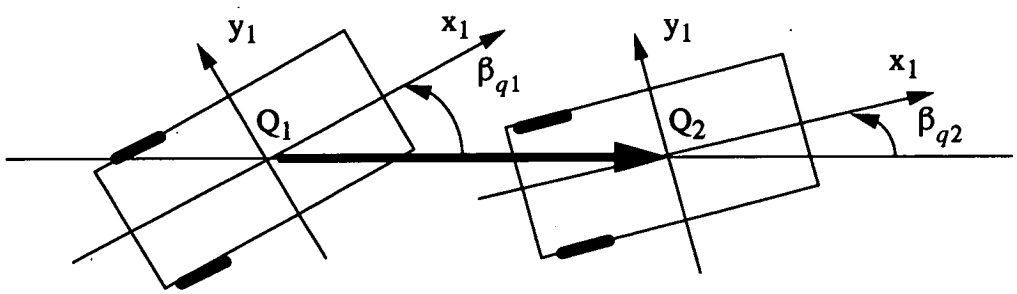

Fig. 6.4 A schematic for straight line motion

Furthermore, if the reference point is chosen at the geometric center (it is usually in front of the rear axle), then the deviation angle monotonically tends to 0^o from its neighborhood

as the robot moves forwards (Fig. 6.4). If the deviation angle at point Q_1 is in the neighborhood of 0^o, then only point Q_1 is needed to be tested for the satisfaction of the steering angle limit. Therefore, we further have the following theorem:

Theorem 6.3: *Provided that the reference point is chosen in front of the rear axle and the deviation angle at point Q_1 is in the neighborhood of 0^o, if the steering angle limit at point Q_1 is satisfied, then the steering angle limit at point Q_2 must also be satisfied.*

Proof. In this case, $x < 0$, the reference point is in front of the rear axle. The conclusion is straightforward from Tables 3.1 and 3.3.

6.4.2 Circular motion

Theorem 6.4: *For a car-like robot moving along a circular arc from point Q_1 to point Q_2, if the deviation angles at Q_1 and Q_2 fall into the feasible intervals, then at any point between Q_1 and Q_2, the deviation angle must also fall into the feasible intervals.*

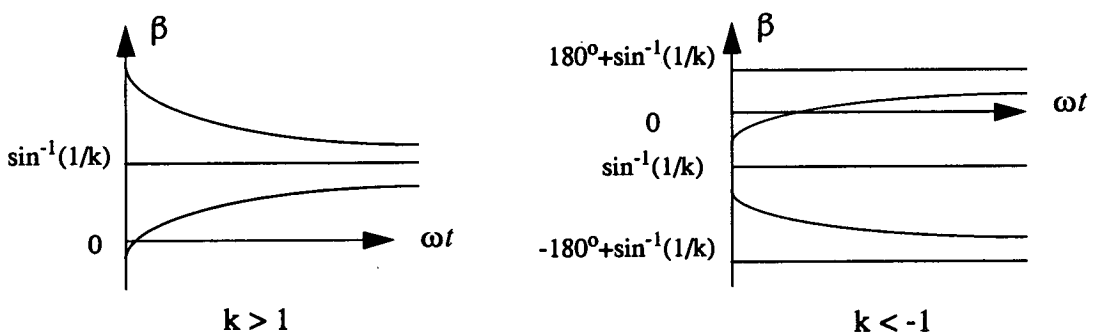

Fig. 6.5 Illustration of the monotony of deviation angle β

Proof. For simplicity and without losing generality, we assume that the circular motion is a right turn motion and Q_1 coincides with S, as shown in Fig. 3.9. Therefore, (3.22), (3.23), and (3.25) also apply. The definition $\beta = \theta - \alpha$ given in chapter 3 and (3.23) result in $\beta = \theta + \omega t - 90°$, which in turn leads to $\frac{d\theta}{d\omega t} = \frac{d\beta}{d\omega t} - 1$. Substituting them into

(3.25) gives

$$\frac{d\beta}{d\omega t} = 1 - k\sin\beta \tag{6.6}$$

where $k = -\frac{R}{x}$. Note that the above derivation does not restrict the sign of x. That is, the reference point may be chosen anywhere. In the following, we will prove the monotony of the deviation angle β with respect to ωt for any k and initial deviation angle β_0.

Case 1: $|k| \le 1$

In this case, it is obvious that the inequality, $\frac{d\beta}{d\omega t} = 1 - k\sin\beta \ge 0$, always holds. β is monotonically non-decreasing with respect to ωt. Therefore theorem 6.4 holds.

Case 2: $|k| > 1$

In this case, the solution of (6.6) is

$$\beta = 2arc\tan\left(c \cdot \frac{(c+z'_0)\cdot e^{\omega td\cdot \mathrm{sgn}(k)} - (c-z'_0)}{(c+z'_0)\cdot e^{\omega td\cdot \mathrm{sgn}(k)} + (c-z'_0)}\right) - 90° \tag{6.7}$$

where $c = \sqrt{\frac{k+1}{k-1}}$, $d = \sqrt{k^2-1}$, $z'_0 = \tan(\frac{90°+\beta}{2})$, and $\mathrm{sgn}(k) = \begin{cases} 1, & k>1 \\ -1, & k<-1 \end{cases}$.

Let $X = (c+z'_0)\cdot e^{\omega td\cdot \mathrm{sgn}(k)} + (c-z'_0)$ and $Y = c[(c+z'_0)\cdot e^{\omega td\cdot \mathrm{sgn}(k)} - (c-z'_0)]$, then

$\frac{dX}{d\omega t} = d\,\mathrm{sgn}(k)\,(c+z'_0)\cdot e^{\omega td\cdot \mathrm{sgn}(k)}$ and $\frac{dY}{d\omega t} = cd\,\mathrm{sgn}(k)\,(c+z'_0)\cdot e^{\omega td\cdot \mathrm{sgn}(k)}$. Thus we have

$$\frac{d\beta}{d\omega t} = 2\cdot\frac{X\frac{dY}{d\omega t} - Y\frac{dX}{d\omega t}}{X^2+Y^2} = 2\cdot\frac{2cd\,\mathrm{sgn}(k)\,(c^2-z'^2_0)\,e^{\omega td\cdot \mathrm{sgn}(k)}}{X^2+Y^2} \tag{6.8}$$

For any given $|k| > 1$ and β_0, either $\frac{d\beta}{d\omega t} \ge 0$ or $\frac{d\beta}{d\omega t} \le 0$ holds for any ωt. Therefore β is

always monotonic with respect to ωt and theorem 6.4 holds.

A typical change of β with respect to ωt when $|k| > 1$ is depicted in Fig. 6.5.

6.4.3 Combination of straight line and circular motions

From theorems 6.2 to 6.4, we can readily reach the following theorem.

Theorem 6.5: *For a car-like robot moving along a line-circular combination, if the reference point is in front of the rear axle and the steering angle limit at every transition point from a circular arc to a straight line is satisfied, then the steering angle limit at the whole path must also be satisfied.*

Theorems 6.5 indicates that the transition points from circular arcs to straight lines are the most possible ones that may violate the steering angle limit. In the following we give a sufficient condition for a saturation-free tracking of the approximate global path. Since the steering angle for tracing a circular motion is monotonic and tends to a constant, denoted as $\phi_{a1\infty}$ which is described in (3.33), if this constant is less than the given steering angle limit δ_{max}, then the steering angle at every transition point must also be less than the steering angle limit. From (3.13) and (3.33) we can obtain the following theorem which gives a conservative estimate for the minimum saturation-free shrinking radius R_s.

Theorem 6.6: *If the shrinking radius R_s satisfies*

$$R_s \geq \sqrt{\left(\frac{L}{\tan(\delta_{max})}\right)^2 + \underline{x}^2} = \left|\frac{\underline{x}}{\sin\beta_{max}}\right| \tag{6.9}$$

then the steering angle needed for tracing the approximate global path must satisfy the steering angle limit.

6.5 Two sufficient conditions for collision-free tracking

In this section, we use a geometric method to derive two sufficient conditions for

collision-free tracking of a straight line and a circular arc generated by the method described in section 6.3.

6.5.1 Straight line motion

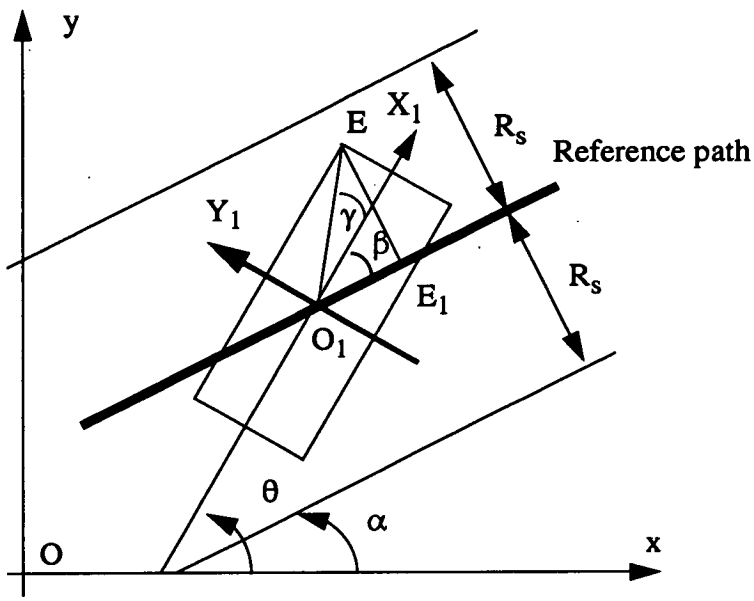

Fig. 6.6 Illustration of the relationship between R_s and the robot for straight line motion

Let TL represent the total length of a rectangular robot and W the width. Then we have (Fig. 6.6)

$$\sin\gamma = \frac{W}{\sqrt{TL^2 + W^2}} \text{ and } \cos\gamma = \frac{TL}{\sqrt{TL^2 + W^2}} \tag{6. 10}$$

The distance of point E to the reference path, EE_1 shown in Fig. 6.6, can be expressed as

$$EE_1 = O_1E\sin(\beta + \gamma) = \frac{TL\sin\beta + W\cos\beta}{2} \tag{6. 11}$$

For a straight line motion, the vertex E of the robot is the most dangerous point for potential collisions, because the reference point is located at the centre and the robot body is symmetric with respect to the center. If the maximum EE_1 corresponding to the

maximum β_{max} is less than the shrinking radius R_s, then the robot must be collision-free. In (6.11), let $\beta = \beta_{max}$, then we have the following theorem:

Theorem 6.7: *If the shrinking radius R_s satisfies*

$$R_s \geq \frac{TL\sin\beta_{max} + W\cos\beta_{max}}{2} \tag{6. 12}$$

then the robot must be collision-free when it tracks a straight line.

6.5.2 Circular motion

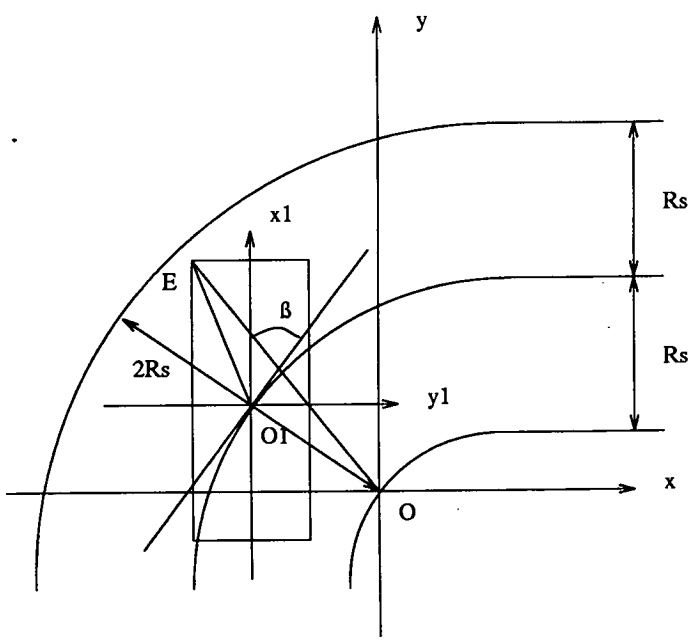

Fig. 6.7 Illustration of the relationship between R_s and robot for circular motion

Fig. 6.7 shows the case of a circular motion. The expression for OE can be obtained from the Cosine theorem as

$$OE^2 = O_1O^2 + O_1E^2 - 2O_1O \cdot O_1E\cos(90° + \beta + \gamma) \tag{6. 13}$$

where $O_1O = R_s$ and $O_1E = (TL^2 + W^2)^{1/2}/2$.

If the maximum OE corresponding to the maximum β_{max} is less than $2R_s$, then the robot must be collision-free. In (6.13), let $\beta = \beta_{max}$, then we have the following theorem (the derivation is omitted).

Theorem 6.8: *If the shrinking radius R_s satisfies*

$$R_s \geq \frac{(W\cos\beta_{max} + TL\sin\beta_{max}) + \sqrt{(W\cos\beta_{max} + TL\sin\beta_{max})^2 + 3(TL^2 + W^2)}}{6} \quad (6.14)$$

then the robot must be collision-free when it tracks a circular arc.

6.5.3 Illustrative example

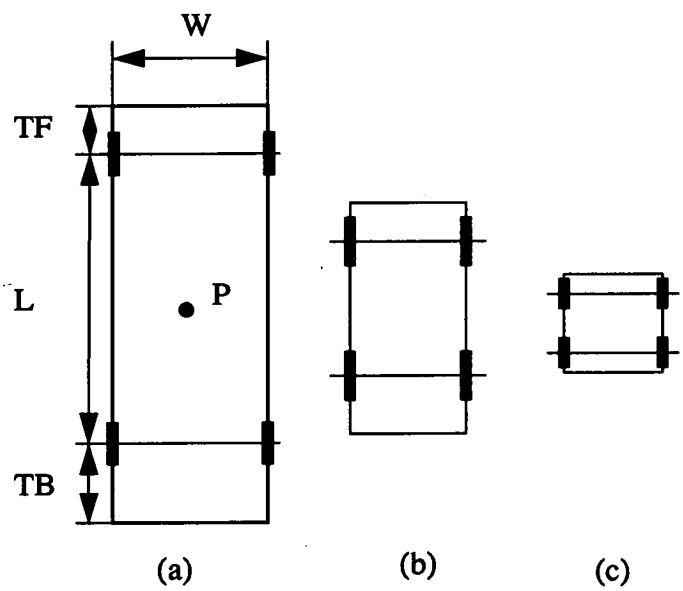

Dimensions (Meter)	(a)	(b)	(c)
W	2.5	1.8	1.5
TF	6.2	0.3	0.2
L	1.3	2.7	1.1
TB	2.5	0.5	0.2
TL	10	3.5	1.5

Fig. 6.8 Three typical vehicles and their dimensions (values in meters)
(a) A commercial design rigid vehicle (b) An ordinary car (c) A Laboratory robot

The sufficient conditions for saturation-free and collision-free motions given in theorems 6.6 ~ 6.8 as well as R_{smin} and R_{mas} defined in section 6.3 provide some important criteria

for choosing the shrinking radius to generate an approximate global path. In the following we use three typical robot dimensions to illustrate this.

Fig. 6.8 shows the three typical vehicles and their dimensions: (a) a commercial design rigid vehicle, (b) an ordinary car, and (c) a laboratory robot, and their dimensions. Suppose their steering angle limits are all 45^o and the safety distance to the obstacles, R_{safe} given in (6.5), is 1 meter. Using these as our simulation parameters, the needed shrinking radius guaranteeing saturation-free (SF) and collision-free (CF) for straight line motion (SM) and circular motion (CM) is shown in Table 6.1.

Table 6.1 The needed shrinking radius guaranteeing saturation-free (SF) and collision-free (CF) for straight line motion (SM) and circular motion (CM) MSA = Maximum Steering Angle; MDA = Maximum Deviation Angle

	MSA δ_{max}	MDA β_{max}	SF R_s for CM	CF R_s for SM	CF R_s for CM	R_{smin}	R_{max}
(a) Vehicle	45°	21.96°	6.69	3.03	4.15	2.25	5.15
(b) Car	45°	24.84°	2.97	1.55	1.76	1.90	3.94
(c) Robot	45°	26.65°	1.23	1.01	1.03	1.75	2.12

Table 6.1 indicates that for short robot (i.e., the TL/W is smaller, in this example, the robot), since R_{smin} is larger than SF R_s for CM and CF R_s for both SM and CM, any approximate global path generated using R_{smin} as shrinking radius must be saturation-free and collision-free; for medium long vehicle (in this example, the car), since R_{smin} is larger than CF R_s for both SM and CM but less than SF R_s for CM, the approximate global path generated using R_{smin} as shrinking radius is only collision-free, and thus, steering saturation must be checked; for long vehicle (the TL/W is bigger), R_{smin} is less than SF R_s for CM and CF R_s for both SM and CM, Saturation and collision testing must be carried

out simultaneously.

6.6 Detecting potential collisions of a polygonal CLR with polygonal obstacles

The subjects of this and next sections are to consider the problem of determining the collisions of a polygonal CLR with polygonal obstacles as the robot moves along a path. In this section, we develop the point-to-point detection method, while the envelope detection method is presented in the next section.

Since only the boundary of the robot has the possibility of collisions with obstacles, the first problem considered here is how to determine the locus of every point on the boundary of the robot and then how to check the possibility of collisions with the obstacles.

Let the vertices of the edge EF for a polygonal robot be E and F. For simplification, we only show in the following how to determine the loci of points on one of its edges, say EF, and how to test its collisions with obstacles in the workspace. The same procedure of derivation applies to the other edges of the polygonal robot.

At any instant, the positions of points E and F can be obtained from (2.1)

$$\begin{bmatrix} x_e \\ y_e \end{bmatrix} = \begin{bmatrix} x_{e1}\cos\theta - y_{e1}\sin\theta + x_p \\ x_{e1}\sin\theta + y_{e1}\cos\theta + y_p \end{bmatrix} \tag{6. 15}$$

$$\begin{bmatrix} x_f \\ y_f \end{bmatrix} = \begin{bmatrix} x_{f1}\cos\theta - y_{f1}\sin\theta + x_p \\ x_{f1}\sin\theta + y_{f1}\cos\theta + y_p \end{bmatrix} \tag{6. 16}$$

Any point in the edge EF can be expressed as an equality and an inequality:

$$y - y_e = k_{ef}(x - x_e),\ k_{ef} = \frac{y_e - y_f}{x_e - x_f} \tag{6. 17}$$

$$min\,(x_e, x_f) \le x \le max\,(x_e, x_f) \tag{6. 18}$$

where x and y represent the coordinates of any point on edge EF in terms of the global reference frame; $min(x_e, x_f)$ means the minimum of x_e and x_f; and $max(x_e, x_f)$ means the maximum of x_e and x_f.

Note that we can also use (6.1) and (6.3) to obtain (6.17) and (6.18), but the derivation is less straightforward than that used here when the robot is a polygon.

Suppose the coordinates of the jth and $(j+1)$th vertices of the ith polygonal obstacle B_i are denoted by $b_{i,j}(x_{i,j},y_{i,j})$ and $b_{i,j+1}(x_{i,j+1},y_{i,j+1})$, respectively, in terms of the global reference frame. Then the coordinates of any point on the segment connecting $b_{i,j}$ and $b_{i,j+1}$ are given in the same forms as those of (6.17) and inequality (6.18):

$$y - y_{i,j} = k_{i,j}(x - x_{i,j}),\ k_{i,j} = \frac{y_{i,j+1} - y_{i,j}}{x_{i,j+1} - x_{i,j}} \tag{6.19}$$

$$min(x_{i,j}, x_{i,j+1}) < x < max(x_{i,j}, x_{i,j+1}) \tag{6.20}$$

The solution of (6.17) and (6.19), i.e., the coordinates of the intersection point of the two straight lines, can be obtained as

$$x = \frac{(k_{ef}x_e - y_e) - (k_{i,j}x_{i,j} - y_{i,j})}{k_{ef} - k_{i,j}} \tag{6.21}$$

$$y = \frac{k_{ef}(y_{i,j} - k_{i,j}x_{i,j}) - k_{i,j}(y_e - k_{ef}x_e)}{k_{ef} - k_{i,j}} \tag{6.22}$$

It is obvious that if and only if the x-coordinate of the intersection point, given in (6.21), does not satisfy both the inequalities (6.18) and (6.20), which means that the edge EF of the CLR has no collisions with the edge $b_{i,j}b_{i,j+1}$ of the ith obstacle B_i, then EF is collision-free with the edge $b_{i,j}b_{i,j+1}$; Furthermore, if and only if EF has no collisions with all the edges of the obstacle B_i, then EF is collision-free with B_i; If and only if all the edges of the robot have no collisions with all the edges of the obstacles in the workspace,

then the robot is collision-free and the approximate path is collision-free.

In implementing the checking algorithm using (6.21), two difficulties with slopes arise. The first one we can see is that for vertical line segments, the denominators of the slopes in both (6.17) and (6.19) are zero, and thus the slopes are infinite. In this case, there is no y-intercept. The second one is that the denominator of (6.21) is zero when the two lines are parallel. These two special cases must be handled. A computer representation that uses the same geometrical ideas but is able to avoid these two special cases can be found in reference [146].

6.7 Envelope of a polygonal CLR

The advantage of the checking method developed in section 6.6 for collisions is that it is very efficient when only some critical points such as the transition points between straight lines and circular arcs are required to be checked. Unfortunately, until now we have not been able to prove that the critical points are sufficient to offer enough information about the potential collisions. When every point along the reference path is needed to be checked, this method is not very efficient.

The envelope of a family of curves is a very important concept used in Computer Aided Design (CAD) and Computer Aided Manufacturing (CAM). It is actually a curve formed by the boundary of the swept area of the family of the curves. The underlying idea to use the envelope for checking collisions is that if the envelope is collision-free, then the family of curves forming the envelope must also be collision-free. In this section, we establish the expression of the envelope of the robot when it follows the approximate path to simplify the detection for the potential collisions with obstacles. The feature of the method developed in this section is that for every part (a segment of a straight line or a circular arc, no matter how long, is called a part) of the whole path, only a nonlinear equation is needed to be solved to check the collisions. In other words, this method do not need to check at

every point, but to check for every part.

6.7.1 Envelope of a family of curves

We first derive the equations which determine the envelope of a family of plane curves. If a family of curves are represented in an implicit equation $f(x, y, t) = 0$ at time t, then each of the points of the boundary curve must satisfy this equation for some value of t. In order to derive the conditions the envelope must satisfy, let consider the intersection between two curves $f(x, y, t) = 0$ and $f(x, y, t+\delta t) = 0$. The intersection between them will be close to the boundary curve for small δt. At this intersection, since both $f(x, y, t) = 0$ and $f(x, y, t+\delta t) = 0$ are zero there, we can write

$$\frac{f(x, y, t+\delta t) - f(x, y, t)}{\delta t} = 0 \tag{6.23}$$

It follows that the boundary point satisfies this equation in the limit as $\delta t \rightarrow 0$. Thus the envelope is found by solving the equations

$$f(x, y, t) = 0 \tag{6.24}$$

and

$$\frac{\partial f}{\partial t}(x, y, t) = 0 \tag{6.25}$$

simultaneously.

If, on the other hand, the curves of the family f(x, y, t)=0 are described by the parametric equations

$$x = x(u, t) \tag{6.26}$$

$$y = y(u, t) \tag{6.27}$$

where u is the parameter describing the points on any given curve, and t is the parameter

distinguishing the different curves of the family, then $f(x, y, t) = f(x(u, t), y(u, t), t) = F(u, t)$, say, so that $F(u, t) = 0$. Thus

$$\frac{\partial F}{\partial u} = \frac{\partial f}{\partial x}\frac{\partial x}{\partial u} + \frac{\partial f}{\partial y}\frac{\partial y}{\partial u} = 0 \tag{6.28}$$

$$\frac{\partial F}{\partial t} = \frac{\partial f}{\partial x}\frac{\partial x}{\partial t} + \frac{\partial f}{\partial y}\frac{\partial y}{\partial t} + \frac{\partial f}{\partial t} = 0 \tag{6.29}$$

for all points on any member of the family.

For points on the envelope, however, (6.25) holds, so that (6.28) and (6.29) become

$$\frac{\partial f}{\partial x}\frac{\partial x}{\partial u} + \frac{\partial f}{\partial y}\frac{\partial y}{\partial u} = 0 \tag{6.30}$$

$$\frac{\partial f}{\partial x}\frac{\partial x}{\partial t} + \frac{\partial f}{\partial y}\frac{\partial y}{\partial t} = 0 \tag{6.31}$$

Considering (6.30) and (6.31) as equations for $\frac{\partial f}{\partial x}$ and $\frac{\partial f}{\partial y}$, we find that, unless $\frac{\partial f}{\partial x} = 0$ and $\frac{\partial f}{\partial y} = 0$, we must have

$$\frac{\partial x}{\partial u}\frac{\partial y}{\partial t} - \frac{\partial x}{\partial t}\frac{\partial y}{\partial u} = 0 \tag{6.32}$$

If, alternatively, $\frac{\partial f}{\partial x}$ and $\frac{\partial f}{\partial y}$ are both zero, then the tangent to the curve $f(x, y, t) = 0$ is not defined and the curve must have a cusp when this occurs.

Thus for a family of smooth curves, we may obtain the parametric equation of the

envelope by eliminating either u or t from (6.26) and (6.27) with the aid of (6.32).

6.7.2 Envelope of a polygonal CLR

In what follows, applying the above theory to our study we derive the envelope of a polygonal robot when it moves along a reference path which is given as

$$\begin{bmatrix} x_p \\ y_p \end{bmatrix} = \begin{bmatrix} x_p(t) \\ y_p(t) \end{bmatrix} \tag{6.33}$$

We still consider one of its edges, say EF, as an example. Any point located between E and F can be expressed in the local coordinate frame and the global coordinate frame, respectively,

$$\begin{bmatrix} x_1 \\ y_1 \end{bmatrix} = \begin{bmatrix} x_{e1} + u(x_{f1} - x_{e1}) \\ y_{e1} + u(y_{f1} - y_{e1}) \end{bmatrix}, \quad 0 \le u \le 1 \tag{6.34}$$

$$\begin{bmatrix} x \\ y \end{bmatrix} = \begin{bmatrix} x_1 \cos\theta - y_1 \sin\theta + x_p \\ x_1 \sin\theta + y_1 \cos\theta + y_p \end{bmatrix} \tag{6.35}$$

Differentiating (6.34) and (6.35), we have

$$\begin{bmatrix} \frac{\partial x}{\partial u} \\ \frac{\partial y}{\partial u} \end{bmatrix} = \begin{bmatrix} \frac{\partial x_1}{\partial u}\cos\theta - \frac{\partial y_1}{\partial u}\sin\theta \\ \frac{\partial x_1}{\partial u}\sin\theta + \frac{\partial y_1}{\partial u}\cos\theta \end{bmatrix} = \begin{bmatrix} (x_{f1} - x_{e1})\cos\theta - (y_{f1} - y_{e1})\sin\theta \\ (x_{f1} - x_{e1})\sin\theta + (y_{f1} - y_{e1})\cos\theta \end{bmatrix} \tag{6.36}$$

$$\begin{bmatrix} \frac{\partial x}{\partial t} \\ \frac{\partial y}{\partial t} \end{bmatrix} = \begin{bmatrix} (-x_1 \sin\theta - y_1 \cos\theta)\dot{\theta} + \dot{x}_p \\ (x_1 \cos\theta - y_1 \sin\theta)\dot{\theta} + \dot{y}_p \end{bmatrix} \tag{6.37}$$

In order to eliminate (x_1, y_1), substituting (6.34) into (6.37) and taking (6.35) into

account, we have

$$\begin{bmatrix} \frac{\partial x}{\partial t} \\ \frac{\partial y}{\partial t} \end{bmatrix} = \begin{bmatrix} \dot{x}_e - u\,(y_f - y_e)\,\dot{\theta} \\ \dot{y}_e + u\,(x_f - x_e)\,\dot{\theta} \end{bmatrix} \tag{6.38}$$

Substituting (6.36) and (6.38) into (6.32), we obtain the expression of u which is used to determine the locus of the envelope of EF

$$u = \frac{\dot{x}_e \frac{\partial y}{\partial u} - \dot{y}_e \frac{\partial x}{\partial u}}{\left[(x_f - x_e) \frac{\partial x}{\partial u} + (y_f - y_e) \frac{\partial y}{\partial u} \right] \dot{\theta}} \tag{6.39}$$

Eq. (6.39) indicates that u is a function of $x_p(t)$ and $y_p(t)$. If substituting (6.33), (6.34) and (6.39) into (6.35), we can observe that the locus of the envelope of the family of EF can be expressed as the function of $x_p(t)$ and $y_p(t)$. Therefore the checking collision problem is converted into the problem of determining the intersection of (6.35) with a straight line, i.e., an edge of the obstacle B_i expressed by (6.19) and (6.20).

6.8 Recovery from failure

When a CLR tracks a straight line, the deviation angle tends to zero. Thus the swept area of the robot will become smaller and smaller. Since the shrinking radius R_s is always bigger than the width of the robot, the possibility of collisions and saturations is relatively lower during a straight line motion than that during a turning. Generally speaking, the most dangerous points of collisions and saturations are located near corners of the obstacles, especially the vertices. The situation is worsen when a sharp turn is encountered.

People can drive a car around a corner easily. That is because the curbs at corners have been designed using design vehicles [232] and the resulting corner curbs consist of

circular arcs and straight lines. In robotic community, the workspace is usually assumed to be full of polygonal obstacles which make the collisions and saturations occur more frequently. In this section, we use two curves introduced by Nelson [137] to recover from collisions and saturations at corners if they are found.

6.8.1 Quintic polynomial paths

Curves that produce a transition between parallel lanes in the same direction are usually called lane-change maneuvers. Here we give a brief introduction of the single quintic polynomial segment that provides a continuous-curvature transition between the parallel lanes of travel [137].

The general expression for a quintic polynomial in Cartesian coodinates is

$$y(x) = a_0 + a_1 x + a_2 x^2 + a_3 x^3 + a_4 x^4 + a_5 x^5 \tag{6.40}$$

Consider the lane-change maneuver in the coordinate frame shown in Fig. 6.9 (a). The six coefficients in (6.40) are chosen to satisfy the position, slope, and curvature constraints of this maneuver, namely

$$y = 0, \frac{dy}{dx} = 0, \kappa = 0 \text{ at } x = 0 \tag{6.41}$$

$$y = y_e, \frac{dy}{dx} = 0, \kappa = 0 \text{ at } x = x_e \tag{6.42}$$

where κ is the curvature of $y(x)$.

The quintic polynomial satisfying constraints (6.41) and (6.42) has only three nonzero coefficients and can be written in the form

$$y(x) = y_e\left[10\left(\frac{x}{x_e}\right)^3 - 15\left(\frac{x}{x_e}\right)^4 + 6\left(\frac{x}{x_e}\right)^5\right] \tag{6.43}$$

The quintic polynomial curve resulting from (6.43) is shown in Fig. 6.9 (a). The curvature

function in Fig. 6.9 (b) shows that the quintic polynomial provides the desired continuous curvature path. The maximum curvature and curvature-rate for the function shown in Fig. 6.9 (b) increase directly with the lane change slope ratio y_e/x_e. This ratio must be chosen sufficiently low so that the resulting continuous steering function does not violate the peak steering and steering-rate constraints for a particular car-like robot. Given that these constraints are met, the simple three term expression (6.43) for the quintic polynomial applies to lane-change segments of arbitrary location and orientation in the workspace layout by transforming from the coordinate frame shown in Fig. 6.9 (a) to the coordinate frame aligned with the lane-change starting point.

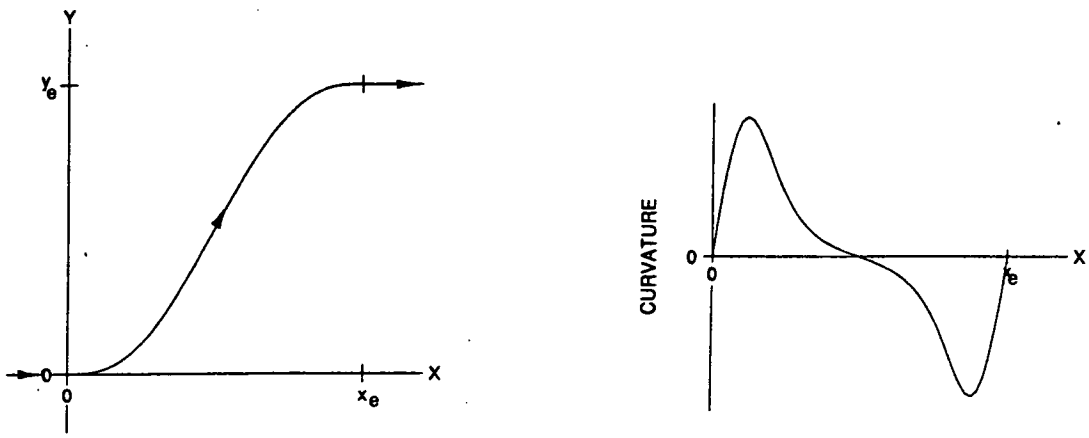

(a) (b)

Fig. 6.9 (a) Lane-change maneuver using a quintic polynomial segment
(b) curvature function of the quintic polynomial

6.8.2 Polar spline paths

Curves that produce a smooth transition between lines intersecting at an arbitrary angle, and are symmetric with respect to the intersection point, are usually called arc turns. The turn angle is measured in the direction of the change of heading with counter-clockwise positive.

A cartesian quintic polynomial, given by (6.40), can be used to provide continuous-curvature turns that are close in shape to arc turns, provided the magnitude of the turn angle is less than about 45°. For larger angles, however, the quintic begins to curve away

from the circular arc and "blows up", i.e., has coefficients tending to infinity, as the turn angle approaches 90° [137]. This problem could be avoided by segmenting a large-angle turn into several smaller turns, but a concatenation of curve segments requires additional computation that should be avoided.

Nelson [137] introduced a single, smooth curve segment that does not deviate far in shape from the circular arc it will replace and yet can satisfy the position, heading, and curvature constraints imposed at the start and end points. The polar coordinates of the curve, with the curve specified by the polar length r, as a function of the polar angle ψ, are chosen so that the independent variable changes relatively uniformly with respect to the distance along the curve, regardless of the total angle. The curve $r(\psi)$, expressed as a polynomial in ψ, has the general form

$$r(\psi) = a_0 + a_1\psi + a_2\psi^2 + a_3\psi^3 + a_4\psi^4 + \ldots\ldots \tag{6.44}$$

where the number of the terms needed depends on the number of conditions imposed.

Consider arc turns in the coordinate frame shown in Fig. 6.10. Here, R is the radius of the circular arc connecting the two line segments, and Φ is the total angle of the turn. The position, slope, and curvature constraints on the polynomial (6.44) for the desired arc turns are

$$r = R,\ r' = 0,\ \kappa = 0 \text{ at } \psi = 0 \tag{6.45}$$

$$r = R,\ r' = 0,\ \kappa = 0 \text{ at } \psi = \Phi \tag{6.46}$$

where $r' = \frac{dr}{d\psi}$, and κ is the curvature of r. The general expression for curvature of any curve is

$$\kappa = \frac{d\alpha}{ds} \tag{6.47}$$

where s is the distance along the reference path, and α is the angle of the tangent to the reference path.

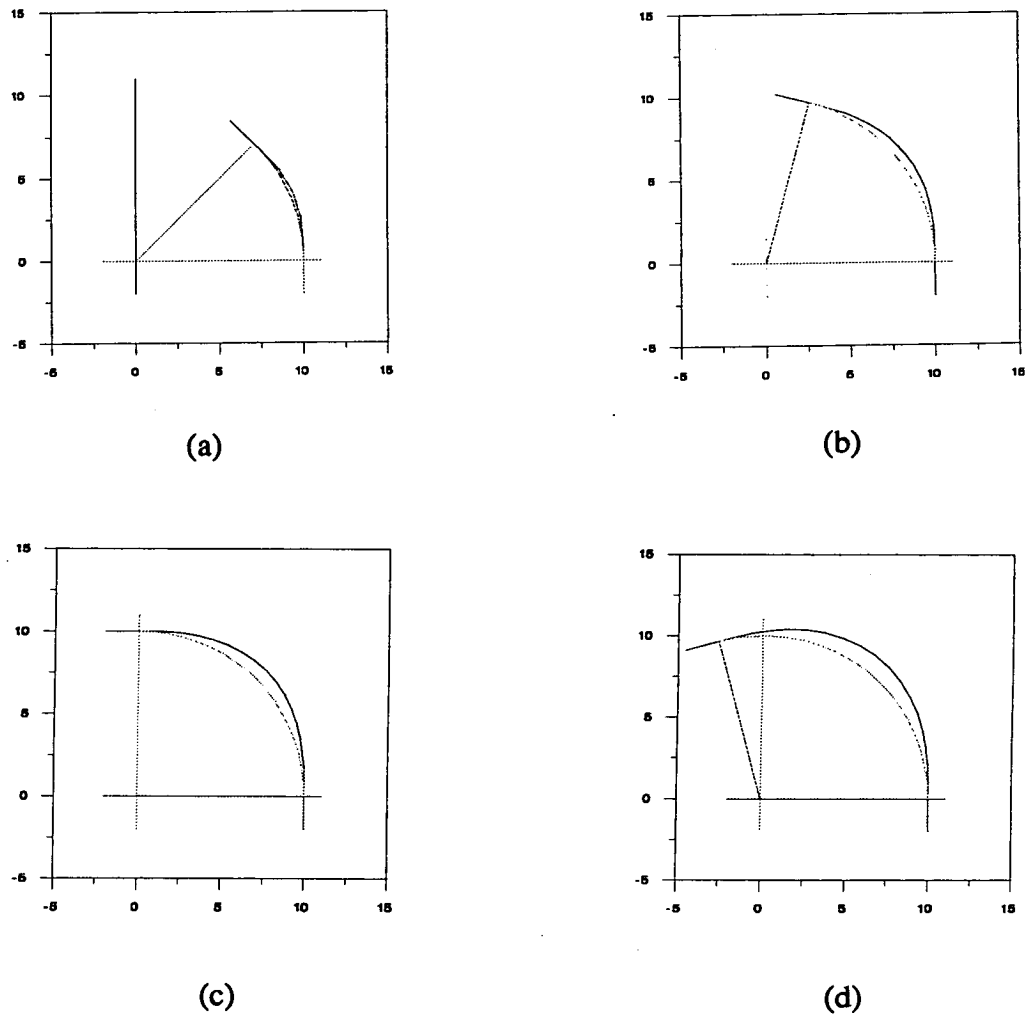

Fig. 6.10 Polar spline segments for arc turns of (a) 45, (b) 75, (c) 90, and (d) 105. The corresponding circular arc turns are shown as dotted lines

For a path defined in polar coordinates (r, ψ), the tangent angle can be expressed as

$$\alpha = \pi/2 + \psi - arc\tan(r'/r) \tag{6.48}$$

Differentiating (6.48) with respect to ψ gives

$$\frac{d\alpha}{d\psi} = 1 - \frac{rr'' - r'^2}{r^2 + r'^2} \tag{6.49}$$

where $r'' = \dfrac{d^2r}{d\psi^2}$.

The infinitesimal change in path length ds is given in polar form by

$$ds = (r^2 + r'^2)^{1/2} d\psi \tag{6.50}$$

Using (6.49) and (6.50) in (6.47) yields the desired expression for the curvature, namely

$$\kappa = \frac{r^2 + 2r'^2 - rr''}{(r^2 + r'^2)^{3/2}} \tag{6.51}$$

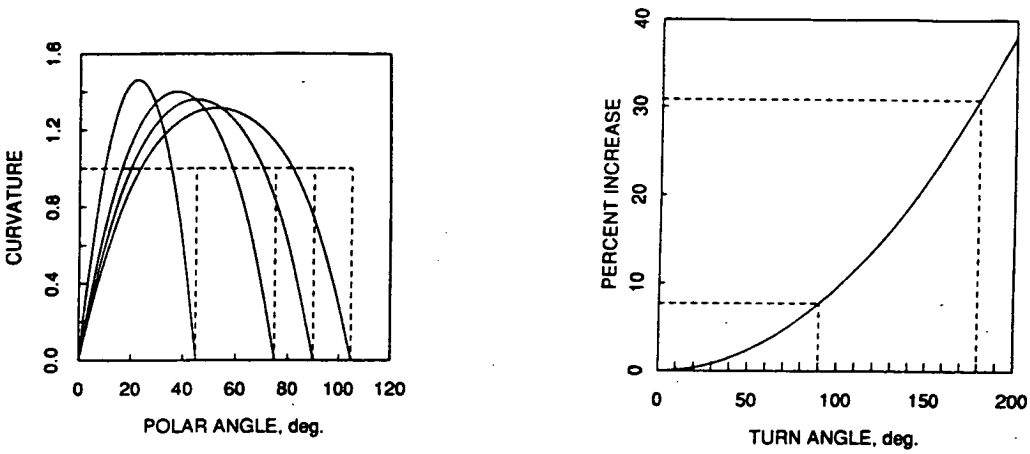

(a) (b)

Fig. 6.11 (a) Curvature functions for the spline segments of Fig. 7.10. The curvature functions for the corresponding circular arcs are shown in dashed lines (b) percent increase in peak radial length for single segment polar splines as compared to circular arc turns as a function of turn angle

Using the position and slope constraints of (6.45) and (6.46) in (6.51), it follows that the zero curvature constraints in (6.45) and (6.46) are equivalent to requiring that $r'' = 0$ at $\psi = 0$ and $\psi = \Phi$. Applying these constraints on r, r' and r'' yields four nonzero coefficients in (6.44), namely $a_0 = R$, $a_2 = R/2$, $a_3 = -R/\Phi$, and $a_4 = R/(2\Phi^2)$.

This polar spline fit between line segments can thus be written as

$$r(\psi) = R\left(1 + \frac{\psi^2}{2} - \frac{\psi^3}{\Phi} + \frac{\psi^4}{2\Phi^2}\right) \tag{6.52}$$

The (x, y) coordinates of the polar spline are then obtained from $x = r\cos\psi$ and $y = r\sin\psi$.

The continuous-curvature polar splines resulting from (6.52) are shown in Fig. 6.10 for four values of the turn angle Φ. The curvature functions (6.51) for these four polar spline segments are shown in Fig. 6.11(a). The paths and curvature functions for the corresponding circular arc turns are also shown (dashed lines in Fig. 11(a)) for comparison. For turn angles of 90° or less, the polar spline curvature functions are very close to parabolic in shape and are very close to the cubic spiral curves of Kanayama and Hartman [85], which are optimally-smooth curves in the sense of minimizing the integral-square-curvature rate (centripetal jerk). In this sense, the single-segment polar splines provide a simple means to achieve near-optimally smooth arc turns of 90° or less.

These results suggest that the polar spline is a very appropriate choice for producing continuous-curvature arc turns of arbitrary angle. It has a closed-form expression, which is a simple function of the turn radius R and turn angle Φ. The curve it produces is symmetric, has near-optimal smoothness in the sense described above, and is reasonably close to the circular arc, although both these qualities begin to degrade for turn angles greater than 90°.

The peak value r_p of $r(\psi)$ in (6.52) occurs at the mid-point of the turn, where $\psi = \Phi/2$. The ratio of this peak value to the radius of the circular arc is thus given by

$$\frac{r_p}{R} = 1 + \frac{\Phi^2}{32} \tag{6.53}$$

where Φ is the turn angle in radians. The second term in (6.53), which represents the

fractional increase in the peak value of the polar spline radial over that of the circular arc, is plotted in Fig. 6.11(b) for turn angles up to 200°. For right angle turns, the increase is only about 8 percent, but it grows as the square of the turn angle, and for 180° turns, it is over 30 percent.

The minimum curvature radius also occurs at the mid-point of the turn. The ratio of this minimum radius to the radius of the circular arc is given by

$$\frac{\rho_{min}}{R} = \frac{(1 + (\Phi/32)^2)^2}{1.5 + (\Phi/32)^2} \tag{6.54}$$

6.8.3 Modification of the approximate global path

Once a saturation of steering angle or a collision with obstacles is found at a corner, the following three strategies are used to find a modified approximate global path, as shown in Fig. 6.12.

1. Use a quintic polynomial fit to produce a lane-change maneuver away from the vertex of the obstacle.

2. Use a polar spline fit to produce a smooth, curvature-continuous maneuver.

3. Use another quintic polynomial to produce another lane-change maneuver.

In Fig. 6.12, the original global path consists of the straight line AG, the circular arc GH, and the straight line HF. The modified path consists of the straight line AB, the quintic polynomial BC, the polar spline CD, the quintic polynomial DE, and the straight line EF. The principle of designing the quintic polynomial fit and the polar spline fit is to have a proper clearance to the corner, neither too far nor too close. Our experience shows that the saturation-free shrinking radius given in (6.9) is the most suitable candidate for the radius R of the circular arc turns a polar spline will replace. The turn angle Φ in (6.52) is determined by the original global path. The difference between R and R_s corresponds to the y_e in (6.43) while the x_e in (6.43) corresponds to the length of BG in Fig. 6.12 and is

determined by the minimum curvature requirement of the quintic polynomial.

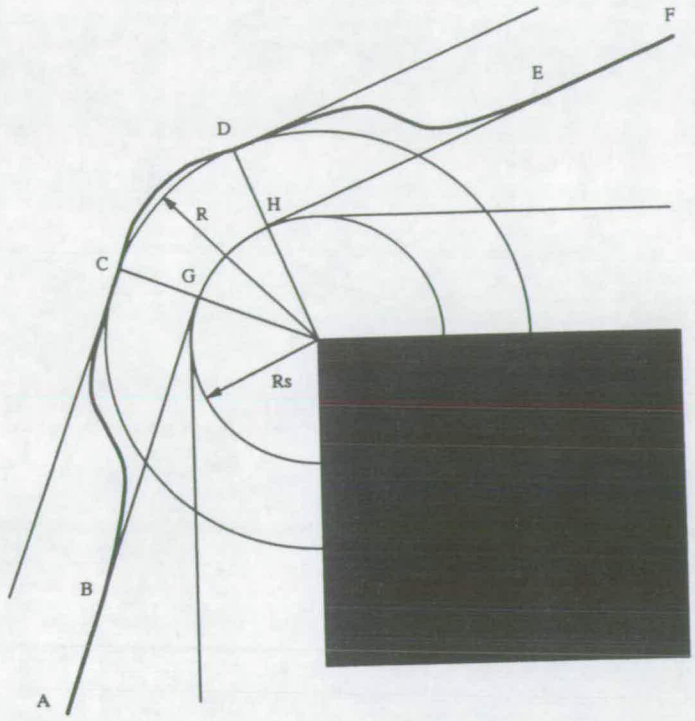

Fig. 6.12 Modified path shown as the segments of the quintic polynomial BC, the polar spline CD, and the quintic polynomial DE

The advantage of these strategies is that they make best use of the clearance everywhere. In other words, it allows a narrow space to be passed by running a straight line motion, thus avoids any waste of effective space.

After the modification of the approximate global path, the checking of collision is carried out again. This time, if collision is found at the corner, then we can say that the channel is too narrow to be passed.

6.9 Summary

In this chapter, a path planning algorithm taking into account the nonholonomic constraint and steering angle limit has been presented. Essentially, path planning is to find a path which avoids the obstacles and is able to be traced. Although the algorithm is heuristic, it has the advantages of robustness, efficiency, smoothness and reliability over the previous

algorithms. Our experience shows that during normal environment, the path generated is quite similar to that traced by a man-driven car or truck.

Chapter 7

Conclusions and scope for future research

7.1 Conclusions

This thesis presents a complete and systematic investigation into some fundamental issues relating to the development of an autonomous wheeled mobile robot, and makes several important contributions to an improved understanding of motion feasibility and smoothness for each of four kinds of wheeled mobile robots. The most important accomplishments are:

1. The concepts of inverse and direct kinematics widely used in manipulators are, for the first time, introduced to wheeled mobile robots, and a unified treatment of kinematics for each of the four kinds of robots is presented. This model is the best in the sense that it is general, applicable to any dimension of vehicle or vehicle combination, and to any path. It also gives the steering angle and the velocity needed for a reference point to tracing a specified path.

2. The concept of feasible deviation angle and its relationship with steering angle limit are developed. This is important for enabling intelligent sensor-based robots to avoid obstacles.

3. Four typical motions, i.e., pure translation, pure rotation, straight line motion and circular motion for car-like and dual drive robots are defined. The conditions and analytic formulas for each of these four motions are given and their applications are discussed.

4. The geometric highway design problem encountered by very large vehicles or vehicle combinations is solved.

5. A critical review of the path planning algorithms presently available is made and the reason why these algorithms are not suitable for the most widely used car-like or dual

drive robots is examined in detail.

6. A formal formulation of the path planning problem is given and a robust, efficient and reliable path planning algorithm for a car-like robot, taking into account nonholonomic constraint and steering angle limit is developed. This algorithm may also apply to a dual drive robot.

In addition, several phenomena which should prove of interest to other robot researchers are also observed and discussed. These include: the phenomenon of a pirouette for a car-like and a dual drive robot, the translation property of a synchro drive and steering robot and the singularity for an omnidirectional robot.

7.2 Future research

The theory described here is the first but necessary step on the long road in the development of competent autonomous robots. The promising areas for future research include:

1. The dynamics for each of the four kinds of wheeled mobile robots

There is a considerable amount of work on the dynamics of a vehicle which is mainly focused on its handling and ride characteristics [1,185,186,219], but this dynamics has no relevance to an autonomous robot. Although research on wheeled robots has been conducted for more than twenty years, there exists no widely accepted dynamic theory for wheeled mobile robots. This is in contrast to the extensive theory developed for manipulators.

2. Nonholonomic motion planning

This problem can be described as: given two arbitrary configurations of a system with nonholonomic constraints (a wheeled mobile robot system is one such system), find the input control variables which satisfy the nonholonomic constraints and drive the system from one configuration to the other. In recent years, there has been a considerable amount

of work on the nonholonomic motion planning problem [101,105,111,134]. This problem is also referred to as the controllability of nonholonomic systems [104] and the stabilization problem [153]. Actually, as the input control variables are always a function of the configuration variables of a robot system, this nonholonomic motion problem can also be treated as the trajectory generation problem, and vice-versa. This is our on-going research. Some results which are not included in this thesis have been achieved [236].

3. Control of each kind of wheeled mobile robots

This topic includes traditional control methods, i.e. kinematic-based control, dynamic-based control and nontraditional control methods, e.g. fuzzy logic based control and neural network based control. A comparative study of fuzzy logic based control and neural network based control for backing up a truck-and-trailer has been reported. A comparative study of traditional and nontraditional methods seems necessary.

4. Sensing and computer vision

This has probably been the most active research area in the past. A wide variety of sensing technologies are available: ultrasonic, infrared and laser range sensing; and monocular, binocular, and trinocular vision have all been explored. The difficulty is in interpreting the sensed data, that is, in deciding what the sensor signals tell us about the external word. The trend is to attack this problem by so-called sensor fusion, that is, by combining the outputs of multiple feature detectors possibly operating on a variety of sensors or simply multiple observations of the same objects. It seems that Kalman filtering is the most promising method [15,20,53,168].

5. Integration of all aspects mentioned above into a Computer Aided Design System

Finally, the problem of integration of all aspects mentioned above into a Computer Aided Design System must be encountered and solved. This CAD system would provide a controller for a mobile robot capable of (1) sensing its environment, (2) interpreting this sensor information to refine its knowledge of its position and the environment's structure, (3) planning a path from an initial to a goal position in the presence of known or perhaps

unknown obstacles, and (4) execute the commands from the computer to achieve the desired motion.

In summary, creating an autonomous wheeled mobile robots is a real challenge. The kinematic models developed, the analyses carried out, and the path planning algorithm presented here can be used as a basis for future research.

REFERENCES

[1] Ackermann, J. and Sienel, W., 1993, Robust Yaw Damping of Cars with Front and Rear Wheel Steering, IEEE Trans. on Control Systems Technology, Vol. 1, pp. 15-20.

[2] Aken, Ir. L. V. and Brussel, H. V., 1988, On-line Robot Trajectory Control in Joint Coodinates by Means of Imposed Acceleration Profiles, Robotica, Vol. 6, pp. 185-195.

[3] Alexander, J. C., 1985, On the Motion of a Trailer-Truck Problem, SIAM Rev., Vol. 27, pp. 578-579.

[4] Alexander, J. C. and Maddocks, J. H., 1988, On the Maneuvering of Vehicles, SIAM J. Appl. Math. Vol. 48, pp. 38-51.

[5] Alexander, J. C. and Maddocks, J. H., 1989, On the Kinematics of Wheeled Mobile Robots, Int. J. Robotics Research, Vol. 8, pp. 15-27.

[6] Arai, T. and Nakano, E., 1983, Development of Measuring Equipment for Location and Direction (MELODI) Using Ultrasonic Waves, Trans. of the ASME, J. Dynamic Systems, Measurement, and Control, Vol. 105, pp. 152-156.

[7] Arkin, R. C. and MacKenzie, D., 1994, Temporal Coordination of Perceptual Algorithms for Mobile Robot Navigation, IEEE Trans. on Robotics and automation, Vol. 10, pp. 276-286.

[8] Badcock, J. M., Dun, J. A., Ajay, K., Kleeman, L. and Jarvis, R. A., 1993, An Autonomous Robot Navigation System--Integrating Environmental Mapping, Path Planning, Location and Motion, Robotica, Vol. 11, pp. 97-103.

[9] Barraquand, J. and Latombe, J. C., 1990, Controllability of Mobile Robots with Kinematic Constraints, Technical Report No. STAN-CS-90-1317, Department of Computer Science, Stanford University.

[10] Barraquand, J., Langlois, B. and Latombe, J. C., 1990, Robot Motion Planning with Many Degrees of Freedom and Dynamic Constraints, In: Miura, H and Arimoto, S. (eds.), The fifth Int. Symposium on Robotics Research, The MIT Press, Cambridge, Massachusetts, pp. 435-444.

[11] Barshan, B. and Kuc, R., 1992, ROBAT: A Sonar-Based Mobile Robot for Bat-Like Prey Capture, Proc. of the 1992 Int. Conf. on Robotics and Automation, Nice, France, pp. 274-279.

[12] Baylis, J., 1973, The Mathematics of a Driving Hazard, Math. Gaz., Vol. 57, pp. 23-26.

[13] Beazel, V. and Red, E., 1993, Inaccuracy Compensation and Piecewise Circular Approximation of Parametric Paths, Robotica, Vol. 11, pp. 413-425.

[14] Bender, E. A., 1979, A Driving Hazard Revisited, SIAM Rev., Vol. 21, pp. 136-138.

[15] Bien, Z., Kwon, H. Y., Youn, J. and Suh, I. H., 1991, A Closed Form 3D Self-Positioning Algorithm for a Mobile Robot Using Vision and Guide-Marks, Robotica, Vol. 9, pp. 265-274.

[16] Billing, J. R. and Mercer, W. R. J., 1986, Swept Paths of Large Trucks in Right Turns of Small Radius, Transportation Research Record 1052, Symposium on Geometric Design for Large Trucks, pp. 116-119.

[17] Blazevic, P., Delaplace, S., Fontaine, J. G., and Rabit, J., 1991, Mobile Robot Using Ultrasonic Sensors: Study of a Degraded Mode, Robotica, Vol. 9, pp. 365-370.

[18] Bloch, A. M., Reyhanoglu, M. and McClamroch, N. H., 1992, Control and Stabilization of Nonholonomic Dynamic Systems, IEEE Trans. on Automatic Control, Vol. 37, pp. 1746-1757.

[19] Borenstein, J. and Koren, Y., 1988, Obstacle Avoidance with Ultrasonic Sensors, IEEE Trans. on Robotics and Automation, Vol. 4, pp. 213-218.

[20] Borenstein, J. and Koren, Y., 1991, Histogramic In-Motion Mapping for Mobile Robot Obstacle Avoidance, IEEE Trans. on Robotics and Automation, Vol. 7., pp. 535-539.

[21] Borenstein, J. and Koren, Y., 1991, The Vector Field Histogram-Fast Obstacle Avoidance for Mobile Robots, IEEE Trans. on Robotics and Automation, Vol. 7, pp. 278-288.

[22] Borenstein, J., 1993, Multi-Layered Control of a Four-Degree-of-Freedom Mobile Robot with Compliant Linkage, Proc. of IEEE Int. Conf. on Robotics and Automation, Vol. 3, pp. 7-12.

[23] Brooks, R. A., 1983, Solving the Find-Path Problem by Good Representation of Free Space, IEEE Trans. on Systems, Man and Cybernetics, Vol. SMC-13, No. 3, pp. 190-197.

[24] Brooks, R. A. and Lozano-Perez, T., 1985, A Subdivision Algorithm in Configuration Space for Findpath with Rotation, IEEE Trans. on Systems, Man and Cybernetics, Vol. SMC-15, No. 2, pp. 224-233.

[25] Brooks, R. A., 1986, A Robust Layered Control System for a Mobile Robot, IEEE J. Robotics and Automation, Vol. 2, pp. 14-23.

[26] Brown, F. T., 1976, Bond Graphs for Nonholonomic Dynamic Systems, Trans. of the ASME, J. Dynamic Systems, Measurement, and Control, Vol. 98, pp. 361-366.

[27] Butler, J., Hack, B. and Tomizuka, M., 1991, Reference Input Generation for High Speed Coordinated Motion of a Two Axis System, Trans. of ASME, J. Dynamic Systems, Measurement, and Control, Vol. 113, pp. 67-74.

[28] Cai, C. and Regtien, P. P. L., 1993, A Versatile Ultrasonic Ranging System, Sensor Review, Vol. 13, pp. 22-25.

[29] Carlise, B., 1983, An Omnidirectional Mobile Robot, Developments in Robotics, Eds. Rocks. B. and Kempston, England: IFS Publishing Ltd., pp. 79-88.

[30] Charles, E. T., 1984, Path Relaxation: Path Planning for a Mobile Robot, CMU-RI-TR-84-5.

[31] Chen, H. F. and Velinsky, S., 1992, Designing Articulated Vehicles for Low-Speed Maneuverability, ASCE, J. Transportation Engineering, Vol. 118, pp. 711-728.

[32] Cheung, E. and Lumelsky, V. J., 1989, Proximity Sensing in Robot Manipulator Motion Planning: System and Implementation Issues, IEEE Trans. on Robotics and Automation, Vol. 5, pp. 740-751.

[33] Connell, J. H., 1990, Minimalist Mobile Robotics, A Colony-style Architecture for an Artificial Creature, Academic Press, New York.

[34] Coron, J. M. and d'Andrea-Novel, B., 1992, Smooth Stabilizing Time-Varying Control Laws for a Class of Nonlinear Systems-Application to Mobile Robots, Proc. IFAC Nonlinear Control System Design, Bordeaux, France, pp. 413-418.

[35] Cox, I. J. and Gehani, N. H., 1989, Exception Handling in Robotics, Computer, Vol. 22, No. 4, pp. 43-49.

[36] Cox, I. J., 1991, Blanche-An Experiment in Guidance and Navigation of an Autonomous Robot Vehicle, IEEE Trans. on Robotics and Automation, Vol. 7, pp. 193-204.

[37] Crowley, J., 1985, Navigation for an Intelligent Mobile Robot, IEEE J. Robotics and Automation, Vol, 1, pp. 31-41.

[38] Curran, A. and Kyriakopoulos, K. J., 1993, Sensor-Based Self-Localization for Wheeled Mobile Robots, Proc. of IEEE Int. Conf. on Robotics and Automation, Vol. 1, pp. 8-13.

[39] Dahl, O. and Nielsen, L., 1990, Torque-Limited Path Following by On-Line Trajectory Time Scaling, IEEE Trans. on Robotics and Automation, Vol. 6, pp. 554-561.

[40] DeCabooter, P. H. and Solberg, C. E., 1988, Designated Highway System Truck Operation Study: Geometric Consideration, Presented at Committee on motor vehicle Size and Weight, Transp. Res. Board, Washington, D.C.

[41] Drake, K. C., Mcvey, E. S. and Inigo, R. M., 1987, Experimental Position and Ranging Results for a Mobile Robot, IEEE J. Robotics and Automation, Vol. 3, pp. 31-42.

[42] Dubins, L., 1957, On Curves of Minimal Length with a Constraint on Average Curvature and with Pre-

scribed Initial and Terminal Positions and Tangents, American J. Mathematics, Vol. 79, pp. 497-516.

[43] Easa, S. D., 1993, Unified Design of Horizontal Circular Curves, ASCE, J. Transportation Engineering, Vol. 119, pp. 94-110.

[44] Elfes, A., 1987, Sonar-Based Real-World Mapping and Navigation, IEEE J. Robotics and Automation, Vol. 3, pp. 249-265.

[45] Elnagar, A. and Basu, A., 1993, Heuristics for Local Path Planning, IEEE Trans. on Systems, Man, and Cybernetics, Vol. 23, pp. 624-634.

[46] Engelberger, J. F., 1993, Health-Care Robotics Goes Commercial: the 'HelpMate' Experience, Robotica, Vol. 11, pp. 517-523.

[47] Ervin, R. D. and Guy, Y, 1986, Axioms Relating Size and Weight Constraints to the Response of Trailers in Combination Trucks, Int. Symp. on Heavy Vehicle Weights and Dimensions, Kelowna, Canada, pp. 35-41.

[48] Evans, J., Krishnamurthy, B., Skewis, T. and Lumelsky, V., 1992, Handling Real-World Motion Planning: A Hospital Transport Robot, IEEE Control Systems, February, pp. 15-20.

[49] Fardanesh, B. and Rastegar, J., 1992, A New Model-Based Tracking Controller for Robot Manipulators Using Trajectory Pattern Inverse Dynamics, IEEE Trans. on Robotics and Automation, Vol. 8, pp. 279-285.

[50] Fearing, R. S. and Binford, T. O., 1991, Using a Cylindrical Tactile Sensor for Determining Curvature, IEEE Trans. on Robotics and Automation, Vol. 7, pp. 806-817.

[51] Feng, L., Fainman, Y. and Koren, Y., 1992, Estimation of the Absolute Position of Mobile Systems by an Optoelectronic Processor, IEEE Trans. on Systems, Man, and Cybernetics, Vol. 22, pp. 953-963.

[52] Feng, L., Koren, Y. and Borenstein, J., 1993, Cross-Coupling Motion Controller for Mobile Robots, IEEE Control Systems, Vol. 13, No. 6, pp. 35-43.

[53] Flynn, A. M., 1988, Combining Sonar and Infrared Sensors for Mobile Robot Navigation, Int. J. Robotics Research, Vol. 7, pp. 5-14.

[54] Fok, K. Y. and Kabuka, M. R., 1991, An Automatic Navigation System for Vision Guided Vehicle Using a Double Heuristic and a Finite State Machine, IEEE Trans. on Robotics and Automation, Vol. 7, pp. 181-189.

[55] Fossum, T. V. and Lewis, G. N., 1981, A Mathematical Model for Trailer-Truck jackknifing, SIAM Rev., Vol. 23, pp. 95-99.

[56] Foux, G., Heymann, M. and Bruckstein, A., 1993, Two-dimensional Robot Navigation among Unknown Stationary Polygonal Obstacles, IEEE Trans. on Robotics and Automation, Vol. 9, pp. 96-102.

[57] Fowler, B. and Bartels, R., 1993, Constraint-Based Curve Manipulation, IEEE Computer Graphics & Applications, Vol. 13, No. 5, pp. 43-49.

[58] Freedman, H. I. and Riemenschneider, S. D., 1983, Determining the Path of the Rear Wheels of a Bus, SIAM Rev., Vol. 25, pp. 561-568.

[59] Fujimura, K. and Samet, H., 1989, A Hierarchical Strategy for Path Planning Among Moving Obstacles, IEEE Trans. on Robotics and Automation, Vol. 5, pp. 61-69.

[60] Graettinger, T. J. and Krogh, B. H., 1989, Evaluation and Time-Scaling of Trajectories for Wheeled Mobile Robots, Trans. of ASME, J. Dynamic Systems, Measurement, and Control, Vol. 111, pp. 222-231.

[61] Griswold, N. C. and Eem, J., 1990, Control for Mobile Robots in the Presence of Moving Objects, IEEE Trans. on Robotics and Automaton, Vol. 6, pp. 263-268.

[62] Gutsche, R. and Wahl, F. M., 1992, A New Navigation Concept for Mobile Vehicles, Proc. of the 1992 Int. Conf. on Robotics and Automation, Nice, France, pp. 215-220.

[63] Hammond, G., 1986, AGVS at Work, Automated Guided Vehicle Systems, IFS Ltd.

[64] Heald, K. L. 1986, Use of the WHI Offtracking Formula, Transportation Research Record 1052, Symposium on Geometric Design for Large Trucks, pp. 45-53.

[65] Hemami, A., and Cheng, R. M. H., 1992, A Preliminary Step for Path Tracking of Coordinated Robot Arms Based on Kinematics, Int. J. Robotics Research, Vol. 11, pp.185-195.

[66] Hemami, A., Mehrabi, M. G. and Cheng, R. M. H., 1992, Synthesis of an Optimal Control Law for Path Tracking in Mobile Robots, Automatica, Vol. 28, pp. 383-387.

[67] Hemami, A., Mehrabi, M. G. and Cheng, R. M. H., 1994, Optimal Kinematic Path Tracking Control of Mobile Robots with Front Steering, Robotica, Vol. 12, pp. 563-568.

[68] Hillier, V. and Pittuck, F. W., 1966, Fundamentals of Motor Vehicle Technology, Hutchinson Educational LTD, London.

[69] Holland, J. M., 1983, Basic Robotic Concepts, Howard W. Sams & Co.

[70] Hongo, T., Arakawa, H., Sugimoto, G., Tange, K. and Yamamoto, Y., 1986, An Automatic Guidance System of a Self-Controlled Vehicle, IEEE Trans. on Industrial Electronics, Vol. 34, pp. 5-10.

[71] Hoogerwoord, R., 1986, An Implementation of Mutual Inclusion, Information Processing Letters, Vol. 23, pp. 77-80.

[72] Hu, T. C., Kahng, A. B. and Robins, G., 1993, Optimal Robust Path Planning in General Environments, IEEE Trans. on Robotics and Automation, Vol. 9, pp. 755-784.

[73] Huang, H. P. and Lee, P. C., 1992, A Real-Time Algorithm for Obstacle Avoidance of Autonomous Mobile Robots, Robotica, Vol. 10, pp. 217-227.

[74] Hung, J. Y., Gao, W. and Hung, J. C., 1993, Variable Structure Control: A Survey, IEEE Trans. on Industrial Electronics, Vol. 40, pp. 2-22.

[75] Hutchinson, B. G., 1990, Large-Truck Properties and Highway Design Criteria, ASCE, J. Transportation Engineering, Vol. 116, pp. 1-21.

[76] Hwang, Y. K. and Ahuja, A., 1992, A Potential Field Approach to Path Planning, IEEE Trans. on Robotics and Automation, Vol. 8, pp. 23-32.

[77] Ilari, J. and Torras, C., 1990, 2D Path Planning: A Configuration Space Heuristic Approach, Int. J. Robotics Research, Vol. 9, pp. 75-91.

[78] Ikeuchi, K. and Robert, J. C., 1991, Modeling Sensor Detectability with the VATAGE Geometric/Sensor Modeler, IEEE Trans. on Robotics and Automation, Vol. 7, pp. 771-784.

[79] Jagannathan, S., Zhu, S. Q. and Lewis, F. L., 1994, Path Planning and Control of a Mobile Base with Nonholonomic Constraints, Robotica, Vol. 12, pp. 529-539.

[80] Jansen, J. F. and Kress, R. L., 1989, Analysis and Control of A Three-Degree-of-Freedom Robot Platform, J. of Mechanical Working Technology, Vol. 18, pp. 269-282.

[81] Kambhampati, S. and Davis, L. S., 1986, Multiresolution Path Planning for Mobile Robots, IEEE J. Robotics and Automation, Vol. 2, pp. 135-145.

[82] Kanatani, K. and Watanabe, K., 1990, Reconstruction of 3-D Road Geometry From Images for Autonomous Land Vehicles, IEEE Trans. on Robotics and Automation, Vol. 6, pp. 127-132.

[83] Kanayama, Y. and Miyake, N., 1986, Trajectory Generation for Mobile Robots, In: Faugeras, D. and Giralt, G. (eds.), The third Int. Symposium on Robotics Research, The MIT Press, Cambridge, Massachusetts, pp. 333-340.

[84] Kanayama, Y. and Yuta, S., 1988, Vehicle Path Specification by a Sequence of Straight lines, IEEE J. Robotics and Automation, Vol. 4, pp. 265-276.

[85] Kanayama, Y. and Hartman, B. I., 1989, Smooth Local Path Planning for Autonomous Vehicles, Proc.

of the 1989 IEEE Int. Conf. on Robotics and Automation, pp. 1265-1270.

[86] Kanayama, Y., Kimura, Y., Miyazaki, F. and Noguchi, T., 1990, A Stable Tracking Control Method for an Autonomous Mobile Robot, Proc. of the 1990 IEEE Int. Conf. on Robotics and Automation, pp. 384-389.

[87] Kanayama, Y., 1990, A Mathematical Theory of Object Centered Path Planning, In: Miura, H and Arimoto, S. (eds.), The fifth Int. Symposium on Robotics Research, The MIT Press, Cambridge, Massachusetts, pp. 387-394.

[88] Kanayama, Y. and Krahn, G., 1993, Two Dimensional Transformation and Its application to Vehicle Motion Control and Analysis, Proc. of IEEE Int. Conf. on Robotics and Automation, pp. 13-18.

[89] Kant, K. and Zucker, S. W., 1986, Toward Efficient Trajectory Planning: The Path-Velocity Decomposition, Int. J. Robotics Research, Vol. 5, pp. 72-89.

[90] Khatib, O., 1986, Real-Time Obstacle Avoidance for Manipulators and Mobile Robots, Int. J. Robotics Research, Vol. 5, pp. 90-98.

[91] Khouri, J. and Stelson, K. A., 1989, An Efficient Algorithm for Shortest Path in Three Dimensions With Polyhedral Obstacles, Trans. of ASME, J. Dynamic Systems, Measurement, and Control, Vol. 111, pp. 433-436.

[92] Kieffer, J. and Litvin, F. J., 1991, Swept Volume Determination and Interface Detection for Moving 3-D Solids, Trans. of ASME, J. Mechanical Design, Vol. 113, pp. 456-463.

[93] Kirecci, A. and Gilmartin, M. J., 1994, Improved Trajectory Planning Using Arbitrary Power Polynomials, Proceedings of the Institute of Mechanical Engineers, Part I, J. of Systems and Control Engineering, Vol. 208, pp. 3-13.

[94] Klein, R. E. and Sehitoglu, H., 1979, An Application of Equation Error Identification Techniques to the Problem of Vehicular Drag Parameter Determination, Proc. of 29th IEEE Vehicle Technology Conference, pp. 292-295.

[95] Koshiyama, A. and Yamafuji, K., 1993, Design and Control of an All-direction Steering Type Mobile Robot, Int. J. Robotics Research, Vol. 12, pp. 411-419.

[96] Kreyszig, E., 1967, Advanced Engineering Mathematics, Second Edition, John Wiley and Sons, New York.

[97] Kutulakos, K. N., Lumelsky, V. J. and Dyer, C. R., 1993, Vision-Guided Exploration: A Step Toward General Motion planning in Three Dimensions, Proc. of IEEE Int. Conf. on Robotics and Automation, Vol. 1, pp. 289-296.

[98] Kyriakopoulos, K. J. and Saridis, G. N., 1993, An Integrated Collision Prediction and Avoidance Scheme for Mobile Robots in Non-stationary Environments, Automatica, Vol. 29, pp. 309-322.

[99] Lamadrid, J. and Zimmerman, J., 1993, Avoidance of Obstacles with Unknown Trajectories: Locally Optimal Paths and Path Complexity, Part I, Robotica, Vol. 11, pp. 299-308.

[100] Lamadrid, J. and Zimmerman, J., 1993, Avoidance of Obstacles with Unknown Trajectories: Locally Optimal Paths and Path Complexity, Part II, Robotica, Vol. 11, pp. 403-412.

[101] Latombe, J. C., 1991, Robot Motion Planning, Kluwer Academic Publishers, Boston.

[102] Laumond, J. P., 1986, Feasible Trajectories for Mobile Robots with Kinematic and Environment Constraints, Preprints of Int. Conf. on Intelligent Autonomous Systems, pp. 346-354.

[103] Laumond, J. P., 1987, Obstacle Growing in a Non-polygonal World, Information Processing letters, Vol. 25, pp. 41-50.

[104] Laumond, J. P., 1993, Controllability of a Multibody Mobile Robot, IEEE Trans. on Robotics and Automation, Vol. 9, pp. 755-763.

[105] Laumond, J. P., Jacobs, P. E., Taix, M. and Murray, R. M., 1994, A Motion Planner for Nonholonomic Mobile Robots, IEEE Trans. on Robotics and Automation, Vol. 10, pp. 577-593.

[106] Lebegue, X. and Aggarwal, J. K., 1993, Significant Line Segments for an Indoor Mobile Robot, IEEE Trans. on Robotics and Automation, Vol. 9, pp. 801-815.

[107] Lee, C. T. and Sheu, P. C., 1992, A Divide-and-Conquer Approach with Heuristics of Motion Planning for a Cartesian Manipulator, IEEE Trans. on Systems, Man, and Cybernetics, Vol. 22, pp. 929-945.

[108] Lee, S. S. and Williams, J. H., 1993, A Fast Tracking Error Control Method for an Autonomous Mobile Robot, Robotica, Vol. 11, pp. 209-215.

[109] Lee, S. S., Williams, J. H. and Rayment, P. J., 1993, An Automatic Guidance System of an Autonomous Vehicle--the Trajectory Generation and the Control Algorithm, Robotica, Vol. 11, pp. 309-314.

[110] Leonard J. J. and Durrant-Whyte, F. D., 1991, Mobile Robot Localization by Tracking Geometric Beacons, IEEE Trans. on Robotics and Automation, Vol. 7, pp. 376-382.

[111] Li, Z. and Canny, J., 1990, Motion of Two Rigid Bodies with Rolling Constraint, IEEE Trans. on Robotics and Automation, Vol. 6, pp. 62-72.

[112] Liu, Y. and Arimoto, S., 1992, Path Planning Using Tangent Graph for Mobile Robots Among Polygonal and Curved Obstacles, Int. J. Robotics Research, Vol. 11, pp. 376-382.

[113] Lloyd, J. and Hayward, V., 1993, Trajectory Generation for Sensor-Driven and Time-Varying Tasks,

Int. J. Robotics Research, Vol. 12, pp. 380-393.

[114] Lozano-perez, T., 1983, Spatial Planning: A Configuration Space Approach, IEEE Trans. on Computers, Vol. C-32, No. 2, pp. 108-119.

[115] Lozano-perez, T. and Wesley, M, 1979, An Algorithm for Planning Collision-free Paths among Polyhedral Obstacles, Commun. Assoc. Comput. Math., Vol. 22, pp. 560-570.

[116] Lumelsky, V. J. and Stepanov, A. A., 1986, Dynamic Path Planning for a Mobile Automation With Limited Information on the Environment, IEEE Trans. on Automatic Control, Vol. AC-31, pp. 1058-1063.

[117] Lumelsky, V. J. and Sun, K., 1987, Computer Simulation of Senser-Based Robot Collision Avoidance in an Unknown Environment, Robotica, Vol. 5, pp. 291-302.

[118] Lumelsky, V. J., 1987, Effect of Kinematics on Motion Planning for Planar Robot Moving Amidst Unknown Obstacles, IEEE J. Robotics and Automation, Vol. 3, pp. 207-223.

[119] Lumelsky, V. J. and Sun, K., 1990, A United Methodology for Motion Planning with Uncertainty for 2D and 3D Two-Link Robot Arm Manipulators, Int. J. Robotics Research, Vol. 9, pp. 89-104.

[120] Lumelsky, V. J., Mukhopadhyay, S. and Sun, K., 1990, Dynamic Path Planning in Sensor-based Terrain Acquisition, IEEE Trans. on Robotics and Automation, Vol. 6, pp. 462-472.

[121] Lumelsky, V. J., 1991, A Comparative Study on Path Length Performance of Maze-Searching and Robot Motion Planning Algorithms, IEEE Trans. on Robotics and Automation, Vol. 7, pp. 57-66.

[122] Lynn, D. K., McCormick, J. B., Bobbett, R. E., Derouin, C. R., Nachamkin, J. and Kerwin, W., 1979, Determination of Vehicle Rolling Resistance and Aerodynamic Drag, Proc. of 29th IEEE Vehicular Technology Conference, pp. 296-300.

[123] Maciejewski, A. A. and Fox, J., 1993, Path Planning and the Topology of Configuration Space, IEEE Trans. on Robotics and Automation, Vol. 9, pp.444-456.

[124] Madarasz, R. L., 1986, The Design of an Autonomous Vehicle for the Disabled, IEEE J. Robotics and Automation, Vol. 2, pp. 117-126.

[125] Matsumoto, N. and Tomizuka, M., 1992, Vehicle Lateral Velocity and Yaw Rate Control with Two Independent Control Inputs, Trans. of the ASME, J. Dynamic Systems, Measurement, and Control, Vol. 114, pp. 606-613.

[126] Martines, A. Tunstel, E. and Jamshidi, M., 1994, Fuzzy Logic Based Collision Avoidance for a Mobile Robot, Robotica, Vol. 12, pp. 521-527.

[127] Maude, C., 1979, Applied Network Optimization, Academic Press, New York.

[128] McGean, T., 1976, Urban Transportation Technology, D. C. Heath and Company.

[129] McGhee, R. B. and Iswandhi, G. I., 1979, Adaptive Location of a Multilegged Robot Over Rough Terrain, IEEE Trans. on Systems, Man, and Cybernetics, Vol. 33, pp. 176-182.

[130] Moigne, J. L., 1988, Domain-Dependent Reasoning for visual Navigation of Roadways, IEEE J. Robotics and automation, Vol. 4, pp. 419-427.

[131] Muir, P. F. and Neuman, C. P.,1987, Kinematic Modeling of Wheeled Mobile Robots, J. Robotic Systems, Vol. 4, pp. 281-340.

[132] Muir, P. F. and Neuman, C. P., 1987, Kinematic Modeling for feedback Control of an Omnidirectional Wheeled Mobile Robot, Proc. of IEEE Int. Conf.Conf. on Robotics and Automation, pp. 1772-1778.

[133] Mukherjee, R. and Sastry, S. S., 1993, Nonholonomic Motion Planning: Steering Using Sinusoids, IEEE Trans. on Automatic Control, Vol. 38, pp. 700-716.

[134] Mukherjee, R. and Anderson, D., 1993, Nonholonomic Motion Planning Using Stokes's Theorem, Proc. of the 1993 IEEE Int. Conf. on Robotics and Automation, Vol. 3, pp. 802-809.

[135] Mukherjee, R. and Anderson, D., 1994, A Surface Integral Approach to the Motion Planning of Nonholonomic Systems, ASME J. of Dynamic Systems, Measurement and Control, Vol. 116, pp.315-325.

[136] Muller, I. T., 1983, Automated Guided Vehicles, IFS Ltd, London.

[137] Nelson, W. L., 1989, Continuous Steering-Function Control of Robot Carts, IEEE Trans. on Industrial Electronics, Vol. 36, No. 3, pp. 330-337.

[138] Nelson, W. L. and Cox, I. J., 1988, Local Path Control for an Autonomous Vehicles, Proc. of the 1988 IEEE Int. Conf. on Robotics and Automation, pp. 1504-1510.

[139] Nicholls, S. and Lee, H., 1989, A Survey of Robot Tactile Sensing Technology, Int. J. Robotics Research, Vol. 8, pp. 3-25.

[140] Niehaus, A. and Stengel, R. F., 1994, Probability-Based Decision Making for Automated Highway Driving, IEEE Trans. on Vehicular Technology, Vol. 43, pp. 626-634.

[141] Nitzan, D., 1985, Development of Intelligent Robots: Achievement and Issues, IEEE J. Robotics and Automation, Vol. 1, pp. 3-13.

[142] Okada, T., 1982, Development of an Optical Distance Sensor for Robots, Int. J. Robotics Research, Vol. 1, pp. 3-13.

[143] Okada, T. O. and Rembold, U., 1991, Proximity senser Using a Light-Emitting Mechanism, IEEE Trans. on Robotics and Automation, Vol. 7, pp. 798-805.

[144] Oommen, B. J., Iyengar, S. S., Rao, N. and Kashyap, R. L., 1987, Robot Navigation in Unknown Graphs. Part I: The Disjoint Convex Obstacle Case, IEEE J. Robotics and Automation, Vol. 3, 672-681.

[145] Oommen, B. J. and Reichstein, I., 1987, On the Problem of Translating an Elliptic Object through a Workspace of Elliptic Obstacles, Robotica, Vol. 5, pp. 187-196.

[146] O'Rourke, J., 1994, Computational Geometry in C, Cambridge University Press, New York, USA.

[147] Ozaki, H. and Mohri, A., 1988, Synthesis of a Minimum-Time Manipulator Trajectories with Geometric Path Constrains Using Time Scaling, Robotica, Vol. 6, pp. 41-46.

[148] Paul, R. P., 1981, Robot Manipulators: Mathematics, Programming, and Control, The MIT Press.

[149] Pegna, J. and Wolter, F., 1992, Geometrical Criteria to Guarantee Curvature Continuity of Blend Surfaces, Trans. of ASME, J. Mechanical Design, Vol. 114, pp. 201-210.

[150] Petriu, E. M., 1991, Automated Guided Vehicle with Encoded Guide-Path, IEEE Trans. on Robotics and Automation, Vol. 7, pp. 562-565.

[151] Petrov. I. P., 1968, Variational Methods in Optimum Control Theory, Academic Press.

[152] Pin, F. G. and Watanabe, Y., 1994, Navigation of Mobile Robots Using a Fuzzy Behaviorist Approach and Custom-designed Fuzzy Inferencing Boards, Robotica, Vol. 12, pp. 491-503.

[153] Pomet, J., Bastin, B. and Campion, G., 1992, A Hybrid Strategy for the Feedback Stabilization of Nonholonomic Mobile Robots, Proc. of the 1992 Int. Conf. on Robotics and Automation, Nice, France, pp. 129-134.

[154] Press, W. H., Teukolsky, S. A., Vetterling, W. T. and Flannery, B. P., 1992, Numerical Recipes in C, second edition, Cambridge University Press, New York.

[155] Pruski, A. and Bourhis, G., 1992, The VAHM Project: a Cooperation Between an Autonomous Mobile Platform and a Disabled Person, Proc. of the 1992 Int. Conf. on Robotics and Automation, Nice, France, pp. 268-273.

[156] Rao, N. S., Iyengar, S. S., Oommen, B. J. and Kashyap, R. L., 1988, On Terrain Model Acquisition by a Point Robot Amidst Polyhedral Obstacles, IEEE J. Robotics and Automation, Vol. 4, pp. 450-455.

[157] Rao, N. S., Stoltzfus, N. and Iyengar, S. S., 1991, A "Retraction" Method for Learned Navigation in Unknown Terrains for a Circular Robot, IEEE Trans. on Robotics and Automation, Vol. 7, pp. 699-

707.

[158] Reeds, J. A. and Shepp, L. A., 1990, Optimal Paths for a Car That Goes both Forwards and Backwards, Pacific J. Mathematics, Vol. 145, 367-393.

[159] Reister, D. B., 1992, A New Wheel Control System for the Omnidirectional HERMIES-III Robot, Robotica, Vol. 10, pp. 351-360.

[160] Reister, D. B. and Pin, F. G., 1994, Time-Optimal Trajectories for Mobile Robots With Two Independent Driven Wheels, Int. J. Robotics Research, Vol. 13, pp. 38-54.

[161] Reister, D. B. and Unseren, M., 1993, Position and Force Control of a Vehicle With Two or More Steerable Drive Wheels, IEEE Trans. on Robotics and Automation, Vol. 9, pp. 723-731.

[162] Rohnert, H., 1986, Shortest Paths in the Plane with Convex Polygonal Obstacles, Information Processing Letters, Vol. 23, pp. 71-76.

[163] Romerio, M. V., and Burckhardt, C. W., 1991, Displacements by Successive Rotations for Vehicles Subject to Given Constraints, Robotica, Vol. 9, pp. 409-415.

[164] Rossignac, J. R. and Requicha, A. A. G., 1987, Piecewise-Circular Curves for Geometric Modeling, IBM J. Res. Develop. Vol. 31, pp. 296-313.

[165] Rowe, N. C., 1990, Roads, Rivers, and Obstacles: Optimal Two-Dimensional Path Planning around Linear Features for a Mobile Agent, Int. J. Robotics Research, Vol. 9, pp. 67-74.

[166] Rowe, N. C. and Ross, R. S., 1990, Optimal Grid-Free Path Planning Across Arbitrarily Contoured Terrain with Anisotropic Friction and Gravity Effects, IEEE Trans. on Robotics and Automation, Vol. 6, pp. 540-553.

[167] Rowe, N. C. and Kanayama, Y., 1994, Near-Minimum-Energy Paths on a Vertical-Axis Cone With Anisotropic Friction and Gravity Effects, Int. J. of Robotics Research, Vol. 13, pp. 408-433.

[168] Safaee-Rad, R., Tchoukanov, I., Smith, K. and Benhabib, B., 1992, Three-Dimensional Location Estimation of Circular Features for Machine Vision, IEEE Trans. on Robotics and Automation, Vol. 8, pp. 624-640.

[169] Saha, S. K., Angeles, J. and Darcovich, J., 1993, The Kinematic Design of a 3-dof Isotropic Mobile Robot, Proc. of IEEE Int. Conf. on Robotics and Automation, Vol. 1, pp. 283-288.

[170] Sahar, G. and Hollerbach, J. M., 1986, Planning of Minimum-Time Trajectories for Robot Arms, Int. J. Robotics Research, Vol. 5, pp. 90-100.

[171] Samson, C., 1993, Time-Varying Feedback Stabilization of Car-like Wheeled Mobile Robots, Int. J.

Robotics Research, Vol. 12, pp. 55-64.

[172] Sano, S., Furukawa, Y. and Shiraishi, S., 1986, Four Wheel Steering System with Rear Wheel Steer Angle Controlled as a Function of Steering Wheel Angle, SAE The Engineering Resource for Advanced Mobility, 860625.

[173] Sayer, M., 1986, Vehicle Offtracking Models, Transportation Research Record 1052, Symposium on Geometric Design for Large Trucks, pp. 53-62.

[174] Schwartz, J. T. and Sharir, M., 1983a, On the "Piano Movers" Problem: I. The Case of a Two-Dimensional Rigid Polygonal Body Moving Amidst Polygonal Barriers, Communications on Pure and Applied Mathematics, Vol. XXXVI, pp. 375-398.

[175] Schwartz, J. T. and Sharir, M., 1983b, On the "Piano Movers" Problem: III. Coordinating the Motion of Several Independent Bodies: The Special Case of Circular Bodies Moving Amidst Polygonal Barriers, Int. J. Robotics Research, Vol. 2, pp. 46-75.

[176] Shan, Y. and Koren, Y., 1993, Design and Motion Planning of a Mechanical Snake, IEEE Trans. on Systems, Man, and Cybernetics, Vol. 23, pp. 1091-1100.

[177] Sharir, M., 1989, Algorithmic Motion Planning in Robotics, Computer, Vol. 22, No. 4, pp. 9-20.

[178] Sharma, R., 1992, Locally Efficient Path Planning in An Uncertain, Dynamic Environment Using a Probabilistic Model, IEEE Trans. on Robotics and Automation, Vol. 8, pp. 105-110.

[179] Sharma, U. K. and Davis, L. S., 1988, Road Boundary Detection in Range Imagery for an Autonomous Robot, IEEE J. Robotics and Automation, Vol. 4, pp. 515-523

[180] Shiller, Z. and Gwo, Y. R., 1991, Dynamic Motion Planning of Autonomous Vehicles, IEEE Trans. on Robotics and Automation, Vol. 7, pp. 241-249.

[181] Shiller, Z. and Lu, H. H., 1992, Computation of Path Constrained Time Optimal Motions with Dynamic Singularities, Trans. of ASME, J. Dynamic Systems, Measurement, and Control, Vol. 114, pp. 34-40.

[182] Shiller, Z., Serate, W. and Hua, M., 1993, Trajectory Planning of Tracked Vehicles, Proc. of IEEE Int. Conf. on Robotics and Automation, Vol. 3, pp. 796-801.

[183] Shiller, Z. and Sundar, S., 1994, Constrained Optimization of Multi-Degree-of-Freedom Mechanisms for Near-Time-Optimal Motions, Trans. of the ASME J. of Mechanical Design, Vol. 116, pp. 412-418.

[184] Shin, S. Y. and Woo, T. C., 1989, An Optimal Algorithm for Finding All Visible Edges in a Simple Polygon, IEEE Trans. on Robotics and Automation, Vol. 5, pp. 202-207.

[185] Shladover, S. E., 1991, Longitudinal Control of Automated Guideway Transit Vehicles within Platoons, Trans. of ASME, J. Dynamic Systems, Measurement and Control, Vol. 100, pp. 302-310.

[186] Shladover, S. E., 1991, Longitudinal Control of Automotive Vehicles in Close-Formation Platoons, Trans. of ASME, J. Dynamic Systems, Measurement and Control, Vol. 113, pp. 231-241.

[187] Skaar, S., Yalda-Mooshabad, I. and Brockman, W., 1992, Nonholonomic Camera-Space Manipulation, IEEE Trans. on Robotics and Automation, Vol. 8, pp. 464-479.

[188] Slotine, J. E. and Yang, H. S., 1989, Improving the Efficiency of Time-Optimal Path-Following Algorithms, IEEE Trans. on Robotics and Automation, Vol. 5, pp. 118-124.

[189] Smith, B. L., 1986, Existing Design Standards, Transportation Research Record 1052, Symposium on Geometric Design for Large Trucks, pp. 116-119.

[190] Sordalen, O. J. and Canudas de Wit, C., 1992, Path Following and Stabilization of a Mobile Robot, Proc. IFAC Nonlinear Control System Design, Bordeaux, France, pp. 471-476.

[191] Sordalen, O. J., Dalsmo, M. and Egeland, O., 1993, An Exponentially Convergent Control law for a Nonholonomic underwater Vehicles, Proc. of IEEE Int. Conf. on Robotics and Automation, Vol. 3, pp. 790-795.

[192] Srakar, N., Yun, X. and Kumar, V., 1993, Control of Mechanical Systems With Rolling Constraints: Application to Dynamic Control of Mobile Robots, Int. J. Robotics Research, Vol. 13, pp. 55-69.

[193] Stappen, A. F., Halperin, D. and Overmars, M. H., 1993, Efficient Algorithms for Exact Motion Planning amidst Fat Obstacles, Proc. of IEEE Int. Conf. on Robotics and Automation, Vol. 1, pp. 297-304.

[194] Steer, B., 1989, Trajectory Planning for a Mobile Robot, Int. J. Robotics Research, Vol. 8, pp. 3-14.

[195] Suh, S. H. and Shin, K. G., 1988, A Variational Dynamic Programming Approach to Robot-Path Planning with a Distance-Safety Criterion, IEEE J. Robotics and Automation, Vol. 4, pp. 334-349.

[196] Suri, S., 1990, On Some Link Distance Problem in a Simple Polygon, IEEE Trans. On Robotics and Automation, Vol. 6, pp. 108-113.

[197] Sutherland, K. T. and Thompson, W. B., 1993, Inexact Navigation, Proc. of IEEE Int. Conf. on Robotics and Automation, Vol. 1, pp. 1-7.

[198] Suzuki, H., and Arimoto, S., 1990, Trajectory Planning Inside Dynamic Environment, In: Miura, H and Arimoto, S. (eds.), The fifth Int. Symposium on Robotics Research, The MIT Press, Cambridge, Massachusetts, pp. 395-403.

[199] Suzuki, Y., Niinomi, S., Saitoh, Y., Tsuchiya, K. and Hatakeyama, T., 1988, A New Control Method

for Motor Vehicles for the Severely Handicapped, Robotica, Vol. 6, pp. 131-139.

[200] Synge, J. L., 1973, A Steering Problem, Quart. Appl. Math., Vol. 31, pp. 295-302.

[201] Takano, M., 1980, Mechanism of an Autonomous Mobile Robot and Its Control, Advanced Robotics, Vol. 4, pp. 187-202.

[202] Tan, H. H. and Potts, R. B., 1988, Minimum Time Trajectory Planning for the Discrete Dynamic Robot Model with Dynamic Constraints, IEEE J. Robotics and Automation, Vol. 4, pp. 174-185.

[203] Tanaka, K. and Sano, M., 1994, A Robust Stabilization Problem of Fuzzy Control Systems and Its Application to Backing up Control of a Truck-Trailer, IEEE Trans. on Fuzzy Systems, Vol. 2, No. 2, pp. 119-134.

[204] Todd, D. J., 1985, Walking Machines, An Introduction to legged robots, Kogan Page Ltd.

[205] Todd, D. J., 1986, Fundamentals of Robot Technology, An Introduction to Industrial Robots, Teleoperators and Robot Vehicles, Kogan Page Ltd.

[206] Turennout, P. V., Honderd, G. and Schelven, L. J., 1992, Wall-following Control of a Mobile Robot, Proc. of the 1992 Int. Conf. on Robotics and Automation, Nice, France, pp. 280-285.

[207] Villalon, E. P. and Dauchez, P., 1988, World Representation and Path Planning for a Mobile Robot, Robotica, Vol. 6, pp. 35-40.

[208] Volpe, R. and Khosla, P., 1990, A Strategy for Obstacle Avoidance and Approach Using Superquadric Potential Function, In: Miura, H and Arimoto, S. (eds.), The fifth Int. Symposium on Robotics Research, The MIT Press, Cambridge, Massachusetts, pp. 445-452.

[209] Wang, W. P. and Wang, K. K., 1986, Geometric Modelling for Swept Volume of Moving Solids, IEEE Computer Graphics and Applications, Vol. 12, pp. 8-17.

[210] Wang, Y., Linnett, J. A. and Roberts, J. W., 1994, Motion Feasibility of a Wheeled Vehicle with a Steering Angle Limit, Robotica, Vol. 12, pp. 217-226.

[211] Wang, Y., Linnett, J. A. and Roberts, J. W., 1994, Kinematics, Kinematic Constraints and Path Planning for Wheeled Mobile Robots, Robotica, Vol. 12, pp. 391-400.

[212] Wang, Y. and Linnett, J. A., 1995, Vehicle Kinematics and its Application to Highway Design, ASCE J. of Transportation Engineering, Vol. 121, pp. 63-74.

[213] Wang, Y. and Linnett, J. A., 1993, On the Maneuvering Problems of Wheeled Vehicles, Proc. of the First Conf. of the Chinese Society of Electrical and Electronic Engineering in U.K., pp. 34-40.

[214] Wang, Y., Linnett, J. A. and Roberts, J. W., 1995, A Unified Approach to Inverse and Direct Kinemat-

ics for Four Kinds of Wheeled Mobile Robots, Submitted to the Proceedings of IMechE, J. of Mechanical Engineering Science.

[215] Wang, Y., Linnett, J. A. and Roberts, J. W., 1995, On the Suitability of Path Planning Algorithms to Four Kinds of Mobile Robots, Submitted to Int. J. Robotics Research.

[216] Weisbin, C., Burks, B. L., Einstein, J. R., Feezell, R., Manges, V. and Thompson, D., 1990, HERMIES-III: A Step Toward Autonomous Mobility, Manipulation and Perception, Robotica, Vol. 8, pp. 7-12.

[217] Weisbin, C. and Perillard, D., 1991, Jet Propulsion Laboratory Robotic Facilities and Associated Research, Robotica, Vol. 9, pp. 7-12.

[218] Wilfong, G., 1988, Motion Planning for an Autonomous Vehicle, Proc. of the 1988 IEEE Int. Conf. on Robotics and Automation, pp. 529-533.

[219] Wong, J. Y., 1978, Theory of Ground Vehicles, John Wiley & Sons, New York.

[220] Yamamoto, Y and Yun, X., 1993, Control of Mobile Manipulators Following a Moving Surface, Proc. of IEEE Int. Conf. on Robotics and Automation, Vol. 1, pp. 1-6.

[221] Yang, D. C. H., 1993, Collision-Free Path Planning by Using Nonperiodic B-Spline Curve, Trans. of the ASME, J. of Mechanical Design, Vol. 115, pp. 679-684.

[222] Yap, C., 1987, How to Move a Chair through a Door, IEEE J. Robotics and Automation, Vol. 3, pp. 172-181.

[223] Yoon, K. and Rao, S. S., 1993, Cam Motion Synthesis Using Cubic Splines, Trans. of the ASME, J. of Mechanical Design, Vol. 115, pp. 441-446.

[224] Zelinsky, A., 1994, Using Path Transforms to Guide the Search for Findpath in 2D, Int. J. Robotics Research, Vol. 13. No. 4, pp. 315-325.

[225] Zhang, C., Agui, T. and Nagahashi, H., 1994, Piecewise Parametric Cubic Interpolation, IEICE Trans. on INF. and SYST., Vol. E77, pp.869-876.

[226] Zhang, H., 1993, Efficient Evaluation of the Feasibility of Robot Displacement Trajectories, IEEE Trans. on Systems, Man, and Cybernetics, Vol. 23, pp. 324-330.

[227] Zhang, H., Weiss, R. and Hanson, A. R., 1993, Automatic Calibration and Visual Servoing for a Robot Navigation System, Proc. of IEEE Int. Conf. on Robotics and Automation, Vol. 1, pp. 14-19.

[228] Zhao, Y. and BeMent, S. L., 1992, Kinematics, Dynamics and Control of Wheeled mobile Robots, Proc. of the 1992 Int. Conf. on Robotics and Automation, Nice, France, pp. 91-96.

[229] Zhu, D. and Latombe, J. C., 1991, New Heuristic Algorithms for Efficient Hierarchical Path Planning, IEEE Trans. on Robotics and Automation, Vol. 7, pp. 9-20.

[230] Zhu, Q., 1991, Hidden Markov Model for Dynamic Obstacle Avoidance of Mobile Robot Navigation, IEEE Trans. on Robotics and Automation, Vol. 7, pp. 390-397.

[231] American Association of State Highway and Transportation Officials, 1973, A Policy on Design of Urban Highways and Arterial Streets.

[232] American Association of State Highway and Transportation Officials, 1990, A Policy on Geometric Design of Highways and Streets.

[233] Freight Transport Association, U. K., 1983, Designing for Deliveries.

[234] Manual of Geometric Design Standards for Canadian Roads, 1986, Metric Edition.

[235] Offtracking Characteristics of Trucks and Truck Combination, WHI Research Committee Report 3, Western Highway Institute, San Bruno, Calif., Feb. 1970.

[236] Wang, Y, Transformation of nonholonomic motion planning problem to polynomial fitting and two point boundary value problem, Submitted to IEEE Trans. on Automatic Control.

Appendix

Publications

The following lists the publications during my Ph.D. Study.

[1] Wang, Y., Linnett, J. A. and Roberts, J. W., 1994, Motion Feasibility of a Wheeled Vehicle with a Steering Angle Limit, Robotica, Vol. 12, pp. 217-226.

[2] Wang, Y., Linnett, J. A. and Roberts, J. W., 1994, Kinematics, Kinematic Constraints and Path Planning for Wheeled Mobile Robots, Robotica, Vol. 12, pp. 391-400.

[3] Wang, Y. and Linnett, J. A., 1995, Vehicle Kinematics and its Application to Highway Design, ASCE J. of Transportation Engineering, Vol. 121, pp. 63-74.

[4] Wang, Y. and Linnett, J. A., 1993, On the Maneuvering Problems of Wheeled Vehicles, Proc. of the First Conf. of the Chinese Society of Electrical and Electronic Engineering in U.K., pp. 34-40.

The following lists the papers which are in review.

[5] Wang, Y., Linnett, J. A. and Roberts, J. W., 1995, A Unified Approach to Inverse and Direct Kinematics for Four Kinds of Wheeled Mobile Robots, Submitted to the Proceedings of IMechE, J. of Mechanical Engineering Science.

[6] Wang, Y., Linnett, J. A. and Roberts, J. W., 1995, On the Suitability of Path Planning Algorithms to Four Kinds of Mobile Robots, Submitted to Int. J. Robotics Research.

[7] Wang, Y, Transformation of nonholonomic motion planning problem to polynomial fitting and two point boundary value problem, Submitted to IEEE Trans. on Automatic Control.

Robotica (1994) volume 12, pp 217–226. © 1994 Cambridge University Press

Motion feasibility of a wheeled vehicle with a steering angle limit

Yongji Wang, J.A. Linnett and J.W. Roberts

(Mechanical Engineering Department, Edinburgh University, Kings Buildings, Edinburgh EH9 3JL U.K.)

(Received in Final Form: September 11, 1993)

SUMMARY

In the problem of automatically controlling a wheeled vehicle so that a given reference point on the vehicle follows a prescribed path, several factors determine how the task can be accomplished; they are the shape of the path, the initial orientation angle, the steering angle limit and the position of the reference point on the vehicle. If the required steering angle exceeds the limit set by the steering mechanism or the required orientation angle is discontinuous at any point along the path, then the path cannot be followed. This paper investigates this motion feasibility problem, taking steering angle limit into consideration. First of all, we determine the dependence of the continuity of the orientation angle, steering angle and their derivatives on the continuity of the reference path and its derivatives, then discuss the relationship between the steering angle limit and the feasible deviation angle intervals. Furthermore, we analyze in detail two typical motions, namely straight line motion and circular motion; some simulation results have been given based on a practical vehicle dimension.

KEYWORDS: Vehicle; Motion; Steering angle; Automatic control.

1. INTRODUCTION

When a vehicle (it may be an autonomous robot, an automated guided vehicle, a car or a truck) is required to run from a start point to a goal point in the workspace, a path has to be planned and a point on the vehicle is designated to follow this path. The path is usually called reference path and the point is called reference point P (it is also called guidepoint by Nelson[1] and reference vertex by Lozano-Perez[2]). Due to the existence of the steering angle limit, the required steering angle may exceed this limit; in this case, the path can not be traced.

The reference path for an automatically guided vehicle around factories or offices generally comprises a concatenation of line-circular segments.[3,4] The path generated by the available algorithms for an autonomous vehicle depends on the assumption of the shapes of the obstacles in the workspace and the autonomous vehicle, and the algorithms. It generally consists of a collection of line–line, line–circular segments. For example, under the assumption of polygonal obstacles and polygonal vehicle body, the path generated by the visibility graph method[2,5] and the cell decomposition method[6,7] comprises line–line segments, as shown in Figure 1(a). The path generated by the generalized visibility graph[8,9] is a combination of line–line and line–circular segments, as shown in Figure 1(b). The common feature of these reference paths is that at the transition point between segments, the path is not smooth enough. For example, at the line–line transition point, the first derivative of the path is not continuous, and at the line–circular transition point, the second derivative of the path is not continuous. In general, the smoothness of the reference path can be described by the continuity of the nth derivative of the path, and the motion smoothness of the vehicle can be judged upon the continuities of the nth derivatives of the steering angle and the orientation angle. Thus an interesting problem investigated in this paper is to determine the dependence of the continuities of the orientation angle and steering angle on that of the nth derivative of the reference point.

The steering angle and orientation angle are two important parameters featuring the motion feasibility of a vehicle. To make a vehicle move along a path, steering is necessary. For wheeled vehicles, steering is normally affected by changing the heading of the steering wheels (for four wheel vehicles) or the single steering wheel (for three wheel vehicles) through the steering system. In practice, the turning capability of most of the steering mechanisms in use is limited, and it can be described by inequality constraints. Due to the steering angle limit, not all the paths are executable. At any time, only when the vehicle steering angle needed to follow a given path satisfies these constraints is the vehicle able to follow the reference path. In this sense, a study of the factors which will affect the steering angle is of importance.

Another reason for studying steering angle lies in the fact that even when the steering angle limit is not exceeded in following a path, a discontinuity of the steering angle may occur at a transition point. The only way for a vehicle to cope with this discontinuity is to stop at the corresponding point, wait for the required adjustment of the steering angle, and then start again. Clearly, this is not desirable.

Vehicle orientation angle is another important parameter which should be investigated. Since the vehicle is modelled as a rigid body with wheels mounted on it, the orientation angle totally determines the space swept by the vehicle when it moves along the reference path. In addition to this, a discontinuity of the orientation angle at transition points will occur if the reference point is not chosen correctly. This implies that

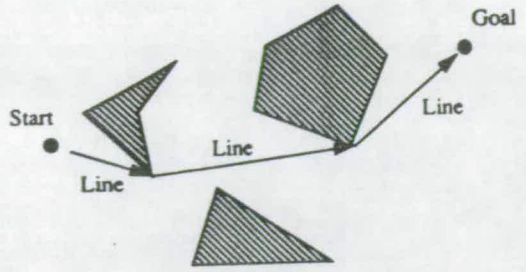

Fig. 1(a). A typical line–line planned path for vehicles.

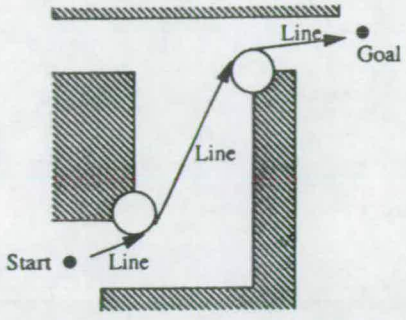

Fig. 1(b). A typical line–circular planned path for vehicles.

the requirement of tracing the planned path by the reference point is not feasible.

In addition to the shape of the reference path, the steering angle and orientation angle of a vehicle depend on many other factors. The most important two are the reference point position and the initial orientation angle. The choice of the reference point is the first thing to be considered. It may be somewhat arbitrary, yet its choice does affect the kinematics and dynamics of the vehicle. The desired steering and drive functions of the vehicle, the space swept out by the vehicle, the actuators needed to drive the vehicle and the control method to be devised for the vehicle all are functions of the position of the reference point. Hence, the analysis of the effect of the reference point position on the motion feasibility of the vehicle is of importance.

The necessity of investigating the initial orientation angle can be seen from tracing the line–line combination shown in Figure 1(a). When the vehicle arrives the end of the first line segment, the orientation angle at that point will become the initial orientation angle for the second line segment; the orientation angle at the end of the second line will, in turn, be the initial angle for the third line, and so on. When the vehicle changes lanes consisting of circular–circular segments, there also exists an initial value problem.

Most of the vehicles in use or in development today are steered by a single wheel or wheel pair.[7,10] It has been proved that from the steering viewpoint, a vehicle steered by a single wheel is an equivalent to that steered by a wheel pair.[11] Hence in this study, we only consider the former kind of vehicle by using the mathematical model developed in reference 11 to analyze the motion feasibility of the vehicle.

Although many researchers have focused their attentions on the study of the motion of trucks[3,12–23] and the motion of automated guided vehicles or autonomous vehicles,[4,7,10,14,24–36] to date, we have not been aware of the detailed analysis of the dependence of the motion feasibility of wheeled vehicles on the shape of the reference path, the reference point position and the initial orientation angle of the vehicle. This paper investigates this problem when the vehicle is required to follow a general path $y_p = f(x_p)$ and two typical paths, i.e. straight line and circle.

Section 2 gives a brief description of the kinematic model. In section 3, the relationship between the continuities of the orientation angle, steering angle and that of the reference path is discussed when reference point is chosen at different points on the vehicle. The steering angle limit and its effects on the feasible deviation angle intervals are discussed in section 4. The subject of section 5 is the analysis of motion feasibility when the reference path is a straight line. This is followed in section 6 by the analysis of motion feasibility when the circular motion is carried out. Finally, the conclusions are drawn in section 7.

2. KINEMATIC MODEL FOR A VEHICLE

To analyze the motion feasibility of a wheeled vehicle, an appropriate kinematical model is necessary. In this section, we briefly introduce the kinematic model developed by Wang and Linnett.[11] Figure 2 is a plan view of a general vehicle model investigated. From the point of view of operating function, wheels used in the vehicle can be categorized into two types, free wheels and fixed wheels. If a wheel can rotate about a vertical axle, it is defined as a free wheel, otherwise, it is defined as a fixed wheel. Based on this definition, steered wheels are free wheels and wheels on the fixed axle are fixed wheels. However, when they are described by a mathematical model, a fixed wheel may be regarded as a special free wheel, so in Figure 2 all the wheels are given in the form of free wheels. For most of the vehicles in

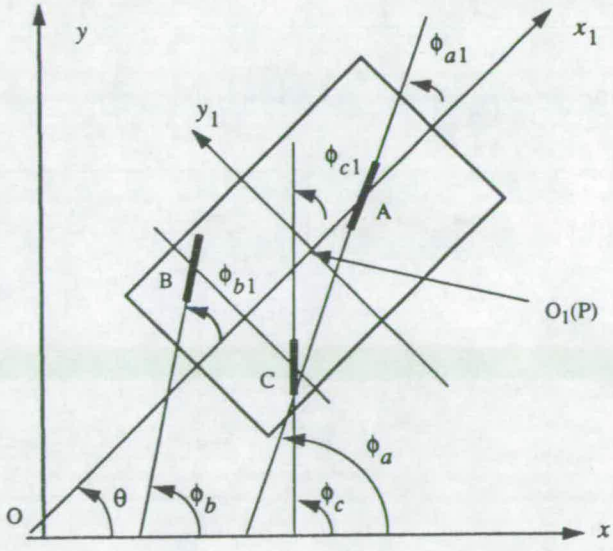

Fig. 2. Global (Oxy) and local ($O_1x_1y_1$) reference coordinate frames, reference point P coincides with O_1.

use and in development, B and C are fixed wheels, i.e. $\phi_{b1} = \phi_{c1} = 0$. A global reference coordinate frame (Oxy) is introduced to describe the motion of the vehicle in terms of the position of the reference point (x_p, y_p) and the orientation angle θ of the vehicle. We also define a local reference coordinate frame $(O_1 x_1 y_1)$, whose origin O_1 is placed at the reference point P of the vehicle with y_1 axis parallel to the rear axle BC. We use M to represent any point in the rigid vehicle body when discussing the motion of the rigid vehicle body and also use it to represent a wheel connected to the corresponding point when discussing steering angle. The coordinates of point M are denoted by $M(x_m, y_m)$ in terms of the global reference frame and $M(x_{m1}, y_{m1})$ in terms of the local reference frame. So the coordinates are constants with respect to the local reference frame.

The angle ϕ_m, $(m = a, b, c)$ is that between the vertical plane of the wheel M and the positive x axis, and ϕ_{m1}, between the vertical plane of the wheel M and the positive x_1 axis. It is noted that ϕ_m, θ, ϕ_{m1} are all in the range from $-180°$ to $180°$. The relation between ϕ_m, θ, and ϕ_{m1} can be written as:

$$\phi_m = \phi_{m1} + \theta \tag{1}$$

The coordinates of point M in the global frame are related to the coordinates of point M measured in the local frame by the transformation:

$$\begin{bmatrix} x_m \\ y_m \end{bmatrix} = \begin{bmatrix} x_{m1}\cos\theta - y_{m1}\sin\theta + x_p \\ x_{m1}\sin\theta + y_{m1}\cos\theta + y_p \end{bmatrix} \tag{2}$$

In the paper, when x, y are functions of time t, we use $\dot{x}$, $\ddot{x}$ to denote $\frac{dx}{dt}$, $\frac{d^2x}{dt^2}$ respectively. Differentiating equation (2) with respect to time, we have:

$$\begin{bmatrix} \dot{x}_m \\ \dot{y}_m \end{bmatrix} = \begin{bmatrix} (-x_{m1}\sin\theta - y_{m1}\cos\theta)\dot{\theta} + \dot{x}_p \\ (x_{m1}\cos\theta - y_{m1}\sin\theta)\dot{\theta} + \dot{y}_p \end{bmatrix} \tag{3}$$

Where $\dot{x}_m$, $\dot{y}_m$, $\dot{x}_p$, $\dot{y}_p$ are the absolute velocity components of point M and the reference point P along x, y-axes and $\dot{\theta}$ is the absolute angular velocity of the vehicle body. Differentiating equation (3) again, we have the absolute acceleration expressions:

$$\begin{bmatrix} \ddot{x}_m \\ \ddot{y}_m \end{bmatrix} = \begin{bmatrix} (-x_{m1}\cos\theta + y_{m1}\sin\theta)\cdot\dot{\theta}^2 + (-x_{m1}\sin\theta - y_{m1}\cos\theta)\cdot\ddot{\theta} + \ddot{x}_p \\ (-x_{m1}\sin\theta - y_{m1}\cos\theta)\cdot\dot{\theta}^2 + (x_{m1}\cos\theta - y_{m1}\sin\theta)\cdot\ddot{\theta} + \ddot{y}_p \end{bmatrix} \tag{4}$$

When the whole vehicle is considered, the ideal rolling condition of all the wheels must be satisfied, that is the motion direction of every wheel rolling forward or backward, whether steered or not, must coincide with the tangent to the vehicle body trajectory at the corresponding wheel center. Mathematically, the above condition can be expressed as:

$$\tan(\phi_m) = \frac{d}{d(x_m)}(y_m) = \frac{\dot{y}_m}{\dot{x}_m} \tag{5}$$

From equations (1) and (5) we can obtain ϕ_{m1}, the angle relative to the vehicle orientation line, which is the steering angle for a steering wheel.

$$\phi_{m1} = a\tan\left(\frac{\dot{y}_m}{\dot{x}_m}\right) - \theta \tag{6}$$

As mentioned above, when the wheels in the vehicle are fixed wheels, then their angles relative to the vehicle orientation line are constants. In this study, wheels B, C are considered as fixed wheels so that $\phi_{b1} = \phi_{c1} = 0$. Therefore, from equation (6), the following constraints are imposed:

$$\tan\theta = \frac{\dot{y}_b}{\dot{x}_b} \tag{7}$$

$$\tan\theta = \frac{\dot{y}_c}{\dot{x}_c} \tag{8}$$

Substituting equation (3) into (7) and (8) respectively and simplifying, we obtain:

$$x_{b1}\cdot\dot{\theta} = \dot{x}_p\sin\theta - \dot{y}_p\cos\theta \tag{9}$$

$$x_{c1}\cdot\dot{\theta} = \dot{x}_p\sin\theta - \dot{y}_p\cos\theta \tag{10}$$

The y_1 axis is parallel to the vehicle's rear axle, so, letting $x_{b1} = x_{c1} = \underline{x}$, equations (9) and (10) become:

$$\underline{x}\cdot\dot{\theta} = \dot{x}_p\sin\theta - \dot{y}_p\cos\theta \tag{11}$$

Equation (11) is what we need to solve for the vehicle's orientation angle θ and angular velocity $\dot{\theta}$ when the reference point velocity components $\dot{x}_p$ and $\dot{y}_p$ are specified. Due to the fact that equation (11) describes the general relationship between the reference point's position relative to the rear axle, its velocity, the vehicle's orientation angle and its first derivative when the reference point is chosen at any point in the vehicle, it is called the general constraint equation.

Once θ and $\dot{\theta}$ are known, the position and absolute velocity of any point can be determined by equations (2) and (3) and the steering angle from equation (6).

3. THE CONTINUITIES OF ORIENTATION ANGLE AND STEERING ANGLE

A geometric curve, which is generated by a path planning algorithm and is required to be followed by the reference point P of the robot, is called a path. Mathematically, a curve can be presented as a general form in $x - y$ plane:

$$y_p = f(x_p) \tag{12}$$

Some characteristics associated with its shape, such as its derivatives and curvature, are referred to as its geometric characteristics. A trajectory is defined as the time course along a path. One can choose velocity from various schedules for a geometrically defined path, which results in various velocity profiles. If a variable is only affected by the geometrical characteristics rather than by vehicle's velocities at any point along the path, it is called an independent variable of velocities. θ, ϕ_{a1} are such defined independent variables. In this section, we discuss the effects of the continuities of the reference path and its derivatives on the continuities of the orientation angle and steering angle of the vehicle.

Equations (6) and (11) cannot be directly used for this purpose as they include time variable. From (11), another form of the general constraint equation can be derived as:

$$\xi\, d\theta = (\sin\theta - f'(x_p)\cos\theta)\, dx_p \tag{13}$$

where $f'(x_p)$ denotes the slope of curve $f(x_p)$ at x_p. It follows from differential equation (13) that the orientation angle of the vehicle is only a function of x-axis coordinate of the reference point.

From equations (3), (6) and (13), we can obtain the expression of steering angle as follows (the detailed derivation is omitted):

$$\phi_{m1} = \tan^{-1}\left(\frac{f'(x_p)\cos\theta - \sin\theta + x_{m1}\dfrac{d\theta}{dx_p}}{f'(x_p)\sin\theta + \cos\theta - y_{m1}\dfrac{d\theta}{dx_p}}\right) \tag{14}$$

Since the reference point at different positions will produce different effects on the orientation angle and steering angle, two cases $\xi = 0$ and $\xi \neq 0$ will be considered.

3.1. The case $\xi = 0$

As defined above, $\xi = 0$ corresponds to the position where reference point is chosen at the rear axle. In this case, from equation (13),

$$\theta = \tan^{-1}(f'(x_p)) \tag{15}$$

Substituting expression (15) into (14) and simplifying,

$$\phi_{a1} = \tan^{-1}\left(\frac{L\kappa_p}{1 - y_{a1}\kappa_p}\right) \tag{16}$$

Where $f''(x_p)$ represents the second derivative of the path of the reference point at x_p,

$$\kappa_p = \frac{f''(x_p)}{(1 + (f'(x_p))^2)^{3/2}}$$

represents the curvature of the reference path at the same point, $L = x_{a1} - \xi$ represents the wheelbase of the vehicle. If the reference point is at the midpoint of the rear axle, then $y_{a1} = 0$ and we obtain the widely used formula:

$$\phi_{a1} = \tan^{-1}(L\kappa_p) \tag{17}$$

It is noted that equations (15) and (17) are independent of the initial orientation angle at any point on the path, that is the direction of the orientation of the vehicle must be the tangent of the path.

Equation (15) indicates that vehicle's orientation angle possesses the same continuity as the first derivative of the path. At the line–line transition point shown in Figure 1(a), $f'(x_p)$ is not continuous, therefore, the orientation of the vehicle is also not continuous. However, at the line–circular transition point shown in Figure 1(b), vehicle's orientation angle is continuous as $f'(x_p)$ at this point is continuous.

Equation (17) shows the dependence of the continuity of the steering angle on that of the followed path. The sufficient and necessary condition for the continuity of the steering angle along the path is the continuity of the second derivative of the path at every point. So at the line–line and line–circular transition points, steering angle is not continuous. This prevents the vehicle from efficient and smooth motion.

Using an inductive method, we can prove the following theorems:

Theorem 3.1: If the $(n+1)$th derivative of the path at any point with respect to x_p is continuous, then the nth derivative of the orientation angle of the vehicle at the corresponding point with respect to x_p is continuous.

Theorem 3.2: If the $(n+2)$th derivative of the path at any point with respect to x_p is continuous, then the nth derivative of the steering angle of the vehicle at the corresponding point with respect to x_p is continuous.

3.2 The case $\xi \neq 0$

When the reference point is chosen away from the rear axle of the vehicle, $\xi \neq 0$. In this case, orientation angle is the solution of the first order differential equation (13) and is a function of $f'(x_p)$ and the initial orientation angle θ_0 of the vehicle. When the vehicle traverses the line–line transition point, although $f'(x_p)$ at that point is not continuous, orientation angle will be continuous because the orientation angle at the end of the first line segment will become the initial angle of the succeeding line segment. The first derivative of the orientation angle with respect to x_p possesses the same continuity as $f'(x_p)$ does. From equation (13) and (14), steering angle can be derived as:

$$\phi_{a1} = \tan^{-1}\left(\frac{L(\sin\theta - f'(x_p)\cos\theta)}{(\xi\cos\theta - y_{a1}\sin\theta) + f'(x_p)(\xi\sin\theta + y_{a1}\cos\theta)}\right) \tag{18}$$

It can be seen from (18) that for most cases, the steering angle is not continuous at the line–line transition point because the orientation angle is continuous and $f'(x_p)$ is not; the steering angle is continuous at the line-circle transition point because both orientation angle and $f'(x_p)$ are continuous.

Since the solution of orientation angle θ depends on the initial orientation angle θ_0 when $\xi \neq 0$, the continuity of orientation angle θ may hold occasionally even if $f'(x_p)$ is not continuous at some transition point. However, the possibility is rare. Generally, we have the following theorems:

Theorem 3.3: If the nth derivative of the path at any point with respect to x_p is continuous, then the nth derivative of the orientation angle of the vehicle at the corresponding point with respect to x_p is continuous.

Theorem 3.4: If the $(n+1)$th derivative of the path at any point with respect to x_p is continuous, then the nth derivative of the steering angle of the vehicle at the corresponding point with respect to x_p is continuous.

From Theorems 3.1 to 3.4, it is easily seen that the position of the reference point does have a significant effect on the motion feasibility of the vehicle. Following the same path, moving the reference point away from the rear axle of the vehicle will improve the smoothness of the motion and steering performance.

4. STEERING ANGLE LIMIT AND THE FEASIBLE DEVIATION ANGLE INTERVALS

To analyze the motion feasibility of a vehicle, the existence of steering angle limit cannot be neglected. The consideration of it helps to understand the critical conditions for distinguishing a feasible motion from an infeasible one. In the range of $-180° \le \phi_{a1} \le 180°$, the limited steering angle can be expressed by the following inequality constraints:

$$-\delta_{max} \le \phi_{a1} \le \delta_{max}, \quad 180° - \delta_{max} \le \phi_{a1} \le 180°,$$
$$-180° \le \phi_{a1} \le -180° + \delta_{max} \tag{19}$$

Where δ_{max} is a positive constant and represents the maximum deviation of the steering wheel from x_1-axis, see Figure 3. When the steering angle is in the range of $-\delta_{max} \le \phi_{a1} \le \delta_{max}$, it means that the direction of the velocity at the midpoint of the vehicle is the same as that of the positive direction of the x_1-axis; when the steering angle falls into the range of $180° - \delta_{max} \le \delta_{a1} \le 180°$ or $-180° \le \phi_{a1} \le -180° + \delta_{max}$, the direction of the velocity at the midpoint of the rear axle is on the negative direction of the x_1-axis. We usually refer to the former as a forward motion and the latter as a backward motion.

Let α represent the motion direction of the reference point P, θ represent the orientation angle of the vehicle at point x_p on the path $f(x_p)$, as shown in Figure 4. Then α can be expressed as:

$$\tan(\alpha) = \frac{\dot{y}_p}{\dot{x}_p} = f'(x_p) \tag{20}$$

We define $\beta = \theta - \alpha$ as the deviation angle of the vehicle at point x_p. Substituting equation (20) into (18), we have:

$$\phi_{a1} = \tan^{-1}\left(\frac{L \sin\beta}{\chi \cos\beta - y_{a1} \sin\beta}\right) \tag{21}$$

Differentiating equation (21) with respect to β:

$$\frac{d\phi_{a1}}{d\beta} = \frac{\chi \cdot L}{(L \sin\beta)^2 + (\chi \cos\beta - y_{a1} \sin\beta)^2} \tag{22}$$

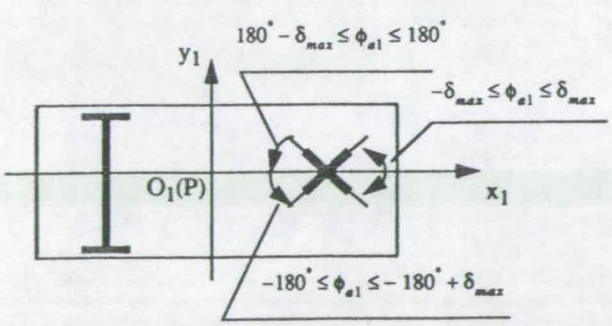

Fig. 3. An illustration of the steering angle inequality constraints.

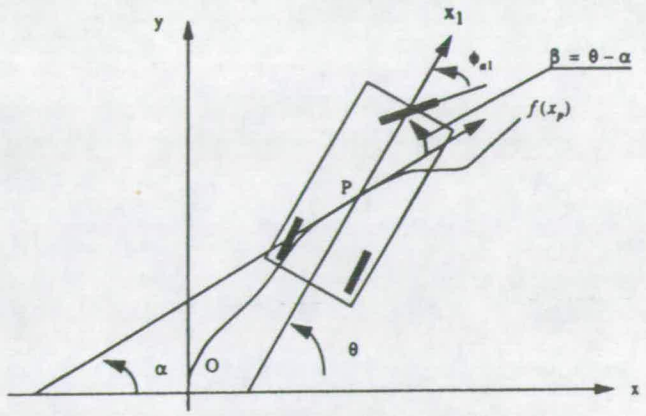

Fig. 4. An illustration of the deviation angle β.

It is clear that when $\chi < 0$, $\frac{d\phi_{a1}}{d\beta} < 0$, steering angle ϕ_{a1} is monotonic decreasing with respect to β; when $\chi > 0$, $\frac{d\phi_{a1}}{d\beta} > 0$, steering angle ϕ_{a1} is monotonic increasing. A typical relationship between steering angle and the deviation angle is shown in Figure 5.

Since the steering angle varies monotonically with respect to the deviation angle, there exist four critical orientation angles β_1, β_2, β_3 and β_4, corresponding to the four critical steering angles δ_{max}, $-\delta_{max}$, $180° - \delta_{max}$ and $-180° + \delta_{max}$. The corresponding feasible intervals of the deviation angles for $\chi < 0$ and $\chi > 0$ are shown in Table I and Table II, respectively.

From Tables I and II, we can draw the following conclusion that if the steering angle limit is taken into consideration, only when the deviation angle falls into the four feasible intervals, i.e. the neighborhood of 0° and that of ±180°, can the steering angle limit be satisfied. We call these four intervals as the feasible deviation intervals and the corresponding orientation angle intervals as feasible orientation intervals.

For a given steering angle limit, in the following, we discuss the effect of χ on the maximum deviation angle. From equation (21), it is easy to obtain:

$$\beta = \tan^{-1}\left(\frac{\chi \tan(\phi_{a1})}{L + y_{a1} \tan(\phi_{a1})}\right) \tag{23}$$

It can be observed from equation (23) that the farther (the larger the value of the $|\chi|$) the reference point is chosen from the rear axle, the larger the magnitude of

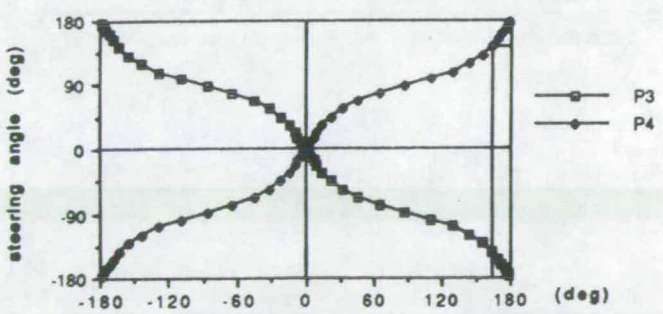

Fig. 5. The relationship between the steering angle and the deviation angle when the reference points are in front of the rear axle ($P3$) and behind the rear axle ($P4$), respectively.

Table I The corresponding relationship between critical steering angles and critical orientation angles when reference point is in front of the rear axle

$\underline{x} < 0$				
Interval ϕ_{s1}	$(0°, \delta_{max})$	$(-\delta_{max}, 0°)$	$(180° - \delta_{max}, 180°)$	$(-180°, -180° + \delta_{max})$
Interval β	$(\beta_1, 0)$	$(0°, \beta_2)$	$(-180°, \beta_3)$	$(\beta_4, 180°)$
Signs	$\beta_1(-)$	$\beta_2(+)$	$\beta_3(-)$	$\beta_4(+)$

Table II The corresponding relationship between critical steering angles and critical orientation angles when reference point is behind the rear axle

$\underline{x} > 0$				
Interval ϕ_{s1}	$(0°, \delta_{max})$	$(-\delta_{max}, 0°)$	$(180° - \delta_{max}, 180°)$	$(-180°, -180° + \delta_{max})$
Interval β	$(0°, \beta_1)$	$(\beta_2, 0°)$	$(\beta_3, 180°)$	$(-180°, \beta_4)$
Signs	$\beta_1(+)$	$\beta_2(-)$	$\beta_3(+)$	$\beta_4(-)$

the permitted deviation angle. It should be noted that above analysis applies to the initial position.

5. THE ANALYSIS OF STRAIGHT LINE MOTION

When the reference path is a straight line, the motion of the vehicle is called straight line motion. Straight line motion is the most basic and widely adopted kind of motion. In this section, we analyze the effects of the position of the reference point and the initial orientation angle on the orientation angle and steering angle of the vehicle when the limit of steering mechanism is taken into consideration.

For simplicity and without losing generality, suppose the straight line is the x-axis, the start point is located at the origin and the motion direction is along the positive direction of the x-axis. Mathematically, it is:

$$y_p = 0, \quad x_p \geq 0 \tag{24}$$

As defined above, in this case, $\alpha = 0$, the deviation angle β of the vehicle is equal to its orientation angle θ. The main problem is how to determine θ.

When the reference point is not chosen at the rear axle, the orientation angle can be expressed as a function of the initial angle θ_0, the relative position of the reference point to the rear axle $\underline{x}$ and the passed length x_p:[11]

$$\theta = 2\tan^{-1}\left(\tan\left(\frac{\theta_0}{2}\right)e^c\right) \tag{25}$$

where $c = x_p/\underline{x}$. Differentiating equation (25) with respect to x_p, we have:

$$\frac{d\theta}{dx_p} = \frac{2\tan\left(\frac{\theta_0}{2}\right)e^c}{\underline{x}\left(1 + \left(\tan\left(\frac{\theta_0}{2}\right)e^c\right)^2\right)} \tag{26}$$

The monotonicity of θ with respect to the passed length x_p is shown in Table III.

5.1 The case $\underline{x} < 0$

In this case, since θ is monotonic decreasing (MD) with respect to x_p when $0° < \theta_0 < 180°$ whereas θ is monotonic increasing (MI) when $-180° < \theta_0 < 0°$, if no steering angle limit is taken into consideration, then whatever the initial orientation angle is in the range from $-180°$ to $180°$, when $x_p \to \infty$, then $\theta \to 0$. When the steering angle limit is not neglected, it can be seen from Table I and III that if the initial orientation angle falls into the feasible range of $(\theta_1, 0°)$ or $(0°, \theta_2)$ which equals to $(\beta_1, 0°)$ or $(0°, \beta_2)$, respectively, when $x_p \to \infty$, then $\theta \to 0$, and the orientation angle is always kept in the feasible range, so the steering angle limit is always satisfied; if the initial orientation angle falls into the other feasible range of $(-180°, \theta_3)$ or $(180°, \theta_4)$ which equals to $(-180°, \beta_3)$ or $(\beta_4, 180°)$, respectively, when $x_p \to \infty$, then the orientation angle will reach θ_3 or θ_4 within a limited passed length, that means that after the steering angle limit is reached, the path can not be traced.

5.2 The case $\underline{x} > 0$

In this case, since θ is monotonic increasing (MI) with

Table III The monotonicity of the orientation angle with respect to x_p when reference point is chosen away from the rear axle of the vehicle (MD = Monotonic Increasing, MD = Monotonic Decreasing)

	$\underline{x} < 0$		$\underline{x} > 0$	
	$0° < \theta_0 < 180°$	$-180° < \theta_0 < 0°$	$0° < \theta_0 < 180°$	$-180° < \theta_0 < 0°$
θ versus x_p	MD	MI	MI	MD

respect to x_p when $0° < \theta_0 < 180°$ whereas θ is monotonic decreasing (MD) when $-180° < \theta_0 < 0°$, if no steering angle limit is taken into consideration, whatever the initial orientation angle falls into the range of $0° < \theta_0 < 180°$, $-180° < \theta_0 < 0°$, when $x_p \to \infty$, then $\theta \to \pm 180°$. Using the similar analysis, we can conclude that only when the initial orientation angle is in the feasible range of $(-180°, \theta_3)$ or $(180°, \theta_4)$, can the vehicle trace the straight line for any length.

5.3 The case $\underset{\sim}{x} = 0$

This means that the initial angle must only be 0° or ±180°. The locus of any point is also straight line and the motion of the vehicle is a translation. Otherwise, the vehicle can not move.

6. THE ANALYSIS OF CIRCULAR MOTION

If the reference path is a circular arc, the motion of the vehicle is called circular motion. In this section, we consider the rigid vehicle travelling along a circle of radius R from S to T, see Figure 6. We may assume that the motion of the reference point P can be described by the following equations:

$$\begin{bmatrix} x_p \\ y_p \end{bmatrix} = \begin{bmatrix} -R\cos(\omega t) \\ R\sin(\omega t) \end{bmatrix} \tag{27}$$

$$\begin{bmatrix} \dot{x}_p \\ \dot{y}_p \end{bmatrix} = \begin{bmatrix} R\omega\sin(\omega t) \\ R\omega\cos(\omega t) \end{bmatrix} \tag{28}$$

Where ω represents the angular velocity of the reference point P, ωt represents the radians of the passed arc. Substituting equation (28) into (20), we have the expression for the motion direction of the reference point:

$$\alpha = 90° - \omega t \tag{29}$$

At the start point, $\omega t = 0$ and $\alpha = 90°$. The feasible initial orientation angle must be in the neighborhoods of ±90°.

The steering angle expression becomes:

$$\phi_{a1} = \tan^{-1}\left(\frac{-L}{\underset{\sim}{x}\tan(\theta + \omega t) + y_{a1}}\right) \tag{30}$$

Like the straight line motion, there are three cases depending on the choice of the reference point P, namely, corresponding to the signs of $\underset{\sim}{x}$.

6.1 The case $\underset{\sim}{x} < 0$

In this case, the orientation angle can be given in the following form:[11]

$$\theta = \begin{cases} 2\tan^{-1}\left(a \cdot \dfrac{z_0' + a \cdot \tan(\omega t \cdot b)}{a - (z_0' \cdot \tan(\omega t \cdot b))}\right) - \omega t, & k < 1 \\ 2\tan^{-1}(\omega t + z_0') - \omega t, & k = 1 \\ 2\tan^{-1}\left(c \cdot \dfrac{(c + z_0') \cdot e^{\omega t d} - (c - z_0')}{(c + z_0') \cdot e^{\omega t d} + (c - z_0')}\right) - \omega t, & k > 1 \end{cases} \tag{31}$$

Where

$$k = -\frac{R}{\underset{\sim}{x}}, \quad z_0' = \tan\left(\frac{\theta_0}{2}\right), \quad a = \sqrt{\frac{1+k}{1-k}}, \quad b = \frac{\sqrt{1-k^2}}{2},$$

$$c = \sqrt{\frac{k+1}{k-1}}, \quad d = \sqrt{k^2 - 1}.$$

Equation (31) indicates that the orientation angle is a function of initial orientation angle, the k and ωt, independent of ω and $R\omega$. That means velocity has no effect on the orientation angle.

Because the monotonicity of the orientation angle with respect to ωt is not as explicit as that of the straight line motion, so in the following, the simulation result is given. Figure 7 illustrates a schematic of a practical rigid vehicle and its key dimensions.[37] This vehicle will be used as the simulation model in this section.

Figure 8 shows the changes of the orientation angle with respect to ωt at different k values and initial orientation angles when ωt changes from 0° to 90°. When the initial orientation angle is in the range of from 90° to 120°, the orientation angle is monotonic decreasing and

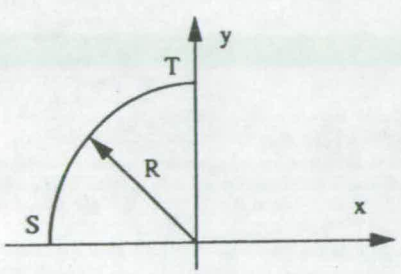

Fig. 6. A schematic for circular motion.

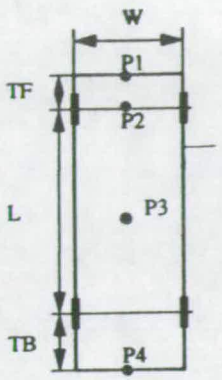

Dimensions (values in meters)	
Body width (W)	2.5
Effective wheelbase (L)	6.2
Front overhang (TF)	1.3
Rear overhang (TB)	2.5

Fig. 7. A schematic of the geometry of a FAT design rigid vehicle.

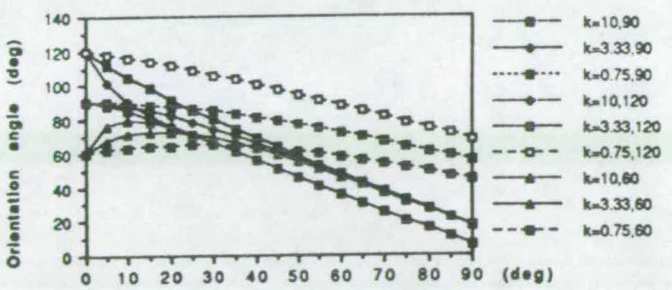

Fig. 8. The change of the orientation angle with respect to the passed arc length when the reference point is in front of the rear axle and the initial orientation angle is in the neighborhood of 90°.

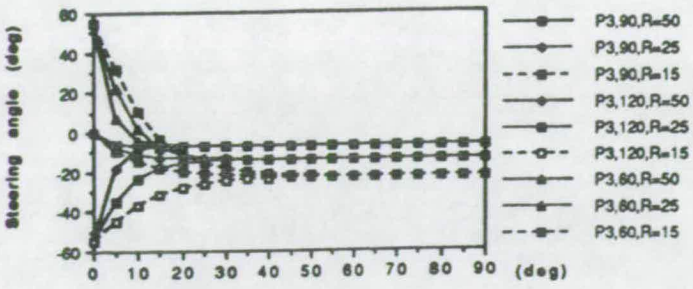

Fig. 9(a). The change of the steering angle with respect to the passed arc length when the reference point is chosen at $P3$ and the initial orientation angle is in the neighborhood of 90°.

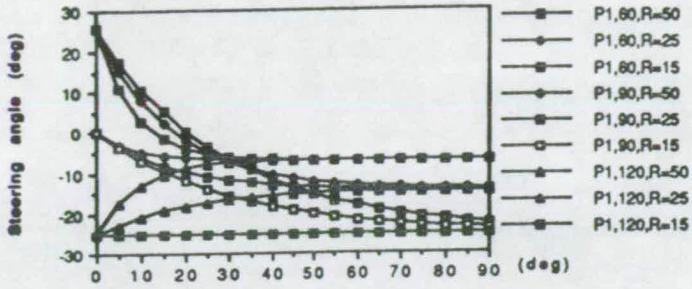

Fig. 9(b). The change of the steering angle with respect to the passed arc length when the reference point is chosen at $P1$ and the initial orientation angle is in the neighborhood of 90°.

the smaller the k, the slower the change of the orientation angle. When initial orientation angle is less than 90°, at the beginning, the orientation angle increases and then decreases. It can also be seen that with the same k and different initial orientation angles, the vehicle's orientation angle tends to be the same value as ωt increases.

Figure 9(a) and (b) show the change of the steering angle with respect to ωt when the initial orientation angle is in the neighborhood of 90° and the reference point are at $P3$ and $P1$ (see Figure 7), respectively. Three factors, namely, the reference point position, the initial orientation angle and k, affect the steering angle. The initial steering angle is dependent on the position of the reference point and the initial orientation angle, not on k. As stated above, moving forward the reference point increases the permitted deviation angle, consequently, makes it easier to satisfy the steering limit. However, as ωt increases, the steering angle tends to be a steady value which is independent of the initial orientation angle but dependent on k. Moving forward the reference point makes the magnitude of the steady steering angle increase. In practice, $k>1$, from equations (30) and (31) by putting $\omega t \to \infty$, it can be obtained:

$$\phi_{a1_\infty} = \lim_{\omega t \to \infty} \phi_{a1} = \tan^{-1}\left(\frac{-L}{-\underline{x}\sqrt{k^2-1}+y_{a1}}\right), \quad (k>1) \tag{32}$$

when reference point is chosen at the center line, namely, $y_{a1}=0$, the condition of equal initial and steady

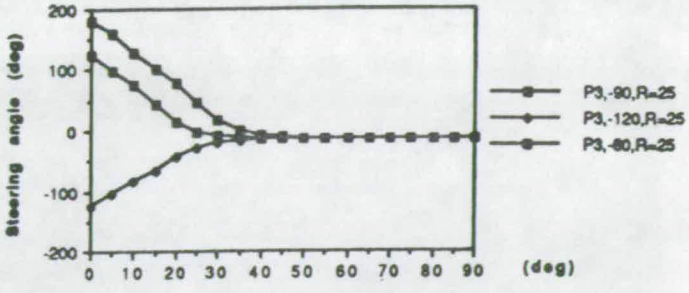

Fig. 10. The change of the steering angle with respect to the passed arc length when the reference point is in front of the rear axle ($P3$) and the initial orientation angle is in the neighborhood of −90°.

steering angles is:

$$\tan(\theta_0) = \pm\sqrt{k^2-1} \tag{33}$$

When initial orientation angles are −60°, −90° and −120°, the orientation angle change with respect to ωt is indicated in Figure 10. The steering angle reaches its saturation limit very quickly, after that, the vehicle can not move.

In summary, from the above analysis we can draw the following conclusions: Only when the initial orientation angle falls into the neighborhood of 90° and satisfying the steering angle limit, then the vehicle can move properly, the needed steering angle tends to a steady value. The farther the reference point is chosen from the rear axle, the smaller the magnitude of the initial steering angle is needed, on the other hand, the bigger the magnitude of the steady steering angle is needed.

6.2 The case $\underline{x}>0$

The orientation angle is as follows:[11]

$$\theta = \begin{cases} 2\tan^{-1}\left(\frac{1}{a}\cdot\frac{az_0'+\tan(\omega t\cdot b)}{1-(az_0'\cdot\tan(\omega t\cdot b))}\right)-\omega t, & k<1 \\ 2\tan^{-1}\left(\frac{z_0'}{1-(\omega t\cdot z_0')}\right)-\omega t, & k=1 \\ 2\tan^{-1}\left(\frac{1}{c}\cdot\frac{(1+cz_0')+(cz_0'-1)\cdot e^{\omega td}}{(1+cz_0')-((cz_0'-1)\cdot e^{\omega td})}\right)-\omega t, & k>1 \end{cases} \tag{34}$$

Where $k=R/\underline{x}$, a, b, c, d, and z_0' are defined as those in the case $\underline{x}<0$. The steering input necessary to follow the circle is still determined by equation (30).

Figure 11 shows the change of the orientation angle

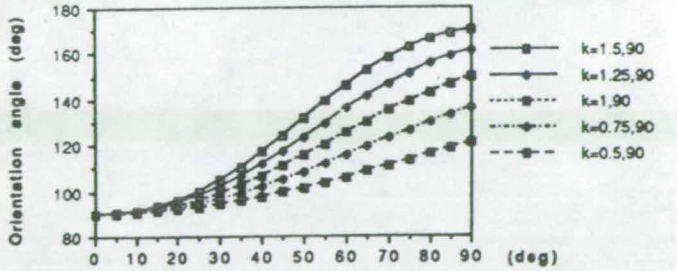

Fig. 11. The change of the orientation angle with respect to the passed arc length when the reference point is behind the rear axle and the initial orientation angle is 90°.

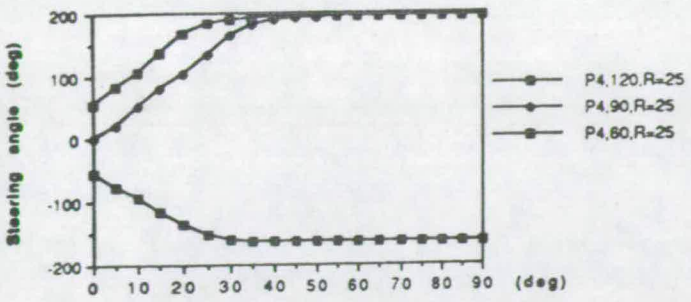

Fig. 12. The change of the steering angle with respect to the passed arc length when the reference point is behind the rear axle ($P4$) and the initial orientation angle is in the neighborhood of 90°.

with respect to ωt when initial orientation angles are 90°. The heading of the vehicle turns left while the reference point is making a right turn. A pirouette occurs. Even if the initial steering angle satisfies the steering limit, the steering angle limit will be reached very quickly. Figure 12 illustrates this point.

Figure 13 is an illustration of orientation angle changes when initial orientation angle are −90°, −120° and −60° respectively. Figure 14 shows the corresponding steering angle changes. Clearly, the steering angle limit will be satisfied all the time if initial and steady steering angles fall into the feasible intervals.

6.3 The case $x = 0$

It is obvious that equations (15) and (28) yield:

$$\theta = 90° - \omega t \tag{35}$$

In this case, equation (2) becomes:

$$x_m^2 + y_m^2 = x_{m1}^2 + (y_{m1} + R)^2 \tag{36}$$

Equation (36) indicates that the path of any point in the vehicle is a circle. At any instant, the tangent of the reference path coincides with the orientation of the vehicle, including the intial time.

7. CONCLUSIONS

In this paper, we have investigated in detail the dependence of the orientation angle and steering angle on the shape of the reference path, the initial orientation angle and the position of the reference point, taking any

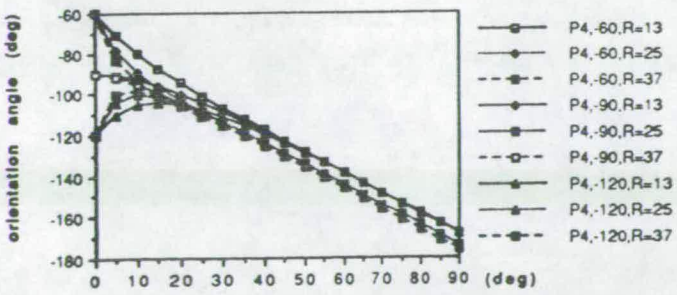

Fig. 13. The change of the orientation angle with respect to the passed arc length when the reference point is behind the rear axle ($P4$) and the initial orientation angle is in the neighbhorhood of −90°.

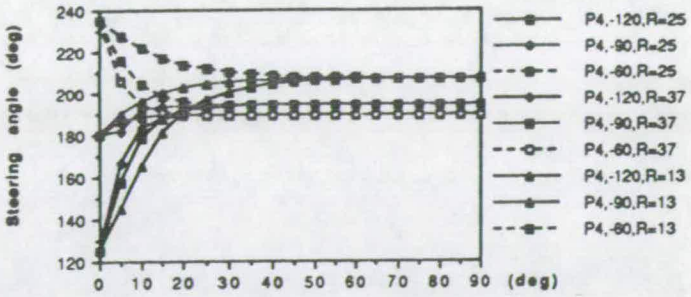

Fig. 14. The change of the steering angle with respect to the passed arc length when the reference point is behind the rear axle ($P4$) and the initial orientation angle is in the neighborhood of −90°.

steering angle limit into consideration. The problem solved is how to judge motion feasibility of a vehicle when it is required to follow a path and, if feasible, how to determine the required steering angle and the velocity.

The continuity of the orientation angle is the first requirement for smooth motion of a vehicle. However, if we choose the reference point on the rear axle of the vehicle and the first derivative of the reference path possesses a discontinuity point, a discontinuity will occur. This will cause difficulty in the localization of the vehicle. Moving the reference point away from the rear axle improves not only the continuity of the orientation angle, but also that of the steering angle, when the same path is followed. A continuous steering angle means that continuous motion without stopping at the transition points of the path is possible.

The steering angle limit is the main factor affecting the maneuvering capacity of the vehicle. Theoretically, if no steering limit exists, any continuous reference path can be traced if the reference point is chosen away from the rear axle. In practice, the steering angle limit cannot be neglected. The concept of the deviation angle has been established to describe the motion feasibility of the vehicle. The advantage of developing the concept is that at any time, the feasible deviation angle intervals are always in the neighborhood of 0° and ±180°. Through the analyses of straight line motion and circular motion, it is further revealed that when the reference point is in front of the rear axle, if the initial deviation angle falls into the feasible interval in the neighborhood of 0°, then the vehicle can trace the straight line or circular arc for any length. However, if the initial deviation angle falls into the other feasible interval, a pirouette will occur and the steering limit will be reached very quickly; after that, the vehicle cannot trace the path any more. When the reference point is chosen behind the rear axle of the vehicle, the initial feasible deviation angle falling in the neighborhood of ±180° means that the straight line or circular arc can be traced for any length and the other feasible interval will cause the pirouette.

The above result tells us that if the vehicle moves forward, the reference point should be chosen in front of the rear axle whereas the reference point should be chosen behind the rear axle when the vehicle moves backward.

For following a circular path, the position of the reference point affects the initial steering angle and the steady state steering angle. The farther the reference point is chosen from the rear axle, the smaller the magnitude of the initial steering angle, but the bigger the magnitude of the steady state steering angle. Therefore, a trade-off must be made.

The aim of this paper is to offer a better understanding of the motion of the vehicle. The results have been tested on a kinematic model of a typical vehicle. Using this model, even if the reference point is not at the mass center of the vehicle, we still can calculate the motion of the mass center of the vehicle, this is important for the analysis of the dynamics of the vehicle. More applications associated with kinematics of a wheeled vehicle are expected.

Acknowledgments

The authors would like to express their gratitude to K.C. Wong Education Foundation for providing living expenses, CVCP committee, U.K. and Mechanical Engineering Department of Edinburgh University for offering tuition fees for the first author during his Ph.D research. Also thanks to Dr. A.S.-T. Lue, Mr. K.H. Wong and Dr. G. Alder for their valuable encouragement and help.

References

1. W.L. Nelson, "Continuous steering-function control of robot carts" *IEEE Trans. on Industrial Electronics* **36,** 330–337 (1989).
2. T. Lozano-Perez, "Spatial Planning: A configuration space approach" *IEEE Trans. on Computers*, **C-32**(2), 108–120 (1983).
3. J.R. Billing and W.R.J. Mercer, "Swept paths of large trucks in right turns of small radius" *Transportation Research Record 1052, Symposium on Geometric Design for Large Trucks* (1986) pp. 116–119.
4. Y. Kanayama and S. Yuta, "Vehicle path specification by a sequence of straight lines" *IEEE J. Robotics and Automation* **4,** 560–570 (1988).
5. T. Lozano-Perez and M. Wesley, "An algorithm for planning collision-free paths among polyhedral obstacles" *Commun. Assoc. Comput. Math.* **22,** 560–570 (1979).
6. R.A. Brooks and T. Lozano-Perez, "A subdivision algorithm in configuration space for findpath with rotation" *IEEE Trans. on Systems, Man and Cybernetics*, **SMC-15**(2), 224–233 (1985).
7. J.C. Latombe, *Robot Motion Planning* (Kluwer Academic Publishers, Boston, Mass., 1990).
8. J.P. Laumond, "Obstacle growing in a non-polygonal world" *Information Processing Letters* **25,** 41–50 (1987).
9. Y.H. Liu and S. Arimoto, "Path Planning Using a Tangent Graph for Mobile Robots Among Polygonal and Curved Obstacles" *Int. J. Robotics Research* **11,** 376–382 (1992).
10. I.J. Cox, "Blanche – An experiment in guidance and navigation of an autonomous robot vehicle" *IEEE Trans. on Robotics and Automation* **7,** 193–204 (1991).
11. Y. Wang and J.A. Linnett, "On the maneuvering problems of wheeled vehicles" *Proc. of the First Conference of the Chinese Society of Electrical and Electronic Engineering in the UK* (1993) pp. 34–60.
12. J.C. Alexander, "On the motion of a trailer-truck" *SIAM Rev.* **27,** 578–579 (1985).
13. J.C. Alexander and J.H. Maddocks, "On the maneuvering of vehicles" *SIAM J. Appl. Math.* **48,** 38–51 (1988).
14. J.C. Alexander and J.H. Maddocks, "On the kinematics of wheeled mobile robots" *Int. J. Robotics Research* **8,** 15–27 (1989).
15. J. Baylis, "The mathematics of a driving hazard" *Math. Gaz.* **57,** 23–26 (1973).
16. E.A. Bender, "A driving hazard revisited" *SIAM Rev.* **21,** 136–138 (1979).
17. T.V. Fossum and G.N. Lewis, "A mathematical model for trailer-truck jackknifing" *SIAM Rev.* **23,** 95–99 (1981).
18. H.I. Freedman and S.D. Riemenschneider, "Determining the path of the rear wheels of a bus" *SIAM Rev.* **25,** 561–568 (1983).
19. K.L. Heald, "Use of the HWI offtracking formula" *Transportation Research Record 1052, Symposium on Geometric Design for Large Trucks* (1986) pp. 45–53.
20. V. Hillier and F.W. Pittuck, *Fundamentals of Motor Vehicle Technology* (Hutchinson Education, London, 1966).
21. M.W. Sayers, "Vehicle offtracking models" *Transportation Research Record 1052, Symposium on Geometric Design for Large Trucks* (1986) pp. 53–62.
22. B.L. Smith, "Existing design standards" *Transportation Research Record 1052, Symposium on Geometric Design for Large Trucks* (1986) pp. 23–29.
23. J.Y. Wong, *Theory of Ground Vehicles* (John Wiley & Sons, New York, 1978).
24. J.M. Badcock, J.A. Dun, K. Ajay, L. Kleeman and R.A. Jarvis, "An autonomous robot navigation system — integrated environmental mapping, path planning, localization and motion" *Robotica* **11,** 97–103 (1993).
25. J. Barraquand and J.C. Latombe, "Controllability of mobile robots with kinematic constraints" *Technical Report No. STAN-CS-90-1317* (Department of Computer Science, Stanford University, USA, 1990).
26. T.J. Graettinger and B.H. Krogh, "Evaluation and time-scaling of trajectories for wheeled mobile robots" *Trans. of ASME J. Dynamics, Systems, Measurement and Control* **111,** 222–231 (1989).
27. A. Hemami, M.G. Mehrabi and R.M.H. Cheng, "Synthesis of an optimal control law for path tracking in mobile robots" *Automatica* **28,** 383–387 (1992).
28. Y. Kanayama and I.H. Bruce, "Smooth local path planning for autonomous vehicles" *Proc. of IEEEE Int. Conf. on Robotics and Automation* (1989) pp. 1256–1270.
29. Y. Kanayama, Y. Kimura, F. Miyazaki and T. Noguchi, "A stable tracking control method for an autonomous mobile robot" *Proc. of IEEE Int. Conference on Robotics and Automation* (1990) pp. 384–389.
30. K.J. Kyriakopoulos and G.N. Saridis, "An integrated collision prediction and avoidance scheme for mobile robots in non-stationary environments" *Automatica* **29,** 309–322 (1993).
31. J.P. Laumond, "Feasible trajectories for mobile robots with kinematic and environment constraints" *Preprints of the International Conference on Intelligent Autonomous Systems* (1986) pp. 346–354.
32. P.F. Muir and C.P. Neuman, "Kinematic modelling of wheeled mobile robots" *J. Robotic Systems* **4,** 281–340 (1987).
33. W.L. Nelson, "Continuous-curvature paths for autonomous vehicles" *Proc. of IEEE Int. Conf. on Robotics and Automation* (1989) pp. 1260–1264.
34. B. Steer, "Trajectory planning for a mobile robot" *Int. J. Robotics Research* **8,** 3–14 (1989).
35. C.K. Yap, "How to move a chair through a door" *IEEE J. Robotics and Automation* **RA-3**(3), 172–181 (1987).
36. R.A. Brooks, "Solving the find-path problem by good representation of free space" *IEEE Trans. on Systems, Man and Cybernetics*, **SMC-13**(3), 190–197 (1983).
37. *Designing for Deliveries* (Freight Transport Association, St. John's Road, Tunbridge Wells TN4 9U2, U.K., 1983).

Robotica (1994) volume 12, pp 391–400.

Kinematics, kinematic constraints and path planning for wheeled mobile robots

Yongji Wang, J.A. Linnett, J. Roberts

Mechanical Engineering Department, The University of Edinburgh, Kings Building, Edinburgh EH9 3JL (UK)

(Received in Final Form: October 9, 1993)

SUMMARY

The problem associated with planning a collision-free path for a wheeled mobile robot (WMR) moving among obstacles in the workspace is investigated in this paper. A kinematic model, including the general nonholonomic constraint equation, is developed first, followed by the analysis of some general maneuvering characteristics of the WMR. The analytic solutions to the typical path curves, such as circle and straight line, which are important in the path planning problem, are also derived. From the analysis of the established kinematic model, some factors which affect the path planning problem for a WMR and therefore must be taken into account are revealed and the general description of the path planning problem for a WMR is formuated. In conclusion, a possible architecture of the algorithm for a practical WMR is presented.

KEYWORDS: Kinematics; Path planning; Mobile robot; Kinematic model.

1. INTRODUCTION

A major objective of current research for wheeled mobile robots is to provide the capability to automatically plan a collision-free path among obstacles. This problem is well-known as a find-path problem.[1] The importance of a find-path problem is obvious and the complexity involved in solving it has been shown.[2] The problem can be described as: given an object (a wheeled mobile robot) with an initial location and orientation, a goal location and orientation, and a set of obstacles located in space, find a continuous path for the object from the initial location and orientation to the goal location and orientation which avoids any collision with obstacles along the way.

To achieve this purpose, numerous efforts have been conducted to solve this seemly simple, but in fact very complicated problem during the past decade. Various methods for dealing with the basic find-path problem and its various extensions, such as roadmap, exact cell decomposition, approximate cell decomposition and potential field approaches, have been developed. A systematic detailed discussion on robot motion planting can be found in reference 3.

Three kinds of constraints should be taken into account for the basic path planning problem, namely planning a path for a WMR moving among a set of fixed obstacles in the work space. The first is the size and location of the obstacles in the work space. The second results from the wheels mounted on the rigid robot body, it can be expressed as a general nonholonomic kinematic constraint. The third comes from the steering mechanism, the saturation limit of steering angle determines the capability to trace a path. We refer to the second and third kinds of constraints as the kinematic constraints. It is not necessary to include the velocity and acceleration at the path planning phase, because it will be shown that changing the velocity has no effect on the swept space of the WMR at low speed when it is tracing a path. This will be proved by the independence of the orientation angle of the WMR to its velocity. However, when the path planning problem is extended to include other robots or moving obstacles or both in the workspace, velocity and acceleration limits can't be ignored.

From the point of view of constraints taken into account in the existing algorithms, these can be categorized into two types. The first type treats a wheeled mobile robot as a free rigid body which can translate and rotate freely in the work space provided that it does not collide with obstacles, i.e. the motions of a WMR are supposed to be only subject to constraints from the obstacles, rather than from any kinematic constraints. Most of the algorithms developed belong to this type.[1,4–20] All the algorithms falling into the first type suffer from the fundamental drawback that kinematic constraints due to the robot's structure are not taken into account. Therefore, the paths generated by these algorithms will not always be reliable. In other words, when an actual robot is required to move along the generated path using this kind of algorithm, there still exists possibility of colliding with obstacles or finding that the path is inexexutable. This is illustrated in Figure 1. In which, Robot 1 and Robot 2 have the identical rigid body shape, but the wheels are mounted in different positions, and therefore, their second and third kinds of constraints are totally different. When the first type of algorithms is utilized to plan the paths for the two robots under the same environment, there will be the same paths generated for their same body shapes. However, in practice, when the two robots are required to follow the same generated path, the locus of any corresponding points except the two reference points in the two robots will be different. That means the swept spaces by the two robots are different. This will be clearly shown in section 2.

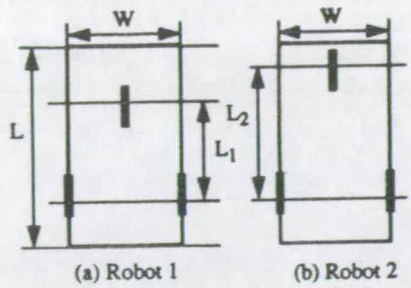

(a) Robot 1 (b) Robot 2

Fig. 1. Two robots with same rigid bodies, different wheel positions.

The second type of path planning algorithms for wheeled mobile robots does take into account the limit imposed by the steering mechanism which defines the minimum radius of curvature of the reference point's path. Path planning with this kind of constraint is a relatively new area of research. Following the work of Laumond,[21] it has recently attracted considerable interest.[3] The kinematic constraints considered by the second type of algorithms can be expressed in the following form:

$$\dot{x}^2 + \dot{y}^2 - \rho_{\min}\dot{\theta}^2 \geq 0 \tag{1}$$

$$-\dot{x}\sin\theta + \dot{y}\cos\theta = 0 \tag{2}$$

$$\frac{1}{\rho_{\min}} = \frac{1}{L_1}\tan(\varphi_{\max}) \tag{3}$$

Where $\dot{x}$, $\dot{y}$ are the velocity components of the midpoint of the rear axle in x-axis and y-axis in terms of the global reference frame respectively, θ is the orientation angle of the mobile robot, $\dot{\theta}$ the rotating angular speed of the robot, L_1 the wheelbase of the robot, $\rho_{\min}$ the minimum radius of curvature of the midpoint of the rear axle, $\varphi_{\max}$ the maximum steering angle determined by the steering mechanism (See Figure 2).

The purpose of developing the second type of algorithms is to remedy the drawback that the radius of curvature of the path generated for the reference point using the first type may be less than $\rho_{\min}$. However, the second kind of algorithms still suffers from some drawbacks:

a. Equations (1) to (3) hold only when the reference point is chosen on the midpoint of the rear axle. If the reference point is chosen on the other point, say one of the vertices of the robot's body or the mass center of the WMR, what kind of the general kinematic constraints can be found? What form can the general steering limit be expressed as? These questions will be answered in the later sections.

b. The algorithms still take no account of the fact that there is unique corresponding relationships between the orientation angle of a WMR and the path followed, which is determined by the rolling conditions of the wheels in the rigid robot body. This is the fundamental drawback.

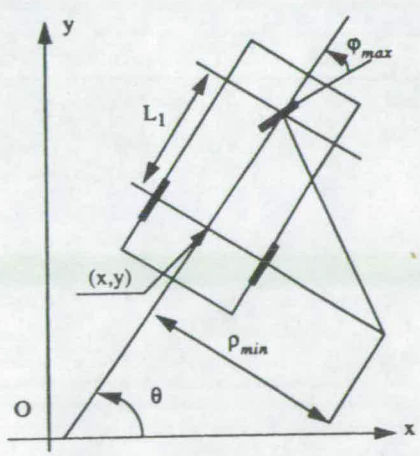

Fig. 2. An illustration of nonholonomic constraints expressed in equations (1)–(3).

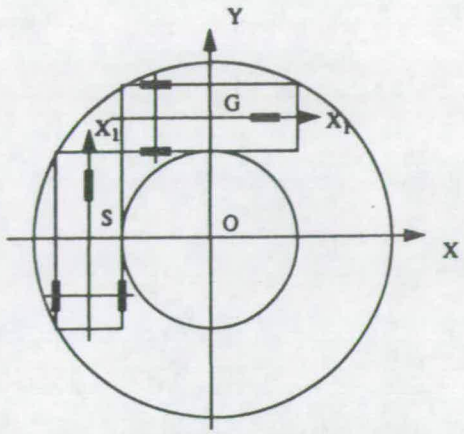

Fig. 3. An illustration of the difference between a free rigid body and a wheeled mobile robot.

Understanding the difference between a free body WMR and a practical WMR is the key to understand the shortcomings of the available algorithms, including the first and second types. A intuitional example of showing it is depicted in Figure 3. The free rigid body WMR is a rectangle and its free space is the part enclosed within the two circles with the same center. It can successfully move from the initial position and orientation S to the goal position and orientation G. However, for a practical WMR, the goal position and orientation is unreachable if the motion is restricted to the space between the circles. This will be seen in section 3.

In this paper, the study begins with the development of a general kinematic model for a wheeled mobile robot, which clearly distinguishes a practical WMR from a free rigid body. By analyzing the kinematic model, we draw some conclusions which are of significance to path planning problems and on which the remainder of the paper is built. Based on the kinematical model and the kinematic constraints, a possible architecture of the path planning algorithm for mobile robots among a set of fixed polygonal obstacles is presented.

The paper is organized as follows: In section 2, we first develop a general kinematic model for a WMR based on the ideal rolling conditions of the wheels mounted on the rigid body, followed by the analysis of its some general maneuvering characteristics. The derivation of the analytic solutions to two typical motions, circular and straight line motions, is the subject of section 3. The

effect of the kinematic constraints on the path planning problem is discussed in section 4 and then a general description of the path planning problem is formulated. The possible architecture of a path planning algorithm is also included in this section. Section 5 gives a coarse subalgorithm for an approximate global path for arbitrary shapes of WMRs moving among fixed polygonal obstacles. Emphasis is put on the discussion of the effects of the choice of the reference point on the computational efficiency. A general technique for detecting a potential collision between a polygonal rigid body and fixed polygonal obstacles is proposed in section 6. Finally, conclusions are drawn in section 7.

2. KINEMATIC MODEL FOR A WHEELED MOBILE ROBOT

To analyze the characteristics of a mobile robot associated with the path planning problem, namely the constraints imposed on it, a correct kinematic model is needed. In this section, we derive the mathematical model for a wheeled mobile robot, establish the general kinematical constraint equation, and then draw some conclusions useful for path planning problems.

2.1. Basic kinematic description of a wheeled mobile robot

Figure 4 is a plan view of the wheeled mobile robot model investigated in this paper. From the point of view of operating function, wheels used in the robot can be categorized into two types, free wheels and fixed wheels. If a wheel can rotate about a vertical axle, it is defined as a free wheel, otherwise, it is defined as a fixed wheel. Based on this definition, steered wheels are free wheels and wheels on the fixed axle, are fixed wheels. However, when they are described by a mathematical model, a fixed wheel may be regarded as a special free wheel, so in Figure 4, all the wheels are given in the form of free wheels. A global reference coordinate frame (Oxy) is introduced to describe the motion of the robot in terms of the position of the reference point (x_p, y_p) and the orientation angle θ of the robot. We define a local reference coordinate frame $(O_1x_1y_1)$, whose origin is placed at the reference point P of the robot with y_1 axis parallel to the rear axle BC of the robot. We use M to represent any point in the rigid robot body when discussing the motion of the rigid robot body and also use it to represent a wheel connected to the corresponding point when discussing wheel motion. The coordinates of point M are denoted by $M\ (x_m, y_m)$ in terms of the global reference frame and $M\ (x_{m1}, y_{m1})$ in terms of the local reference frame. So the coordinate of central point of a wheel is constant with respect to the local reference frame.

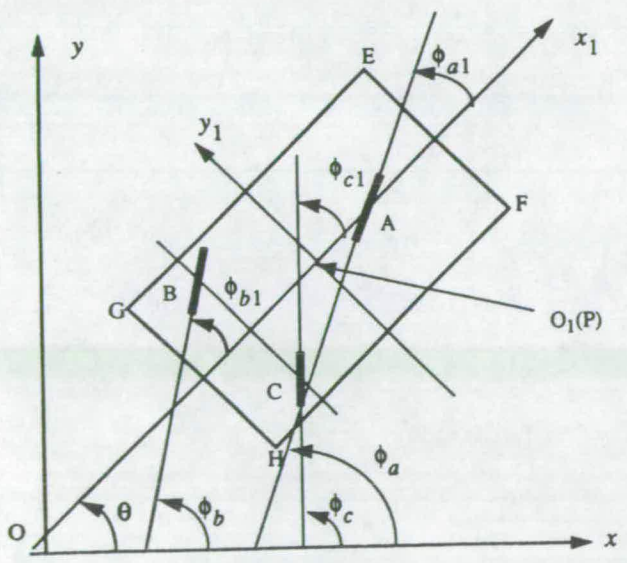

Fig. 4. Global (Oxy) and local $(O_1x_1y_1)$ reference coordinate frames, reference point P coincides with O_1.

The angle ϕ_m, $(m = a, b, c)$ is measured from the vertical plane the wheel M makes to the positive x axis, and ϕ_{m1}, from the vertical plane of the wheel M to the positive x_1 axis. The relation between ϕ_m, θ, ϕ_{m1} can be written as:

$$\phi_m = \phi_{m1} + \theta \tag{4}$$

The coordinates of point M in the global frame are related to the coordinates of point M measured in the local frame by the transformation:

$$\begin{bmatrix} x_m \\ y_m \end{bmatrix} = \begin{bmatrix} x_{m1}\cos\theta - y_{m1}\sin\theta + x_p \\ x_{m1}\sin\theta + y_{m1}\cos\theta + y_p \end{bmatrix} \tag{5}$$

The relationships between reference point velocity, orientation angle θ, robot turning angular rate and central velocities of wheels A, B, C are found by differentiating equation (5) with respect to time:

$$\begin{bmatrix} \dot{x}_m \\ \dot{y}_m \end{bmatrix} = \begin{bmatrix} (-x_{m1}\sin\theta - y_{m1}\cos\theta)\dot{\theta} + \dot{x}_p \\ (x_{m1}\cos\theta - y_{m1}\sin\theta)\dot{\theta} + \dot{y}_p \end{bmatrix} \tag{6}$$

Where $\dot{x}_m$, $\dot{y}_m$, $\dot{x}_p$, $\dot{y}_p$ are the velocity components of the corresponding wheel central point and the reference point along x, y-axes in terms of the global reference frame, $\dot{\theta}$ is the rotating angular rate of the robot body in terms of the global reference frame. Differentiating equation (6) again, we have the acceleration expressions:

$$\begin{bmatrix} \ddot{x}_m \\ \ddot{y}_m \end{bmatrix} = \begin{bmatrix} (-x_{m1}\cos\theta + y_{m1}\sin\theta)\cdot\dot{\theta}^2 \\ \quad + (-x_{m1}\sin\theta - y_{m1}\cos\theta)\cdot\ddot{\theta} + \ddot{x}_p \\ (-x_{m1}\sin\theta - y_{m1}\cos\theta)\cdot\dot{\theta}^2 \\ \quad + (x_{m1}\cos\theta - y_{m1}\sin\theta)\cdot\ddot{\theta} + \ddot{y}_p \end{bmatrix} \tag{7}$$

Equations (5), (6), (7) give the mathematical description of any point on the robot boy in terms of the reference point position, velocity, acceleration and orientation angle as well as their derivatives. When the whole robot is considered, the ideal rolling conditions must be satisfied:

a. The direction of every wheel rolling forward or backward, whether steered or not, must coincide with the tangent to the robot body trajectory in the corresponding wheel center.

b. The velocity of every wheel center point must be equal to the product of wheel rotating angular velocity about its own horizontal axle and its radius.

Mathematically, the above conditions can be expressed

as:

$$\tan(\phi_m) = \frac{d}{(x_m)}(y_m) = \frac{\dot{y}_m}{\dot{x}_m} \tag{8}$$

$$v_m = \varpi_m \times r \tag{9}$$

Where ϖ_m $(m = a, b, c)$ represents the angular velocity of wheels A, B, C, respectively; v_m the velocity of the center point of wheels A, B, C; and r the radius of every wheel. v_m is equal to the vector sum of $\dot{x}_m$ and $\dot{y}_m$:

$$(v_m)^2 = (\dot{x}_m)^2 + (\dot{y}_m)^2 \tag{10}$$

From equations (4), (8), we can obtain ϕ_{m1}, the relative angle to the robot orientation line, which is the steering angle for steering wheel.

$$\phi_{m1} = \tan^{-1}\left(\frac{\dot{y}_m}{\dot{x}_m}\right) - \theta \tag{11}$$

When the wheels in the robot are fixed wheels, then their relative angles to the robot orientation line are constants. For example, in Figure 3, wheels B, C are fixed wheels and $\phi_{b1} = \phi_{c1} = 0$, therefore, from equation (11), the following constraint is imposed:

$$\tan\theta = \frac{\dot{y}_b}{\dot{x}_b} = \frac{\dot{y}_c}{\dot{x}_c} \tag{12}$$

As defined above, y_1 axis is parallel to the robot's rear axle, so that $x_{b1} = x_c = \underline{x}$. Substituting equation (6) into (12) and simplifying we obtain:

$$\underline{x} \cdot \dot{\theta} = \dot{x}_p \sin\theta - \dot{y}_p \cos\theta \tag{13}$$

Equation (13) is what we need to solve for the robot's orientation angle θ when the reference point velocity components $\dot{x}_p$ and $\dot{y}_r$ are specified. Due to the fact that equation (13) describes the general relationship among reference point's position relative to the rear axle, its velocity and the robot's orientation angle and its first derivative when reference point is chosen at any point in the robot, it is called the general constraint equation. It can be seen that equations (1)–(3) are the special results when $\underline{x} = 0$ in equation (13). It can be noted that y_{b1}, y_{c1} are not included in equation (13), which illustrates the fact that only $\underline{x}$ effects on robot's orientation angle.

2.2 The independence of robot's orientation angle θ, steering angle to its velocity

A geometric curve, which is generated by a path planning algorithm and is required to be followed by the reference point P of the robot, is called a path. Mathematically, a curve can be presented as a general form in x-y plane:

$$y_p = f(x_p) \tag{14}$$

Some characteristics associated with its shape, such as its derivatives and curvature, are referred to as its geometric characteristics. A trajectory is defined as the time course along a path. One can choose velocity from various schedules for a geometrically defined path, which results in various velocity profiles. If a wheeled robot moves along any curve at different velocity profiles, how the velocities affect the robot's orientation θ and steering angle is an important problem for path planning of a mobile robot. If a variable is only affected by the geometrical characteristics rather than by robot's velocities, it is called an independent variable of velocities. If θ is an independent variable, it is easily derived that the swept space by a robot travelling along a specified path will be also independent of the robot's velocities (suppose the robot's motion is so low that ideal rolling occurs). When the limited steering angle of the steering mechanism is taken into consideration, whether or not the steering angle is an independent variable is of interest. In this subsection, we will prove that they are such defined independent variables.

Let $f'(x_p)$ denote the slope of curve $f(x_p)$ at x_p, we have:

$$dy_p = f'(x_p)\,dx_p \tag{15}$$

Substituting equation (15) into equation (13) gives:

$$\underline{x}\frac{d\theta}{dt} = (\sin\theta - f'(x_p)\cos\theta)\frac{dx_p}{dt} \tag{16}$$

Which reduces at once to,

$$\underline{x}\,d\theta = (\sin\theta - f'(x_p)\cos\theta)\,dx_p \tag{17}$$

Equation (17) is another form of the general constraint equation. Although the explicit analytic solution θ to the above equation can't be obtained, it is obviously dependent on x_p rather than on the velocity of the robot's reference point.

From the general constraint equation (17), the following two conclusions can be made:

a. When a WMR moves along a curved path, it is impossible for it to purely translate without rotation. As shown later, it is only when it moves along a straight line and its initial orientation angle coincides with the direction of the straight line that pure translation occurs.

b. When a WMR moves along a path, its instantaneous orientation angle is unique at every point on the path. This characteristic distinguishes a WMR from a free rigid body and has direct effects on path-planning problem for a WMR.

The robot's steering angle is presented by equation (11). After proving that θ is an independent variable, we must show that the ratio of $\dot{\theta}$ to $\dot{x}_p$ is independent of robot's velocities.

Substituting equation (6) into equation (11) yields:

$$\phi_{m1} = \tan^{-1}\left(\frac{(x_{m1}\cos\theta - y_{m1}\sin\theta)\dfrac{\dot{\theta}}{\dot{x}_p} + f'(x_p)}{(-x_{m1}\sin\theta - y_{m1}\cos\theta)\dfrac{\dot{\theta}}{\dot{x}_p} + 1}\right) - \theta \tag{18}$$

From equation (17), it follows that:

$$\frac{\dot{\theta}}{\dot{x}_p} = \frac{(\sin\theta - f'(x_p)\cos\theta)}{\underline{x}} \tag{19}$$

Equations (18) and (19) indicate that $\dot{\theta}/\dot{x}_p$ and ϕ_{m1} are

independent of the robot's velocity, so the steering angle of the robot is an independent variable.

3. TWO TYPICAL MOTIONS: CIRCULAR MOTION AND STRAIGHT LINE MOTION

In this section, we use the mathematical model from the previous secton to analyze the two typical robot motions: 1) circular motion. 2) straight line motion. Exactly speaking, circular motion or straight line motion means that the path followed by the reference point is a circle or a straight line because paths of the other points on the robot are not necessarily a circle or a straight line. The circular motion and straight line motion are chosen as examples because of the following two reasons: a) most analyses, especially for practical applications, assume that the reference point path is a circle; for example, the offtracking problem is defined only for circular turn.[22,23] b) the effects of some parameters, such as the circular radius, driving velocity, the position of the refence point, on the driving characteristics can be illustrated clearly. In path planning problem, most of the generated paths also consist of circles and straight lines.[3]

3.1 Right turn circular motion

A circular motion in clockwise direction is called a right turn circular motion, and the circular motion in counter-clockwise direction is called a left-turn circular motion. As proven above, some parameters, such as the robot's orientation angle and steering angle, are independent variables to its velocity. Therefore, for convenience and without losing generality, we may use parameterized expressions. Consider a WMR travelling along a circle of radius R at a constant rate from starting point S, see Figure 5. We may assume that the motion of the reference point P can be described by the following equations:

$$\begin{bmatrix} x_p \\ y_p \end{bmatrix} = \begin{bmatrix} \bar{x} + R\cos(\omega t - \varphi_0) \\ \bar{y} - R\sin(\omega t - \varphi_0) \end{bmatrix} \tag{20}$$

$$\begin{bmatrix} \dot{x}_p \\ \dot{y}_p \end{bmatrix} = \begin{bmatrix} -R\omega\sin(\omega t - \varphi_0) \\ -R\omega\cos(\omega t - \varphi_0) \end{bmatrix} \tag{21}$$

Where $\bar{x}$, $\bar{y}$ present the coordinates of the center of the circle, ω the angular rate, φ_0, $0° \le \varphi_0 < 360°$, presents the initial phase angle. There are three cases depending on the choice of the reference point P, corresponding to the signs of χ in equation (13). Suppose that L_r represents the distance from P to the rear axle, then $\chi = -L_r$, $\chi = 0$ and $\chi = L_r$ correspond to the following three cases where the reference point is chosen in front of, at and behind the robot's rear axle, respectively. In the following, we will study these three cases respectively.

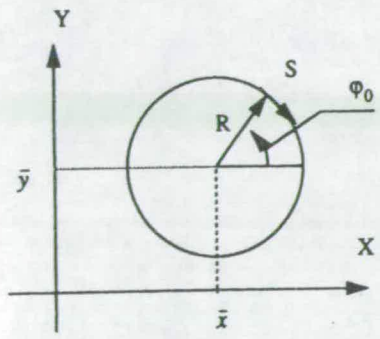

Fig. 5. A schematic for right turn circular motion.

I. The case $\chi = -L_r$

In this case, by substituting equation (21) into (13), we have:

$$-L_r\dot{\theta} = \dot{x}_p\sin\theta - \dot{y}_p\cos\theta = R\omega\cos(\omega t + \theta - \varphi_0) \tag{22}$$

As it is not possible to separate the variables in equation (22), the method of changing the variables must be used to solve it. The substitution $z = \omega t + \theta - \varphi_0$ gives $\dot{z} = \omega + \dot{\theta}$. In equation (22), putting $k = R/L_r$ for convenience:

$$\frac{dz}{dt} = \omega\cdot(1 - k\cos z) \tag{23}$$

Separating the variables and integrating

$$\int_0^t \omega\,dt = \int_{z_0}^{z}\frac{dz}{(1 - k\cos z)} \tag{24}$$

where $z_0 = \theta_0 - \varphi_0$, and θ_0 is the initial orientation angle of the robot at start point S. Equation (24) is an integral of rational function of $\cos z$. Put

$$z' = \tan\left(\frac{z}{2}\right), \quad dz' = \tfrac{1}{2}\cdot\left(\sec\frac{z}{2}\right)^2\cdot dz$$

so that

$$dz = \frac{2}{1 + (z')^2}\cdot dz',$$

hence:

$$\omega t = \int_{z_0'}^{z'}\frac{2\,dz'}{(1-k) + (1+k)(z')^2} \tag{25}$$

The solution from equation (25) is:

$$\omega t = \begin{cases} \dfrac{1}{b}\tan^{-1}(az') - \dfrac{1}{b}\tan^{-1}(az_0'), & a = \sqrt{\dfrac{1+k}{1-k}}, \\ b = \dfrac{\sqrt{1-k^2}}{2}, \quad k<1 & \dfrac{1}{z_0'} - \dfrac{1}{z_0}, \quad k = 1; \\ \dfrac{1}{d}\cdot\left(\ln\dfrac{cz'-1}{cz'+1} - \ln\dfrac{cz_0'-1}{cz_0'+1}\right), & c = \sqrt{\dfrac{k+1}{k-1}}, \\ d = \sqrt{k^2-1}, \quad k>1 \end{cases} \tag{26}$$

Considering the substitutions used above, we finally obtain the expression of θ in terms of k, ω, z_0' and t:

$$\theta = \begin{cases} 2\tan^{-1}\left(\dfrac{1}{a}\cdot\dfrac{az_0' + \tan(\omega t\cdot b)}{1 - (az_0'\cdot\tan(\omega t\cdot b))}\right) - \omega t + \varphi_0, \\ \quad k<1 \\ 2\tan^{-1}\left(\dfrac{z_0'}{1 - (\omega t\cdot z_0')}\right) - \omega t + \varphi_0, \quad k = 1 \\ 2\tan^{-1}\left(\dfrac{1}{c}\cdot\dfrac{(1+cz_0') + (cz_0'-1)\cdot e^{\omega t d}}{(1+cz_0') - ((cz_0'-1)\cdot e^{\omega t d})}\right) \\ \quad - \omega t + \varphi_0, \quad k>1 \end{cases} \tag{27}$$

Substituting equation (20) into (5) and simplifying, we obtain:

$$\begin{bmatrix} x_m - \bar{x} \\ y_m - \bar{y} \end{bmatrix} = \begin{bmatrix} L_m \cos(\theta + \beta) + R\cos(\omega t - \varphi_0) \\ L_m \sin(\theta + \beta) - R\sin(\omega t - \varphi_0) \end{bmatrix} \quad (28)$$

Where

$$\sin\beta = \frac{y_{m1}}{L_m}, \quad \cos\beta = \frac{x_{m1}}{L_m}, \quad L_m = \sqrt{x_{m1}^2 + y_{m1}^2}.$$

In order to understand better the locus of any point in the robot, squaring the two sides of (28) and adding, we can write:

$$(x_m - \bar{x})^2 + (y_m - \bar{y})^2 = L_m^2 + R^2 + 2RL_m \times \cos(\theta + \beta + \omega t - \varphi_0) \quad (29)$$

Equations (27) and (29) show that when the reference point moves along a circle, the locus of any other point is not necessarily a circle. This verifies the correctness of the example depicted in Figure 3.

II. the case $\underline{x} = 0$

$L_r = 0$ is a special case that means the reference point is chosen at the axle of the two rear wheels. It is obvious that equation (13) and (21) yields:

$$\theta = 270° - \omega t + \varphi_0 \quad (30)$$

At any instant, the tangent of the reference path coincides with the orientation of the robot. In this case, equation (29) becomes:

$$(x_m - \bar{x})^2 + (y_m - \bar{y})^2 = x_{m1}^2 + (y_{m1} + R)^2 \quad (31)$$

Equation (31) indicates that the path of any point in the robot is a circle.

III. The case $\underline{x} = L_r$

Using the similar procedure as above, we can obtain the expression of θ as follows:

$$\omega t = \begin{cases} \frac{1}{b}\tan^{-1}\left(\frac{z'}{a}\right) - \frac{1}{b}\tan^{-1}\left(\frac{z_0'}{a}\right), & a = \sqrt{\frac{1+k}{1-k}}, \\ b = \frac{\sqrt{1-k^2}}{2}, & k < 1, \quad z' - z_0', \quad k = 1 \\ \frac{1}{d}\cdot\left(\ln\frac{c+z'}{c-z'} - \ln\frac{c+z_0'}{c-z_0'}\right), & c = \sqrt{\frac{k+1}{k-1}}, \\ d = \sqrt{k^2-1}, & k > 1 \end{cases} \quad (32)$$

$$\theta = \begin{cases} 2\tan^{-1}\left(a\cdot\frac{z_0' + a\cdot\tan(\omega t\cdot b)}{a - (z_0')\cdot\tan(\omega t\cdot b))}\right) \\ \quad - \omega t + \varphi_0, \quad k > 1 \\ 2\tan^{-1}(\omega t + z_0') - \omega t + \varphi_0, \quad k = 1 \\ 2\tan^{-1}\left(c\cdot\frac{(c+z_0')\cdot e^{\omega t d} - (c - z_0')}{(c+z_0')\cdot e^{\omega t d} + (c - z_0')}\right) \\ \quad - \omega t + \varphi_0, \quad k > 1 \end{cases} \quad (33)$$

Where k, a, b, c, d and z_0' are defined as those in the case $\underline{x} = -L_r$. Equation (29) also applies to this case.

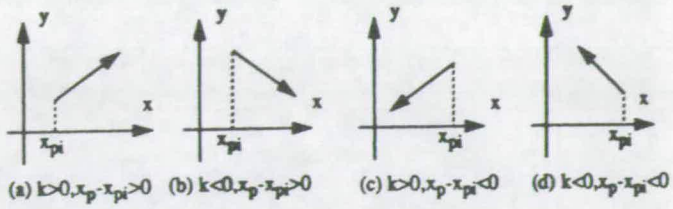

Fig. 6. An illustration of the signs of k and $(x_p - x_{pi})$.

3.2 Straight line motion

Let us consider the case when a robot moves along a straight line as shown in Figure 6, at any velocity. Without losing the generality, suppose that the motion of the reference point P is described by the following equation:

$$y_p = kx_p + b \quad (34)$$

Where k is the slope of the straight line and b the intercept on y axis, hence:

$$f'(x_p) = k \quad (35)$$

Substituting equation (35) into (17), we have:

$$\underline{x}\cdot d\theta = (\sin\theta - k\cos\theta)\,dx_p = \sqrt{1+k^2}\sin(\theta - \gamma)\,dx_p \quad (36)$$

Where

$$\sin\gamma = \frac{k}{\sqrt{1+k^2}}, \quad \cos\gamma = \frac{1}{\sqrt{1+k^2}},$$

γ is a constant ranging from $-90°$ to $90°$ for a followed path. The solution of the above equation is:

$$\theta - \gamma = 2\tan^{-1}\left(\tan\frac{\theta_0 - \gamma}{2}\cdot e^{k'}\right), \qquad k' = \frac{\sqrt{1+k^2}}{\underline{x}}(x_p - x_{pi}) \quad (37)$$

and x_{pi} is the initial x-coordinate. In this formula, the signs of k and $x_p - x_{pi}$ indicate the moving direction, as shown in Figure 6, the sign of $\underline{x}$ indicates the relative position of reference point on the robot to its rear axle. θ_0, the initial orientation angle, is in the range of 0° to 360°.

From equation (37), it can be drawn that if and only if the initial orientation angle θ_0 satisfies the following relation:

$$\theta_0 = \gamma + n\cdot 180°, \quad n = 0, 1 \quad (38)$$

then $\theta = \theta_0$ holds at any instant, which means the motion of the WMR is a translation.

When a WMR moves along a straight line parallel to y axis, the solution to orientation angle for a WMR is:

$$\theta = 2\tan^{-1}\left(\tan\frac{\theta_0 - 90°}{2}\cdot e^{k'}\right) + 90°, \qquad k' = \frac{y_p - y_{pi}}{\underline{x}} \quad (39)$$

When $\underline{x} = 0$, the orientation of the robot must be in the same direction as the tangent of the path at any instant.

4. EFFECT OF KINEMATIC CONSTRAINTS ON AND THE GENERAL FORMULATION OF THE PATH PLANNING PROBLEM FOR A WMR

In the previous sections, we have established the kinematic model and analyzed the kinematic characteristics of a WMR. From the analysis, it can be seen that the following four points are the key ones for path planning problems for a WMR and must be taken into account.

a. Rotation. Rotation of a WMR when it follows a curved path must occur. Only in one case where the path followed is a straight line and the WMR's initial orientation angle coincides with the direction of the straight line, does pure translation occur. However, in practice, this situation rarely appears.

b. Relationships between orientation angle and the path followed. A WMR's orientation angle is obtained by solving the general constraint equation (17) when it follows a specified path. Corresponding to every given initial orientation angle and every generated path, there exists a unique solution to equation (17) for θ. This inherent characteristic of a practical WMR shows that before a path is found (if it exists), one can not know exactly the WMR's orientation angle when the WMR follows it. This implies that the orientation of a WMR can not be arbitrary.

c. Saturation of the steering mechanism. Whenever we generate an approximate global path for a WMR, equation (18) must be used to check the feasibility of the generated path against the steering limit of the steering mechanism.

d. Goal. The goal orientation must be satisfied.

In order to satisfy the kinematic constraints, we first introduce the following definitions. In path planning problem for a WMR, we call a path from the starting point to the goal point feasible if and only if it satisfies both the requirements of being collision-free and being within the saturation limits. A feasible path only means it is safe and can be followed, but it offers no guarantee of the satisfaction of the goal orientation requirement. We call a feasible path a final path if it satisfies the goal orientation requirement. Obviously, the purpose for planning a path is to find a final path.

In the remainder of this subsection, we attempt to give a general formulation of the path planning problem for a WMR while taking into account the kinematic constraints, and then a possible algorithm structure for solving the find-path problem is proposed.

Suppose that the boundary of the WMR is presented as the following form in terms of the local reference frame:

$$\Gamma_A(x_{m1}, y_{m1}) = 0 \tag{40}$$

The boundary of the ith obstacle is presented as the following form in terms of the global reference frame:

$$\Gamma_{B_i}(x_m, y_m) = 0, \quad i = 1, 2, \ldots, n \tag{41}$$

Where $\Gamma_A(x_{m1}, y_{m1})$ and $\Gamma_{B_i}(x_m, y_m)$ are compact (i.e. closed and bounded) and continuous functions of the coordinates (x_{m1}, y_{m1}) and (x_m, y_m). In most cases, they are piecewise continuous functions. From equation (5), it follows that:

$$\begin{bmatrix} x_{m1} \\ y_{m1} \end{bmatrix} = \begin{bmatrix} (x_m - x_p)\cos\theta + (y_m - y_p)\sin\theta \\ -(x_m - x_p)\sin\theta + (y_m - y_p)\cos\theta \end{bmatrix} \tag{42}$$

Substituting equation (42) into (40) yields the expression of the boundary of the WMR in terms of the global reference frame:

$$\Gamma_A((x_m - x_p)\cos\theta + (y_m - y_p)\sin\theta, \\ -(x_m - x_p)\sin\theta + (y_m - y_p)\cos\theta) = 0 \tag{43}$$

As the initial position of the WMR is collision-free, and the WMR and obstacles are compact, if there is a path taken by the reference point of the WMR such that the boundary curve of the WMR expressed by equation (43) and the boundary curves of the obstacles expressed by equation (41) do not intersect each other, this path must be a collision-free path. In equation (43), the orientation angle θ is determined by the general constraint equation (17).

If a collision-free path satisfies the requirement of the saturation limit, it then becomes a feasible path. The purpose for path planning is to find a final path as defined above. Therefore, mathematically, a path planning problem for a WMR can be described formally as: Given $\Gamma_A(x_{m1}, y_{m1}) = 0$, $\Gamma_{B_i}(x_m, y_m) = 0$, the initial position (x_{pi}, y_{pi}) of the reference point and initial orientation angle θ_i of the WMR, and the goal position (x_{pg}, y_{pg}) of the reference point and the goal orientation angle θ_g of the WMR, find a continuous function $y_p = f(x_p)$ as the reference point's path such that it satisfies the following conditions:

a. $y_{pi} = f(x_{pi})$ and $y_{pg} = f(x_{pg})$

b. equations (41) and (43) have no points of intersection while the WMR's reference point follows the whole path.

c. the steering angle obtain from equation (18) satisfies the steering limit of the steering mechanism on the whole path.

d. the goal orientation obtained from equation (17) at the goal point satisfies θ_g.

A very common approach to the path planning problem for a WMR is the configuration space approach.[1] The idea is to build the explicit representations of the subsets of the WMR's configuration, the free space, which a reference point of the WMR can occupy without colliding with any obstacles. Conceptually, a configuration space method can be viewed as shrinking a WMR to a point while at the same time expanding the obstacles to the shape of the WMR. Therefore, two steps are needed to find a safe path. First, computing the Cspace obsetacles, and then a graph search method is employed. More generally, due to the size of a practical WMR, any algorithms considering a WMR as a point must take the first step to compute the Cspace obstacles by shrinking the WMR and then growing the obstacles. So the first step is the basis for most algorithms for planning a collision-free path for a WMR. If the orientation of the WMR is fixed, then the computation of the Cspace obstacles is not a very difficult job.[24] However, as already pointed out, in most cases,

the orientation angle of the WMR changes along the path, rotations must be dealt with. As we know, to obtain Cspace obstacles, an orientation angle of a WMR must be assumed before a reference path is generated. Thus, there is a potential conflict between the assumed orientation angle and that generated when the reference path is followed. Therefore, even if the Cspace obstacles are computed without considering the kinematic constraints, there is no guarantee that the generated path is really collision-free because of the existence of the kinematic constraints. The generated global path is only an approximation to the real one. On the other hand, an approximate global path is indeed necessary as it is a very useful guide to avoiding the blind try to find a safe path for the WMR. For this reason, we discard the time-consuming computation of the Cspace obstacles used in reference 1, use the following strategy to grow the obstacles, and still call the grown obstacles as Cspace obstacles.

For any generated path is to be followed and it must be safe and executable, the kinematic constraints can not be ignored in the path planning phase. In this sense, a path generated by the available algorithms can not be guaranteed to be collision free and they must be modified. A possible way one can do to alleviate this difficulty is first to find an approximate global path as fast as possible and then test it for potential collisions with obstacles and saturation of the steering mechanism. If collisions or saturation are detected, then use the information obtained during the tests to plan a local path for correcting the collision or saturation. The procedure of testing and correcting continues until a feasible path is found. After that, check the requirement of goal orientation. If it is not satisfied, another local planning for adjusting the goal orientation angle must be devised. Clearly, this work can only be done after a feasible path has been found. A possible path planning algorithm may consist of the following parts:

a. A coarse subalgorithm for finding an approximate global path

b. A testing subalgorithm for testing collision with obstacles, saturation of the steering mechanism, and goal orientation

c. A local path planning subalgorithm for correcting collision, saturation and goal orientation

5. Finding an approximate global path for a WMR

The choice of the reference point is the first consideration in path planning for a WMR. Its choice is affected by kinematic constraints, the algorithms devised to compute the Cspace obstacles and other factors. For example, when the reference point is chosen at any point on the rear axle, if the first derivative of the followed path is discontinuous, a discontinuity of the orientation angle will occur at the discontinuous point and, in turn, this also causes discontinuities of the velocity and acceleration of any point in the WMR. This undesired characteristic an be alleviated by moving the reference point away from the rear axle. This is an example of the effect of the kinematic constraints on the choice of the reference point. The algorithmic effect on it is also clear. In reference 1, when the WMR and obstacles are closed and bounded polygonal bodies, and the slice projection technique is employed, the reference point is chosen at one of the vertices of the WMR to generate a polygonal Cspace obstacles, thus to reduce the computational complexity of the followed graph searching procedure.

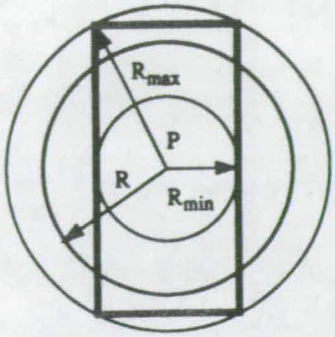

Fig. 7. The boundary of the WMR is encompassed by two circles with the same center.

Let the WMR A be a bounded convex polygon and its boundary be Γ_A (marked by the thick lines in Figure 7.). Let a_i be any point on Γ_A. Choose an origin, i.e. the reference point P, and two coordinate axes x_1, y_1. Let d_i be the distance from a_i to the origin. In this paper, the origin is chosen so that $\max_{a_i \in \Gamma_A} d_i$ is minimized over all possible origins. For a rectangular rigid body, it is located at the symmetric center. For a circular body, it is in the center. Obviously, for these two typical structures, this choice also has the important property that $\min_{a_i \in \Gamma_A} d_i$ is maximized. After the reference point is chosen as defined above, let R_{max} denote the $\min(\max_{a_i \in \Gamma_A} d_i)$ and R_{min} denote the $\max(\min_{a_i \in \Gamma_A} d_i)$. Consequently, the difference between R_{max} and R_{min} is also minimized. The boundary of the WMR will be encompassed by two circles, one with the central point at the origin and the radius of R_{max} and another with the same central point but different radius of R_{min}. As shown in Figure 7. The direction of the x_1 axis is always chosen to be perpendicular to the rear axle of the WMR and from the rear axle to the front axle.

In this paper, for every shrinking radius $R \in [R_{min}, R_{max}]$, shown also in Figure 7, two steps are required to find an approximate global path for a WMR. The first step is to compute the grown obstacles. We expand the obstacles by a circle with radius R to reduce the computational burden. The second step is to use an algorithm to search the Cspace obstacles, which is called generalized polygonal obstacles.[25] Fortunately, the tangent graph methods for a point robot among such generalized polygonal obstacles have been presented by references 25 and 26 and can be employed here. Clearly, the encompassed part of the robot by the circle of radius R is collision-free if an approximate global path can be found corresponding to the shrinking radius R.

If R_{max} is used to grow the polygonal obstacles, any path generated for a point among the grown obstacles will certainly be a collision-free path whatever the orientation angle of the WMR is and it is an approximate

global path. In this case, test for collision with obstacles is not needed. For $R_{max} = \min(\max_{a_i \in \Gamma_A} d_i)$, the choice of the reference point makes it most possible to find a collision-free, approximate global path.

If R_{min} is used to grow the obstacles, and no path is found by the algorithm[26] for a point robot among the grown obstacles, then it can be concluded that there exists no path for the WMR. In this case, for $R_{min} = \max(\min_{a_i \in \Gamma_A} d_i)$, the choice of the reference point increases the possibility to find that there is no path available in a cluttered environment.

The above mentioned two cases are easily handled. If the opposite search results are reached, namely, the first two iterations of using R_{max} and R_{min} fail and succeed in finding an approximate global path respectively, then we devise an equal-interval decreasing search scheme for R between R_{max} and R_{min}. Divide the interval $[R_{min}, R_{max}]$ into n equal subintervals, thus, the length of every subinterval equals to

$$\Delta = \frac{R_{max} - R_{min}}{n}.$$

Let $R_3 = R_{max} - \Delta$ and $R_i = R_{i-1} - \Delta$, $i = 4, 5, \ldots, n+1$, then use R_3 as the next shrinking radius. If the third iteration fails, choose R_4, and so on until an approximate global path for the biggest shrinking radius R is found provided n is big enough. Note that this is not the only possible search order. In fact, the order of the choice of R in $[R_{min}, R_{max}]$ is perfectly arbitrary.

In practice, if uncertainty is taken into account, a safety distance δ is assumed, then the actual minimum shrinking radius R_c equals to $\delta + R_{min}$.

6. DETECTING THE POTENTIAL COLLISIONS OF THE POLYGONAL WMR WITH POLYGONAL OBSTACLES

In this section, we consider the problem of determining the collisions of the polygonal robot with polygonal obstacles as it moves along a path. Because only the edges of the robot have the possibility of collisions with obstacles, the first problem considered here is how to determine the locus of every point on the boundary of the robot and then check the possibily of collisions with the obstacles.

Let the vertices of the robot by E, F, G, H, as shown in Figure 4. For simplification, in the following, we only show how to determine the locus of points on one of its edges, say EF, and test its collisions with obstacle in the workspace, the same procedure of derivation applies to the other edges of the polygonal robot.

At any instant, the positions of points E and F can be obtained from equation (5):

$$\begin{bmatrix} x_e \\ y_e \end{bmatrix} = \begin{bmatrix} x_{e1}\cos\theta - y_{e1}\sin\theta + x_p \\ x_{e1}\sin\theta + y_{e1}\cos\theta + y_p \end{bmatrix} \tag{44}$$

$$\begin{bmatrix} x_f \\ y_f \end{bmatrix} = \begin{bmatrix} x_{f1}\cos\theta - y_{f1}\sin\theta + x_p \\ x_{f1}\sin\theta + y_{f1}\cos\theta + y_p \end{bmatrix} \tag{45}$$

Any point in the edge EF can be expressed as the form of an equality and an inequality:

$$y - y_e = k_{ef}(x - x_e), \quad k_{ef} = \frac{y_e - y_f}{x_e - x_f} \tag{46}$$

$$\min(x_e, x_f) \le x \le \max(x_e, x_f) \tag{47}$$

Where x and y present the coordinates of any point on edge EF in terms of the global reference frame, $\min(x_e, x_f)$ means the minimum of x_e and x_f, $\max(x_e, x_f)$ means the maximum of x_e and x_f.

Suppose that the coordinates of the jth and $(j+1)$th vertices of the ith polygonal obstacle B_i are denoted by $b_{i,j}(x_{i,j}, y_{i,j})$ and $b_{i,j+1}(x_{i,j+1}, y_{i,j+1})$ respectively in terms of the global reference frame, then the coordinates of the points on the segment connecting $b_{i,j}$ and $b_{i,j+1}$ are given in the same form as equation (46) and inequality (47):

$$y - y_{i,j} = k_{i,j}(x - x_{i,j}), \quad k_{i,j} = \frac{y_{i,j+1} - y_{i,j}}{x_{i,j+1} - x_{i,j}} \tag{48}$$

$$\min(x_{i,j}, x_{i,j+1}) < x < \max(x_{i,j}, x_{i,j+1}) \tag{49}$$

The solution of equation (46) and (48), namely the coordinates of the point of intersection of the two straight lines, can be obtained as:

$$x = \frac{(k_{ef}x_e - y_e) - (k_{i,j}x_{i,j} - y_{i,j})}{k_{ef} - k_{i,j}} \tag{50}$$

$$y = \frac{k_{ef}(y_{i,j} - k_{i,j}x_{i,j}) - k_{i,j}(y_e - k_{ef}x_e)}{k_{ef} - k_{i,j}} \tag{51}$$

It is obvious that if and only if the x-coordinate of the point of intersection, given in equation (50), satisfies two inequalities (47) and (49), then the edge EF of the WMR have no collisions with the edge $b_{i,j}b_{i,j+1}$ of the ith obstacle B_i; Furthermore, if and only if EF have no collisions with all the edges of the obstacles B_i, EF is collision-free with B_i, because the initial position of EF is collision-free and B_i is compact polygon; If and only if all the edges of the robot is collision-free with all the obstacles in the workspace, then the approximate path is collision-free.

7. CONCLUSIONS

In this paper, we have clearly shown the difference between a free rigid body and a practical wheeled mobile robot from the viewpoint of kinematic constraints. The interdependence of its orientation angle on the path followed makes the path planning problem for a wheeled mobile robot much more complicated.

The conclusion drawn from this difference is that the path generated by the algorithms available is not definitely safe and executable. By safe we mean that there still exists the possibility to collide with obstacles. By executable we mean that the needed steering angle may exceed the maximum limit of the steering angle. The general constraint equation reflects the inherent characteristic of a wheeled mobile robot. However, as the steering saturation results from the Ackermann layout,[27] it is possible to remove the saturation limit by a new design of the steering mechanism. Consequently, the path planning algorithm for a WMR is simplified.

Another direct benefit from such a no saturation limit steering mechanism is the improvement of the maneuverability of the WMR. A mechanism which might be used for this purpose has been described in reference 28.

Path planning taking account of the kinematic constraints for a WMR is an area for the future research. In this work, we only addressed how to find an approximate global path and how to test for the collision with obstacles and for the steering saturation. More effort will have to be conducted for designing the local path without collision and saturation. This work must be built on the better understanding of the combination of the available algorithms and the kinematic characteristics of a wheeled mobile robot.

ACKNOWLEDGMENTS

The authors would like to express their gratitude to K.C. Wong Education Foundation for providing living expenses, CVCP committee, U.K. and Mechanical Engineering department of Edinburgh University for offering tuition fees for the first author during his Ph.D research. Also thanks to Dr. A.S-T. Lue, Mr. K.H. Wong and Dr. G. Alder for their valuable encouragement and help.

REFERENCES

1. T. Lozano-Perez, "Spatial Planning: A Configuration Space Approach" *IEEE Trans. on Computers* **C-32(2),** 108–120 (1983).
2. M. Sharir, "Algorithmic Motion Planning in Robotics" *IEEE Trans. on Computers* **39,** 9–20 (1989).
3. J.C. Latombe, *Robot Motion Planning* (Kluwer Academic Publishers, Boston, 1991).
4. R.A. Brooks, "Solving the Find-path Problem by Good Representation of Free Space" *IEEE Trans. on Systems, Man and Cybernetics* **SMC-13**(3), 190–197 (1983).
5. R.A. Brooks and T. Lozano-Perez, "A Subdivision Algorithm in Configuration Space for Findpath with Rotation" *IEEE Trans. on Systems, Man and Cybernetics* **SMC-15(2),** 224–233 (1985).
6. K. Fujimura and H. Samet, "A Hierarchical Strategy for Path Planning Among Moving Obstacles" *IEEE Trans. on Robotics and Automation* **5,** 61–69 (1989).
7. H.P. Huang and P.C. Lee, "A Real-Time Algorithm for Obstacle Avoidance of Autonomous Mobile Robots" *Robotica* **10,** 217–227 (1992).
8. Y.K. Hwang and N. Ahuja, "A Potential Field Approach to Path Planning" *IEEE Trans. on Robotics and Automation* **8,** 23–32 (1992).
9. J. Ilari and C. Torras, "2D Path planning: A Configuration Space Heuristic Approach" *Int. J. of Robotics Research* **9,** 75–91 (1990).
10. S. Kambhampati and L.S. Davis, "Multiresolution Path Planning for Mobile Robots" *IEEE J. of Robotics and Automation* **RA-2,** 135–145 (1986).
11. K. Kant and S.W. Zucker, "Toward Efficient Trajectory Planning: the Path-Velocity Decomposition" *Int. J. of Robotics Research* **5,** 72–89 (1986).
12. O. Khatib, "Real Time Obstacle Avoiding for Manipulators and Mobile Robots" *Int. J. of Robotics Research* **7,** 90–98 (1986).
13. V.J. Lumelsky, "A Comparative Study on the Path Length Performance of Maze-Searching and Robot Motion Planning Algorithms" *IEEE Trans. on Robotics and Automation* **7,** 57–66 (1991).
14. V.J. Lumelsky and A.A. Stepnov, "Dynamic Path Planning for a Mobile Robot Automation with Limited Information on the Environment" *IEEE Trans. on Automatic Control* **31,** 1058–1063 (1986).
15. J.T. Schwartz and M. Sharir, "On the 'piano Movers' Problem I. The Case of a Two-Dimensional Rigid Polygonal Body Moving Amidst Polygonal Barriers" *Communications on Pure and Applied Mathematics* **36,** 345–398 (1983).
16. S.H. Suh and K.G. Shin, "A Variational Dynamic Programming Approach to Robot-Path Planning with a Distance-Safety" *IEEE J. of Robotics and Automation* **4,** 334–349 (1988).
17. O. Takahashi and R.J. Schiling, "Motion Planning in a Plane Using Generalized Voronoi Diagrams" *IEEE Trans. on Robotics and Automation* **6,** 143–150 (1990).
18. G.T. Wilfong, "Motion Planning for an Autonomous Vehicle" Proc. of the *IEEE International Conf. on Robotics and Automation* pp. 529–533. (1988).
19. C.K. Yap, "How to Move a Chair through a Door" *IEEE J. of Robotics and Automation* **3,** 173–181 (1987).
20. D. Zhu and J.C. Latombe, "New Heuristic Algorithms for Efficient Hierarchical Path Planning" *IEEE Trans. on Robotics and Automation* **7,** 9–22 (1991).
21. J.P. Laumond, "Feasible Trajectories for Mobile Robots with Kinematic and Environment Constraints" *Preprints of the International Conference on Intelligent Autonomous Systems* pp. 346–354 (1986).
22. J.R. Billing and W.R.J. Mercer," Swept Paths of Large Trucks in Right Turns of Small Radius" *Transportation Research Record* 1052, *Symposium on Geometric Design for Large Trucks* pp. 116–119. (1986).
23. H.I. Freedman and S.D. Riemenschneider, "Determining the Path of the Rear Wheels of a Bus" *SIAM Rev.* **25,** 561–568 (1983).
24. T. Lozano-Perez and M. Wesley, "An Algorithm for Planning Collision-free Paths among Polyhedral Obstacles" *Commun. Assoc. Comput. Math.* **22,** 560–570 (1969).
25. J.P. Laumond, "Obstacle Growing in a Non-polygonal World" *Information Processing Letters* **25,** 41–50 (1987).
26. Y.H. Liu and S. Arimoto, "Path Planning Using a Tangent Graph for Mobile Robots Among Polygonal and Curved Obstacles" *Int. J. of Robotics Research* **11,** 376–382 (1992).
27. J.Y. Wang, *Theory of Ground Vehicles* (John Wiley and Sons, Chichester, UK, 1978).
28. J.L. Synge, "A Steering Problem" *Quarterly of Applied Mathematics* **31,** 295–302 (1973).

Vehicle Kinematics and Its Application to Highway Design

By Yongji Wang,[1] and J. A. Linnett[2]

(Reviewed by the Highway Division)

Abstract: This paper presents a mathematical model for computing the path of any one point on a wheeled vehicle, which may be a bus, an articulated truck, or a wheeled robot, and the steering angle necessary for a reference point to travel a specified curve. This problem arises in applications that require determination of the swept space of a vehicle and in the automatic control of a mobile robot while the reference point on the vehicle moves along a specified path. The mathematical model is applicable to any dimension of a rigid vehicle or vehicle combination. It can be shown that the widely used Western Highway Institute (WHI) formula for highway design is a special case of the mathematical model presented in this paper. Based on this model, some inherent characteristics of wheeled vehicles, such as curvature, radius of instantaneous rotation of a point on the vehicle, and their relationship; and the independence of vehicle's orientation angle, steering angle, curvature, and radius of instantaneous rotation to its velocity, are also analyzed. The analytic solutions of two typical motions, circular and straight-line motions, have been developed, and the comparison of the simulation results with the existing standards has been conducted.

INTRODUCTION

A driving hazard problem was proposed by Baylis (1973) and revised by Bender (1979). The problem can be described as follows: when making a left turn at a crossroad, one moves to the left as far as possible on one's side of the roadway and then turns. Unfortunately, the rear of the vehicle swings rightward as the left turn is begun—toward the unsuspecting driver passing on the right (Fig. 1). This can be quite noticeable if the turning vehicle is a long bus. Hence, the problem—just how far to the right will the back corner of the bus (P in Fig. 1) swing towards the right as the bus driver negotiates the left turn—was proposed.

Another similar problem, studied by Freedman and Riemenschneider (1983), is how to determine the path of the rear wheels of a bus while the front wheels of the bus track a given path. The solution to this problem is useful for highway design and for the placement of curbs at intersections.

A third problem, which is related to the previous ones but a little more complicated, arises from the motion of a trailer-truck and was dealt with by Fossum and Lewis (1981) and Alexander (1985). A comprehensive discussion of the maneuvering of vehicles such as buses or articulated trucks was carried out by Alexander and Maddocks (1988). In their work, attention was focused on intrinsic properties of rigid-body trajectories, such as curvature and centers of rotation. They derived a relation between the radius of rotation of the body and the radii of curvatures of the trajectories of the wheels. Based on that relation, the problems of circular steering, offtracking, and optimal steering were considered.

In addition to the aforementioned researchers from the mathematical field, many others (Alexander and Maddocks, 1989; Graettinger and Krogh 1989; Hemami et al. 1992; Kanayama et al. 1990; Muir and Newman 1987; Steer 1989) have focused their attentions on the kinematics of mobile robots and different methods have been developed. The motion problems of wheeled vehicles have also attracted the interest of many researchers devoted to road design for vehicles, especially large vehicles (Billing and Mercer 1986; Heald 1986; Sayers 1986; Smith 1986).

A mobile robot is a wheeled vehicle that executes the commands of computers rather than of a driver. However, from the viewpoint of the structure of the vehicle, a mobile robot has the identical kinematical model as the ordinary human-driven wheeled vehicle, due to their same structure. Therefore, research on wheeled vehicles can contribute insights to the problems related to both human-driven vehicles and problems associated with intelligent and autonomous

[1]PhD Student, Dept. of Mech. Engrg., Univ. of Edinburgh, King's Buildings, Edinburgh EH9 3JL, Scotland, United Kingdom.

[2]Endowment Fellow, Dept. of Mech. Engrg., Univ. of Edinburgh, King's Buildings, Edinburgh EH9 3JL, Scotland, United Kingdom.

Note. Discussion open until July 1, 1995. To extend the closing date one month, a written request must be filed with the ASCE Manager of Journals. The manuscript for this paper was submitted for review and possible publication on October 4, 1993. This paper is part of the *Journal of Transportation Engineering*, Vol. 121, No. 1, January/February, 1995. ©ASCE, ISSN 0733-947X/95/0001-0063–0074/$2.00 + $.25 per page. Paper No. 7099.

robots. Therefore, the investigation into this problem is of practical importance. In the present paper, a different method is proposed. Compared with the other models, it has the following advantages.

- The mathematical model is general in the sense that the reference point can be chosen at any point on the vehicle, not only on the midpoint of the rear axle or the front left wheel.
- The model can apply to any dimension of rigid vehicle or vehicle combination, not only to small vehicles, because it gives a transient description of the motion for a vehicle.
- The steering angle needed for a reference point to trace a specified path can be given, which is essential for automatically controlling a mobile robot by computer and useful for determining the minimum turning-radius when the steering angle limit is taken into consideration.
- The analytic solutions to straight-line motion and circular motion have been developed, which make the computation of the swept space by the vehicle more efficient and accurate.

STEERING GEOMETRY

Fig. 2 shows a vehicle cornering without any side-slip of the wheels. For a road vehicle, steering is normally affected by changing the heading of the front wheels through the steering system. At low speeds, there is a simple relation between the direction of motion of the vehicle and the steering wheel angle, and the turning behavior mainly depends on the geometry of the steering linkage. The prime consideration in the design of the steering system geometry is minimum tire-scrub during cornering. This requires that during the turn all tires should be in pure rolling without lateral sliding. Let us assume for simplicity that the planes of all four wheels, two front wheels (D, E) and two rear wheels (B, C), are vertical. Then the condition to be satisfied is this: the perpendicular to the planes of the front wheels, drawn through their centers, must meet at a projected point on the back axle. This establishes the proper relationship between the steering angle of the inside front wheel α_i and that of the outside front wheel α_o. When the local right-hand coordinate frame $O_1x_1y_1$ is introduced, as shown in Fig. 2, it is evident that α_o and α_i are negative angles. Therefore, in Fig. 2 it can be seen readily that α_i and α_o should satisfy the following relationship:

$$\cot \alpha_o - \cot \alpha_i = -\frac{W}{L} \tag{1}$$

where W = track; and L = wheelbase of the vehicle, respectively. Eq. (1) is usually referred to as the Jeantaud condition, which must be fulfilled if tire wear is to be kept to a minimum (Hillier and Pittuck 1966).

A mechanism that might be used in the steering of a four-wheeled vehicle with theoretically perfect satisfaction of the Jeantaud condition has been designed using suitably shaped oval wheels (or cams), which engage without slipping (Synge 1973). In practice, the Ackermann layout (Hillier and Pittuck 1966) is widely used, although it does not completely achieve the Jeantaud condition and is only accurate in three positions: straight-ahead, and one position in each lock. Since pneumatic tires are used, any slight inaccuracy can be overcome by the deflection of the tires.

It is obvious that the steering angle of the inside front wheel, α_i, is greater than that of the outside front wheel, α_o, when a vehicle turns. In our study, to gain simplicity without losing generality, we introduce a virtual steering angle α when we discuss the steering angle needed to follow a prespecified path, where α is the angle between the path of the midpoint of the two front wheels and the center line of the vehicle (Fig. 2).

MATHEMATICAL MODEL FOR RIGID VEHICLE

Three types of vehicle are considered: rigid, articulated, and drawbar. In this section, we derive the mathematical model for a rigid vehicle, which is the basis of the other two types, and prove that the established mathematical model satisfies the Jeantaud condition. Some useful characteristics will be analyzed.

Basic Kinematic Description of Rigid Vehicle

Fig. 3 is a plan view of the rigid vehicle model investigated in the present paper. From the point of view of the operating function, wheels used in the vehicle can be categorized into two types: free wheels and fixed wheels. If a wheel can rotate about a vertical axle, it is defined as a free wheel; otherwise, it is defined as a fixed wheel. Based on this definition, steered wheels are free wheels and wheels on the fixed axis, i.e., the two rear wheels, are fixed wheels. However, when they are described by a mathematical model, a fixed wheel may be regarded as a special

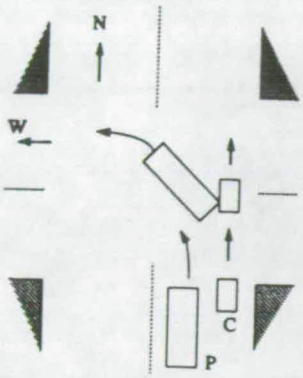

FIG. 1. Driving Hazard Problem

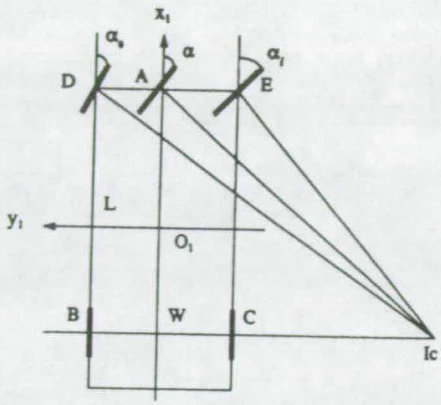

FIG. 2. Vehicle Cornering with Unique Center of Rotation on Back-Axle Projection

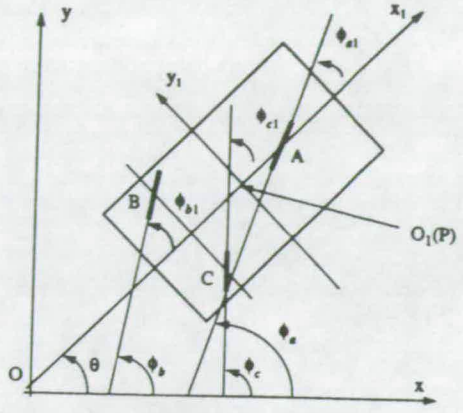

FIG. 3. Global (Oxy) and Local ($O_1x_1y_1$) Reference Coordinate Frames (Reference Point P Coincides with O_1)

free wheel. Therefore, in Fig. 3 all the wheels are given in the form of free wheels. A global reference coordinate frame (Oxy) is introduced to describe the motion of the vehicle in terms of the position of the reference point $P(x_p, y_p)$ and the orientation angle θ of the vehicle. We define a local reference coordinate frame ($O_1x_1y_1$), whose origin is placed at the reference point P of the vehicle with y_1-axis parallel to the rear axle BC of the vehicle. We use M to represent any point in the rigid vehicle body when discussing the motion of the rigid vehicle body, and also use it to represent a wheel connected to the corresponding point when discussing wheel motion. The coordinate of point M is given by $M(x_m, y_m)$ in terms of the global reference frame and $M(x_{m1}, y_{m1})$ in terms of the local reference frame. The coordinate of the central point of a wheel is constant with respect to the local reference frame.

The angle ϕ_m ($m = a, b, c, d$, and e) is measured from the vertical plane that the wheel M makes to the positive x-axis, and ϕ_{m1} is measured from the vertical planes of the wheel M to the positive x_1-axis (see Fig. 3). The relation between ϕ_m, θ, and ϕ_{m1} can be written as

$$\phi_m = \phi_{m1} + \theta \tag{2}$$

The coordinates of point M in the global frame are related to the coordinates of point M measured in the local frame by the transformation

$$\begin{pmatrix} x_m \\ y_m \end{pmatrix} = \begin{pmatrix} x_{m1} \cos\theta - y_{m1} \sin\theta + x_p \\ x_{m1} \sin\theta + y_{m1} \cos\theta + y_p \end{pmatrix} \tag{3}$$

The relationships between reference point velocity, orientation angle θ, vehicle turning angular rate, and wheel central velocities of wheels A, B, and C are found by differentiating (3) with respect to time

$$\begin{pmatrix} \dot{x}_m \\ \dot{y}_m \end{pmatrix} = \begin{bmatrix} (-x_{m1} \sin\theta - y_{m1} \cos\theta)\dot{\theta} + \dot{x}_p \\ (x_{m1} \cos\theta - y_{m1} \sin\theta)\dot{\theta} + \dot{y}_p \end{bmatrix} \tag{4}$$

where $\dot{x}_m$, $\dot{y}_m$, $\dot{x}_p$, and $\dot{y}_p$ = velocity components of the corresponding wheel central point and reference point along the x- and y-axes in terms of the global reference frame; and $\dot{\theta}$ = rotating angular rate of the vehicle body in terms of the global reference frame. Differentiating (4) again, we have the acceleration expressions

$$\begin{pmatrix} \ddot{x}_m \\ \ddot{y}_m \end{pmatrix} = \begin{bmatrix} (-x_{m1} \cos\theta + y_{m1} \sin\theta)\cdot\dot{\theta}^2 + (-x_{m1} \sin\theta - y_{m1} \cos\theta)\cdot\ddot{\theta} + \ddot{x}_p \\ (-x_{m1} \sin\theta - y_{m1} \cos\theta)\cdot\dot{\theta}^2 + (x_{m1} \cos\theta - y_{m1} \sin\theta)\cdot\ddot{\theta} + \ddot{y}_p \end{bmatrix} \tag{5}$$

Eqs. (3), (4), and (5) give the mathematical description of any point on the vehicle body in terms of the reference point position, velocity, acceleration, and orientation angle, as well as their derivatives. When the whole vehicle is considered, the ideal rolling conditions must be satisfied: (1) The direction of every wheel rolling forward, whether steered or not, must coincide with the tangent to the vehicle body trajectory in the corresponding wheel center; and (2) the velocity of every wheel center point must be equal to the product of wheel rotating angular rate about its own horizontal axle and its radius.

Mathematically, the foregoing conditions can be expressed as

$$\tan(\phi_m) = \frac{d}{d(x_m)}(y_m) = \frac{\dot{y}_m}{\dot{x}_m} \tag{6}$$

$$v_m = \frac{y}{\gamma}\bar{\omega}_m \tag{7}$$

where $\dot{\omega}_m$ (m = a, b, c, d, and e) = rotating angular rate of wheels A, B, C, D, and E, respectively; v_m = velocity of wheel center point of wheels A, B, C, D, and E; and r = radius of every wheel. Here, v_m = vector sum of $\dot{x}_m$ and $\dot{y}_m$

$$(v_m)^2 = (\dot{x}_m)^2 + (\dot{y}_m)^2 \tag{8}$$

From (2) and (6), we can obtain ϕ_{m1}, the relative angle to the vehicle orientation line, which is the steering angle for the steering wheel

$$\phi_{m1} = \arctan\left(\frac{\dot{y}_m}{\dot{x}_m}\right) - \theta \tag{9}$$

When the wheels in the vehicle are fixed wheels, $\phi_{b1} = \phi_{c1} = 0$, and, from (9), the following constraint is added:

$$\tan\theta = \frac{\dot{y}_b}{\dot{x}_b} = \frac{\dot{y}_c}{\dot{x}_c} \tag{10}$$

Assume that $x_{b1} = x_{c1} = \underline{x}$. Substituting (4) into (10) and simplifying we obtain

$$\underline{x}\cdot\dot{\theta} = \dot{x}_p \sin\theta - \dot{y}_p \cos\theta \tag{11}$$

Eq. (11) is what we need to solve for the vehicle orientation angle θ when the reference point velocity components $\dot{x}_p$ and $\dot{y}_p$ are specified. It is interesting that y_{b1} and y_{c1} are not included in (11), which illustrates the fact that only $\underline{x}$ has effects on a vehicle's orientation angle. Eq. (11) also indicates that

- When different fixed wheels in the vehicle have the same x-coordinates in terms of the local reference frame, that means they are installed in the same fixed horizontal axle, and only one constraint is added.
- If a vehicle has more than one fixed horizontal axle, two constraint equations are added. In this case, the two equations must conflict with one another, and the vehicle cannot move properly. Therefore, in a rigid vehicle the number of the fixed horizontal axles cannot exceed one.

Satisfaction of Jeantaud Condition

In the following, we prove that the mathematical model established in the foregoing satisfies the Jeantaud condition [(1)]. Suppose that the coordinates of the outside front wheel (D), the inside front wheel (E), and the two rear wheels (B and C) are denoted by $D(x_{d1}, y_{d1})$, $E(x_{e1}, y_{e1})$, $B(x_{b1}, y_{b1})$, and $C(x_{c1}, y_{c1})$, respectively, in terms of the local reference frame. Then we have the following equations (Fig. 2):

$$\begin{pmatrix} x_{b1} \\ y_{b1} \end{pmatrix} = \begin{pmatrix} x_{c1} \\ y_{d1} \end{pmatrix} \tag{12}$$

$$\begin{pmatrix} x_{e1} \\ y_{e1} \end{pmatrix} = \begin{pmatrix} x_{d1} \\ y_{c1} \end{pmatrix} \tag{13}$$

$$\begin{pmatrix} x_{d1} - x_{b1} \\ y_{b1} - y_{c1} \end{pmatrix} = \begin{pmatrix} x_{e1} - x_{c1} \\ y_{d1} - y_{e1} \end{pmatrix} = \begin{pmatrix} L \\ W \end{pmatrix} \tag{14}$$

From (9), we obtain the following relationship:

$$\cot(\phi_{m1}) = \frac{\dot{x}_m + \dot{y}_m \tan\theta}{\dot{y}_m - \dot{x}_m \tan\theta} \tag{15}$$

Substituting (4) into (15)

$$\cot(\phi_{m1}) = \frac{-y_{m1}\cdot\dot{\theta} + \dot{x}_p \cos\theta + \dot{y}_p \sin\theta}{x_{m1}\cdot\dot{\theta} + \dot{y}_p \cos\theta - \dot{x}_p \sin\theta} \tag{16}$$

When choosing M to be D and E, respectively, and taking (11), (13), and (14) into account, we have

$$\cot(\alpha_o) - \cot(\alpha_i) = \cot(\phi_{d1}) - \cot(\phi_{e1}) = \frac{\dot{\theta}\cdot(y_{e1} - y_{d1})}{\dot{\theta}\cdot(x_{d1} - x_{b1})} = -\frac{W}{L} \tag{17}$$

Eq. (17) illustrates that our mathematical model satisfies the Jeantaud condition and therefore its correctness is verified.

Curvature, Radius of Instantaneous Rotation, and Their Relationship

The expressions of the curvature and the radius of instantaneous rotation of any one point in the vehicle will be given in this subsection by using the basic kinematic description developed previously with respect to the position of the reference point, the vehicle orientation angle, and their derivatives. Some conclusions will also be made.

When x and y are expressed in terms of a parameter t, using $\dot{x}$ and $\ddot{x}$ to denote dx/dt, d^2x/dt^2, etc., we have $dy/dx = (dy/dt)/(dx/dt) = \dot{y}/\dot{x}$, while $d^2y/dx^2 = d(\dot{y}/\dot{x})/dx = d(\dot{y}/\dot{x})/dt \cdot dt/dx = (\dot{x}\ddot{y} - \ddot{x}\dot{y})/\dot{x}^3$. Therefore, for any point M in the vehicle, the curvature κ_m can be expressed by the following formula:

$$\kappa_m = \frac{\dfrac{d^2y_m}{d(x_m)^2}}{\left(1 + \left(\dfrac{dy_m}{dx_m}\right)^2\right)^{3/2}} = \frac{(\dot{x}_m \cdot \ddot{y}_m) - (\dot{y}_m \cdot \ddot{x}_m)}{[(\dot{x}_m)^2 + (\dot{y}_m)^2]^{3/2}} \tag{18}$$

Let R_m = radius of instantaneous rotation of point M in the vehicle. Then R_m is defined as the ratio of v_m to $\dot{\theta}$

$$R_m = \frac{v_m}{\dot{\theta}} = \frac{[(\dot{x}_m)^2 + (\dot{y}_m)^2]^{1/2}}{\dot{\theta}} \tag{19}$$

Taking (9) into consideration, we obtain the relationship between κ_m and R_m

$$R_m \cdot \kappa_m = \frac{[(\dot{x}_m)^2 + (\dot{y}_m)^2]^{1/2}}{\dot{\theta}} \cdot \frac{(\dot{x}_m \cdot \ddot{y}_m) - (\dot{y}_m \cdot \ddot{x}_m)}{[(\dot{x}_m)^2 + (\dot{y}_m)^2]^{3/2}} = 1 + \frac{\dot{\phi}_{m1}}{\dot{\theta}} \tag{20}$$

Eq. (20) reaches the same result as proposition 2 in Alexander and Maddocks (1988), which results in the following conclusions.

- It is apparent that the center of instantaneous rotation of a point in the vehicle and its center of curvature do not necessarily coincide. Their relationship is described by (20).
- If a point lies in the fixed axle, then $\dot{\phi}_{m1} = 0$, and the two aforementioned points do coincide.

Independence of θ, α, κ_m, and R_m to Velocity

A geometric curve in space is called a path. Mathematically, a curve can be presented by the following form in x, y plane:

$$y = f(x) \tag{21}$$

Some characteristics associated with its shape, such as its derivatives and curvature, are referred to as its geometric characteristics. A trajectory is defined as the time course along a path. One can choose its velocity from various schedules for a geometrically defined path, which results in various velocity profiles. If a wheeled vehicle moves along any curve at different velocity profiles, how the velocities will affect the vehicle's orientation θ and steering angle α is an important problem. If a variable is only affected by the geometrical characteristics, rather than by vehicle's velocities, it is called an independent variable of velocities. If θ is an independent variable, it is easily derived that the space swept by a vehicle traveling along a specified path also will be independent of the vehicle's velocities (suppose the vehicle's motion is so low that ideal rolling occurs). In this case, the highway design problem can be treated geometrically. When the limited steering angle of the steering mechanism is taken into consideration, whether or not the steering angle is an independent variable is of interest. In this subsection, we will prove that θ and α are such defined independent variables.

Eq. (11) cannot be directly used for this purpose, because it includes the time variable. From (11), another form of the general constraint equation can be derived

$$\underline{x} d\theta = [\sin\theta - f'(x_p)\cos\theta]\, dx_p \tag{22}$$

where $f'(x_p)$ = slope of curve $f(x_p)$ at x_p. It follows from the differential equation (22) that the orientation angle of the vehicle is only a function of the x-axis coordinate of the global reference frame.

From (4) and (9), we can obtain the expression of the steering angle as follows (the detailed derivation is omitted):

$$\phi_{m1} = \arctan\left[\frac{f'(x_p)\cos\theta - \sin\theta + x_{m1}\dfrac{d\theta}{dx_p}}{f'(x_p)\sin\theta + \cos\theta - y_{m1}\dfrac{d\theta}{dx_p}}\right] \tag{23}$$

Eqs. (22) and (23) show that vehicle's orientation angle θ and steering angle α depend only on the geometric characteristics of the followed curve.

The fact that κ_m and R_m are independent variables may be seen directly from (18) and (19); therefore the proofs are omitted.

ANALYTICAL SOLUTIONS FOR RIGID VEHICLE

In this section, we use the mathematical model from the previous section to analyze the two typical vehicle motions, circular motion and straight-line motion. The circular motion and straight-line motion are chosen because of the following two reasons: (1) Most analyses, especially for applications, assume that the reference point path is a circle and a straight line (for example, offtracking problem is defined only for circular turn); and (2) the effects of some parameters, such as the circular radius, driving velocity, the position of the reference point, etc., on the driving characteristics can be illustrated clearly.

Circular Motion

Consider the rigid vehicle traveling at a constant rate along a circle of radius R from S to T (Fig. 4). We may assume that the motion of the reference point P can be described by the following equations:

$$\begin{pmatrix} x_p \\ y_p \end{pmatrix} = \begin{bmatrix} -R\cos(\omega t) \\ R\sin(\omega t) \end{bmatrix} \tag{24}$$

$$\begin{pmatrix} \dot{x}_p \\ \dot{y}_p \end{pmatrix} = \begin{bmatrix} R\omega\sin(\omega t) \\ R\omega\cos(\omega t) \end{bmatrix} \tag{25}$$

There are three cases for $\underline{x}$ in (11), depending on the choice of the reference point P. Suppose that L_r represents the distance from P to the rear axle. Then $\underline{x} = -L_r$, $\underline{x} = 0$, and $\underline{x} = L_r$ correspond to the cases in which the reference points are chosen in front of, at, and behind the vehicle's rear axle, respectively. In the following, we will study these three cases.

Case 1: $\underline{x} = -L_r$

In this case, by substituting (25) into (11), we have

$$L_r\dot{\theta} = \dot{y}_p\cos\theta - \dot{x}_p\sin\theta = R\omega\cos(\omega t + \theta) \tag{26}$$

For convenience, let $k = R/L_r$. Because (26) is not an equation in t, θ with separable variables, the method of changing the variables must be used to solve it. The substitution $z = \omega t + \theta$ gives $\dot{z} = \omega + \dot{\theta}$. Substituting them into (26) gives the following:

$$\frac{dz}{dt} = \omega\cdot(1 + k\cos z) \tag{27}$$

Integrating (27)

$$\int_0^t dt = \int_{z_0}^{z} \frac{dz}{\omega\cdot(1 + k\cos z)} \tag{28}$$

where $z_0 = \theta(0) = \theta_0$ = initial orientation angle of the vehicle at start point S. Eq. (28) is an integral of rational function of $\cos\theta$. Let $z' = \tan(z/2)$; and $dz' = 1/2\cdot[\sec(z/2)]^2\cdot dz$, so that $dz = \{2/[1 + (z')^2]\}\cdot dz'$, hence

$$\omega t = \int_{z_0'}^{z'} \frac{2dz'}{(1 + k) + (1 - k)(z')^2} \tag{29}$$

The solution from (29) is

$$\frac{1}{b}\left[\arctan\left(\frac{z'}{a}\right) - \arctan\left(\frac{z_0'}{a}\right)\right]; \quad \text{for } a = \sqrt{\frac{1 + k}{1 - k}}; \quad b = \frac{\sqrt{1 - k^2}}{2}; \quad k < 1 \tag{30a}$$

$$\omega t = z' - z_0'; \quad \text{for } k = 1 \tag{30b}$$

$$\omega t = \frac{1}{d}\cdot\left[\ln\left(\frac{c + z'}{c - z'}\right) - \ln\left(\frac{c + z_0'}{c - z_0'}\right)\right]; \quad \text{for } c = \sqrt{\frac{k + 1}{k - 1}}; \quad d = \sqrt{k^2 - 1}; \quad k > 1 \tag{30c}$$

Considering the previous substitutions, we finally obtain the expression of θ in terms of k, ω, z_0', and t

$$\theta = 2 \arctan \left\{ a \cdot \frac{z_0' + a \cdot \tan(\omega t \cdot b)}{a - [z_0' \cdot \tan(\omega t \cdot b)]} \right\} - \omega t; \qquad \text{for } k < 1 \tag{31a}$$

$$\theta = 2 \arctan(\omega t + z_0') - \omega t; \qquad \text{for } k = 1 \tag{31b}$$

$$\theta = 2 \arctan \left[c \cdot \frac{(c + z_0') \cdot e^{\omega t d} - (c - z_0')}{(c + z_0') \cdot e^{\omega t d} + (c - z_0')} \right] - \omega t; \qquad \text{for } k > 1 \tag{31c}$$

When calculating the steering angle α from (9), we must know $\dot{\theta}$, which can be obtained by differentiating (31). Another reason for calculating $\dot{\theta}$ lies in the fact that $\dot{\theta}$ cannot exceed some value that corresponds to the driver's reaction rate (Billing and Mercer 1986). Substituting (24) into (3) and simplifying, we obtain

$$\begin{pmatrix} x_m \\ y_m \end{pmatrix} = \begin{bmatrix} L_m \cos(\theta + \beta) - R \cos \omega t \\ L_m \sin(\theta + \beta) + R \sin \omega t \end{bmatrix} \tag{32}$$

where $\sin \beta = y_{m1}/L_m$, $\cos \beta = x_{m1}/L_m$; and $L_m = \sqrt{x_{m1}^2 + y_{m1}^2}$. In order to understand better the locus of any point in the vehicle, squaring the two sides of (32), we write

$$x_m^2 + y_m^2 = L_m^2 + R^2 - 2RL_m \cos(\theta + \beta + \omega t) \tag{33}$$

Eq. (31) verifies that θ is only dependent on ωt, rather than dependent on ω alone. If R is fixed, ω represents the velocity of the reference point P; and ωt represents the radians of the arc traveled. Eqs. (31) and (33) show that

- When the vehicle moves along a path, the geometry of the path, such as its slope, curvature, and the choice of reference point, rather than the velocity of the reference point, decide the orientation angle of the vehicle.
- When reference point moves along a circle, the locus of the other point is not necessarily a circle.

Case 2: $\underline{x} = 0$

As mentioned previously, the choice of reference point has a very important effect on the orientation angle as well as on all the other parameters, such as position, velocity of a point in the vehicle, and steering angle. $L_r = 0$ is a special case that means the reference point is chosen at the axle of the two rear wheels. It is obvious that (26) yields

$$\theta = 90° - \omega t \tag{34}$$

In this case, (33) becomes

$$x_m^2 + y_m^2 = x_{m1}^2 + (y_{m1} + R)^2 \tag{35}$$

Eq. (35) indicates that the path of any point in the vehicle is a circle. At any instant, the tangent of the reference path coincides with the orientation of the vehicle, including the initial time.

Case 3: $\underline{x} = L_r$

In this case, the reference point P is chosen after the rear axle. For the sake of simplification, the procedure of deriving the vehicle's orientation angle θ is omitted. Using a procedure similar to the foregoing, we can obtain the expression of θ as follows:

$$\theta = 2 \arctan \left\{ \frac{1}{a} \cdot \frac{az_0' + \tan(\omega t \cdot b)}{1 - [az_0' \cdot \tan(\omega t \cdot b)]} \right\} - \omega t; \qquad \text{for } k < 1 \tag{36a}$$

$$\theta = 2 \arctan \left[\frac{z_0'}{1 - (\omega t \cdot z_0')} \right] - \omega t; \qquad k = 1 \tag{36b}$$

$$\theta = 2 \arctan \left\{ \frac{1}{c} \cdot \frac{(1 + cz_0') + (cz_0' - 1) \cdot e^{\omega t d}}{(1 + cz_0') - [(cz_0' - 1) \cdot e^{\omega t d}]} \right\} - \omega t; \qquad \text{for } k > 1 \tag{36c}$$

where k, a, b, c, d, and z_0' are defined as they were in case 1, $\underline{x} = -L_r$. Eq. (33) also applies to case 3.

Straight Line Motion

Let us consider the cases in which a vehicle moves forward from position T in the direction shown in Fig. 4, at a constant acceleration a with the initial velocity $R\omega$. The question is how long it will take for the vehicle to adjust its orientation angle θ to coincide with its moving

direction. Without losing the generality, suppose the motion of the reference point P is described by the following equations:

$$\begin{pmatrix} x_p \\ y_p \end{pmatrix} = \begin{pmatrix} \int_0^t \dot{x}_p \, dt \\ R \end{pmatrix} = \begin{pmatrix} R\omega t + \frac{1}{2} \cdot at^2 \\ R \end{pmatrix} \tag{37}$$

$$\begin{pmatrix} \dot{x}_p \\ \dot{y}_p \end{pmatrix} = \begin{pmatrix} R\omega + at \\ 0 \end{pmatrix} \tag{38}$$

Case 1: $\underline{x} = -L_r$

Substituting (38) into (11), we have

$$L_r \cdot \dot{\theta} = -\dot{x}_p \cdot \sin\theta = -(R\omega + at)\sin\theta \tag{39}$$

The solution of (39) is

$$\theta = 2 \arctan\left[\tan\frac{\theta_0}{2} \cdot \exp\left(-\frac{x_p}{L_r}\right)\right] = 2 \arctan\left[\tan\frac{\theta_0}{2} \cdot \exp\left(-\frac{2R\omega t + at^2}{2L_r}\right)\right] \tag{40}$$

This is a very interesting result, which illustrates the following:

- The length needed by a vehicle to adjust its own orientation angle within the required accuracy limitation is independent of the velocity, and infinite length is needed to reach $\theta = 0$ theoretically.
- One important factor affecting on the adjustment of θ is the position of the reference point P, namely L_r. The larger L_r is, the longer the path needed for the vehicle to travel to reach the required limitation. Of course, θ_0 has direct influence on θ.

In our coordinate frame, when $\theta = 0°$, the orientation of the vehicle is in the same direction as its moving direction. The problem we are interested in is under what condition the orientation will reach the required accuracy limitation from θ_0. Assuming that the accuracy limitation is 5°, we have the following form:

$$|\theta| < 5° \tag{41}$$

That is

$$-0.0437 < \tan\frac{\theta_0}{2} \cdot e^{-k'} < 0.0437; \qquad \text{for } k' = \frac{x_p}{L_r} \tag{42}$$

This is the inequality we need in order to analyze the relationship between θ_0, x_p, and L_r. It will find its applications in road design for road vehicles and in workspace design for mobile robots working in the factory environment.

The position of any point in the vehicle for straight-line motion can be obtained by substituting (40) into (3)

$$\begin{pmatrix} x_m \\ y_m \end{pmatrix} = \frac{1}{1 + \tan^2\gamma} \cdot \begin{bmatrix} (x_{m1} + x_p) - 2y_{m1}\tan\gamma + (x_p - x_{m1})\tan^2\gamma \\ (y_{m1} + y_p) + 2x_{m1}\tan\gamma + (y_p - y_{m1})\tan^2\gamma \end{bmatrix} \tag{43}$$

where $\tan\gamma = \tan(\theta_0/2) \cdot e^{-k'}$.

Case 2: $\underline{x} = 0$

When $\underline{x} = 0$, the orientation of the vehicle at any instant must be in the same direction as the tangent of the path. In straight-line motion, the orientation must coincide with the direction of the road.

MATHEMATICAL MODEL FOR SERIALLY LINKED VEHICLE

In the previous sections, a mathematical model dealing with the motion of a rigid vehicle has been developed. Before studying the motion of a combined vehicle, it is useful to distinguish a vehicle unit from a combined vehicle. A vehicle unit is composed of: (1) A rigid body; (2) a fixed axle on which some wheels are mounted; and (3) some steering wheels or a hitch point. In this sense, a rigid vehicle is a single-unit vehicle with two front steering wheels like that in Fig. 2. A combined vehicle, such as an articulated vehicle or a drawbar vehicle, can be regarded as a combination of two or more vehicle units linked in series at their hitch points (Fig. 5).

From a motion analysis standpoint, multiple axles of an axle group operating together within

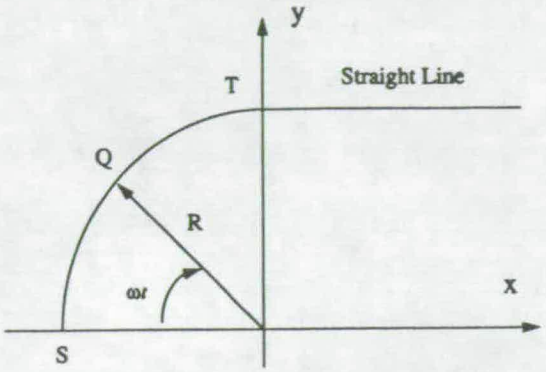

FIG. 4. Circular and Straight Line Motions

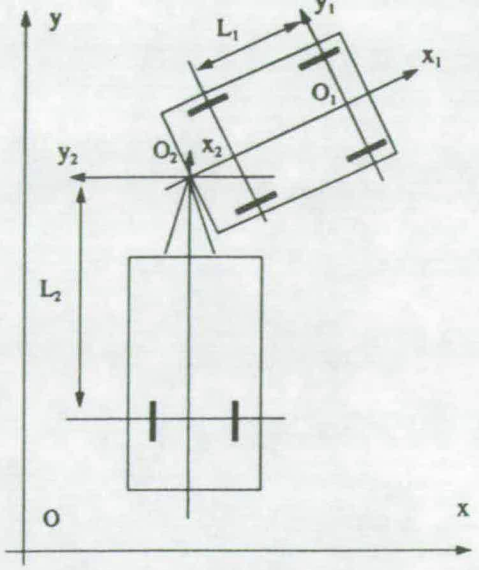

FIG. 5. Articulated Vehicle

TABLE 1. Design Vehicle Dimensions

Vehicle dimensions (1)	Design Vehicle Type: Passenger car[a] (2)	Single-unit truck[b] (3)	Single-unit bus[c] (4)	Semitrailer intermediate[d] (5)	Combination large[e] (6)
Wheelbase	3.35	6.10	7.62	12.19	15.24
Front overhang	0.91	1.22	2.13	1.22	0.91
Rear overhang	1.52	1.83	2.44	1.83	0.61
Overall length	5.79	9.14	12.19	15.24	16.76
Overall width	2.13	2.59	2.59	2.59	2.59
Height	—	4.11	4.11	4.11	4.11

Note: Dimensions are in m.
[a]Passenger car = *P* for Fig. G-1 in *A Policy* . . . (1973).
[b]Single-unit truck = SU for Fig. G-2 in *A Policy* . . . (1973).
[c]Single-unit bus = BUS for Fig. G-3 in *A Policy* . . . (1973).
[d]Semitrailer intermediate = WB-40 for Fig. G-4 in *A Policy* . . . (1973).
[e] Combination large = WB-50 for Fig. G-5 in *A Policy* . . . (1973).

a single suspension system, which is simplified as a rigid body, are treated as though they were a single axle located at the geometric center of the group.

Fig. 5 shows a two-linked vehicle model. The first vehicle unit is one with two steering wheels, while the second has a hitch point instead of two steering wheels. Two local reference coordinate frames $(O_1x_1y_1)$ and $(O_2x_2y_2)$ are each put on one of the two vehicle units. For convenience, the origin of the second frame coincides with the hitch point. We know that for the first vehicle unit, if the position and velocity of the reference point O_1 are given, then the orientation angle of vehicle unit 1 can be obtained by solving the differential equation, (11). The position and velocity of the hitch point O_2, which is a point in the vehicle unit 1, can be calculated using (3) and (4). That means that the position and velocity of the second vehicle unit's reference point O_2 have been obtained. Consequently, by means of the identical procedure used in the calculations of the vehicle unit one, the position and velocity and other interesting parameters of all the points in the second vehicle unit can be calculated. If more than two vehicle units are serially linked, the procedure for dealing with the motion problem of the complicated vehicle is analogous to the previous one. In every step, a numerical method must be used to solve a simple first-order differential equation [(11)].

SIMULATION RESULTS AND COMMENTS

The WHI offtracking formula is widely used for highway design. In their 1973 volume, the Society of Automotive Engineers (SAE) included the following statement (Heald 1986):

> In recent years, there have been developed data which are accurate enough to use for all practical purposes. The method was developed by the Western Highway Institute. . . . It is this method, easy to calculate and simple to apply, which is recommended as a general practice.

TABLE 2. Comparison of Results from Present Model with Existing Standards

(1)	DESIGN VEHICLE TYPE														
	Passenger Car[a]			Single-Unit Truck[b]			Single-Unit Bus[c]			Semitrailer Intermediate[d]			Combination Large[e]		
	Standard (2)	Present model (3)	Error (4)	Standard (5)	Present model (6)	Error (7)	Standard (8)	Present model (9)	Error (10)	Standard (11)	Present model (12)	Error (13)	Standard (14)	Present model (15)	Error (16)
Minimum turning radius (m)	7.31	7.31	—	12.8	12.8	—	12.8	12.8	—	12.19	12.19	—	13.71	13.71	—
Minimum inside radius (m)	4.66	4.66	0%	8.66	8.69	0.4%	6.19	7.74	25%	6.06	5.91	2.5%	6.03	6.00	0.3%
Maximum outside radius (m)	7.86	7.89	0.4%	13.38	13.41	0.2%	14.35	14.17	1.3%	12.56	12.65	0.7%	14.08	14.11	0.2%
Maximum steering angle (rad)	—	−0.62	—	—	−0.61	—	—	−0.77	—	—	−0.42	—	—	−0.50	—

[a]Passenger car = P for Fig. G-1 in *A Policy . . .* (1973).
[b]Single-unit truck = SU for Fig. G-2 in *A Policy . . .* (1973).
[c]Single-unit bus = BUS for Fig. G-3 in *A Policy . . .* (1973).
[d]Semitrailer intermediate = WB-40 for Fig. G-4 in *A Policy . . .* (1973).
[e]Combination large = WB-50 for Fig. G-5 in *A Policy . . .* (1973).

Heald (1986) also pointed out that the WHI formula may break down for long units on short-radius curves. Essentially, this formula describes the steady-state motion of a truck or truck combination. The model in the present paper gives a transient description of the vehicles. Using this mathematical model, we can prove that the WHI formula is a special result of this model. This can be observed from (31) when ωt tends to infinite. In this case, $\theta + \omega t \rightarrow 2 \arctan(c)$, a constant. The path of each point on the vehicle becomes a circle. Eq. (31) also indicates that d is an important factor affecting the speed needed to reach the steady-state condition. If the radius of the circle is fixed, then the bigger the length of the wheelbase of a truck, the smaller d, and the longer the length of the path passed by the reference point, the larger the error when the WHI formula is used. This explains that the WHI formula can give a reasonable approximation when the truck's wheelbase is small, but is not applicable for very large trucks.

The assumption used in the model and the WHI is the same, i.e., all the wheels roll without slipping. The only difference is that our model gives a transient description of the vehicle while the WHI describes the steady-state motion.

In highway design, the determination of the minimum turning paths of design vehicles is essential. In the following, the simulation results are compared with the standards (Figs. G1–G5) given in *A Policy . . .* (1973). The boundaries of the turning paths of the several design vehicles when making the sharpest turn are established by the outer trace of the front overhang and the path of the inner rear wheel. This turn assumes that the outer front wheel first follows a circular arc, which is the minimum turning radius as determined by the vehicle steering mechanism, and then follows a straight line. Figures G1–G5 of *A Policy . . .* (1973) are not shown here due to limitation of space; however, the design vehicle dimensions are given in Table 1. Based on these geometric dimensions, the minimum outside and inside wheel paths from this model and from the standards are all shown in Table 2.

In the practical programming, the reference point is chosen at the front left wheel, and the initial orientation angle for the circular curve is 90°. More attention should be paid to the transition from the circular curve to the straight line (Fig. 4). The calculated orientation angle of the vehicle at the end of the circular curve must be treated as the initial orientation angle for the straight line motion.

Table 2 shows that the error of the maximum outside radius is smaller than that of the minimum inside radius. This is because the overhang of each vehicle is much smaller than the corresponding wheelbase. For small vehicles (i.e., passenger cars and single-unit trucks), both of the errors are reasonable. However, as the wheelbase increases (i.e., for a single unit bus), the error of the minimum inside radius increases rapidly, reaching 25%. If a larger vehicle is allowed, then a model that can describe the transient motion of the vehicle is necessary. The model described previously can meet this requirement. For semitrailer intermediate vehicles and combination large vehicles, the minimum inside radii and maximum outside radii from the simulation are, respectively, smaller and larger than those from the standards. Table 2 also shows the maximum steering angle needed for the outer front wheel to follow the circular arc. This is not given in *A Policy . . .* (1973).

CONCLUSIONS

A mathematical model has been developed for computing the path of any one point on a wheeled vehicle as well as the steering angle necessary for a reference point to travel a specified curve. This model has constituted the basis for the analysis of the motion of wheeled vehicles. The key problems that have been solved are: (1) How to describe the constraints added due to the existence of fixed wheels on the vehicle; and (2) how to solve (11) to obtain the orientation angle of the vehicle. It has been proven that the model satisfies the ideal rolling condition, i.e., the Jeantaud condition, which is normally given in the geometric form by (1). When a path is specified, a vehicle may pass a fixed point in the path at different velocities. To consider the

effect of velocity on vehicle's orientation angle, steering angle, curvature, and radius of instantaneous rotation of any point on the vehicle, an independent variable has been defined as one that is only affected by the geometric characteristics of the curve, rather than by the vehicle's velocity. It has been shown that the vehicle's orientation angle, steering angle, curvature, and radius of instantaneous rotation of any point are all such independent variables. This explains why the design for an intersection of an urban road can be treated as a pure geometric problem.

In the model, to obtain the vehicle's orientation angle, only a simple first-order differential equation [(11)] is required to be solved. The other parameters can be obtained using the given analytic formulas. For the case when the path followed is a typical one, such as a circle or a straight line, direct analytic formulas have been given. Compared with other models, it has the following advantages.

- The mathematical model is general in the sense that the reference point can be chosen at any point on the vehicle, not only on the midpoint of the rear axle or the front left wheel.
- The model can apply to any dimension of rigid vehicle or vehicle combination, not only to small vehicles, because it gives a transient description of the motion for a vehicle.
- The needed steering angle for tracing a specified path can be given by the reference point, which is essential for automatically controlling a mobile robot by computer, and useful for determining the minimum turning radius when the steering angle limit is taken into consideration.
- The analytic solutions for straight-line motion and circular motion have been developed, which make the computation of the space swept by the vehicle more efficient and accurate.
- It makes the programming easier.

The model can simulate all the highway vehicles and handle arbitrarily complex turn geometries. Therefore, for a particular vehicle of interest virtually any geometric design can be evaluated.

ACKNOWLEDGMENTS

The writers would like to express their gratitude to the K. C. Wong Education Foundation for providing living expenses, the Committee of Vice-Chancellors and Principals of the Universities of the United Kingdom (CVCP), and the mechanical engineering department of Edinburgh University for offering tuition fees for the first writer during his PhD research. Also, thanks to Dr. A. S.-T. Lue, K. H. Wong, Dr. W. Peng, and Dr. G. Alder for their valuable encouragement and help.

APPENDIX I. REFERENCES

Alexander, J. C. (1985). "On the motion of a trailer-truck." *SIAM Rev.*, 27(4), 578–579.
Alexander, J. C., and Maddocks, J. H. (1988). "On the maneuvering of vehicles." *SIAM J. Appl. Math.*, 48(1), 38–51.
Alexander, J. C., and Maddocks, J. H. (1989). "On the kinematics of wheeled mobile robots." *Int. J. Robotics Res.*, 8(5), 15–27.
Baylis, J. (1973). "The mathematics of a driving hazard." *Math. Gaz.*, 57(399), 23–26.
Bender, E. A. (1979). "A driving hazard revisited." *SIAM Rev.*, 21(1), 136–138.
Billing, J. R., and Mercer, W. R. J. (1986). "Swept paths of large trucks in right turns of small radius." *Transp. Res. Record 1052: Symp. on Geometric Des. for Large Trucks*, Transportation Research Board, Washington, D.C., 116–119.
Fossum, T. V., and Lewis, G. N. (1981). "A mathematical model for trailer-truck jackknifing." *SIAM Rev.*, 23(1), 95–99.
Freedman, H. I., and Riemenschneider, S. D. (1983). "Determining the path of the rear wheels of a bus." *SIAM Rev.*, 25(4), 561–568.
Graettinger, T. J., and Krogh, B. H. (1989). "Evaluation and time-scaling of trajectories for wheeled mobile robots." *J. Dynamic Systems, Measurement, and Control*, 111(2), 222–231.
Heald, K. L. (1986). "Use of the HWI offtracking formula." *Transp. Res. Rec. 1052: Symp. on Geometric Des. for Large Trucks*, Transportation Research Board, Washington, D.C., 45–53.
Hemami, A., Mehrabi, M. G., and Cheng, R. M. H. (1992). "Synthesis of an optimal control law for path tracking in mobile robots." *Automatica*, 28(2), 383–387.
Hillier, V., and Pittuck, F. W. (1966). *Fundamentals of motor vehicle technology*. Hutchinson Educational Ltd., London, England.
Kanayama, Y., Kimura, Y., Miyazaki, F., and Noguchi, T. (1990). "A stable tracking control method for an autonomous mobile robot." *Proc., IEEE Conf. on Robotics and Automation*, The Institute of Electrical and Electronics Engineers, Inc., New York, N.Y., 384–389.
Lozano-perez, T., and Wesley, M. (1979). "An algorithm for planning collision-free paths among polyhedral obstacles." *Communications of the Assoc. for Computing Machinery*, 22(10), 560–570.
Muir, P. F., and Neuman, C. P. (1987). "Kinematic modelling of wheeled mobile robots." *J. Robotic Systems*, 4(2), 281–340.
A policy on design of urban highways and arterial streets. (1973). American Association of State Highway and Transportation Officials, Washington, D.C.

Sayers, M. W. (1986). "Vehicle offtracking models." *Transp. Res. Record 1052: Symp. on Geometric Des. for Large Trucks*, Transportation Research Board, Washington, D.C. 53–62.
Smith, B. L. (1986). "Existing design standards." *Transportation Research Record 1052: Symp. on Geometric Des. for Large Trucks*, Transportation Research Board, Washington, D.C., 23–29.
Steer, B. (1989). "Trajectory planning for a mobile robot." *Int. J. Robotics Res.*, 8(5), 3–14.
Synge, J. L. (1973). "A steering problem." *Quarterly of Appl. Math.*, 31(3), 295–302.
Wong, J. Y. (1978). *Theory of ground vehicles*. John Wiley & Sons, Inc., New York, N.Y.

APPENDIX II. NOTATION

The following symbols are used in this paper:

A, B, C, D, E = wheels;
a, b, c, d, k, k' = coefficients;
L = wheelbase of vehicle;
L_1 = wheelbase of first vehicle unit;
L_2 = distance between hitch point and rear axle of second vehicle unit;
L_m = length between point M and point P;
L_r = distance of reference point P to rear axle;
M = any wheel on vehicle, and its corresponding point;
(Oxy) = global coordinate frame;
$(O_1x_1y_1)$ = local coordinate frame;
P = reference point;
R = radius of circular motion;
R_m = radius of instantaneous rotation of point M;
r = radius of wheel;
W = track of vehicle;
(x_m, y_m) = absolute coordinates of point M with respect to global coordinate frame;
(x_{m1}, y_{m1}) = relative coordinates of point M with respect to local coordinate frame;
$\underline{x}$ = relative position of reference point P to rear axle;
z_0 = coefficient;
z_0' = coefficient;
α = virtual steering angle;
α_i = steering angle of inside front wheel;
α_o = steering angle of outside front wheel;
β_m = angle measured from point M to x_1-axis;
γ = coefficient;
θ = orientation angle of vehicle with respect to global coordinate frame;
θ_0 = initial orientation angle;
κ_m = curvature of point M;
v_m = velocity of center point of wheel M;
ϕ_m = angle measured from vertical plane of wheel M to positive x-axis;
ϕ_{m1} = angle measured from vertical plane of wheel M to positive x_1-axis;
ω = rotating angular rate of reference point P for circular motion; and
$\tilde{\omega}$ = rotating angular rate of wheel M.